Quantum walk and Wigner function on a lattice

Doctoral thesis in Physics

Author:
Margarida Hinarejos Doménech
Supervisor:
Dr. Armando Pérez Cañellas
Dr. Mari Carmen Bañuls Polo

N'Armando Pérez Cañellas, Doctor de Física, Catedràtic d'Universitat al departament de Física Teòrica de la Universitat de València, i Na Mari Carmen Bañuls Polo, Doctora en Física, Wissenschaftliche Mitarbeiterin al Max-Planck-Institut für Quantenoptik

CERTIFIQUEN

que la memòria present "Quantum Walk and Wigner function on a lattice" resumeix el treball d'investigació realitzat, sota la seua direcció, per Margarida Hinarejos Doménech i constitueix la seua Tesi per optar al grau de Doctora en Ciències Físiques.

I per que així conste, i en compliment de la legislació vigent, signen el present certificat a València, vint-i-sis de juny de l'any dos mil catorze.

Dr. Armando Pérez Cañellas

Dra. Mari Carmen Bañus Polo

A Ángel García Bernal, siempre cerca.
Danzar...

El progreso experimental en la manipulación detallada de las propiedades cuánticas de los átomos consolida la posibilidad de poder construir un ordenador cuántico en un futuro todavía lejano, pero ineludible.
El ego científico lo garantiza.

José Ignacio Latorre

Agraïments

En primer lloc, he d'agrair a la Generalitat Valenciana i al Govern Espanyol per donar suport econòmic a aquesta tesis. Res m'agardaria més que tindre la possibilitat de dedicar el meu treball, esforç i dedicació vinent en poder tornar tot allò que ha sigut invertit en la meua formació, però sé, que soles és un desig i no una realitat. Espere que canvie radicalment la politica actual, i que en un futur no molt llunyà hi haja un lloc en aquest país per a tanta gent tan capacitada que poden fer d'ell, un lloc millor.

Per descomptat, vull agrair al meu director Armando Pérez Cañellas, per donar-me la possibilitat de realitzar aquesta tesi, i més enllà, per ser una persona d'extrema bellesa, perque la seua compressió i ajuda han estat peces fonamentals d'aquesta tesi.

A mi codirectora Mari Carmen Bañuls, gran ejemplo de mujer luchadora, ha sido una gran suerte y un honor para mi poder trabajar con ella.

Al grup d'Óptica Quàntica i no lineal de la Universitat de València. M'alegra molt haver estat una infiltrada a la tercera planta i haver pogut compartir amb tots ells bons moments de rialles i desconexió. A Eugenio Roldán i a Germán de Valcárcel, perque sense cap dubte treballar amb ells ha sigut molt enriquidor per a aquesta tesi i per a la meua persona. A Luis A. Brú con quien he tenido el gran placer de volver a disfrutar de una de las cosas que más he echado de menos, el trabajo codo a codo, el compartir el proceso, aunque breve. Mucha suerte Luis! A Joaquin Ruiz-Rivas, por su ayuda con cálculos infinitos.

A Alejandro Romanelli, quien me brindó la oportunidad de realizar una estancia en su gran país, donde disfruté mucho trabajando con él, gracias. Y a toda la gente que allá encontré, que tan lejos de casa, me hicieron sentir mejor que en ella.

También quiero agradecer a todos aquellos profesores que supieron transmitirme algo más que sus conocimientos y sin duda, marcaron mi rumbo. A Pedro Cortés Vicedo, maestro, amigo, es un honor saber que *puedo contar contigo*. A Julio Pellicer, a quien le debo no haber abandonado. A José Antonio Manzanares que me contagió de su pasión. A Pedro Gonzalez, porque sigo admirando sus verdaderas clases magistrales. A Vicent Giménez i Armando Pérez per despertar-me la passió per la Física Quàntica. A Vicent Vento, sempre oferint-me la seua ajuda per a tot.

Por supuesto quiero agradecer el apoyo de mi familia, en especial a mis hermanos, M.Luz y Alberto, gracias por vuestros vitales cuidados, ahora, siempre, y para siempre. Y a Marta, por llenarlo todo con su inmenso cariño y su inocente

alegría.

Y a toda la gente que durante este proceso me ha apoyado y soportado a partes iguales. A Raimundo Seguí, muchos años y siempre ahí cuando lo necesito, gracias. A María Granero y Amparo Tatay, encargadas siempre de facilitarme el camino del aprendizaje. A Jesús Mallo, que conoce todo el contenido de esta tesis sin entender palabra. A Diego López, hábil especialista con los entuertos de mi cabeza. A Guadalupe Médico, porque solo su olor me llena de paz. A Carolina Salvador, por todos los momentos compartidos y los que nos quedan. A Jan García, maestro en el arte del cuidado desde el cinismo y la ironía, gracias. A Johanna I. Fuks, sense dubte, una de les millors coses que m'emporte, gràcies per tot el suport. Con pequeños gestos, he sentido un gran apoyo por parte de Esther Carrascosa, Lucía Sans Selma y Gracia Hernández, tal vez, porque ellas saben lo que esto supone, gracias! A Ángela Moreno y Virgina Giménez, porque no importa el tiempo ni la distáncia. A Pury García Bernal, quien tiene el don de aparecer cuando más lo necesito, gracias. A Álex Martí, con quien empecé esta aventura y siempre supo poner un toque de humor a cualquier situación, y el toque final, no podría ser mejor.

A Rubén Miró, quien tanto me ha enseñado en estos últimos años y ha formado un sostén fundamental de esta tesis. Gracias por dirigirme *ese otro doctotado*, gracias por todo, por tanto.

Y a todos los "a pesar de" que también forman parte de esta tesis.

En último lugar, pero sin duda el más importante, quiero agradecer a Ángel García Bernal, por todo lo que aprendí y sigo aprendiendo, y porque tu recuerdo, siempre presente, me ayuda a ser mejor persona. Siempre confiaste en mí y me animaste para que esta tesis algún día fuera posible. Nada me gustaría más que compartir esta alegría contigo. Va por ti!

Resum

La informació quàntica és un camp relativament jove de la Física, que té com a objectiu explorar les lleis de la mecànica quàntica per a la transmissió i el processament de la informació. Com a exemple d'aplicacions es poden esmentar les comunicacions segures, basades en la distribució de clau quàntica, i algoritmes quàntics que superen als seus homòlegs clàssics per a un determinat nombre de problemes. A més, les eines desenvolupades en el context de la informació quàntica han demostrat ser de gran utilitat per aprofundir en la comprensió dels sistemes quàntics, per exemple, en el context dels problemes de molts cossos quàntics.

Una de les principals aplicacions de la potència de la mecànica quàntica en tasques computacionals és la manipulació de sistemes quàntics al laboratori per tal de realitzar simulacions quàntiques, i els diferents estudis experimentals s'estan realitzant en l'actualitat cap aquest objectiu. Especialment prometedores són les primeres simulacions quàntiques de sistemes atòmics ultrafreds atrapats en xarxes òptiques, on els resultats superen els càlculs clàssics.

Aquesta tesi aplica eines d'informació quàntica a la descripció i l'estudi de diversos sistemes quàntics i a processos que succeeixen en un espai discret, és a dir, en una xarxa. Fins i tot una sola partícula quàntica amb espín 1/2 pot donar lloc a fenomens que difereixen de forma radical de qualsevol analogia clàssica. En alguns casos, la nostra comprensió dels processos físics és més intuïtiva per al cas continu, i per tant, el nostre estudi es connecta fins al límit continu adequat.

La tesi s'estructura en dues parts. La primera d'elles s'emmarca en l'estudi i comprensió d'un algoritme quàntic en particular, el passeig quàntic. Per tal d'explotar el passeig quàntic i aplicar-lo a la construcció d'algoritmes quàntics, és important entendre i controlar el seu comportament tant com siga possible.

Una de les característiques analitzades en aquesta tesi és el passeig quàntic discret en N dimensions des de la perspectiva de les relacions de dispersió. Fent ús de condicions inicials esteses en l'espai de posicions, s'obté una equació d'ona en el límit continu. Aquesta equació ens permet d'entendre algunes propietats conegudes i dissenyar interessants comportaments. Apliquem l'estudi al passeig quàntic en dos i tres dimensions per a la moneda de Grover, on la relació de

dispersió presenta punts i interseccions particulars on la dinàmica és especialment diferent.

D'altra banda, s'analitza el comportament del passeig quàntic com un procés Markovià. Amb aquest objectiu, s'investiga l'evolució temporal de la matiu densitat reduïda per un passeig quàntic de temps discret en una xarxa unidimensional. S'analitza la dinàmica de la matriu densitat reduïda en el cas estàndard, sense decoherència, i quan el sistema està exposat als efectes de decoherència. Analitzem el comportament Markovià de l'evolució en el sentit definit en [1] examinant la distància de traça per a possibles parells de estats inicials com una funció del temps. Arribem a la conclusió que l'evolució de la matriu densitat reduïda en el cas lliure és no Markoviana i, quan el nivell de soroll augmenta, la dinàmica s'aproxima a un procés Markovià.

La segona part d'aquesta tesi proposa una generalització de la coneguda funció de Wigner per a una partícula que es mou en una xarxa infinita en una dimensió. L'estudi de la mecànica quàntica en l'espai de fases a través de les distribucions de quasi-probabilitat s'aplica en molts camps de la física i la funció de Wigner és probablement la més utilitzada.

S'estudia la funció de Wigner per a un sistema quàntic en un espai d'Hilbert discret, de dimensió infinita, tal com una partícula sense spin en moviment en una xarxa infinita unidimensional. Es discuteixen les peculiaritats d'aquest escenari i la construcció de l'espai fàsic associat, i es proposa una definició significativa de la funció de Wigner en aquest cas, a més es caracteritza el conjunt d'estats purs per als quals la funció de Wigner és no negativa. També ampliem la definició proposada per incloure un grau intern de llibertat, com ara l'spin.

La dinàmica d'una partícula en una xarxa amb, i sense spin, en diferents casos, també s'analitza en termes de la funció de Wigner corresponent. Mostrem solucions explícites en el cas d'evolució hamiltoniana sota un potencial depenent de la posició que pot incloure un acoblament d'spin, i per a l'evolució governada per una equació mestra sota alguns simples models de decoherència.

Proposem una mesura de la no-classicitat dels estats en un sistema amb un espai d'Hilbert discret i infinit que és consistent amb el límit continu. I, en darrer lloc, discutim la possibilitat d'ampliar el concepte de negativitat de la funció de Wigner al cas en el qual s'inclou el grau de llibertad d'spin.

Abstract

Quantum information is a relatively young field of Physics, that aims to exploit the laws of quantum mechanics for the transmission and processing of information. As illustrative applications one can mention secure communications, based on quantum key distribution, and quantum algorithms that outperform their classical counterparts for a number of problems. Furthermore, the tools developed in the context of Quantum Information have proven extremely useful to deepen the understanding of quantum systems, for instance in the context of quantum many-body problems.

One of the main applications of the power of quantum mechanics to computational tasks is the manipulation of quantum systems in the lab in order to perform quantum simulations, and different experimental approaches are currently being pursued towards this goal. Especially promising are ultracold atomic systems trapped in optical lattices, where the first quantum simulations that outperform the feasible classical calculations have already been realized.

This thesis applies quantum information tools to the description and the study of several quantum systems and processes that happen on a discrete space, i.e. on a lattice. Even a single quantum particle with spin 1/2 hopping on a lattice can give rise to phenomena that dramatically differ from any classical analogy. In some cases, our understanding of the physical processes is more intuitive for the continuous case, and hence we connect our study to the proper continuum limit.

The thesis is structured in two parts. The first one is framed within the study and understanding of a particular quantum algorithm, namely the quantum walk. In order to exploit the quantum walk and apply it to the construction of quantum algorithms, it is important to understand and control its behavior as much as possible.

One of the features analyzed in this thesis is the discrete time quantum walk in N dimensions from the perspective of its dispersion relations. Making use of the spatially extended initial conditions, a wave equation in the continuum limit is obtained. This equation allows us to understand some known properties, and to design interesting behaviors. We apply the study to the two and three dimen-

sional Grover quantum walk, where the dispersion relation presents particular points and intersections where the dynamics is specially distinct.

On the other hand, we analyze the behavior of the quantum walk as a Markovian process. With this aim, we investigate the time evolution of the chirality reduced density matrix for a discrete time quantum walk on a one-dimensional lattice. We analyze the dynamics of the reduced density matrix in the standard case, without decoherence, and when the system is exposed to the effects of decoherence. We analyze the Markovian behavior in the sense defined in [1] examining the trace distance for possible pairs of initial states as a function of time which gives us the distinguishability of two states and it is related with the Markovian behavior of the system. We conclude that the evolution of the reduced density matrix in the free case is non-Markovian and, as the level of noise increases, the dynamics approaches a Markovian process.

The second part of this thesis proposes a generalization of the known Wigner function for a particle moving on an infinite lattice in one dimension. The study of the quantum mechanics in phase space through quasi-probability distributions is applied in many fields of physics and the Wigner function is probably the most commonly used one.

We study the Wigner function for a quantum system with a discrete, infinite dimensional Hilbert space, such as a spinless particle moving on a one dimensional infinite lattice. We discuss the peculiarities of this scenario and of the associated phase space construction, propose a meaningful definition of the Wigner function in this case, and characterize the set of pure states for which it is non-negative. We also extended the proposed definition to include an internal degree of freedom, such as the spin.

The dynamics of a particle on a lattice with and without spin in different cases are also analyzed in terms of the corresponding Wigner function. We show explicit solutions for the case of Hamiltonian evolution under a position-dependent potential that may include a spin coupling, and for the evolution governed by a master equation under some simple models of decoherence.

We propose a measure of non-classicality for states in the system with a discrete infinite dimensional Hilbert space which is consistent with the continuum limit. And we discuss the possibility of extending a negativity concept for the Wigner function in the case in which the spin degree of freedom is included.

Contents

Part I

Quantum Walk

1 Passeig quàntic en una línea

1.1 Introducció

El passeig aleatori clàssic és un procés estocàstic que té una gran varietat d'aplicacions en molts camps i obri camins a resoldre determinats problemes de la física. Existeixen exemples que van des de l'estudi del moviment Brownià fins a la informàtica, on molts algoritmes es basen en passejos aleatoris clàssics. El passeig quàntic és l'anàleg del passeig aleatori clàssic expressat en termes de la mecànica quàntica. Una qüestió fonamental de la computació quàntica és determinar si un ordinador quàntic pot resoldre problemes de forma més ràpida que un ordinador clàssic, es a dir, ser més eficient que qualsevol algoritme clàssic. A causa del gran interès i a les moltes aplicacions del passeig aleatori clàssic en el disseny d'algoritmes, és natural preguntar-se si el passeig quàntic serà una eina útil per als algoritmes quàntics. Existeixen dos models per descriure el passeig quàntic:

- A temps discret, on l'operador evolució només s'aplica en passos de temps discret a dos sistemas quàntics: una moneda i un passejant.

- A temps continu, on l'evolució està donada per l'Hamiltonià que descriu el sistema definit en temps continu.

En ambdós models, el passeig quàntic es porta a terme en gràfics o en xarxes discretes.

L'estudi del passeig quàntic motivat per les possibles aplicacions en els algoritmes quàntics fou proposat per Ambainis et al. [2] i Aharonov et al. [3] on introduïren el passeig quàntic a temps discret, i demostraren que el passeig quàntic sobre una línia s'estén en el temps de forma quadràtica, el que suposa una millora computacional en temps respecte al passeig aleatori clàssic. D'altra banda, Childs et al. [4], introduïren els "arbres enganxats," un algoritme on trobaren que un passejant quàntic partint d'una de les arrels podria trobar l'arrel oposada exponencialment més ràpid que qualsevol algoritme clàssic. E.Farhi i S.Gutmann [5] introduïren el passeig quàntic contínu que també presenta una acceleració sobre la

varietat clàssica. A més, Childs [6] demostrà que la passeig quàntic en temps continu pot ser considerat computacionalment universal amb qualsevol computació quàntica codificada en alguns gràfics. Més tard, Lovvet et al. [7] demostraren que el passeig quàntic a temps discret també és capaç d'aplicar el mateix conjunt de porta universal i per tant, ambdós, el passeig quàntic a temps continu i discret són computacionals universals.

En aquesta primera part de la tesi, ens centrem en el passeig quàntic discret. El terme discret es refereix a l'aplicació del corresponent operador d'evolució del sistema en temps discret. La partícula també es mou en una xarxa discreta. En primer lloc, s'introdueixen els principals conceptes, tant del passeig quàntic discret com del continu però centrant la nostra atenció en passeig quàntic discret. Després de donar una amplia introducció, ens endinsem en l'estudi del passeig quàntic N-dimensional mitjançant l'estudi de les relacions de dispersió. Veurem com aquest estudi ens permet determinar el subsegüent comportament del passejant. En un capítol posterior, s'introdueix el concepte de Markovianitat quàntica, i s'estudia el comportament no Markovià del passeig quàntic, i com es converteix en Markovià quan s'introdueixen efectes de decoherència.

1.2 Passeig aleatori clàssic

Un passeig aleatori clàssic discret és un procés estocàstic, i pot ser considerat com una cadena de Markov que s'introduirà en el capítol 4. En el passeig aleatori clàssic a temps discret, que és el cas més simple que es pot estudiar, un passejant es mou en una línia infinita, fent passos a l'esquerra o a la dreta en funció del llançament d'una moneda amb probabilitats p i q, respectivament $(p + q = 1)$.

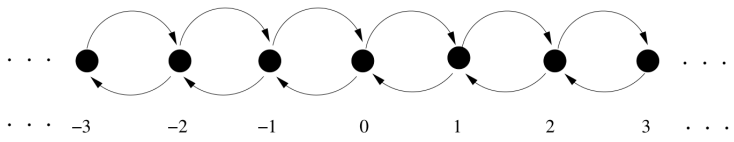

Si tenim en compte el passeig simètric, el passejant tindrà la mateixa probabilitat de saltar a la dreta o a l'esquerra, $q = p = \frac{1}{2}$ en cada pas de temps. Si deixem que evolucione amb el temps, la distribució de probabilitat $P(n, t)$ de trobar el passejant en el lloc n en el temps t sobre una línia infinita amb una condició inicial localitzada $P(n, t = 0) = \delta_{n,0}$ està donada per

$$P(n,t) = \frac{1}{2^t} \begin{pmatrix} t \\ \frac{n+t}{2} \end{pmatrix} \tag{1.1}$$

Només hi ha probabilitat diferent de zero de trobar el passejant en els llocs que tenen la mateixa paritat que el nombre de passos t. La distribució de probabilitat final, l'equació (2.1), és una distribució de probabilitat binomial que es pot aproximar per una distribució gaussiana centrada en $n = 0$ en el límit t gran. Una de les característiques més importants a considerar, és la desviació estàndard de la distribució de probabilitat (magnitud que ens dóna una idea de com de lluny podem trobar al passejant, respecte a la seua posició inicial) que és proporcional al quadrat del temps d'evolució i estableix la principal diferència amb el seu anàleg quàntic. En la figura (2.1) es mostren la distribució de probabilitat i la desviació estàndard del passejant clàssic amb un passeig simètric $p = \frac{1}{2}$

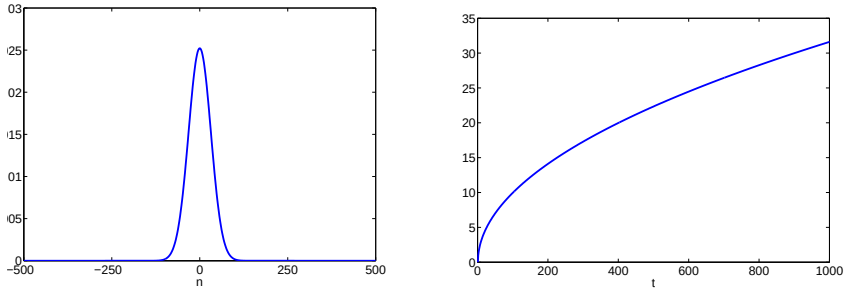

(a) (b)

Figure 1.1: (a) Distribució de probabilitat clàssica en funció de la posició per a 1000 passos d'evolució. (b) Desviació estàndard de la distribució de probabilitat en un funció del nombre de passos

1.3 Passeig quàntic discret sobre una línea

El passeig quàntic a temps discret sobre una línia es defineix directament com l'anàleg del passeig aleatori clàssic. El passejant ha estat substituït per una partícula quàntica i per tant té un nou grau de llibertat: la moneda o quiralitat, amb un sistema quàntic de dos estats. L'estat del passejant està donat per la seua posició i el seu estat de quiralitat. Per tant, els principals components del passeig

quàntic a temps discret són el passejant, és a dir, la partícula quàntica, i la moneda que hi actuarà. El passejant es troba sobre una línia unidimensional discreta i es pot moure a als llocs adjacents. L'espai d'Hilbert associat amb la posició del passejant, $\mathcal{H}_P$, té dimension infinita però comptable i està genreat per la base $\{\mid i\rangle : i \in \mathbb{Z}\}$, el que ens dóna l'estat de posició per al passejant. La moneda és un sistema quàntic que es troba en un espai de Hilbert de 2 dimensions $\mathcal{H}_C$, generat per la base $\{\mid L\rangle, \mid R\rangle\}$. Per tant, l'espai total d'Hilbert del sistema el dóna el producte tensorial de l'espai de posició i l'espai de la moneda $\mathcal{H} = \mathcal{H}_C \otimes \mathcal{H}_P$.

L'evolució del sistema consisteix en l'aplicació d'un operador evolució sobre la moneda, seguit d'un operador desplaçament condicional a la totalitat del sistema quàntic. La transformació més general que es pot escriure actuant sobre l'espai total d'Hilbert és:

$$U(\theta) = S \cdot (C(\theta) \otimes I) \tag{1.2}$$

I llavors, l'evolució del passeig quàntic després d'intervals de temps t és:

$$\mid \psi(t)\rangle = U^t(\theta) \mid \psi(0)\rangle \tag{1.3}$$

on I és l'operador identitat en l'espai posició, $C(\theta)$ és l'operador que actua sobre la quiralitat, equivalent a llançar la moneda, i S és un operador unitari que provoca un desplaçament condicional en el sistema donat per

$$S = \mid R\rangle\langle R \mid \otimes \sum_n \mid n+1\rangle\langle n \mid + \mid L\rangle\langle L \mid \otimes \sum_i \mid n-1\rangle\langle n \mid$$

S transforma els estats $\mid R\rangle \otimes \mid n\rangle$ en $\mid R\rangle \otimes \mid n+1\rangle$ i els estats $\mid L\rangle \otimes \mid n\rangle$ en estats $\mid L\rangle \otimes \mid n-1\rangle$ és a dir, el desplaçament en l'espai de la moneda depén del grau de llibertat de la quiralitat: els estats amb quiralitat dreta es mouen cap a la dreta, mentre que els estats amb quiralitat esquerra es mouen cap a l'esquerra. A més, tenim una procés unitari translacionalment invariant. El primer pas en el passeig quàntic és una rotació en l'espai $C(\theta)$ de la moneda, el qual és anàleg al passeig aleatori clàssic. La transformació unitària $C(\theta)$ és arbitrària i un munt de passejades amb diferents comportaments es poden definir canviant $C(\theta)$. Per tant, la transformació més general, excepte per fases addicionals que es poden reabsorbir en la definició de l'estat inicial, es pot escriure com

$$C(\theta) = \begin{pmatrix} \cos\theta & \sin\theta \\ \sin\theta & -\cos\theta \end{pmatrix}$$

Si volem obtenir una transformació actuant amb la mateixa probabilitat sobre la quiralitat, és a dir, un desplaçament a la dreta amb probabilitat $\frac{1}{2}$ i un desplaçament a l'esquerra amb probabilitat $\frac{1}{2}$ cal utilitzar la transformació donada per la coneguda moneda d'Hadamard per a la qual $\theta = \pi/4$

$$H = \frac{1}{\sqrt{2}} \begin{pmatrix} 1 & 1 \\ 1 & -1 \end{pmatrix}$$

Vegem-ho amb un exemple. Suposem que partim d'un estat inicial localitzat en la posició $\mid 0\rangle$ i prenem l'estat de la moneda com $\mid R\rangle$, és a dir, el nostre estat inicial està donat per $\mid 0\rangle \otimes \mid R\rangle$. Després d'un pas de temps, (una transformació en l'espai de la moneda, H, i un translació condicional, S), obtenim

$$\begin{aligned} \mid 0\rangle \otimes \mid R\rangle = & \mid 0\rangle \otimes \begin{pmatrix} 1 \\ \\ 0 \end{pmatrix} \xrightarrow{H} \\ & \frac{1}{\sqrt{2}} \mid 0\rangle \otimes (\mid R\rangle + \mid L\rangle) \xrightarrow{S} \\ & \frac{1}{\sqrt{2}} (\mid 1\rangle \otimes \mid R\rangle + \mid -1\rangle \otimes \mid L\rangle) \end{aligned} \tag{1.4}$$

Ja que la probabilitat s'obté del mesurament de les amplituds, el resultat obtingut es un desplaçament a la dreta amb probabilitat $\frac{1}{2}$ i un desplaçament a l'esquerra, amb una probabilitat $\frac{1}{2}$. Si continuem amb el següent pas de l'evolució, i mesurem les probabilitats resultants cada vegada que la transformació U s'aplica, s'obtindria el passeig aleatori clàssic sobre una línia. Per descomptat, al passeig aleatori quàntic no mesurem en cada iteració. D'aquesta manera la naturalesa quàntica del sistema sorgeix: es produeix interferència quàntica en el nostre estat, i apareix l'entrellaçament entre l'espai de la moneda i l'espai de posició. Com a resultat, el nostre estat és una superposició coherent. Així que, si no mesurem, la interferència quàntica causa un comportament completament diferent. Per il·lustrar-ho veurem les conseqüències després d'uns pocs passos quan no es mesura. Si comencem en l'estat inicial $\mid \phi_{ini}\rangle = \mid L\rangle \otimes \mid 0\rangle$

$$
\begin{aligned}
\mid \phi_{ini}\rangle &\xrightarrow{U} \frac{1}{\sqrt{2}}(\mid 1\rangle\otimes \mid R\rangle - \mid -1\rangle\otimes \mid L\rangle) \\
&\xrightarrow{U} \frac{1}{2}(\mid 2\rangle\otimes \mid R\rangle - \mid 0\rangle \otimes (\mid R\rangle - \mid L\rangle) + \mid -2\rangle\otimes \mid L\rangle) \\
\xrightarrow{U} \frac{1}{2\sqrt{2}}(\mid 3\rangle\otimes \mid R\rangle + \mid 1\rangle\otimes \mid L\rangle + \mid -1\rangle\otimes \mid R\rangle - 2 \mid -1\rangle\otimes \mid L\rangle - \mid -3\rangle\otimes \mid L\rangle)
\end{aligned}
\tag{1.5}
$$

Aquest exemple mostra com la distribució de probabilitat induïda pel passeig quàntic difereix del passeig aleatori clàssic. A la taula (2.1) es mostra la distribució de probabilitat si permetrem que el sistema evolucione durant 5 passos de temps.

t\n	-5	-4	-3	-2	-1	0	1	2	3	4	5
0						1					
1					1/2	0	1/2				
2				1/4	0	1/2	0	1/4			
3			1/8	0	5/8	0	1/8	0	1/8		
4		1/16	0	5/8	0	1/8	0	1/8	0	1/16	
5	1/32	0	17/32	0	1/8	0	1/8	0	5/32	0	1/32

Table 1.1: Probabilitat d'estar a la posició n després de 5 pasos de temps per a l'estat inicial donat per $\mid \phi_{ini}\rangle = \mid L\rangle\otimes \mid 0\rangle$

En la figura (2.2) es representa la distribució de probabilitat del passeig quàntic amb la moneda d'Hadamard partint de l'estat inicial $\mid \phi_{ini}\rangle = \mid L\rangle\otimes \mid 0\rangle$ després de 1000 passos de temps. Només es mostra la probabilitat de les posicions parelles, ja que per les senars és zero. És clar que la distribució de probabilitat d'aquest passeig és molt més complexa que la obtinguda en el passeig aleatori clàssic.

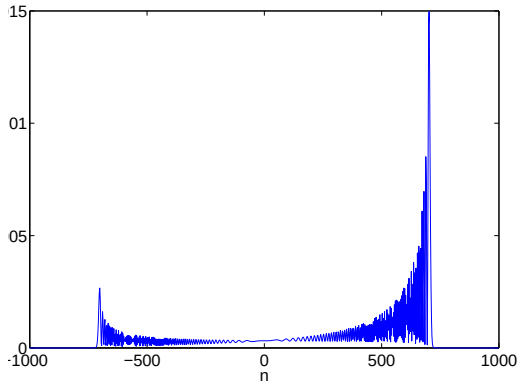

Figure 1.2: Distribució de probabilitat del passeig quàntic després de 1000 passos de temps amb un estat inicial donat per $\mid \phi_{ini}\rangle = \mid L\rangle \otimes \mid 0\rangle$

Veiem a la figura (2.2) que la distribució de probabilitat és asimètrica. Aquesta asimetria és a causa que la moneda d'Hadamard tracta les quiralitats ($\mid R\rangle$ and $\mid L\rangle$) de manera diferent, només $\mid L\rangle$ es multiplica per una fase – 1 i per tant es produeixen més cancel·lacions (interferència destructiva) per a les contribucions que es mouen cap a la equerra, mentre que hi ha interferència constructiva per a les que es mouen cap a la dreta. Hi ha dues maneres d'evitar aquesta asimetria, una és començar amb un estat que és una combinació de $\mid R\rangle$ i $\mid L\rangle$ i assegurar-nos que no hi interfereixen. Per a això podem partir de l'estat inicial $\mid \phi_{ini}\rangle = \frac{1}{\sqrt{2}}(\mid R\rangle + i \mid L\rangle) \otimes \mid 0\rangle$ i com la moneda Hadamard no introdueix cap amplada complexa, el camí per $\mid R\rangle$ serà real, mentre que el camí per $\mid L\rangle$ serà imaginari, de manera que no hi interfereixen i la distribució de probabilitat serà simètrica.

Una altra forma d'obtenir exactament el mateix resultat és utilitzar la següent moneda

$$Y = \frac{1}{\sqrt{2}} \begin{pmatrix} 1 & i \\ i & 1 \end{pmatrix}$$

En la figura (2.3) es representen conjuntament la distribució de probabilitat per al passeig quàntic i clàssic.

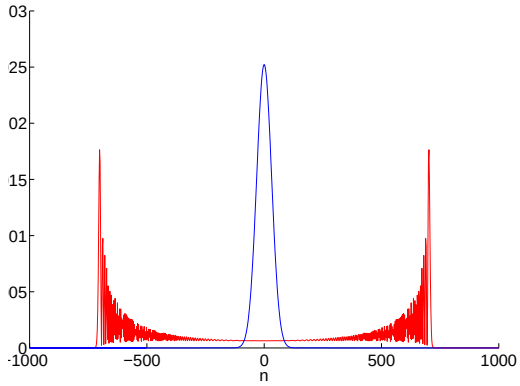

Figure 1.3: Comparació entre la distribució de probabilitat del passeig aleatori quàntic i clàssic després de 1.000 passos de temps. Per al passeig quàntic hem utiliztat la moneda d'Hadamard començant en l'estat de la moneda simetric $\mid \phi_{ini}\rangle = \frac{1}{\sqrt{2}}(\mid R\rangle + i \mid L\rangle)\otimes \mid 0\rangle$.

La desviació estàndard de la distribució de probabilitat és una de les característiques més importants del passeig quàntic, estableix la principal diferència amb el seu anàleg clàssic i es pot utilitzar per dissenyar algoritmes més eficients. La distribució de probabilitat quàntica és molt més dispersa que la distribució de probabilitat clàssica, ja que la probabilitat de trobar al passejant prop del punt de partida és molt baixa. Aquest comportament és contrari al clàssic on la distribució de probabilitat mostra un pic centrat en l'origen i decau exponencialment. El valor màxim de la distribució de probabilitat del passeig aleatori clàssic es troba en el centre, $n = 0$, mentre que els pics màxims de probabilitat en la versió quàntica són en els extrems $n = \pm\frac{t}{\sqrt{2}}$. En altres paraules, el passeig quàntic mostra una propagació balística, en lloc d'una propagació difusiva. Aquestes diferències són causades per l'existència del fenomen d'interferència només en el cas quàntic.

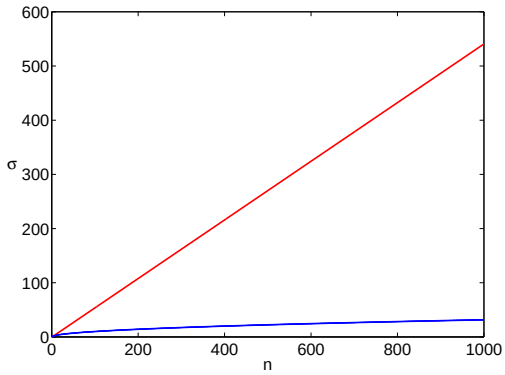

Figure 1.4: Comparació entre la desviació estàndard del passeig aleatori clàssic i quàntic després de 1000 passos de temps. Per al passeig quàntic hem utiliztat la moneda d'Hadamard començant en l'estat de la moneda simetric $\mid \phi_{ini}\rangle = \frac{1}{\sqrt{2}}(\mid R\rangle + i \mid L\rangle) \otimes \mid 0\rangle$

En la figura (2.4) es representa la desviació estàndard dels passejos aleatori clàssic i quàntic. Com s'ha esmentat anteriorment, per al cas clàssic la desviació estàndard creix com l'arrel quadrada del nombre de passos $\sigma \sim \sqrt{t}$, mentre que per al cas quàntic creix amb el nombre de passos $\sigma \sim t$. Aquest resultat ha estat analíticament demostrat per diversos autors [3, 8]. Per tant, per a un determinat nombre de passos, el passejant quàntic és capaç d'escanejar una part significativament major de l'espai accessible que el passejant clàssic, i es mou en una línia quadràticament més ràpid que el passeig aleatori clàssic. Aquest fet té una forta implicació per als algoritmes, i és una de les raons per les quals el passeig aleatori quàntic s'ha estudiat en les últimes dècades.

1.4 Passeig quàntic a temps continu

Childs et al. en [4] donaren una definició general del passeig aleatori a temps continu. Aquesta es basa en una descripció hamiltoniana, en la qual el grau de llibertat de la quiralitat no és necessari. A causa de la connexió directa entre els passejos continu clàssic i quàntic, la forma més senzilla d'introduir la descripció quàntica és començar amb el passeig aleatori clàssic en un gràfic. El passeig aleatori clàssic a temps continu és un procés Markovià que descriurem al capítol 4. La idea principal és considerar el conjunt de vèrtexs $\{1, 2, 3...v\}$ i

les connexions entre els vèrtexs. Un pas en l'evolució del cas clàssic només és possible si els vèrtexs estan connectats. Aquestes connexions poden ser definides per la $v \times v$ matriu generadora infinitesimal M:

$$M_{ab} = \begin{cases} -\gamma & a \neq b, a \text{ i } b \text{ connectats} \\ 0 & a \neq b, a \text{ i } b \text{ no connectats} \\ k\gamma & a = b, k \text{ és la valència del vèrtex } a \end{cases} \tag{1.6}$$

On γ denota la taxa de salt. La probabilitat d'estar en el vèrtex a en el temps t es descriu com:

$$\frac{dp_a(t)}{dt} = -\sum_b M_{ab} p_b(t) \tag{1.7}$$

D'aquesta senzilla manera es pot descriure l'evolució del passeig aleatori clàssic. Per explicar el passeig quàntic a temps continu és necesari definir dos requeriments : l'espai d'Hilbert v-dimensionals generat pels vèrtexs del graf $\mid 1\rangle$, $\mid 2\rangle$,...$\mid v\rangle$ i l'hamiltonià responsable de l'evolució, els elements de la matriu del qual es donen per $\langle a \mid H \mid b\rangle$. Ara, l'evolució d'un estat quàntic $\mid \psi(t)\rangle$ ve expressat per l'equació de Schrödinger

$$i\frac{d\langle a \mid \psi(t)\rangle}{dt} = \sum_b \langle a \mid H \mid b\rangle\langle b \mid \psi(t)\rangle \tag{1.8}$$

En una xarxa unidimensional l'Hamiltionià es defineix com

$$H \mid n\rangle = -\frac{a}{\Delta^2}(\mid n-1\rangle - 2 \mid n\rangle + \mid n+1\rangle) \tag{1.9}$$

que és l'aproximació discreta de l'operador d^2/dx^2, on Δ és l'espaiat de la xarxa. D'aquesta manera l'estat evolucionat es pot escriure com

$$\mid \psi(t)\rangle = e^{-iHt} \mid \psi(0)\rangle \tag{1.10}$$

L'equació (2.10) defineix un passeig quàntic contínu en un gràfic: note que és continu en el temps i discret en l'espai. En aquest cas, la desviació estàndard també creix linealment en el temps i quadràticament més ràpid que la difusió clàssica. Per tant, és més eficaç que el seu contrapart clàssic. És important esmentar que hi ha una correspondència que transforma el passeig quàntic discret en continu. Es proposà a [38] i mostrà que prenent un tipus particular de límit en el passeig quàntic a temps discret s'obtenen dues còpies del continu. Aquest limit també és vàlid per a dimensions majors.

1.5 Passeig quàntic discret en l'espai de moments

L'evolució unitària del passeig quàntic descrit anteriorment, es pot estudiar tenint en compte la funció d'ona resultant. Quan describim la posició de la partícula com un espinor de dos components de les amplituds de la partícula al punt n en el temps t, la funció d'ona resultant la podem escriure com:

$$\psi(n,t) = \begin{pmatrix} a(n,t) \\ b(n,t) \end{pmatrix}. \tag{1.11}$$

amb notació d'operadors: $\mid \psi(n,t)\rangle = a(n,t) \mid R\rangle + b(n,t) \mid L\rangle$. Mitjançant l'aplicació de l'operador d'evolució Eq. (2.2) l'estat en $t+1$ es pot relacionar amb l'estat en el temps anterior t. Llavors, podem descriure la dinàmica de $\psi(n,t)$ en notació matricial com:

$$\psi(n,t) = \begin{pmatrix} \cos\theta & \sin\theta \\ 0 & 0 \end{pmatrix} \psi(n+1,t) + \begin{pmatrix} 0 & 0 \\ \sin\theta & -\cos\theta \end{pmatrix} \psi(n-1,t). \tag{1.12}$$

Si definim:

$$M_+ = \begin{pmatrix} \cos\theta & \sin\theta \\ 0 & 0 \end{pmatrix} \qquad M_- = \begin{pmatrix} 0 & 0 \\ \sin\theta & -\cos\theta \end{pmatrix}, \tag{1.13}$$

Per tant,

$$\psi(n,t+1) = M_+\psi(n+1,t) + M_-\psi(n-1,t) \tag{1.14}$$

L'equació (2.14) es pot rescriure amb les seues components:

$$\begin{aligned} a(n,t+1) &= a(n+1,t)\cos\theta + b(n+1,t)\sin\theta \\ b(n,t+1) &= a(n-1,t)\sin\theta - b(n-1,t)\cos\theta \end{aligned} \tag{1.15}$$

L'anàlisi del passeig quàntic es redueix a resoldre un sistema de recurrència de dues dimensions. A causa de la invariància translacional, el passig quàntic té una simple descripció passant de l'espai de posicions a l'espai de moments, fent ús de la transformada de Fourier. En aquesta base, seguit el tractament desenvolupat en [3], el passeig quàntic es pot resoldre fàcilment i és possible tornar a l'espai real revertint la transformada de Fourier.

Transformada de Fourier a temps discret. La transformada de Fourier espacial $\psi(k,t)$, de la funció d'ona sobre $\mathcal{Z}$ està donada per

$$\psi(k,t) = \sum_n \psi(n,t) e^{ikn} \tag{1.16}$$

on $k \in [-\pi, \pi]$ és el vector quasi-moment i la seua inversa està donada per:

$$\psi(n,t) = \frac{1}{2\pi} \int_{-\pi}^{\pi} \psi(k,t) e^{-ikn} \tag{1.17}$$

De la mateixa menera, la base es pot definir com:

$$\mid k\rangle = \sum_{n=-\infty}^{n=\infty} \mid n\rangle e^{ikn} \tag{1.18}$$

$$\mid n\rangle = \frac{1}{2\pi} \int_{-\pi}^{\pi} \mid k\rangle e^{-ikn} \tag{1.19}$$

La dinàmica de l'equació (2.14) es pot escriure com

$$\begin{aligned} \psi(k,t) &= \sum_n (M_+ \psi(n+1,t) + M_- \psi(n-1,t)) e^{ikn} \\ &= e^{-ikn} M_+ \sum_n \psi(n+1) e^{ik(n+1)} + e^{ikn} M_+ \sum_n \psi(n-1) e^{ik(n-1)} \\ &= (e^{-ik} M_+ + e^{ik} M_-) \psi(k,t) \end{aligned} \tag{1.20}$$

Com a resultat, tenim

$$\begin{gathered} \psi(k,t+1) = M_k \psi(k,t) \\ M_k = e^{-ik} M_+ + e^{ik} M_- = \\ \begin{pmatrix} e^{-ik}\cos\theta & e^{-ik}\sin\theta \\ e^{ik}\sin\theta & -e^{ik}\cos\theta \end{pmatrix} \end{gathered} \tag{1.21}$$

L'equació de recurrència en l'espai de Fourier pren la forma simple

$$\psi(k,t) = M_k^t \psi(k,0) \tag{1.22}$$

on M_k es defineix com l'operador de la moneda en l'espai de moments. El mapa del passeig quàntic ha passat de ser una equació no local (2.14) en l'espai de posicions a una equació local (2.21) en l'espai de moments. Això fa que l'anàlisi de la dinàmica siga més fàcil de resoldre. Per procedir amb la resolució necessitem conèixer els valors i els vectors propis de la matriu M_k. Si $\mid \phi_k^1\rangle$ i $\mid \phi_k^2\rangle$ són els vectors propis i λ_k^1 i λ_k^2 els valors propis, podem escriure M_k com:

$$M_k = \lambda_k^1 \mid \phi_k^1\rangle\langle\phi_k^1 \mid + \lambda_k^2 \mid \phi_k^2\rangle\langle\phi_k^2 \mid, \tag{1.23}$$

i per tant, la matriu d'evolució temporal pren la forma

$$M_k^t = (\lambda_k^1)^t \mid \phi_k^1\rangle\langle\phi_k^1 \mid + (\lambda_k^2)^t \mid \phi_k^2\rangle\langle\phi_k^2 \mid . \tag{1.24}$$

A causa del fet que M_k és una matriu unitària amb $det(M_k) = -1$, els valors propis es poden escriure com $\lambda_k^1 = e^{i\omega_k}$ i $\lambda_k^2 = e^{i(\pi-\omega_k)}$, on $\omega_k = -\arcsin(\sin k \cos\theta)$ és la relació de dispersió. En el cas del passeig donat per la moneda d'Hadamard,

$$M_k = \frac{1}{\sqrt{2}} \begin{pmatrix} e^{-ik} & e^{-ik} \\ e^{ik} & -e^{ik} \end{pmatrix} \tag{1.25}$$

Els vectors propis corresponents es poden obtenir a través de la diagonalització de la matriu M_k, Eq. (2.24)

$$\begin{aligned} \phi_k^1 &= \frac{1}{\sqrt{2N(k)}} \begin{pmatrix} e^{-ik} \\ \sqrt{2}e^{i\omega_k} + e^{-ik} \end{pmatrix} \\ \phi_k^2 &= \frac{1}{\sqrt{2N(\pi-k)}} \begin{pmatrix} e^{-ik} \\ -\sqrt{2}e^{-i\omega_k} + e^{-ik} \end{pmatrix} \end{aligned} \tag{1.26}$$

on el factor de normalització està donat per

$$N(k) = (1 + \cos^2 k) + \cos k\sqrt{1 + cos^2 k} \tag{1.27}$$

A la base de Fourier l'estat inicial està representat per $\psi(k,t) = (0,1)^\intercal$ per a tot k. Fent ús de les relacions (2.22) i (2.23), la funció d'ona en qualsevol temps t està donada per

$$a(k,t) = \frac{1}{2}(1 + \frac{\cos k}{\sqrt{1+\cos^2 k}})e^{i\omega_k t} + \frac{(-1)^t}{2}(1 - \frac{\cos k}{\sqrt{1+\cos^2 k}})e^{-i\omega_k t} \tag{1.28}$$

$$b(k,t) = \frac{e^{-ik}}{2\sqrt{1+cos^2 k}}(e^{i\omega_k t} - (-1)^t e^{-i\omega_k t}) \tag{1.29}$$

Ara, cal tornar a l'espai real, per tant, hem de calcular la transformada de Fourier inversa. Les funcions d'ona en l'espai real es poden escriure com

$$a(n,t) = \frac{1+(-1)^{n+t}}{2}\int_{-\pi}^{\pi}\frac{dk}{2\pi}(1+\frac{\cos k}{\sqrt{1+cos^2 k}})e^{-i(kn+\omega_k t)} \tag{1.30}$$

$$b(n,t) = \frac{1+(-1)^{n+t}}{2}\int_{-\pi}^{\pi}\frac{dk}{2\pi}(\frac{e^{ik}}{\sqrt{1+cos^2 k}})e^{-i(kn+\omega_k t)} \tag{1.31}$$

Aquestes expressions són una solució formal tancada per a la dinàmica del passeig quàntic amb la moneda d'Hadamard, el problema s'ha resolt amb una expressió analítica per a $a(n,t)$ i $b(n,t)$, a pesar que les integrals no es podem resoldre de forma analítica. Simulacions numèriques ens permeten obtenir la distribució de probabilitat per al passeig quàntic i comparar-lo amb el seu contrapart clàssic. Com era d'esperar a partir de la definició del passeig quàntic, les amplituds per a n parell a t senar, i per a n senar a t parell són zero.

L'estudi del passeig quàntic en l'espai de moments dóna la posibilitat de predir i controlar el subsegüent comportament del passeig quàntic mitjançant el coneixement de la relació de dispersió. En el treball presentat per Valcárcel et al [9], es presenta un estudi sobre la dinàmica del passeig quàntic quan l'estat inicial és un paquet d'ones proper a alguns dels vectors propis. Explorarem en profunditat el passig quántic en N-dimensions mitjançant relacions de dispersió al capitol 3. En aquest context, les ones planes

$$\mid \psi(n,t)\rangle = e^{i(kn-\omega t)} \mid \phi_k\rangle \tag{1.32}$$

són solucions del mapa (4.30), on ω és la freqüència del mapa que defineix la relació de dispersió en el sistema. La velocitat de grup està donada per $v_g^{(1,2)} = d\omega/dk^{(1,2)}$. Quan l'estat inicial és un paquet d'ones en el qual l'estat de la moneda és un vector propi de la moneda en l'espai de moments, M_k, és a dir,

$$\mid \psi(n,0)\rangle = f_x^{(1,2)} e^{ik_0 n} \mid \phi_{k_0}^{(1,2)}\rangle \tag{1.33}$$

on $f_x^{(1,2)}$ és una envoltant suau, la propagació de la passeig quàntic es regeix per la velocitat de grup. Per a la moneda Hadamard, $\omega = -\arcsin(\frac{1}{\sqrt{2}}\sin k)$, per tant, si $k_0 = \pm\pi/2$, llavors $v_g(\pm\pi/2) = 0$, i el paquet d'ones ha de romandre en repòs, mentre que si $k_0 = 0$, la velocitat de grup pren el seu valor màxim i s'ha de moure amb velocitat màxima. A la figura 2.5 es mostren la relació dispersió i la velocitat de grup per a aquest cas.

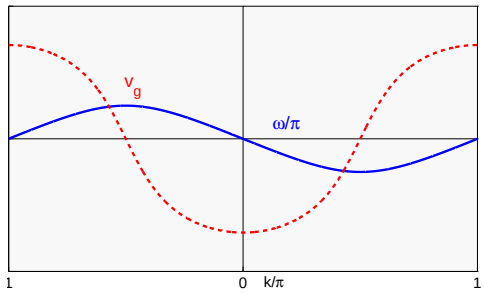

Figure 1.5: Relació de dispersió (línia blava) i velocitat de grup (línia vermella) per a la moneda d'Hadamard.

1.6 Propietats asimptòtiques de la funció d'ona

El comportament de la funció d'ona donada per les equacions (2.29) i (2.30) a temps gran és important per a aplicacions del passeig quàntic a algoritmes quàntics. Per obtenir el comportament asimptòtic de la funció d'ona resultant és necessàri enfrontar integrals de la forma

$$I(\alpha) = \frac{1}{2\pi} \int_{-\pi}^{\pi} g(k) e^{i\phi(k,\alpha)t} dk \tag{1.34}$$

where $\alpha = n/t$

El mètode de la fase estacionària [10, 11] proporciona coneixement en el comportament asimptòtic d'aquest tipus d'integrals quan t tendeix a infinit. Aquest mètode s'ha fet servir a [8] per trobar la distribució de probabilitat asimptòtica del passeig quàntic amb la moneda d'Hadamard en un estat inicial donat per $\psi(0,0) = (0,1)^{\intercal} \otimes \mid 0\rangle$. Ells proven el següent teorema:

Theorem 1.6.1. *Siga $\epsilon > 0$ qualsevol constant, i α comprès en l'interval $(\frac{-1}{\sqrt{2}} + \epsilon, \frac{1}{\sqrt{2}} - \epsilon)$. Llavors, quan $t \to \infty$, tenim (uniformement en n)*

$$p_L(n,t) \sim \frac{2}{\pi\sqrt{1-2\alpha^2 t}} \cos^2(-\omega t + \frac{\pi}{4} - \rho) \tag{1.35}$$

$$p_R(n,t) \sim \frac{2(1+\alpha)}{\pi(1-\alpha\sqrt{1-2\alpha^2 t}} \cos^2(-\omega t + \frac{\pi}{4}) \tag{1.36}$$

on $\omega = \alpha\rho + \theta$, $\rho = arg(-B + \sqrt{\Delta})$, $\theta = arg(B + 2 + \sqrt{\Delta})$, $B = 2\alpha/(1-\alpha)$, and $\Delta = B^2 - 4(B+1)$.

En aquest teorema gairebé tota la probabilitat es concentra en l'interval $(\frac{-1}{\sqrt{2}} + \epsilon, \frac{1}{\sqrt{2}} - \epsilon)$. De fet, el valor exacte de la probabilitat en aquest interval és $(1 - \frac{2\epsilon}{\pi} - \frac{O(1)}{t})$

En la figura (2.6) es mostra una comparació entre la distribució de probabilitat del passeig quàntic obtinguda mitjançant les equacions (2.34) i (2.35) i la obtinguda numèricament. En el treball presentat per Venegas podem trobar altres propietats asimptòtiques del passeig quàntic com són els teoremes límits del passeig quàntic presentats per Konno et al. [12–16].

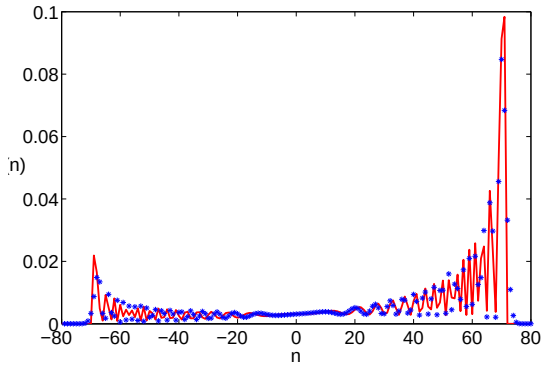

Figure 1.6: Comparació entre les dos distribucions de probabilitat, amb línia vermella es mostra la distribució de probabilitat obtinguda numèricament, i amb punts blaus l'obtinguda amb l'anàlisis asimptòtic.

1.7 Implementacions físiques

S'ha demostrat que molts algoritmes quàntics poden ser construïts sobre la base del passeig quàntic, mostrant una major eficiència que la seua contrapart clàssica, que són una part essencial de molts algoritmes clàssics. A [17] es presenta un algoritme de cerca basat en una arquitectura quàntica. Es mostra que aquest algoritme realitza un oracle de cerca en una base de dades de N elements amb $O(\sqrt{N})$, produint un augment de la velocitat similar a altres algoritmes de cerca quàntica. La referència [18] construeix un problema de tipus "caixa negra" per a travessar un graf, basat en el passeig quàntic en temps continu que pot ser resolt exponencialment més ràpid en un ordinador quàntic que en un ordinador

clàssic. No obstant això, una possible implementació física encara està en desenvolupament primerenc. Es necesita un major desenvolupament en la detallada manipulació d'una partícula quàntica, com poden ser els fotons. Moltes implementacions experimentals han estat proposades i portades a terme per a un petit nombre de passos de temps.

La posició del passejant $\mid n\rangle$ pot ser qualsevol grau discret de llibertat, no necessàriament ha de ser la posició real en la implementació física. De la mateixa manera, l'espai de la moneda no ha de correspondre amb l'spín d'una partícula. Hi ha una gran varietat de propostes, però la següent llista conté les principals: *trampes d'ions, electrodinàmica quàntica* i *xarxes òptiques*.

La primera proposta fou demostrada per Travaglione i Milburn [19] per a l'execució del passeig quàntic a temps discret ja siga en la línia o el cercle utilitzant *trampes d'ions*. La implementació descrita en [20] es basa en un sol ió $^9Be^1$, confinat en una trampa d'ions en un ressonador coaxial de ràdiofreqüència. Les posicions $\mid n\rangle$, es codifiquen en l'estat de moviment de l'ió en el parany, i l'estat electrònic intern dels ions codifica l'estat de la moneda. La moneda i l'operador desplaçament es poden realitzar mitjançant l'aplicació de polsos de feix Raman. La decoherència en l'estat intern de l'ió limita el possible nombre de passos en aquest esquema.

Sanders et al. [21] introduïren altre suggeriment per implementar el passeig quàntic discret en un cercle utilitzant *electrodinàmica quàntica en una cavitat*. Els estats de la moneda es codifiquen amb els estats atòmics interns, mentre que els estats de posició són els modes de la cavitat. El camp de la cavitat pateix canvis de fase, depenent de l'estat en l'àtom. El temps de decoherència de la cavitat fa possible que només uns pocs passos de temps puguen ser realitzats.

Dur et al. [22] proposaren una realització experimental del passeig quàntic discret utilitzant àtoms neutres atrapats en *xarxes òptiques*. Una xarxa òptica està formada per la interferència de raigs làser, creant un potencial espacialment periòdic. Per a cada un dels estats interns d'un àtom neutre (que podria correspondre amb estats hiperfins de l'spín nuclear de l'àtom) existeix una xarxa òptica on es queden atrapats. Els polsos làser s'utilitzen per alterar el seu estat intern. A continuació, els àtoms es desplacen periòdicament, esquerra o dreta, depenent de l'estat intern de l'àtom.

Noves propostes s'han fet per implementar majors dimensions del passeig quàntic com en [23] seguint les idees proposades en [22]. En aquest esquema Roldán i Soriano [24] proposaren una simulació amb cavitats òptiques, que només fa ús de recursos clàssics. El camp de la llum pot seguir quatre camins espacials diferents

que corresponen als estats de la moneda, i el paper del passejant està codificat amb la freqüència del camp.

La primera aplicació experimental del passeig quàntic en temps continu en un cercle fou proposada per Du et al. [25]. Utilitzaren un ordinador quàntic que simula dos qubits amb ressonància magnètica nuclear, i trobaren que la propietat d'aquest passeig quàntic fortament depén de l'entrellaçament quàntic entre els dos qubits.

Poc temps després d'aquesta aplicació experimental Mandel et al. [26] mostraren experimentalment transport coherent d'àtoms neutres en xarxes òptiques fora del context de la passeig quàntic, però és una bona aplicació de l'operador desplaçament del passeig quàntic en temps discret. La primera aplicació del passeig quàntic a temps discret fou realitzada per Ryan et al. [27]. Utilitzaren un processador quàntic que simula tres qubits amb ressonància magnètica nuclear d'estat sòlid en un cercle de 4 vèrtexs en 8 passos de temps. També mostraren la transició al passeig aleatori clàssic afegint decoherència després de cada pas.

Altres propostes i implementacions físiques s'han realitzat en anys recents. Dins l'esquema de trampes d'ions, en [28] basant-se en la proposta donada en [29], s'estudia el passeig quàntic amb ions $^{25}Mg^{+}$ en una trampa de Paul lineal multizona. El nombre de passos es limita a 3 passos. Proposaren un esquema amb sistemes làser que proporcionen polsos curts i intensos, que permet aconseguir un nombre arbitrari de pasos d'evolució. A [30] es desenvolupà una realització similar amb trampes d'ions en l'espai de fases. Es suggerí que aquest mètode podria tenir altres aplicacions en experiments d'òptica quàntica o simulacions quàntiques. Les inestabilitats en la freqüència del parany dóna la limitació en el nombre de passos. No obstant això, s'aconsegueixen 23 passos d'evolució.

En els últims anys diferents grups experimentals han realitzat molts experiments. Seguint [19] Matjeschk et al. [31] analitzaren en detall les limitacions d'aquest protocol. Van explicar la desviació del comportament observat respecte del passeig quàntic ideal per a diferents realitzacions experimentals tenint en compte termes d'ordre superior de l'evolució quàntica. A [32] s'ha implementat e1 passeig quàntic en la línia amb àtoms neutres sobre els llocs d'una xarxa òptica unidimensional amb dependència sobre l'spin per a 10 passos de temps. Es controla l'observació de la transició quàntica-clàssica i la funció d'ona final es caracteritza per la tomografia de l'estat quàntic. Es mostrant un gran control sobre la coherència i l'estat quàntic final.

En el context del passeig quàntic a temps continu una implementació física a [33] demostra la forta correspondència entre passeig quàntic i la propagació

de la llum en els enreixats de guies d'ones. A causa de les baixes taxes de decoherència assolides en els experiments d'enreixats de guies d'ones, alegaren que poden servir com un predilecte esquema experimental, ideal i versàtil per a l'estudi del passeig quàntic i de algoritmes quàntics. Les guies d'ones també s'han utilitzat per a l'aplicació del passeig quàntic amb dos passejants utilitzant fotons entrellaçats [34]. Variant els paràmetres característics de les guies d'ones, es possible investigar passejos quàntics correlacionats en sistemes desordenats, i verificar els efectes de la localització d'Anderson. A [35] es realitzà el primer passeig quàntic en una estructura de guia d'ones 3D amb genuïnes entrades no clàssiques. Estudiaren el passeig quàntic amb diversos pasetjants en 2D en un xip òptic, que conté una disposició elíptica d'acoblament entre les guies d'ona. Alhora, a [36] s'introdueix una novell geometria tridimensional en un circuit de guia d'ona per investigar com les diferents estadístiques de les partícules, ja siga bosònica o fermiònica, influeixen en un passeig quàntic discret de dues partícules.

D'altra banda, a [37] estudiren el passeig quàntic discret en dues dimensions per a un nombre de 20 pasos d'evolució. Simularen molts sistemes quàntics diferents utilitzant un xicotet nombre de components òptics simples disposats en una configuració Mach-Zehnder de trajectòria múltiple. Controlant la quantitat i el tipus de desodre present en el sistema, mostren les conseqüències dels diferents efectes ambientals: desodre espacial dinàmic, desfasament dinàmic sense desordre espacial, i desordre espacial estàtic.

L'experiment d'elecció retardada, proposat per Wheeler [38] i demostrat en diferents configuracions [39–41] s'utilitzà en un article recent [42]. Aquest experiment consta d'un fotó, viatjant en un interferòmetre de Mach-Zehnder, que pot o no pot auto-interferir (i per tant es comporta com una ona o una partícula) depenent de la configuració del propi interferòmetre. En el seu experiment, el patró d'interferència depén la polarització del fotó, i això es determina després de que el fotó haja estat detectat. És el primer experiment del passeig quàntic multidimensional utilitzant un únic fotó i la moneda Grover. Un altre article recent [43] presenta la implementació d'un passeig quàntic òptic de dues dimensions en una xarxa amb fotons obtinguts a partir de polsos de làser atenuats. Els dos estats interns de la moneda estan representats per dos polaritzacions d'un fotó, que es poden moure en quatre camins diferents en una xarxa de fibra depenent en la seua polarització. Aconsegueixen un passeig quàntic coherent de més de 12 passos i 169 posicions. L'arquitectura experimental es pot generalitzar a més de dues dimensions.

El passeig quàntic s'ha convertit en una plataforma versàtil per a l'exploració

d'una àmplia gamma d'efectes topològics no trivials [44–48]. En un article recent [49] es presenta una observació experimental de estructures topològiques, generades a través de l'aplicació controlada de dues rotacions consecutives, no commutatives en el passeig quàntic discret amb fotons. Introduint aquestes rotacions al llarg de la trajectòria, els permet conduir el sistema entre els diferents sectors topològics caracteritzats per diferents invariants topològics.

2 Quantum walk on a line

2.1 Introduction

The classical random walk is a stochastic process that has a huge variety of applications in many fields and provides insights to many problems in physics. Examples range from the study of the Brownian motion to computer science, where many algorithms are based on classical random walks. The quantum walk (QW) is the analogous of the classical random walk expressed in the quantum mechanical form. A fundamental question of quantum computation is to determine if a quantum computer can solve problems faster than a classical computer, i.e. be more efficient than any classical algorithm. Due to the great interest and applications of the classical random walk to algorithm design, it is natural to wonder if the QW will be a useful tool for quantum algorithms.

There are two models of QWs. In the first one, named the discrete time QW, the operator evolution is only applied in discrete time steps to two quantum mechanical systems (a coin and a walker). In the second one, the continuous time QW, the evolution is given by a Hamiltonian which is applied to a system continuously. In both models, the QW is carried out on discrete graphs or lattices.

The study of the QW motivated by potential applications in quantum algorithms was proposed by Ambainis et al. [2] and Aharonov et al. [3]. They introduced the discrete time QW, and proved that a QW on the line or cycle spreads in time quadratically faster than the classical random walk. On the other hand, Childs et al. [4] introduced the "glued trees" graph algorithm, where they found that a quantum walker starting at one on the roots could find the opposite root exponentially faster than any classical algorithm. E.Farhi and S.Gutmann [5] introduced the continuous time QW which also present a speedup over the classical variety. In addition, it has been shown by Childs [6] that the continuous time QW can be considered as a universal computational primitive with any quantum computation encoded in some graph. Later on, Lovvet et al. [7] proved that the discrete time QW is also able to implement the same universal gate set, and thus both, discrete and continuous time QWs are universal computational primitives.

In this first part of the thesis, we focus on the discrete time QW. In this case, the term discrete refers to the application of the corresponding evolution operator of the system in discrete time steps. The particle also moves in a discrete lattice. First, we introduce the main concepts of both the discrete and the continuous time QWs, but focusing our attention on the discrete time QW. After giving a broad introduction, we move into the study of the N-dimensional discrete time QW throughout dispersion relations. We will see how this study allows us to determine the subsequent behavior. In a later chapter, we introduce the concept of quantum Markovianity, and we study the non-Markovian behavior of the QW, and how it becomes Markovian when decoherence effects are introduced.

2.2 Classical Random Walk

A classical discrete random walk is a simple case of stochastic process; it can be seen as a Markov chain that is introduced in chapter 4. In the classical one-dimensional discrete time random walk, which is the simplest case, a walker moves on a line, making steps to the left or to the right depending on the toss of a coin with probability p and q, respectively ($p + q = 1$).

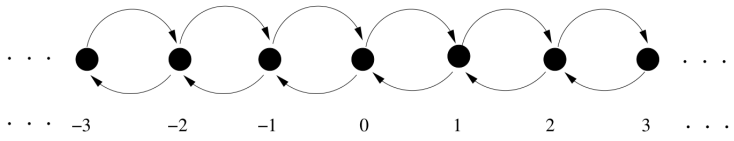

If we consider the symmetric walk, the walker has the same probability of moving either to the right or left, $q = p = \frac{1}{2}$ at each time step. If we let it evolve over time, the probability distribution $P(n, t)$ of finding the walker at site n at time t on the infinite line with a localized initial condition given by $P(n, t = 0) = \delta_{n,0}$ is:

$$P(n,t) = \frac{1}{2^t} \begin{pmatrix} t \\ \frac{n+t}{2} \end{pmatrix} \tag{2.1}$$

There is only non-zero probability of finding the walker at sites that have the same parity as the number of step t. The final probability distribution, Eq. (2.1), is a binomial probability distribution which can be approximated by a Gaussian distribution centered at $n = 0$ in the large t limit. One of the most important features to consider, is the standard deviation of the distribution (magnitude

that gives us an idea of how far, with respect to its initial position, we can find the walker) which is proportional to the square root of the evolution time and establishes the main difference with its quantum analogue. The probability distribution of the classical walker with a symmetric walk $p = \frac{1}{2}$ and the standard deviation of the process are shown in the figure (2.1).

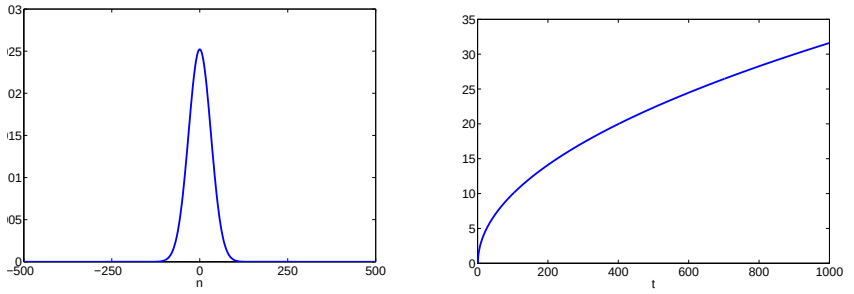

(a) (b)

Figure 2.1: (a) Classical probability distribution as a function of the walker position on the line for 1000 steps. (b) Standard deviation of the probability distribution as a function of the number of steps

2.3 Discrete time Quantum Walk on a line

The discrete time QW on a line is defined directly as the analogous of the classical random walk. The walker is now replaced by a quantum particle with an additional degree of freedom: the coin or chirality with a two state quantum system. Afterwards, the main components of the discrete time QW are the walker, i.e. the quantum particle, and the coin. The walker is located on a discrete one-dimensional line and it can be moved on to nearby places. The Hilbert space associated with the position of the walker has infinite but countable dimensions $\mathcal{H}_P$ and is spanned by the basis $\{|\, x_i\rangle : x_i \in \mathbb{Z}\}$, giving us the position state for the walker. The coin is a quantum system living in a 2-dimensional Hilbert space, $\mathcal{H}_C$, spanned by the basis $\{|\, L\rangle, |\, R\rangle\}$. Therefore, the total Hilbert space of the system is given by the tensor product of the position space and the coin space $\mathcal{H} = \mathcal{H}_C \otimes \mathcal{H}_P$.

The evolution of the system consists in applying an evolution operator to the

coin state followed by a conditional shift operator to the total quantum system. The most general QW transformation that can be written acting on the total Hilbert space is given by

$$U(\theta) = S \cdot (C(\theta) \otimes I) \tag{2.2}$$

And then, the evolution of the QW after t time steps is:

$$\mid \psi(t)\rangle = U^t(\theta) \mid \psi(0)\rangle \tag{2.3}$$

where I is the identity operator in the position space, $C(\theta)$ is the operator that acts on the chirality, equivalent to tossing the coin, and S is a unitary operator which causes a conditional displacement on the system given by

$$S = \mid R\rangle\langle R \mid \otimes \sum_n \mid n+1\rangle\langle n \mid + \mid L\rangle\langle L \mid \otimes \sum_i \mid n-1\rangle\langle n \mid$$

S transforms the states $\mid R\rangle \otimes \mid n\rangle$ into $\mid R\rangle \otimes \mid n+1\rangle$ and the states $\mid L\rangle \otimes \mid n\rangle$ into states $\mid L\rangle \otimes \mid n-1\rangle$ i.e a displacement over the space of the coin that depends on the degree of freedom of the chirality: states with right chirality move to the right, while states with left chirality move to the left. Furthermore, we have a translationally invariant unitary process. The first step in the QW is a rotation in the coin space $C(\theta)$, which is analogous to the classical random walk, followed by a conditional displacement. The unitary transformation $C(\theta)$ is arbitrary and a lot of walks with different behaviors can be defined by changing $C(\theta)$. Therefore, the most general transformation, except for additional phases that can be reabsorbed in the definition of the initial state, can be written as

$$C(\theta) = \begin{pmatrix} \cos\theta & \sin\theta \\ \sin\theta & -\cos\theta \end{pmatrix}$$

If we want to obtain a transformation acting with the same probability of chirality, i.e, a displacement to the right with probability $\frac{1}{2}$ and a displacement to the left with probability $\frac{1}{2}$, the known balanced Hadamard coin transformation given by $\theta = \pi/4$ can be used:

$$H = \frac{1}{\sqrt{2}} \begin{pmatrix} 1 & 1 \\ 1 & -1 \end{pmatrix}$$

Let us see it with an example. Assume that we start from an initial localised state at position $\mid 0\rangle$ and take the state of the coin as $\mid R\rangle$, i.e, our initial state is

given by $\mid 0\rangle\otimes \mid R\rangle$. After one time step, (a transformation on the space of the coin, H, and the conditional translation, S), we obtain

$$\begin{aligned} \mid 0\rangle\otimes \mid R\rangle =\mid 0\rangle \otimes \begin{pmatrix} 1 \\ \\ 0 \end{pmatrix} \xrightarrow{H} \\ \frac{1}{\sqrt{2}} \mid 0\rangle \otimes (\mid R\rangle + \mid L\rangle) \xrightarrow{S} \\ \frac{1}{\sqrt{2}}(\mid 1\rangle\otimes \mid R\rangle + \mid -1\rangle\otimes \mid L\rangle) \end{aligned} \tag{2.4}$$

Since the probability is the result of measuring amplitudes, a shift to the right with probability $\frac{1}{2}$ and a shift to the left with probability $\frac{1}{2}$ is obtained. Should we continue with the next step in the evolution, measuring the resulting probabilities each time the transformation U is applied, the classical random walk on a line would be obtained. Of course, in the quantum random walk, we do not measure at each iteration. In this way the quantum nature of the system arises: quantum interference occurs in our state and entanglement between coin space and position space appears. As a result our state is in a coherent superposition. So, if we do not measure, the quantum interference causes a completely different behavior. To illustrate this, we are going to see the consequences after a few steps when a measure is not made. If we start in the initial state $\mid \phi_{ini}\rangle =\mid L\rangle\otimes \mid 0\rangle$

$$\begin{aligned} \mid \phi_{ini}\rangle \xrightarrow{U} \frac{1}{\sqrt{2}}(\mid 1\rangle\otimes \mid R\rangle - \mid -1\rangle\otimes \mid L\rangle) \\ \xrightarrow{U} \frac{1}{2}(\mid 2\rangle\otimes \mid R\rangle - \mid 0\rangle \otimes (\mid R\rangle - \mid L\rangle) + \mid -2\rangle\otimes \mid L\rangle) \\ \xrightarrow{U} \frac{1}{2\sqrt{2}}(\mid 3\rangle\otimes \mid R\rangle + \mid 1\rangle\otimes \mid L\rangle + \mid -1\rangle\otimes \mid R\rangle - 2 \mid -1\rangle\otimes \mid L\rangle - \mid -3\rangle\otimes \mid L\rangle) \end{aligned} \tag{2.5}$$

This example shows how the probability distribution induced by the QW differs from the classical random walk. In the table (2.1) the probability distribution is shown if we allow the system to evolve during 5 time steps.

t\n	-5	-4	-3	-2	-1	0	1	2	3	4	5
0						1					
1					1/2	0	1/2				
2				1/4	0	1/2	0	1/4			
3			1/8	0	5/8	0	1/8	0	1/8		
4		1/16	0	5/8	0	1/8	0	1/8	0	1/16	
5	1/32	0	17/32	0	1/8	0	1/8	0	5/32	0	1/32

Table 2.1: Probability of being at position n after 5 steps for the initial state given by $\mid \phi_{ini}\rangle = \mid L\rangle \otimes \mid 0\rangle$

The probability distribution of the QW with the Hadamard coin is plotted in figure (2.2), starting in the initial state $\mid \phi_{ini}\rangle = \mid L\rangle \otimes \mid 0\rangle$ after 1000 time steps. It only shows the probability for even positions, since for odd positions it is zero. It is clear that the probability distribution for this walk is much more complicated than the probability distribution obtained in the classical random walk.

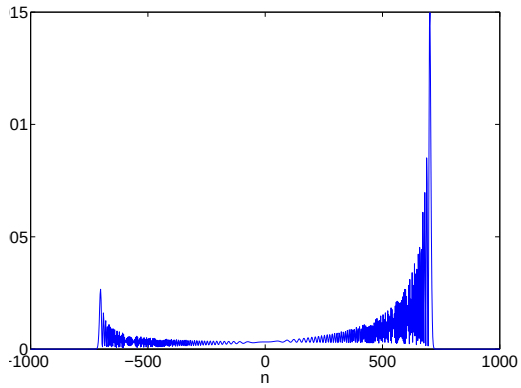

Figure 2.2: Probability distribution of the QW after 1000 time steps with a initial state given by $\mid \phi_{ini}\rangle = \mid L\rangle \otimes \mid 0\rangle$

We see in figure (2.2) that the probability distribution is asymmetrical. This asymmetry is due to the fact that the Hadamard coin treats the ($\mid R\rangle$ and $\mid L\rangle$) chiralities in a different way, only $\mid L\rangle$ is multiplied by a phase -1. More cancellations (destructive interference) are produced for contributions that move to the left, while there is constructive interference for the ones that move to the

right. There are two ways to avoid this asymmetry, one of them is to start with a state that is a combination of $\mid R\rangle$ and $\mid L\rangle$ and make sure they do not interfere with each other. To do this we start with $\mid \phi_{ini}\rangle = \frac{1}{\sqrt{2}}(\mid R\rangle + i \mid L\rangle)\otimes \mid 0\rangle$ and because the Hadamard coin does not introduce any complex amplitude, the path for $\mid R\rangle$ will be real, while the path for $\mid L\rangle$ will be imaginary, so that they do not interfere and the probability distribution will be symmetrical.

Another way to get exactly the same result is to use the following coin

$$Y = \frac{1}{\sqrt{2}} \begin{pmatrix} 1 & i \\ i & 1 \end{pmatrix}$$

The distribution probability for the classical random walk and the QW are represented in figure (2.3).

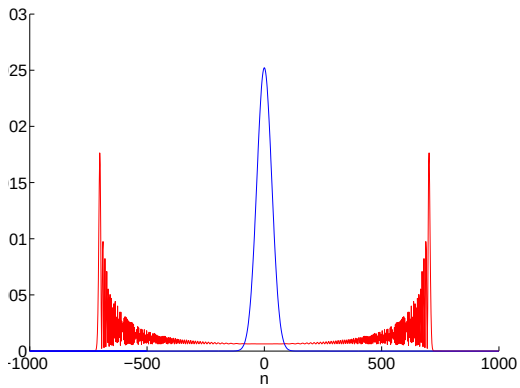

Figure 2.3: Comparison between the quantum and classical random walks probability distribution after 1000 time steps. The QW is evolved using the Hadamard coin, starting in the symmetric coin state $\mid \phi_{ini}\rangle = \frac{1}{\sqrt{2}}(\mid R\rangle + i \mid L\rangle)\otimes \mid 0\rangle$.

The standard deviation of the probability distribution is one of the most important characteristics of the QW. It differs from its classical analogue and can be used to design a more efficient algorithm. The quantum probability distribution is far more dispersed than the classical probability distribution, since the probability of finding the particle near the starting point is very low. This behavior is opposite to the classical one, whose distribution shows a peak centered at the origin and exponentially decaying. The maximum value of the probability distri-

bution of the classical random walk is at the center, $n = 0$, while the maximum probability peaks in the quantum version are at $n = \pm\frac{t}{\sqrt{2}}$.

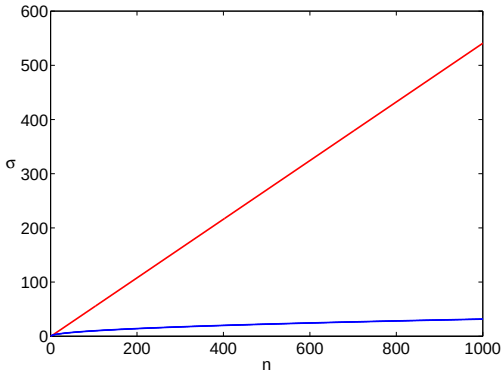

Figure 2.4: Comparison between the quantum and classical random walks standard deviation after 1000 time steps. The QW is evolved using the Hadamard coin, starting in the symmetric coin state $\mid \phi_{ini}\rangle = \frac{1}{\sqrt{2}}(\mid R\rangle + i \mid L\rangle)\otimes \mid 0\rangle$

The standard deviation for the quantum and classical random walk are represented in figure (2.4). As previously mentioned, for the classical case the standard deviation grows as the square root of the step number $\sigma \sim \sqrt{t}$, while for the quantum case it grows as the number of steps $\sigma \sim t$. This result has been analytically proven by several authors [3, 8]. So, for a given number of steps, the quantum walker is capable of scanning a significantly greater portion of the accessible space than the classical walker, and moves in a line quadratically faster than the classical random walk. In other words, the QW shows ballistic propagation, rather than diffusive spreading. These differences are due to the existence of the interference phenomenon present in the quantum case. This fact has strong implications for the algorithms, and is one of the reasons why it has been studied in the last decades.

2.4 Continuous time Quantum Walk

A general definition of the continuous time QW is given by Childs et al. in [4]. This definition is based on a Hamiltonian description, and in this case,

the chirality degree of freedom is not needed. The simplest way to introduce this description is to start with the classical random walk on a graph due to the direct connection between them. The continuous time random walk is also a Markov process that we will describe in chapter 4. The main idea is to consider the set of vertices $\{1, 2, 3...v\}$ and given connections between them. A jump on a random classical walk is only possible if the vertices are connected. These connections can be defined by the $v \times v$ infinitesimal generator matrix M:

$$M_{ab} = \begin{cases} -\gamma & a \neq b, a \text{ and } b \text{ connected} \\ 0 & a \neq b, a \text{ and } b \text{ not connected} \\ k\gamma & a = b, k \text{ is the valence of vertex } a \end{cases} \tag{2.6}$$

Where γ denotes the jumping rate. The probability of being at vertex a at time t is given by

$$\frac{dp_a(t)}{dt} = -\sum_b M_{ab} p_b(t) \tag{2.7}$$

In this simple way the evolution of the classical random walk can be described. In order to introduce the continuous time QW, there are two requirements to be defined: the v-dimensional Hilbert space spanned by the vertices of the graph $\mid 1\rangle$, $\mid 2\rangle$,...$\mid v\rangle$, and the Hamiltonian responsible for the evolution whose matrix elements are given by $\langle a \mid H \mid b\rangle$. Now, the evolution of a quantum state $\mid \psi(t)\rangle$ is given by the Schrödinger equation

$$i\frac{d\langle a \mid \psi(t)\rangle}{dt} = \sum_b \langle a \mid H \mid b\rangle\langle b \mid \psi(t)\rangle \tag{2.8}$$

In a one-dimensional lattice the Hamiltonian can be defined by

$$H \mid n\rangle = -\frac{a}{\Delta^2}(\mid n-1\rangle - 2 \mid n\rangle + \mid n+1\rangle) \tag{2.9}$$

which is just a discrete approximation to the operator d^2/dx^2, where Δ is the lattice spacing. The evolved state can be written as

$$\mid \psi(t)\rangle = e^{-iHt} \mid \psi(0)\rangle \tag{2.10}$$

Eq. (2.10) defines a continuous time QW on a graph: notice that it is continuous in time and discrete in space. In the continuous case, the standard deviation also grows linearly in time and quadratically faster than the classical diffusion. Thus it is more efficient scanning the accessible space than its classical counterpart. It is important to mention that a correspondence exists to transform the

discrete time QW into continuous QW as in the classical case. It was proposed in [50] and shows that two copies of the continuous time QW were obtained taking a particular kind of continuous time limit in the discrete time QW. It is valid for one and higher dimensions.

2.5 Discrete time Quantum Walk in momentum space.

The unitary evolution of the discrete time QW described above can be studied considering the resulting wave function. Describing the position of the particle as a two component spinor of amplitudes of the particle being at point n at time t, with the chirality being right (upper component) or left (lower component), the resulting wave function is given by:

$$\psi(n,t) = \begin{pmatrix} a(n,t) \\ b(n,t) \end{pmatrix}. \tag{2.11}$$

In operator notation: $\mid \psi(n,t)\rangle = a(n,t) \mid R\rangle + b(n,t) \mid L\rangle$. By applying the evolution operator Eq.(2.2) the state at $t+1$ can be related to the state at previous time, t. Then, the dynamics for ψ can be written in matrix notation as:

$$\psi(n,t) = \begin{pmatrix} \cos\theta & \sin\theta \\ 0 & 0 \end{pmatrix} \psi(n+1,t) + \begin{pmatrix} 0 & 0 \\ \sin\theta & -\cos\theta \end{pmatrix} \psi(n-1,t). \tag{2.12}$$

If we define:

$$M_+ = \begin{pmatrix} \cos\theta & \sin\theta \\ 0 & 0 \end{pmatrix} \qquad M_- = \begin{pmatrix} 0 & 0 \\ \sin\theta & -\cos\theta \end{pmatrix}, \tag{2.13}$$

thus

$$\psi(n,t+1) = M_+\psi(n+1,t) + M_-\psi(n-1,t) \tag{2.14}$$

Eq (2.14) can be written as its components

$$\begin{aligned} a(n,t+1) &= a(n+1,t)\cos\theta + b(n+1,t)\sin\theta \\ b(n,t+1) &= a(n-1,t)\sin\theta - b(n-1,t)\cos\theta \end{aligned} \tag{2.15}$$

Then, the analysis of the QW is reduced to solving a two dimensional recurrence system. Due to translational invariance, the QW has a simple description in the Fourier domain. In this basis, following [3] it can easily be solved and then we

can go back to the real space by reverting the Fourier transform.
Discrete Time Fourier Transform. The spatial Fourier transform $\psi(k,t)$, of the wave function over $\mathcal{Z}$ is given by

$$\psi(k,t) = \sum_n \psi(n,t)e^{ikn} \tag{2.16}$$

where $k \in [-\pi, \pi[$ is the quasi-momentum vector and its inverse is given by:

$$\psi(n,t) = \frac{1}{2\pi}\int_{-\pi}^{\pi} \psi(k,t)e^{-ikn}dk \tag{2.17}$$

In the same way, the basis $\mid k\rangle$ and $\mid n\rangle$ can be defined as:

$$\begin{aligned} \mid k\rangle &= \sum_{n=-\infty}^{n=\infty} \mid n\rangle e^{ikn} \\ \mid n\rangle &= \frac{1}{2\pi}\int_{-\pi}^{\pi} \mid k\rangle e^{-ikn}dk \end{aligned} \tag{2.18}$$

The dynamics of Eq. (2.14) can be written as

$$\begin{aligned} \psi(k,t) &= \sum_n (M_+\psi(n+1,t) + M_-\psi(n-1,t))e^{ikn} \\ &= e^{-ikn}M_+\sum_n \psi(n+1)e^{ik(n+1)} + e^{ikn}M_+\sum_n \psi(n-1)e^{ik(n-1)} \\ &= (e^{-ik}M_+ + e^{ik}M_-)\psi(k,t) \end{aligned} \tag{2.19}$$

As a result, we have

$$\begin{aligned} \psi(k,t+1) &= M_k\psi(k,t) \\ M_k &= e^{-ik}M_+ + e^{ik}M_- = \\ &\begin{pmatrix} e^{-ik}\cos\theta & e^{-ik}\sin\theta \\ e^{ik}\sin\theta & -e^{ik}\cos\theta \end{pmatrix} \end{aligned} \tag{2.20}$$

The recurrence in Fourier space takes the simple form

$$\psi(k,t) = M_k^t\psi(k,0) \tag{2.21}$$

Where M_k is defined as the coin operator in quasi-momentum space. The QW map has gone from non-local Eq. (2.14) in the space representation to local Eq.

(2.21) in the momentum representation. It makes the analysis of the dynamics easier to solve. To proceed with the resolution the eigenvalues and eigenvectors of M_k should be obtained. If M_k has eigenvectors $\mid \phi_k^1\rangle, \mid \phi_k^2\rangle$ and corresponding eigenvalues λ_k^1, λ_k^2, it can be can written as:

$$M_k = \lambda_k^1 \mid \phi_k^1\rangle\langle\phi_k^1 \mid + \lambda_k^2 \mid \phi_k^2\rangle\langle\phi_k^2 \mid, \tag{2.22}$$

and then the time evolution matrix has the form

$$M_k^t = (\lambda_k^1)^t \mid \phi_k^1\rangle\langle\phi_k^1 \mid + (\lambda_k^2)^t \mid \phi_k^2\rangle\langle\phi_k^2 \mid . \tag{2.23}$$

Due to the fact that M_k is a unitary matrix with $det(M_k) = -1$, the eigenvalues can be written as $\lambda_k^1 = e^{i\omega_k}$ and $\lambda_k^2 = e^{i(\pi-\omega_k)}$, where $\omega_k = -\arcsin(\sin k \cos\theta)$ is the dispersion relation. In the case of the Hadamard walk,

$$M_k = \frac{1}{\sqrt{2}} \begin{pmatrix} e^{-ik} & e^{-ik} \\ e^{ik} & -e^{ik} \end{pmatrix} \tag{2.24}$$

The corresponding eigenvectors can be obtained through the diagonalization of the matrix M_k, Eq. (2.24)

$$\begin{aligned} \phi_k^1 &= \frac{1}{\sqrt{2N(k)}} \begin{pmatrix} e^{-ik} \\ \sqrt{2}e^{i\omega_k} + e^{-ik} \end{pmatrix} \\ \phi_k^2 &= \frac{1}{\sqrt{2N(\pi-k)}} \begin{pmatrix} e^{-ik} \\ -\sqrt{2}e^{-i\omega_k} + e^{-ik} \end{pmatrix} \end{aligned} \tag{2.25}$$

where the normalization factor is given by

$$N(k) = (1 + \cos^2 k) + \cos k\sqrt{1 + cos^2 k} \tag{2.26}$$

In the Fourier basis the initial state is represented by $\psi(k,t) = (0,1)^\intercal$ for all k. Making use of the relations (2.22) and (2.23), the wave function at any time t is given by

$$a(k,t) = \frac{1}{2}(1 + \frac{\cos k}{\sqrt{1+\cos^2 k}})e^{i\omega_k t} + \frac{(-1)^t}{2}(1 - \frac{\cos k}{\sqrt{1+\cos^2 k}})e^{-i\omega_k t} \tag{2.27}$$

$$b(k,t) = \frac{e^{-ik}}{2\sqrt{1+cos^2 k}}(e^{i\omega_k t} - (-1)^t e^{-i\omega_k t}) \tag{2.28}$$

Now, it is necessary to return to real space. For that, the inverse Fourier transformation has to be calculated. The wave functions in real space can be written in the form:

$$a(n,t) = \frac{1 + (-1)^{n+t}}{2} \int_{-\pi}^{\pi} \frac{dk}{2\pi}(1 + \frac{\cos k}{\sqrt{1+cos^2 k}})e^{-i(kn+\omega_k t)} \tag{2.29}$$

$$b(n,t) = \frac{1+(-1)^{n+t}}{2}\int_{-\pi}^{\pi}\frac{dk}{2\pi}\left(\frac{e^{ik}}{\sqrt{1+cos^2 k}}\right)e^{-i(kn+\omega_k t)} \tag{2.30}$$

These expressions are a closed formal solution for the dynamics of the Quantum Walk with a Hadamard coin for a particular initial state, the problem has been solved with a formal expression for $a(n,t)$ and $b(n,t)$, although the integrals cannot be solved in analytical form. Numerical simulations allow us to obtain the probability distribution for the QW and compare it with the classical counterpart. As expected from the definition of the QW, the amplitudes for even n at odd t, and for odd n at even t are zero.

The study of the QW in momentum space gives the possibility to predict and to control the subsequent behavior of the QW through the knowledge of the dispersion relation. In the work presented by Valcárcel et al [9], a study about the QW dynamics when the initial state is a wavepacket close to some of the eigenvectors is shown. We explore it in depth for N-dimensions in chapter 3. In this context, plane waves

$$\mid \psi(n,t)\rangle = e^{i(kn-\omega_k t)} \mid \phi_k\rangle \tag{2.31}$$

are solutions to the map (2.15), where ω_k is the frequency of the map which defines a dispersion relation in the system. The group velocity is given by $v_g^{(1,2)} = d\omega/dk^{(1,2)}$. When the initial state is a wavepacket in which the coin state is an eigenvector of the coin in momentum space, i.e,

$$\mid \psi(n,0)\rangle = f_x^{(1,2)} e^{ik_0 n} \mid \phi_{k_0}^{(1,2)}\rangle \tag{2.32}$$

with $f_x^{(1,2)}$ a smooth envelope, the propagation of the QW is governed by the group velocity. For the Hadamard coin, $\omega = -\arcsin(\frac{1}{\sqrt{2}}\sin k)$, hence, if $k_0 = \pm\pi/2$, then $v_g(\pm\pi/2) = 0$ and the wavepacket should stay at rest, while if $k_0 = 0$, the group velocity is maximal and it should move with maximum velocity. In figure 2.5 the dispersion relation and the group velocity are plotted.

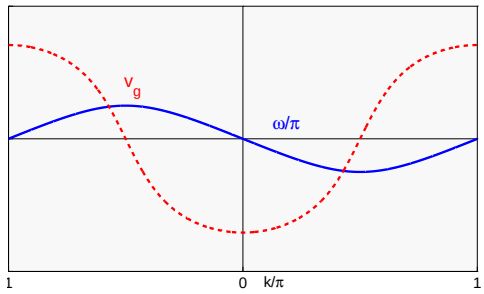

Figure 2.5: Dispersion relation (blue line) and group velocity (red line) for the Hadamard coin.

2.6 Asymptotic properties of the wave function in the long time limit

The behavior of the wave function Eq. (2.29) and Eq. (2.30) at large times is important for QW applications to quantum algorithms. To obtain the asymptotic behavior of the resulting wave function it is necessary to solve integrals of the form

$$I(\alpha) = \frac{1}{2\pi}\int_{-\pi}^{\pi} g(k)e^{i\phi(k,\alpha)t}dk \tag{2.33}$$

where $\alpha = n/t$

The method of stationary phase [10, 11] provides insight in the asympotical behavior of these kind of integrals as t tends to infinity. This method has been used in [8] to found the asymptotic probability distribution for the Hadamard walk with an initial state given by $\psi(0,0) = (0,1)^{\intercal}\otimes \mid 0\rangle$. They proof the following theorem:

Theorem 2.6.1. *Let $\epsilon > 0$ be any constant, and α be in the interval $(\frac{-1}{\sqrt{2}} + \epsilon, \frac{1}{\sqrt{2}} - \epsilon)$. Then, as $t \to \infty$, we have (uniformly in n)*

$$p_L(n,t) \sim \frac{2}{\pi\sqrt{1-2\alpha^2 t}}\cos^2(-\omega t + \frac{\pi}{4} - \rho) \tag{2.34}$$

$$p_R(n,t) \sim \frac{2(1+\alpha)}{\pi(1-\alpha\sqrt{1-2\alpha^2 t}}\cos^2(-\omega t + \frac{\pi}{4}) \tag{2.35}$$

where $\omega = \alpha\rho + \theta$, $\rho = arg(-B + \sqrt{\Delta})$, $\theta = arg(B + 2 + \sqrt{\Delta})$, $B = 2\alpha/(1-\alpha)$, *and* $\Delta = B^2 - 4(B+1)$.

In this theorem almost all the probability is concentrated in the interval $(\frac{-1}{\sqrt{2}} + \epsilon, \frac{1}{\sqrt{2}} - \epsilon)$. In fact, the exact probability value in that interval is $(1 - \frac{2\epsilon}{\pi} - \frac{O(1)}{t})$

In figure (2.6) a comparation between the probability distribution obtained from Eq.(2.34) and Eq.(2.35) and the probability distribution obtained numerically is shown. In the review presented by Venegas in [51] other asymptotic properties of the QW can be found, such as the limit theorems for quantum walks presented by Konno et al. [12–16].

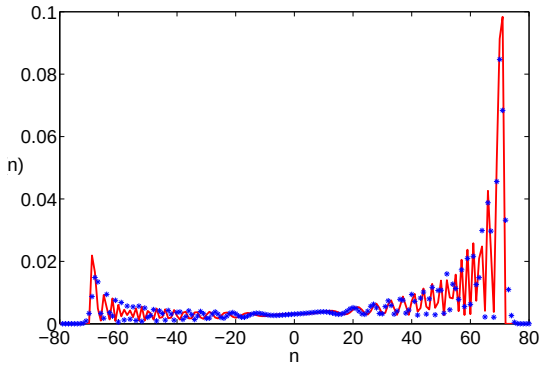

Figure 2.6: A comparison between two probability distributions. The red line shows the probability distribution as obtained numerically, while blue dots show the one obtained from an asymptotic analysis of the quantum walk. The number of steps in the walk was taken to be 100.

2.7 Physical implementations

It has been proven that many quantum algorithms can be constructed based on the QWs structure, showing a greater efficiency than their classical counterpart, which are an essential part of many classical algorithms. In [17] a quantum search algorithm based on a quantum architecture is presented. It is shown that this algorithm performs an oracle search on a database of N items with $O(\sqrt{N})$ calls to the oracle, yielding a speedup similar to other quantum search algorithms. Reference [18] constructs a black box graph traversal problem based on a continuous time QW that can be solved exponentially faster on a quantum computer than on

a classical computer. However, a possible physical implementation is still in early development. Further development in the detailed manipulation of a quantum particle, such as photons, is needed. Many experimental implementations have been proposed and carried out for a small number of time steps.

The position of the walker $\mid n\rangle$ can be any discrete degree of freedom, it does not need necessarily be the real position in the physical implementation. In the same way, the coin space does not need to correspond to the spin of a particle.

There is a huge variety of proposals, but the following list contains the main ones: *ion-traps, quantum electrodynamics* and *optical lattices*.

The first proposal was shown by Travaglione and Milburn [19] for implementing the discrete time QW on either the line or the cycle using *ion traps*. The implementations are based on a single $^9Be^1$ ion, confined in a coaxial resonator radio frequency ion trap, as described in [20]. The positions, $\mid n\rangle$, are encoded into the motional state of the ion in the trap, and the electronic internal state of the ion encodes the coin state. The coin and shift operators can be performed by applying Raman beam pulses. The decoherence in the internal state of the ion limits the possible number of steps in this scheme.

Another suggestion to implement the discrete time QW on a circle using *cavity quantum electrodynamics* was introduced by Sanders et al [21]. The coin states are encoded into the internal atomic states, whereas the position states are the cavity modes. The cavity field undergoes phase shifts, depending on the state of the atom. The decoherence time of the cavity makes it possible only a few time steps.

Dür et al. [22] proposed an experimental realization of discrete time QWs using neutral atoms trapped in *optical lattices*. An optical lattice is formed by the interference of counter-propagating laser beams, creating a spatially periodic potential. Different internal states of a neutral atom (they could correspond to hyperfine states of the nuclear spin of the atom) can be trapped on an optical lattice. Laser pulses are used to alter their internal state. Then the atoms periodically shift, left or right, depending on the internal state of the atom. In the work presented by Knight et al. [52] showed that the discrete time quantum walk can be understood as an interference phenomenon, can be simulated in a purely classical implementation, involving nothing more than wave interference of electromagnetic fields.

New proposals have been made to implement higher dimensional QWs such as in [23] following the ideas proposed in [22]. In the same scheme Roldán and Soriano [24] proposed a simulation with optical cavities, which only makes use of

classical resources. There are four different spatial paths that the light field can follow which correspond to the states of the coin, and the walker role is encoded into the field frequency.

The first experimental implementation of the continuous time QW on a circle was proposed by Du et al. [25]. They used a two-qubit nuclear-magnetic-resonance quantum computer and found that the properties such as uniform distribution of this QW strongly depends on the quantum entanglement between the two qubits.

A short time after this experimental implementation Mandel et al. [26] experimentally showed coherent transport of neutral atoms in optical lattices outside the context of the QWs, although is a nice implementation of the shift operator of the discrete time QW. The first implementation of the discrete time QW was done by Ryan et al. [27]. A three-qubit liquid-state nuclear-magnetic-resonance quantum-information processor has been used on a circle of 4 vertices for 8 time steps. They also showed the transition to the classical random walk adding decoherence after each step.

Other proposals and physical implementations have been made in recent years. In [28], in the scheme of trapped ions based on the proposal [29], the QW with $^{25}Mg^{+}$ ion in a linear multizone Paul trap is studied. The number of time steps is limited to 3. A scheme for laser systems providing short, intense pulses,allowing arbitrarily many steps was proposed. In [30] a similar realization with ion traps in phase space was made. It was suggested that this method might have further applications in quantum optics experiments or quantum simulations. The instabilities in the trap frequency gives a limitation in the number of steps. However, 23 time steps have been achieved.

In recent years many experiments have been made by experimental groups. Following [19] Matjeschk et al. [31] analyzed in detail the limitations of this protocol. The deviations from the idealized QW for different experimental realizations and an increasing number of steps have been explained by taking into account higher-order terms of the quantum evolution. In [32] a QW on the line with single neutral atoms over the sites of a one-dimensional spin-dependent optical lattice has been implemented with 10 time steps. The observation of the quantum-to-classical transition is controlled and the final wave function is characterized by local quantum state tomography. Its spatial coherence is demonstrated showing a great control over coherence and the quantum state.

In the context of the continuous time QW, a physical implementation in [33] demonstrated the strong correspondence between QWs and light propagation

in waveguide lattices. Due to the low decoherence rates achieved in waveguide lattices experiments, the authors claimed that it can serve as an ideal and versatile experimental playground for the study of QWs and quantum algorithms. Waveguides have also been used for implementing the QW with two walkers using entangled photons [34]. Varying the characteristical parameters of the waveguide allows one to investigate correlated QWs in disordered systems, and to verify the effects of Anderson localization. In [35] the first QW in a 3D waveguide structure with genuine non-classical inputs was performed. They studied the multi-walker continuous time 2D QW in an optical chip containing an elliptical arrangement of coupled direct-write waveguides. At the same time, in [36] a novel three-dimensional geometry for the waveguide circuit is introduced to investigate how the particle statistics, either bosonic or fermionic, influences a two-particle discrete time QW.

On the other hand, in [37] the two dimensional discrete time QW for 20 time step was studied, using a small number of simple optical components arranged in a multipath Mach-Zehnder-like configuration, which allows them to simulate many different quantum systems. Controlling the amount and type of disorder present in the system, they showed the consequences of different environmental effects: dynamical spatial disorder, dynamical dephasing without spatial disorder, and static spatial disorder.

The delayed-choice experiment, proposed by Wheeler [38] and demonstrated in different setups [39–41] was used in a recent article [42]. The delayed-choice experiment consists of a photon, traveling in a Mach-Zehnder interferometer, which can or cannot self-interfere (and thus behave as a wave or a particle) depending on the configuration of the interferometer itself. In their experiment, the interference pattern depends on the polarization of the photon, which is determined after the photon has already been detected. It is the first experiment on multi-dimensional QW with a single-photon source and the first one using the Grover walk. Another recent article [43] presents the implementation of a two-dimensional optical QW on a lattice with photons obtained from attenuated laser pulses. The two internal coin states are represented by two polarization modes of a photon that can move in four different paths in a fiber network depending on their polarization. They achieve a coherent QW over 12 steps and 169 positions The experimental architecture can be generalized to more than two dimensions.

The QW has become a versatile platform for the exploration of a wide range of nontrivial topological effects [44–48] . In a recent article [49] an experimental observation of topological structures generated via the controlled implementation

of two consecutive noncommuting rotations in photonic discrete time quantum walks is presented. The authors introduce two consecutive non- commuting rotations along the walk that allow them drive the system between topological sectors characterized by different topological invariants.

The classical random walk is a deterministic process that has a huge variety of applications in many fields and provides insights to many problems in physics. Examples range from the study of the Brownian motion to computer science, where many algorithms are based on classical random walks. The quantum walk (QW) is the analogous of the classical random walk expressed in the quantum mechanical form. A fundamental question of quantum computation is to determine if a quantum computer can solve problems faster than a classical computer, i.e. be more efficient than any classical algorithm. Due to the great interest and applications of the classical random walk to algorithm design, it is natural to wonder if the QW will be a useful tool for quantum algorithms.

There are two models of QWs. In the first one, named the discrete time QW, the operator evolution is only applied in discrete time steps to two quantum mechanical systems (a coin and a walker). In the second one, the continuous time QW, the evolution is given by a Hamiltonian which is applied to a system continuously. In both models, the QW is carried out on discrete graphs or lattices.

The study of the QW motivated by potential applications in quantum algorithms was proposed by Ambainis et al. [2] and Aharonov et al. [3]. They introduced the discrete time QW, and proved that a QW on the line or cycle spreads in time quadratically faster than the classical random walk. On the other hand, Childs et al. [4] introduced the "glued trees" graph algorithm, where they found that a quantum walker starting at one on the roots could find the opposite root exponentially faster than any classical algorithm. E.Farhi and S.Gutmann [5] introduced the continuous QW which also present a speedup over the classical variety. In addition, it has been shown by Childs [6] that the continuous time QW can be considered as a universal computational primitive with any quantum computation encoded in some graph. Later on, Lovvet et al. [7] proved that the discrete-time QW is also able to implement the same universal gate set, and thus both, discrete and continuous-time QWs are universal computational primitives.

In this first part of the thesis, we focus on the discrete QW. In this case, the term discrete refers to the application of the corresponding evolution operator of the system in discrete time steps. The particle also moves in a discrete lattice. First, we introduce the main concepts of both the discrete and the continuous QWs, but focusing our attention on the discrete QW. After giving a broad intro-

duction, we move into the study of the N-dimensional QW throughout dispersion relations. We will see how this study allows us to determine the subsequent behavior. In a later chapter, we introduce the concept of quantum Markovianity, and we study the non-Markovian behavior of the QW, and how it becomes Markovian when decoherence effects are introduced.

3 Understanding and controlling N-dimensional quantum walks via dispersion relations.

3.1 Introduction

In chapter 2 we introduced the work presented by Valcarcel et al. [9] in which the dynamics of coined QWs from the perspective of their dispersion relation has been analyzed. It has been also used for different purposes (see, e.g., [54, 55]). When the initial state is described by a probability distribution extending over a finite region in the lattice, the evolution of the QW can be derived, to a good degree of approximation, from familiar linear partial differential wave equations. Certainly the use of extended initial conditions has been rare up to now [56], but we show that they allow us to reach final probability distributions which, interestingly, can be tailored to some extent. It is also worth mentioning that extended initial conditions also make a connection with multiparticle quantum walks for noninteracting particles [57].

The authors in [53] have applied the above viewpoint in studying *alternate* QWs [58] in N dimensions. In this chapter we shall carry out, from the dispersion relation viewpoint, the study of multidimensional QWs using standard coin operators. Below we make a general treatment, valid for N dimensions, and illustrate our results with the special cases of the Grover two- and three-dimensional QWs. We notice that the 2D Grover QW has received most of the theoretical attention paid to multidimensional QWs [16, 17, 59–69].

We shall derive continuous wave equations, whose form depends on the probability distribution at time $t = 0$. To the leading order in a derivative expansion, these equations are partial differential equations that can be written in the form

$$\mathrm{i}\frac{\partial A^{(s)}\left(\mathbf{X},t\right)}{\partial t} = -\frac{1}{2}\sum_{i,j=1}^{N}\varpi_{ij}^{(s)}\frac{\partial^2 A^{(s)}}{\partial X_i \partial X_j} + \cdots, \tag{3.1}$$

with $A^{(s)}$ a continuous amplitude probability, the coefficients $\varpi_{ij}^{(s)}$ determined by the QW dispersion relation properties, and X_i the spatial coordinates in a reference frame moving with the group velocity (see below for full details).

The accumulated knowledge regarding the solutions of the above continuous equations allows us, to some extent, for a qualitative estimation of the long term probability distribution of the QW for particular initial conditions.

We are interested, not in obtaining approximate continuous solutions to the discrete time QW, but in getting a quick intuition of the QW evolution for different initial probability distributions. This allows, in particular, to reach a desired asymptotic distribution by suitably tailoring the initial (extended) state [9]. Of course, this study will be only approximate (as the continuous solutions are strictly valid only for infinitely extended initial distributions) but, as we show below, even for relatively narrow initial distributions the approximation turns out to be quite accurate. In each case, we will present an exact numerical simulation, obtained from the discrete map of the QW, that illustrates the agreement with the qualitative analysis described above. As far as we know, this is the first time that continuous approximations to the discrete time QW are derived for a multidimensional QW.

The continuous equations we derive, however, cannot be applied near degeneracies in the dispersion relations, since in their vicinity the eigensolutions of the QW vary wildly from point to point. In the two dimensional Grover QW, they appear under the form of canonical intersections. These canonical intersections called *diabolical points* [70–72], determine a type of dynamics similar to that of massless Dirac fermions or electrons in graphene [53, 73–77] and appear in very different systems: quantum triangular billiards [70], conical refraction in crystal optics [71, 72], the already mentioned graphene electrons [73–77], the spectra of polyatomic molecules [78, 79], optical lattices [80] or acoustic surface waves [81], just to mention a few. Diabolical points in the dispersion relations play also a role on the analysis of topological properties of the QW [82].

In three dimensional Grover walk, we also find degeneracies, but of a different nature. In this chapter we develop in mathematical detail the specific treatment necessary to study the evolution close to degeneracies, and we apply it to the two-dimensional Grover walk.

3.2 N-dimensional discrete time quantum walks. Generalities

In the N-dimensional QW the walker moves at discrete time steps $t \in \mathbb{N}$ across an N-dimensional lattice of sites $\mathbf{x} \equiv (x_1, \ldots, x_N) \in \mathbb{Z}^N$. The walker is endowed with a $2N$-dimensional coin which, after a convenient unitary transformation, determines the direction of displacement. The Hilbert space of the whole system (walker+coin) has then the form

$$\mathcal{H} = \mathcal{H}_{\mathrm{P}} \otimes \mathcal{H}_{\mathrm{C}}, \tag{3.2}$$

where the position space, $\mathcal{H}_{\mathrm{P}}$, is spanned by the basis $\{|\mathbf{x}\rangle \equiv |x_1, \ldots, x_N\rangle : x_\alpha \in \mathbb{Z};\ \alpha = 1, \ldots, N\}$ ($\langle \mathbf{x} | \mathbf{x}' \rangle = \delta_{\mathbf{x},\mathbf{x}'}$), and the coin space, $\mathcal{H}_{\mathrm{C}}$, is spanned by $2N$ orthonormal quantum states $\{|\alpha_\eta\rangle : \alpha = 1, \ldots, N; \eta = \pm\}$. Note that α is associated with the axis and η with the direction. For example, in the popular one dimensional QW ($N = 1$) we would have just $|1_+\rangle$ and $|1_-\rangle$, which are the equivalent to the $|\mathrm{R}\rangle$ and $|\mathrm{L}\rangle$ (for right and left) states commonly used in the literature. This notation is introduced in order to deal easily with an arbitrary number of dimensions.

The state of the total system at time t is represented by the ket $|\psi_t\rangle$, which can be expressed in the form

$$|\psi_t\rangle = \sum_{\mathbf{x}} \sum_{\alpha=1}^{N} \sum_{\eta=\pm} \psi_{\mathbf{x},t}^{\alpha,\eta} \ |\mathbf{x}\rangle \otimes |\alpha_\eta\rangle \,, \tag{3.3}$$

where the projections

$$\psi_{\mathbf{x},t}^{\alpha,\eta} = (\langle \alpha_\eta | \otimes \langle \mathbf{x} |) \, |\Psi_t\rangle \,, \tag{3.4}$$

are wave functions on the lattice. We find it convenient to define, at each point $\mathbf{x}$, the following ket

$$|\psi_{\mathbf{x},t}\rangle = \langle \mathbf{x} \, |\psi_t\rangle = \sum_{\alpha=1}^{N} \sum_{\eta=\pm} \psi_{\mathbf{x},t}^{\alpha,\eta} \, |\alpha_\eta\rangle \,, \tag{3.5}$$

which is an (unnormalized) coin state, so that $\psi_{\mathbf{x},t}^{\alpha,\eta} = \langle \alpha_\eta \mid \psi_{\mathbf{x},t} \rangle$. As $\left|\psi_{\mathbf{x},t}^{\alpha,\eta}\right|^2 = |(\langle \alpha_\eta | \otimes \langle \mathbf{x} |) \, |\psi_t\rangle|^2$ is the probability of finding the walker at $(\mathbf{x}, t)$, and the coin in state $|\alpha_\eta\rangle$, the probability of finding the walker at $(\mathbf{x}, t)$ irrespectively of the coin state is, then,

$$P_{\mathbf{x},t} = \sum_{\alpha=1}^{N} \sum_{\eta=\pm} \left|\psi_{\mathbf{x},t}^{\alpha,\eta}\right|^2 = \langle \psi_{\mathbf{x},t} \, |\psi_{\mathbf{x},t}\rangle \,, \tag{3.6}$$

where we used the fact that $\sum_{\alpha=1}^{N}\sum_{\eta=\pm}|\alpha_\eta\rangle\langle\alpha_\eta|$ is the identity in $\mathcal{H}_{\mathrm{C}}$. Clearly $\sum_{\mathbf{x}}P_{\mathbf{x},t}=1$ because $\sum_{\mathbf{x}}|\mathbf{x}\rangle\langle\mathbf{x}|$ is the identity in $\mathcal{H}_{\mathrm{P}}$.

The dynamical evolution of the system is ruled by

$$|\psi_{t+1}\rangle=\hat{U}\,|\psi_t\rangle\,, \tag{3.7}$$

where the unitary operator

$$\hat{U}=\hat{D}\circ\left(\hat{I}\otimes\hat{C}\right) \tag{3.8}$$

is given in terms of the identity operator in $\mathcal{H}_{\mathrm{P}}$, $\hat{I}$, and two more unitary operators. On the one hand $\hat{C}$ is the so-called coin operator (an operator in $\mathcal{H}_{\mathrm{C}}$), which can be written in its more general form as

$$\hat{C}=\sum_{\alpha,\alpha'=1}^{N}\sum_{\eta,\eta'=\pm}C_{\alpha',\eta'}^{\alpha,\eta}\,|\alpha_\eta\rangle\left\langle\alpha'_{\eta'}\right|, \tag{3.9}$$

where the matrix elements $C_{\alpha',\eta'}^{\alpha,\eta}\equiv\langle\alpha_\eta|\,\hat{C}\,|\alpha'_{\eta'}\rangle$ can be arranged as a $2N\times 2N$ unitary square matrix C. On the other hand $\hat{D}$ is the conditional displacement operator in $\mathcal{H}$

$$\hat{D}=\sum_{\mathbf{x}}\sum_{\alpha=1}^{N}\sum_{\eta=\pm}|\mathbf{x}+\eta\mathbf{u}_\alpha\rangle\langle\mathbf{x}|\otimes|\alpha_\eta\rangle\langle\alpha_\eta|\,, \tag{3.10}$$

where $\mathbf{u}_\alpha$ is the unit vector along direction x_α; note that, depending on the coin state $|\alpha_\eta\rangle$, the walker moves one site to the positive or negative direction of x_α if $\eta=+$ or $\eta=-$, respectively.

Projecting (3.7) onto $\langle\mathbf{x}|$ and using (3.4) and (3.8)–(3.10) we get straightforwardly

$$|\psi_{\mathbf{x},t+1}\rangle=\sum_{\alpha=1}^{N}\sum_{\eta=\pm}|\alpha_\eta\rangle\langle\alpha_\eta|\,\hat{C}\,|\psi_{\mathbf{x}-\eta\mathbf{u}_\alpha,t}\rangle\,, \tag{3.11}$$

which further projected onto $\langle\alpha_\eta|$ leads to

$$\psi_{\mathbf{x},t+1}^{\alpha,\eta}=\sum_{\alpha'=1}^{N}\sum_{\eta'=\pm}C_{\alpha',\eta'}^{\alpha,\eta}\psi_{\mathbf{x}-\eta\mathbf{u}_\alpha,t}^{\alpha',\eta'}. \tag{3.12}$$

Equation (3.11), or equivalently (3.12), is the NDQW map in position representation; it shows that, at each (discrete) time, the wavefunctions at each point are coherent linear superpositions of wavefunctions at neighboring points at previous

time, the weights of the superposition being given by the coin operator matrix elements $C^{\alpha,\eta}_{\alpha',\eta'}$. Next we proceed to derive the solution of map (3.12).

Given the linearity of the map and the fact that it is space-invariant ($C^{\alpha,\eta}_{\alpha',\eta'}$ do not depend on space) a useful technique here is the spatial Discrete Fourier Transform (DFT), which has been used many times in QW studies (see, for example, [3]). First we define the DFT pair

$$\left|\tilde{\psi}_{\mathbf{k},t}\right\rangle \equiv \sum_{\mathbf{x}} e^{-\mathrm{i}\mathbf{k}\cdot\mathbf{x}} \left|\psi_{\mathbf{x},t}\right\rangle, \tag{3.13}$$

$$\left|\psi_{\mathbf{x},t}\right\rangle \equiv \int \frac{\mathrm{d}^N\mathbf{k}}{(2\pi)^N} e^{\mathrm{i}\mathbf{k}\cdot\mathbf{x}} \left|\tilde{\psi}_{\mathbf{k},t}\right\rangle, \tag{3.14}$$

where $\mathbf{k} = (k_1, \ldots, k_N)$ and $k_\alpha \in [-\pi, \pi]$ is the (quasi-)momentum vector [83]. Applying the previous definitions to the map (3.11) we readily get

$$\left|\tilde{\psi}_{\mathbf{k},t+1}\right\rangle = \hat{C}_{\mathbf{k}} \left|\tilde{\psi}_{\mathbf{k},t}\right\rangle, \tag{3.15}$$

where we defined a coin operator in the quasi-momentum space

$$\hat{C}_{\mathbf{k}} \equiv \sum_{\alpha=1}^{N} \sum_{\eta=\pm} \left|\alpha_\eta\right\rangle \left\langle\alpha_\eta\right| \hat{C} e^{-\mathrm{i}\eta k_\alpha}, \tag{3.16}$$

$k_\alpha = \mathbf{k}\cdot\mathbf{u}_\alpha$, whose matrix elements read

$$\left\langle\alpha_\eta\right| \hat{C}_{\mathbf{k}} \left|\alpha'_{\eta'}\right\rangle \equiv (C_{\mathbf{k}})^{\alpha,\eta}_{\alpha',\eta'} = e^{-\mathrm{i}\eta k_\alpha} C^{\alpha,\eta}_{\alpha',\eta'}. \tag{3.17}$$

Projection of (3.15) onto $\langle\alpha_\eta|$ and use of (3.16,3.17) leads to

$$\tilde{\psi}^{\alpha,\eta}_{\mathbf{k},t+1} = \sum_{\alpha'=1}^{N} \sum_{\eta'=\pm} e^{-\mathrm{i}\eta\mathbf{k}\cdot\mathbf{u}_\alpha} C^{\alpha,\eta}_{\alpha',\eta'} \tilde{\psi}^{\alpha',\eta'}_{\mathbf{k},t}. \tag{3.18}$$

Hence the nonlocal maps (3.11,3.12) become local in the momentum representation (3.15,3.18). This allows solving formally the QW dynamics very easily because map (3.15) implies

$$\left|\tilde{\psi}_{\mathbf{k},t}\right\rangle = \left(\hat{C}_{\mathbf{k}}\right)^t \left|\tilde{\psi}_{\mathbf{k},0}\right\rangle, \tag{3.19}$$

and hence the eigensystem of $\hat{C}_{\mathbf{k}}$ (or of $C_{\mathbf{k}}$ in matrix form) is most useful for solving the problem, as we do next.

As the operator $\hat{C}_{\mathbf{k}}$ is unitary, its eigenvalues have all the form $\lambda_{\mathbf{k}}^{(s)} = \exp\left(-\mathrm{i}\omega_{\mathbf{k}}^{(s)}\right)$, $s = 1, \ldots, 2N$, with $\omega_{\mathbf{k}}^{(s)}$ real. We will need to know the $\hat{C}_{\mathbf{k}}$ eigenstates too, $\left\{\left|\phi_{\mathbf{k}}^{(s)}\right\rangle\right\}_{s=1}^{2N}$. Once the eigensystem of $\hat{C}_{\mathbf{k}}$ is known, implementing (3.19) is trivial: Given an initial distribution of the walker in position representation $|\psi_{\mathbf{x},0}\rangle$ we compute its DFT $\left|\tilde{\psi}_{\mathbf{k},0}\right\rangle$ via (3.13), as well as the projections

$$\tilde{f}_{\mathbf{k}}^{(s)} = \left\langle \phi_{\mathbf{k}}^{(s)} \middle| \tilde{\psi}_{\mathbf{k},0} \right\rangle, \tag{3.20}$$

so that $\left|\tilde{\psi}_{\mathbf{k},0}\right\rangle = \sum_s \tilde{f}_{\mathbf{k}}^{(s)} \left|\phi_{\mathbf{k}}^{(s)}\right\rangle$. Now recalling (3.19) we arrive to

$$\left|\tilde{\psi}_{\mathbf{k},t}\right\rangle = \sum_{s=1}^{2N} e^{-\mathrm{i}\omega_{\mathbf{k}}^{(s)} t} \tilde{f}_{\mathbf{k}}^{(s)} \left|\phi_{\mathbf{k}}^{(s)}\right\rangle, \tag{3.21}$$

where we used $\lambda_{\mathbf{k}}^{(s)} = \exp\left(-\mathrm{i}\omega_{\mathbf{k}}^{(s)}\right)$, while in position representation we get, using (3.14),

$$|\psi_{\mathbf{x},t}\rangle = \sum_{s=1}^{2N} \left|\psi_{\mathbf{x},t}^{(s)}\right\rangle, \tag{3.22}$$

$$\left|\psi_{\mathbf{x},t}^{(s)}\right\rangle = \int \frac{\mathrm{d}^N \mathbf{k}}{(2\pi)^N} e^{\mathrm{i}\left(\mathbf{k}\cdot\mathbf{x} - \omega_{\mathbf{k}}^{(s)} t\right)} \tilde{f}_{\mathbf{k}}^{(s)} \left|\phi_{\mathbf{k}}^{(s)}\right\rangle. \tag{3.23}$$

Hence the QW is formally solved: all we need is to compute the eigensystem of $\hat{C}_{\mathbf{k}}$ and the initial state in reciprocal space $\left|\tilde{\psi}_{\mathbf{k},0}\right\rangle$, which determines the weight functions $\tilde{f}_{\mathbf{k}}^{(s)}$ through (3.20).

Equation (3.22) shows that the QW dynamics corresponds to the superposition of $2N$ independent walks, labeled by s. According to (3.23) the $\omega_{\mathbf{k}}^{(s)}$'s are the frequencies of the map, each of which defines a dispersion relation in the system ($2N$ in total). Note as well that what we have done in the end is to decompose the QW dynamics in terms of plane waves. In particular, if $\tilde{f}_{\mathbf{k}}^{(s)} = \delta^{(N)}(\mathbf{k} - \mathbf{k}_0)$, what means that $\left|\tilde{\psi}_{\mathbf{k},0}\right\rangle$ is different from zero only for $\mathbf{k} = \mathbf{k}_0$, $\left|\psi_{\mathbf{x},t}^{(s)}\right\rangle = (2\pi)^{-N} \exp\left[\mathrm{i}\left(\mathbf{k}_0 \cdot \mathbf{x} - \omega_{\mathbf{k}_0}^{(s)} t\right)\right] \left|\phi_{\mathbf{k}_0}^{(s)}\right\rangle$, which is an unnormalizable plane wave and thus unphysical.

In order to avoid possible confusions, to conclude this initial part we state that the ordering of the coin base elements we will be using in the matrix representations of operators and kets is $|1_+\rangle, |1_-\rangle, \ldots |N_+\rangle, |N_-\rangle$.

3.3 Continuous wave equations for spatially extended initial conditions

In this section we describe the evolution of spatially extended initial conditions that are close to the plane waves we have introduced. We define such spatially extended states as those having a width which is appreciably larger than the lattice spacing (taken as unity in this work). This type of initial states are wavepackets which are easily expressed in reciprocal space,

$$\left|\tilde{\psi}_{\mathbf{k},0}\right\rangle = \sum_{s=1}^{2N} \tilde{F}^{(s)}_{\mathbf{k}-\mathbf{k}_0} \left|\phi^{(s)}_{\mathbf{k}_0}\right\rangle, \tag{3.24}$$

where $\mathbf{k}_0$ is a reference (carrier) wavevector, chosen at will, $\left|\phi^{(s)}_{\mathbf{k}_0}\right\rangle$ are the associated eigenvectors, and $\tilde{F}^{(s)}_{\mathbf{k}}$ is a narrow function of $\mathbf{k}$, centered at $\mathbf{k}=0$ ($\tilde{F}^{(s)}_{\mathbf{k}-\mathbf{k}_0}$ is centered at $\mathbf{k}=\mathbf{k}_0$) and having a very small width $\Delta k^{(s)} \ll \pi$ [1]. Notice that we have chosen an initial coin state which is independent of $\mathbf{k}$. From here one must distinguish between *regular points*, where eigenvectors $\left|\phi^{(s)}_{\mathbf{k}}\right\rangle$ have a smooth dependence on $\mathbf{k}$ close to $\mathbf{k}_0$, and *degeneracy points*, where eigenvectors have wild variations around them, as we will see later.

According to (3.14) the initial condition (3.24) reads in position representation

$$|\psi_{\mathbf{x},0}\rangle = e^{\mathrm{i}\mathbf{k}_0\cdot\mathbf{x}} \sum_{s=1}^{2N} F^{(s)}_{\mathbf{x},0} \left|\phi^{(s)}_{\mathbf{k}_0}\right\rangle, \tag{3.25}$$

where

$$F^{(s)}_{\mathbf{x},0} = \int \frac{\mathrm{d}^N\mathbf{k}}{(2\pi)^N} e^{\mathrm{i}(\mathbf{k}-\mathbf{k}_0)\cdot\mathbf{x}} \tilde{F}^{(s)}_{\mathbf{k}-\mathbf{k}_0} \tag{3.26}$$

is a wide and smooth function of $\mathbf{x}$ because $\tilde{F}^{(s)}_{\mathbf{k}}$ is concentrated around $\mathbf{k}=0$. Hence in real space our initial condition consists of a coin state $\left|\phi^{(s)}_{\mathbf{k}_0}\right\rangle$ equal at

[1] Obviously this width will be different, in general, along different directions in $\mathbf{k}$-space. However we are just interested in an order-of-magnitude estimate for $\Delta k^{(s)}$. To be conservative this width can be taken as the largest standard deviation of $\left|\tilde{F}^{(s)}_{\mathbf{k}}\right|^2$ in any direction or, more formally, as the largest eigenvalue of the covariance matrix σ, such that $\left(\sigma^2\right)_{ij} = \int \mathrm{d}^N\mathbf{k}\left(k_i-\bar{k}_i\right)\left(k_j-\bar{k}_j\right)\rho^{(s)}_{\mathbf{k}}$ with $\rho^{(s)}_{\mathbf{k}} = \left|\tilde{F}^{(s)}_{\mathbf{k}}\right|^2 / \int \mathrm{d}^N\mathbf{k}\left|\tilde{F}^{(s)}_{\mathbf{k}}\right|^2$ and $\bar{k}_i = \int \mathrm{d}^N\mathbf{k} k_i \rho^{(s)}_{\mathbf{k}}$, $i,j \in \{1,\ldots,N\}$. In our case $\bar{k}_i = 0$ as $\tilde{F}^{(s)}_{\mathbf{k}}$ is assumed to be centered at the origin, hence $\tilde{F}^{(s)}_{\mathbf{k}-\mathbf{k}_0}$ is centered at $\mathbf{k}_0$. Indeed it is this condition that determines the value of $\mathbf{k}_0$

all points, multiplied by the carrier $\exp\left[\mathrm{i}\left(\mathbf{k}_0\cdot\mathbf{x}\right)\right]$ and by a wide and smooth function of space, $F^{(s)}_{\mathbf{x},0}$. We see then that the type of initial conditions we are dealing with are very close to the plane waves of momentum $\mathbf{k}_0$ of the QW, given by $e^{\mathrm{i}\mathbf{k}_0\cdot\mathbf{x}}\left|\phi^{(s)}_{\mathbf{k}_0}\right\rangle$.

3.3.1 Regular points

For regular points (i.e., far from degeneracies) the initial condition (3.24) determines the weight functions (3.20) as

$$\tilde{f}^{(s)}_{\mathbf{k}}=\sum_{s'}\tilde{F}^{(s')}_{\mathbf{k}-\mathbf{k}_0}\langle\phi^{(s)}_{\mathbf{k}}\mid\phi^{(s')}_{\mathbf{k}_0}\rangle=\tilde{F}^{(s)}_{\mathbf{k}-\mathbf{k}_0}+O\left(\Delta k^{(s)}\right),\tag{3.27}$$

where we took into account that the eigenvectors $\left|\phi^{(s)}_{\mathbf{k}_0}\right\rangle$ vary smoothly around $\mathbf{k}=\mathbf{k}_0$ and that only for $\mathbf{k}\approx\mathbf{k}_0$ the function $\tilde{F}^{(s)}_{\mathbf{k}-\mathbf{k}_0}$ is non-vanishing. Note that we cannot make such an approximation in the case of degeneracy points because of the strong variations of the eigenvectors around them.

Now, the system will evolve according to (3.23). Approximating the eigenvector $\left|\phi^{(s)}_{\mathbf{k}}\right\rangle$ appearing in (3.23) by $\left|\phi^{(s)}_{\mathbf{k}_0}\right\rangle$ using the same arguments as before, the partial waves $\left|\psi^{(s)}_{\mathbf{x},t}\right\rangle$ can be written as

$$\left|\psi^{(s)}_{\mathbf{x},t}\right\rangle=F^{(s)}_{\mathbf{x},t}\exp\left[\mathrm{i}\left(\mathbf{k}_0\cdot\mathbf{x}-\omega^{(s)}_{\mathbf{k}_0}t\right)\right]\left|\phi^{(s)}_{\mathbf{k}_0}\right\rangle+O\left(\Delta k^{(s)}\right),\tag{3.28}$$

$$F^{(s)}_{\mathbf{x},t}=\int\frac{\mathrm{d}^N\mathbf{k}}{(2\pi)^N}\exp\left(\mathrm{i}\left[(\mathbf{k}-\mathbf{k}_0)\cdot\mathbf{x}-\left(\omega^{(s)}_{\mathbf{k}}-\omega^{(s)}_{\mathbf{k}_0}\right)t\right]\right)\times\tilde{F}^{(s)}_{\mathbf{k}-\mathbf{k}_0},\tag{3.29}$$

where we have defined new functions $\left\{F^{(s)}_{\mathbf{x},t}\right\}_{s=1}^{2N}$. Note that, at $t=0$, $\left|\psi^{(s)}_{\mathbf{x},0}\right\rangle=F^{(s)}_{\mathbf{x},0}\exp\left[\mathrm{i}\left(\mathbf{k}_0\cdot\mathbf{x}\right)\right]\left|\phi^{(s)}_{\mathbf{k}_0}\right\rangle$, in agreement with (3.25).

The problem is then solved if functions $\left\{F^{(s)}_{\mathbf{x},t}\right\}_{s=1}^{2N}$ are determined. Instead of doing so by brute force, i.e. by integrating –maybe numerically– Eq. (3.29), what we do now is to look for a continuous wave equation that, by comparison with other known cases, sheds light onto the expected behavior of the QW. In order to test the quality of our analysis based on our continuous equations and the knowledge of the dispersion relations, we will present some plots that are obtained directly by iteration of Eq. (3.12) without any approximation.

To avoid confusion, we introduce a function $F^{(s)}(\mathbf{x},t)$ of continuous real arguments exactly in the same way as in (3.29) as there is nothing forbidding such

a definition. We have then $F^{(s)}_{\mathbf{x},t} = F^{(s)}(\mathbf{x},t)$ for $\mathbf{x} \in \mathbb{Z}^N$ and $t \in \mathbb{N}$. In order to simplify the derivation we rewrite Eq. (3.29) by making the variable change $\mathbf{k} - \mathbf{k}_0 \to \mathbf{k}$. Finally, as for the limits of integration (originally from $-\pi$ to $+\pi$ for each dimension), we extend them from $-\infty$ to $+\infty$ in agreement with the continuous limit. We then have

$$F^{(s)}(\mathbf{x},t) \equiv \int \frac{\mathrm{d}^N\mathbf{k}}{(2\pi)^N} \exp\left[\mathrm{i}\left(\mathbf{k}\cdot\mathbf{x} - \left[\omega^{(s)}_{\mathbf{k}_0+\mathbf{k}} - \omega^{(s)}_{\mathbf{k}_0}\right]t\right)\right] \times \tilde{F}^{(s)}_{\mathbf{k}}. \tag{3.30}$$

Let us obtain the (approximate) wave equation. First we take the time derivative of (3.30) and get

$$\begin{aligned}\mathrm{i}\partial_t F^{(s)}(\mathbf{x},t) = \int \frac{\mathrm{d}^N\mathbf{k}}{(2\pi)^N} \exp\left[\mathrm{i}\left(\mathbf{k}\cdot\mathbf{x} - \left[\omega^{(s)}_{\mathbf{k}_0+\mathbf{k}} - \omega^{(s)}_{\mathbf{k}_0}\right]t\right)\right] \\ \times \left[\omega^{(s)}_{\mathbf{k}_0+\mathbf{k}} - \omega^{(s)}_{\mathbf{k}_0}\right]\tilde{F}^{(s)}_{\mathbf{k}}.\end{aligned} \tag{3.31}$$

Then we Taylor expand the function $\left[\omega^{(s)}_{\mathbf{k}_0+\mathbf{k}} - \omega^{(s)}_{\mathbf{k}_0}\right]$ (except in the exponent: otherwise large errors at long times would be introduced) around $\mathbf{k} = 0$,

$$\omega^{(s)}_{\mathbf{k}_0+\mathbf{k}} - \omega^{(s)}_{\mathbf{k}_0} = \sum_{i=1}^{N} \varpi^{(s)}_i k_i + \frac{1}{2!}\sum_{i,j=1}^{N} \varpi^{(s)}_{ij} k_i k_j + \cdots, \tag{3.32}$$

where

$$\begin{aligned}\varpi^{(s)}_i &= \partial\omega^{(s)}_{\mathbf{k}_0+\mathbf{k}}/\partial k_i\Big|_{\mathbf{k}=0} \\ &= \partial\omega^{(s)}_{\mathbf{k}}/\partial k_i\Big|_{\mathbf{k}=\mathbf{k}_0} = \left[\mathbf{v}^{(s)}_{\mathrm{g}}(\mathbf{k}_0)\right]_i,\end{aligned} \tag{3.33}$$

$$\begin{aligned}\varpi^{(s)}_{ij} &= \partial^2\omega^{(s)}_{\mathbf{k}_0+\mathbf{k}}/\partial k_i\partial k_j\Big|_{\mathbf{k}=0} \\ &= \partial^2\omega^{(s)}_{\mathbf{k}}/\partial k_i\partial k_j\Big|_{\mathbf{k}=\mathbf{k}_0},\end{aligned} \tag{3.34}$$

etc. In the latter equation, $\mathbf{v}^{(s)}_{\mathrm{g}}(\mathbf{k}_0) = \nabla_{\mathbf{k}}\omega^{(s)}_{\mathbf{k}}\Big|_{\mathbf{k}=\mathbf{k}_0}$ is the group velocity at the point $\mathbf{k} = \mathbf{k}_0$ (see discussion below). Now it is trivial to transform the so-obtained right hand side of Eq. (3.31) as a sum of spatial derivatives of $F^{(s)}(\mathbf{x},t)$, leading to the result

$$\mathrm{i}\frac{\partial F^{(s)}(\mathbf{x},t)}{\partial t} = -\mathrm{i}\mathbf{v}^{(s)}_{\mathrm{g}}(\mathbf{k}_0)\cdot\nabla F^{(s)} - \frac{1}{2!}\sum_{i,j=1}^{N} \varpi^{(s)}_{ij}\frac{\partial^2 F^{(s)}}{\partial x_i\partial x_j} + \cdots, \tag{3.35}$$

which is the sought continuous wave equation. One should understand that, in general, few terms are necessary on the right hand side of Eq. (3.35) because $F^{(s)}(\mathbf{x},t)$ is a slowly varying function of space, as commented.

The first term on the right hand side of the wave equation is an advection term, implying that the initial condition $F_0^{(s)}(\mathbf{x}) \equiv F^{(s)}(\mathbf{x},0)$ is shifted in time as $F^{(s)}(\mathbf{x},t) = F_0^{(s)}\left(\mathbf{x} - \mathbf{v}_{\mathrm{g}}^{(s)}(\mathbf{k}_0)\,t\right)$ without distortion, to the leading order. In fact we can get rid of this term by defining a moving reference frame $\mathbf{X}$ such that

$$\mathbf{X} = \mathbf{x} - \mathbf{v}_{\mathrm{g}}^{(s)}(\mathbf{k}_0)\,t, \quad A^{(s)}(\mathbf{X},t) = F^{(s)}(\mathbf{x},t)\,, \tag{3.36}$$

and then Eq. (3.35) becomes

$$\mathrm{i}\frac{\partial A^{(s)}(\mathbf{X},t)}{\partial t} = -\frac{1}{2}\sum_{i,j=1}^{N} \varpi_{ij}^{(s)} \frac{\partial^2 A^{(s)}}{\partial X_i \partial X_j} + \cdots\,, \tag{3.37}$$

which is an N-dimensional Schrödinger-like equation, to the leading order. This means that the evolution of the wave packet consists of the advection of the initial wave packet at the corresponding group velocity and, on top of that, the wavefunction itself evolves according to (3.37). Equation (3.37) is a main result of this chapter as it governs the nontrivial dynamics of the QW when spatially extended initial conditions, as we have defined them, are considered. It evidences the role played by the dispersion relations as anticipated: For distributions whose DFT is centered around some $\mathbf{k}_0$, the local variations of ω around $\mathbf{k}_0$ determine the type of wave equation controlling the QW dynamics.

A few additional remarks: First, if the initial condition only projects onto one of the sheets of the dispersion relation (hence the sum in s in (3.24) reduces to a single element), all $F^{(s)}(\mathbf{X},t)$ will be zero, except the one corresponding to the chosen eigenvector. This means that the coin state is preserved along the evolution, to the leading order. Second, if the initial state projects onto several eigenvectors the probability of finding the walker at $(\mathbf{x},t)$, irrespectively of the coin state, follows from (3.6), (3.22) and (3.28), and reads

$$P_{\mathbf{x},t} = \sum_s \left|F_{\mathbf{x},t}^{(s)}\right|^2 = \sum_s \left|A^{(s)}(\mathbf{X},t)\right|^2, \tag{3.38}$$

to the leading order, where we used $\langle \phi_{\mathbf{k}_0}^{(s)} \mid \phi_{\mathbf{k}_0}^{(s')} \rangle = \delta_{s,s'}$. Hence $P_{\mathbf{x},t}$ is just the sum of partial probabilities: there is not interference among the different sub-QW's.

Finally, one might consider an initial condition consisting in a linear combination of initial terms of the form Eq. (3.25), each having a different $\mathbf{k}_0$. It is easy to see that we can generalize the above treatment to this case, each term evolving in accordance to the corresponding $\mathbf{k}_0$: Of course, this situation may show a more complicated behavior arising from interference effects among the different terms. We have not considered this richer evolution here, and we have restricted ourselves to a simpler study, where the evolution can be traced back to the analysis of the dispersion relation around a single $\mathbf{k}_0$ point.

3.3.2 Degeneracy points

This case requires special care because there are eigenvectors of the QW that vary strongly around the degeneracy, forbidding the very initial approximation taken in the case of regular points, namely Eq. (3.27). Given the singular nature of the problem we will try to give a rather general (but not fully general) theory here: We will present a treatment that covers the case of (hyper-) conical intersections. These appear in the 2D Grover walk (as we will see in the next section), in the 3D Alternate QW [53] (that will not be treated here) and, very likely, in some other cases. The basic assumptions are: (i) There are just two (hyper-)sheets in the dispersion relation that display a conical intersection at $\mathbf{k} = \mathbf{k}_{\mathrm{D}}$ (diabolical point) and we label them by $s = 1, 2$ for the sake of definiteness; and (ii) There are other sheets, degenerate with the diabolical ones at $\mathbf{k} = \mathbf{k}_{\mathrm{D}}$, whose associated frequencies $\omega_{\mathbf{k}}^{(s)}$ are constant around the diabolical point.

In order to alleviate the notation we will denote by ω_{D} the value of the degenerate frequencies at $\mathbf{k} = \mathbf{k}_{\mathrm{D}}$

$$\omega_{\mathrm{D}} = \omega_{\mathbf{k}_{\mathrm{D}}}^{(1)} = \omega_{\mathbf{k}_{\mathrm{D}}}^{(2)}. \tag{3.39}$$

Notice that there can be other sheets with $\omega_{\mathbf{k}_{\mathrm{D}}}^{(s\neq 1,2)} = \omega_{\mathrm{D}}$ (as it happens with $\omega_{\mathbf{k}_{\mathrm{D}}}^{(3)}$ in the 2D Grover map).

We consider an initial wave packet defined in reciprocal space by

$$\left|\tilde{\psi}_{\mathbf{k},0}\right\rangle = \tilde{F}_{\mathbf{k}-\mathbf{k}_{\mathrm{D}}} \left|\Xi\right\rangle, \tag{3.40}$$

where $|\Xi\rangle$ is an eigenstate of the coin operator $\hat{C}_{\mathbf{k}}$ at $\mathbf{k} = \mathbf{k}_{\mathrm{D}}$, and $\tilde{F}_{\mathbf{k}-\mathbf{k}_{\mathrm{D}}}$ is again a narrow function centered at $\mathbf{k} = \mathbf{k}_{\mathrm{D}}$. In the position representation this initial condition reads, see (3.14),

$$|\,\psi_{\mathbf{x},0}\rangle = e^{\mathrm{i}\mathbf{k}_{\mathrm{D}}\cdot\mathbf{x}} F_{\mathbf{x},0} \left|\Xi\right\rangle, \tag{3.41}$$

where $F_{\mathbf{x},0} = \int \frac{\mathrm{d}^N\mathbf{k}}{(2\pi)^N} e^{\mathrm{i}(\mathbf{k}-\mathbf{k}_\mathrm{D})\cdot\mathbf{x}} \tilde{F}_{\mathbf{k}-\mathbf{k}_\mathrm{D}}$ is the DFT of $\tilde{F}_\mathbf{k}$. Hence, as in the regular case, $|\Xi\rangle$ represents the state of the coin at the initial condition. Clearly $|\Xi\rangle$ is not unique because of the degeneracy. We do not use the notation $\left|\phi^{(s)}_{\mathbf{k}_\mathrm{D}}\right\rangle$ but instead $|\Xi\rangle$ because the former are ill defined, as we have seen in the example of the 2D Grover walk.

The initial condition (3.40) determines the weight functions (3.20) as

$$\tilde{f}^{(s)}_\mathbf{k} = \tilde{F}_{\mathbf{k}-\mathbf{k}_\mathrm{D}} \langle \phi^{(s)}_\mathbf{k} \mid \Xi\rangle. \tag{3.42}$$

We will assume that $|\Xi\rangle$ does not project on regular sheets (those not degenerate with the conical intersection); otherwise those projections will evolve as described in the previous case of regular points. This is equivalent to saying that, in the remainder of this subsection, all sums on s will be restricted to sheets that are degenerate at the conical intersection.

Definition (3.42) poses no problem but for $\mathbf{k} = \mathbf{k}_\mathrm{D}$. However, as this is a single point (a set of null measure) its influence on the final result, given by integrals in $\mathbf{k}$, is null [2].

A main difference with the regular case is seen at this stage because there is not any choice of the initial coin state $|\Xi\rangle$ making that only one value of s be populated (remind that $\left|\phi^{(s)}_\mathbf{k}\right\rangle$ vary strongly around $\mathbf{k} = \mathbf{k}_\mathrm{D}$). This has consequences as we see next.

Now the system will evolve according to (3.23). The partial waves $\left|\psi^{(s)}_{\mathbf{x},t}\right\rangle$ read now

$$\left|\psi^{(s)}_{\mathbf{x},t}\right\rangle = e^{\mathrm{i}\left(\mathbf{k}_\mathrm{D}\cdot\mathbf{x}-\omega_\mathrm{D}t\right)} \left|\mathbf{F}^{(s)}_{\mathbf{x},t}\right\rangle \tag{3.43}$$

$$\left|\mathbf{F}^{(s)}_{\mathbf{x},t}\right\rangle = \int \frac{\mathrm{d}^N\mathbf{k}}{(2\pi)^N} \exp\left[\mathrm{i}\left(\mathbf{k}\cdot\mathbf{x} - \left[\omega^{(s)}_{\mathbf{k}_\mathrm{D}+\mathbf{k}} - \omega_\mathrm{D}\right] t\right)\right] \times \tilde{F}_\mathbf{k}\ \langle \phi^{(s)}_{\mathbf{k}_\mathrm{D}+\mathbf{k}} \mid \Xi\rangle \mid \phi^{(s)}_{\mathbf{k}_\mathrm{D}+\mathbf{k}}\rangle, \tag{3.44}$$

where we made the variable change $\mathbf{k} - \mathbf{k}_\mathrm{D} \to \mathbf{k}$, and extended the limits of integration to infinity as corresponding to the continuous limit. Note that $\omega^{(s\neq 1,2)}_{\mathbf{k}_\mathrm{D}} - \omega_\mathrm{D} = 0$ according to assumption (ii) above. As in the regular case, the evolution has a fast part, given by the carrier wave $e^{\mathrm{i}\left(\mathbf{k}_\mathrm{D}\cdot\mathbf{x}-\omega_\mathrm{D}t\right)}$, and a slow part (both in time and in space) given by $\left|\mathbf{F}^{(s)}_{\mathbf{x},t}\right\rangle$.

[2] The only problematic case would be when $\tilde{F}_{\mathbf{k}-\mathbf{k}_0}$ equals the Dirac delta $\delta^N(\mathbf{k}-\mathbf{k}_\mathrm{D})$. This is however an unphysical case as it represents an unnormalizable state.

Note that the previous approximations reproduce the correct result at $t = 0$, Eq. (3.41), upon using that $\sum_s \left|\phi^{(s)}_{\mathbf{k}_\mathrm{D}+\mathbf{k}}\right\rangle \left\langle\phi^{(s)}_{\mathbf{k}_\mathrm{D}+\mathbf{k}}\right|$ is very approximately the unit operator in the *degenerate* subspace, to which $|\Xi\rangle$ belongs.

It is important to understand that the vector (coin) part of the state evolves in time in this diabolical point situation, because more than one of the sheets that become degenerate at the conical intersection become necessarily populated, i.e. there are at least two s values for which $\langle\phi^{(s)}_{\mathbf{k}_\mathrm{D}+\mathbf{k}} \mid \Xi\rangle \neq 0$, unlike the regular case.

Finding a wave equation in this case is by far more complicated than in the regular case, as the vector part of $\left|\mathbf{F}^{(s)}_{\mathbf{x},t}\right\rangle$ depends on time (because $\left|\phi^{(s)}_{\mathbf{k}_\mathrm{D}+\mathbf{k}}\right\rangle$ cannot be approximated by $\left|\phi^{(s)}_{\mathbf{k}_\mathrm{D}}\right\rangle$), unlike the regular case where it can be approximated by the constant vector $\left|\phi^{(s)}_{\mathbf{k}_0}\right\rangle$, see (3.28). We will not try deriving such a wave equation but conform ourselves with trying to understand the evolution of the system under the assumed conditions.

What we can say is that the frequency offsets $\left[\omega^{(s=1,2)}_{\mathbf{k}_\mathrm{D}+\mathbf{k}} - \omega_\mathrm{D}\right]$ in (3.44) are conical for small $\mathbf{k}$ (i.e. in the vicinity of the diabolical point, which is the region selected by $\tilde{F}_\mathbf{k}$); in other words, $\left[\omega^{(s=1,2)}_{\mathbf{k}_\mathrm{D}+\mathbf{k}} - \omega_\mathrm{D}\right] \approx \pm ck$, where c is the group speed (the modulus of the group velocity) and $k = |\mathbf{k}|$; see the 2D Grover walk case in Eq. (3.52), where $c = 1/\sqrt{2}$. For the rest of sheets we have assumed $\omega^{(s\neq 1,2)}_{\mathbf{k}_\mathrm{D}} - \omega_\mathrm{D} = 0$. Hence we can write, from (3.44)

$$\left|\mathbf{F}^{(s=1,2)}_{\mathbf{x},t}\right\rangle = \int \frac{\mathrm{d}^N\mathbf{k}}{(2\pi)^N} \exp\left[\mathrm{i}\left(\mathbf{k}\cdot\mathbf{x} \mp ckt\right)\right] \times \tilde{F}_\mathbf{k} \langle\phi^{(s)}_{\mathbf{k}_\mathrm{D}+\mathbf{k}} \mid \Xi\rangle \mid \phi^{(s)}_{\mathbf{k}_\mathrm{D}+\mathbf{k}}\rangle, \tag{3.45}$$

while the rest of partial waves verify

$$\left|\mathbf{F}^{(s\neq 1,2)}_{\mathbf{x},t}\right\rangle = \int \frac{\mathrm{d}^N\mathbf{k}}{(2\pi)^N} \exp\left[\mathrm{i}\left(\mathbf{k}\cdot\mathbf{x}\right)\right] \times \tilde{F}_\mathbf{k} \langle\phi^{(s)}_{\mathbf{k}_\mathrm{D}+\mathbf{k}} \mid \Xi\rangle \mid \phi^{(s)}_{\mathbf{k}_\mathrm{D}+\mathbf{k}}\rangle = \left|\mathbf{F}^{(s\neq 1,2)}_{\mathbf{x},0}\right\rangle, \tag{3.46}$$

which is a constant, equal to its initial value. Hence, the projection of the initial state onto the sheets of constant frequency does not evolve, as expected, leading to a possible localization of a part of the initial wave packet. We thus consider in the following that $\langle\phi^{(s\neq 1,2)}_{\mathbf{k}_\mathrm{D}+\mathbf{k}} \mid \Xi\rangle = 0$.

Regarding the sheets $s = 1, 2$ we cannot progress unless we assume some property of the eigenvectors $\left|\phi^{(s)}_{\mathbf{k}_\mathrm{D}+\mathbf{k}}\right\rangle$. We will assume that $\left|\phi^{(s=1,2)}_{\mathbf{k}_\mathrm{D}+\mathbf{k}}\right\rangle$ (for $\mathbf{k}$ close to zero, i.e. around the diabolical point) depend just on the angular part of $\mathbf{k}$ (let us call it Ω) but not on its modulus k. We also restrict ourselves to cases in which

$\tilde{F}_{\mathbf{k}}$ only depends on k (spherical symmetry), i.e. $\tilde{F}_{\mathbf{k}} = \tilde{F}_k$. Hence we write the integral in (3.45) in (N-dimensional) spherical coordinates as

$$\left|\mathbf{F}_{\mathbf{x},t}^{(s=1,2)}\right\rangle = (2\pi)^{-N} \int \mathrm{d}k \exp\left(\mp \mathrm{i}ckt\right) k^{N-1} \tilde{F}_k \left|\mathbf{E}_{\mathbf{x}}^{(s)}\left(k\right)\right\rangle, \tag{3.47}$$

$$\left|\mathbf{E}_{\mathbf{x}}^{(s)}\left(k\right)\right\rangle = \int \mathrm{d}^N\Omega \exp\left(\mathrm{i}\mathbf{k}\cdot\mathbf{x}\right) \langle \phi_{\mathbf{k}_\mathrm{D}+\mathbf{k}}^{(s)} \mid \Xi\rangle \mid \phi_{\mathbf{k}_\mathrm{D}+\mathbf{k}}^{(s)}\rangle, \tag{3.48}$$

where we wrote $\mathrm{d}^N\mathbf{k} = k^{N-1}\mathrm{d}k\mathrm{d}^N\Omega$ and $\mathrm{d}^N\Omega$ is the N-dimensional solid angle element.

As we mentioned at the end of the previous subsection, one might also study more complicated initial situations, by combining initial terms, each consisting on a different $\mathbf{k}_0$. As an example, assume that $\mathbf{k}_0$ can take two different values $\mathbf{k}_{01}$ and $\mathbf{k}_{02}$. We can face different situations. If both values are far from degeneracies, the discussion of subsection 3.3.1 applies. If one of them, say $\mathbf{k}_{01}$, shows a degeneracy, the treatment developed on the present subsection has to be taken into account for that particular term in the initial state. Finally, one can have a situation in which both values are close to each other and lie close to a degeneracy point $\mathbf{k}_{01} \simeq \mathbf{k}_{02} \simeq \mathbf{k}_D$. This case might lead to very complicated behaviors, which are beyond the scope of this thesis (in fact, as we show later, even an initial condition consisting on a single value $\mathbf{k}_0$ close to a degeneracy can give rise to very reach phenomena).

Up to here the theory is somehow general. However we cannot progress unless we particularize to some special case. We shall do this below for the 2D Grover walk.

3.4 Application to the 2D Grover QW

So far we have derived general expressions for the N–dimensional QW. In this section we consider the special case of the two–dimensional QW using the Grover coin operator.

3.4.1 Diagonalization of the 2D Grover map: Dispersion relations and diabolical points

The so-called Grover coin of dimension $2N$ has matrix elements $C_{\alpha',\eta'}^{\alpha,\eta} = 1/N - \delta_{\alpha,\alpha'}\delta_{\eta,\eta'}$. In the present case ($N = 2$), the corresponding matrix $C_{\mathbf{k}}$ (3.17), with

$\mathbf{k} = (k_1, k_2)$, has the form

$$C_{\mathbf{k}} = \frac{1}{2}\begin{pmatrix} -e^{-\mathrm{i}k_1} & e^{-\mathrm{i}k_1} & e^{-\mathrm{i}k_1} & e^{-\mathrm{i}k_1} \\ e^{\mathrm{i}k_1} & -e^{\mathrm{i}k_1} & e^{\mathrm{i}k_1} & e^{\mathrm{i}k_1} \\ e^{-\mathrm{i}k_2} & e^{-\mathrm{i}k_2} & -e^{-\mathrm{i}k_2} & e^{-\mathrm{i}k_2} \\ e^{\mathrm{i}k_2} & e^{\mathrm{i}k_2} & e^{\mathrm{i}k_2} & -e^{\mathrm{i}k_2} \end{pmatrix}, \tag{3.49}$$

whose diagonalization yields the eigenvalues $\lambda_{\mathbf{k}}^{(s)} = \exp\left(-\mathrm{i}\omega_{\mathbf{k}}^{(s)}\right)$ with

$$\omega_{\mathbf{k}}^{(1)} = \pi + \Omega_{\mathbf{k}},\ \omega_{\mathbf{k}}^{(2)} = \pi - \Omega_{\mathbf{k}},\ \omega_{\mathbf{k}}^{(3)} = \pi,\ \omega_{\mathbf{k}}^{(4)} = 0, \tag{3.50}$$

where

$$\Omega_{\mathbf{k}} = \arccos\left[\frac{1}{2}\left(\cos k_1 + \cos k_2\right)\right] \in [0, \pi]\,. \tag{3.51}$$

Note that adding a multiple integer of 2π to any of the ω's does not change anything because time is discrete and runs in steps of 1, see (3.23).

We see, according to (3.50), that the last two eigenvalues $\lambda_{\mathbf{k}}^{(3,4)} = \exp\left(-\mathrm{i}\omega_{\mathbf{k}}^{(3,4)}\right) = -1, 1$ do not depend on $\mathbf{k}$, and the first two eigenvalues $\lambda_{\mathbf{k}}^{(1,2)} = \exp\left(-\mathrm{i}\omega_{\mathbf{k}}^{(1,2)}\right) = -\exp\left(\mp\mathrm{i}\Omega_{\mathbf{k}}\right)$ are complex-conjugate of each other, hence we can choose $\Omega_{\mathbf{k}} \in [0, \pi]$ without loss of generality. A plot of the dispersion relations (3.50) is given in Fig.3.1, where five degeneracy points (the origin and the four corners, see also Fig.3.2) are observed with 3-fold degeneracies. Moreover the frequencies $\pm\Omega_{\mathbf{k}}$ have a conical form (diabolo-like) at those degeneracies and this is why we call them *diabolical points*, in analogy to other diabolos found in different systems [70–74, 78–81]. At the central diabolical point the degeneracy is between $\omega_{\mathbf{k}}^{(s=1,2,4)}$, while at the corners it is between $\omega_{\mathbf{k}}^{(s=1,2,3)}$.

For the sake of later use we note that the frequency $\Omega_{\mathbf{k}}$ reads, close to the diabolical point $\mathbf{k} = 0$,

$$\Omega_{\mathbf{k}} \simeq \frac{k}{\sqrt{2}} - \frac{k^3 \cos(2\theta)}{48\sqrt{2}} + O\left(k^5\right), \tag{3.52}$$

where $\mathbf{k} = k\,(\cos\theta, \sin\theta)$. This means that, very close to the diabolical point, the frequency $\Omega_{\mathbf{k}}$ actually has a conical dependence on the wavenumber. Later we will understand the consequences of the existence of these points.

The fact that $\omega_{\mathbf{k}}^{(s=3,4)}$ are constant causes that $\left|\psi_{\mathbf{x},t}^{(s=3,4)}\right\rangle$, see (3.23), do not have a wave character; only $\left|\psi_{\mathbf{x},t}^{(s=1,2)}\right\rangle$ are true waves. Hence propagation in the 2D Grover walk occurs only if the initial condition projects onto subspaces 1 or

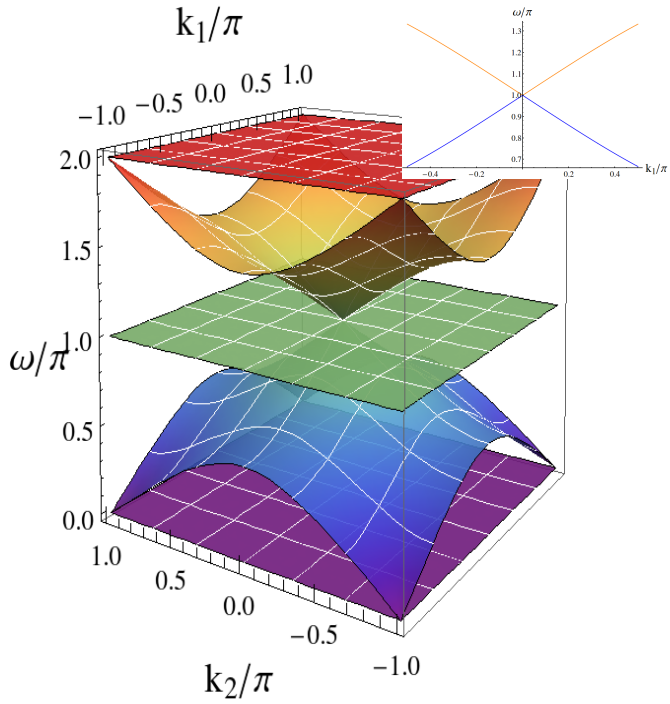

Figure 3.1: (Main Figure): Dispersion relation sketch around the diabolic point. The value of ω/π is plotted for the different sheets (i.e., different eigenvalues). The middle (flat) surface corresponds to $\omega_k^{(3)} = \pi$, the surface with values ranging from 1 to 2 corresponds to $\omega_k^{(1)}$. The bottom plane is associated with $\omega_k^{(4)}$ and the surface with values ranging from 0 to 1 corresponds to $\omega_k^{(2)}$. (Inset): Detail of $\omega_k^{(1)}$ and $\omega_k^{(2)}$ around the origin (orange and blue curves, respectively) for $k_2 = 0$ as a function of k_1, showing the intersection at the diabolical point.

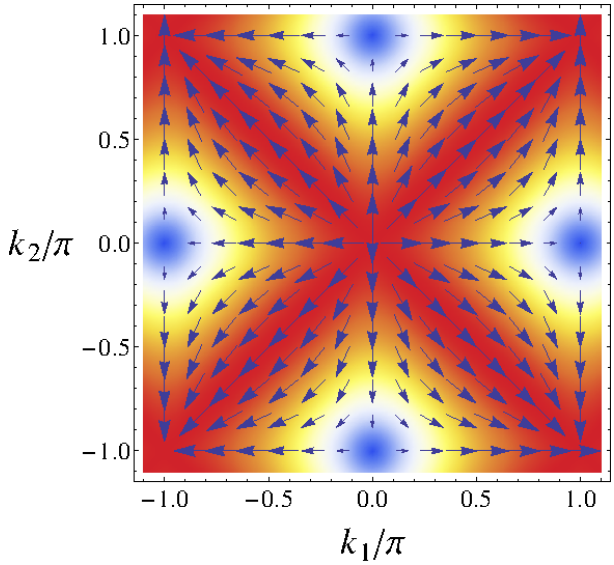

Figure 3.2: Vector plot of the group velocity (shown as arrows), superimposed to a density plot of the velocity modulus Eq. (3.51).

2; otherwise the walker remains localized. This explains why strong localization in the 2D Grover map is usually observed, as first noted in Ref. [61]. All this can be put more formally in terms of the group velocity $\mathbf{v}_{\mathrm{g}}(\mathbf{k})$ of the waves in the system, given by the gradient (in $\mathbf{k}$) of the wave frequency. The group velocity, as in any linear wave system, has the meaning of velocity at which an extended wave packet, centered in $\mathbf{k}$-space around some value $\mathbf{k}_0$, moves (there are other effects affecting extended wavepackets which we analyze below). In our case $\omega_{\mathbf{k}}^{(s=3,4)}$ are constant, hence their gradient is null: these eigenvalues entail no motion. On the contrary $\omega_{\mathbf{k}}^{(s=1,2)}$ depend on $\mathbf{k}$ (3.50,3.51) and then define non null group velocities:

$$\mathbf{v}_{\mathrm{g}}^{(1,2)}(\mathbf{k}) = \pm\nabla_{\mathbf{k}}\Omega_{\mathbf{k}}, \tag{3.53}$$

where the plus and minus signs stand for $s = 1, 2$, respectively. Using (3.51) these velocities become

$$\mathbf{v}_{\mathrm{g}}^{(1,2)}(\mathbf{k}) = \pm\frac{(\sin k_1, \sin k_2)}{\sqrt{4 - (\cos k_1 + \cos k_2)^2}}. \tag{3.54}$$

Hence the maximum group velocity modulus in the 2D Grover walk is $\frac{1}{\sqrt{2}}$, as can be easily checked and is obtained, in particular, along the diagonals $k_2 = \pm k_1$.

This is the maximum speed at which any feature of the QW can propagate. Figure 3.2 displays a vector plot of $\mathbf{v}_{\mathrm{g}}^{(1,2)}(\mathbf{k})$ where a number of interesting points (in $\mathbf{k}$ space) is revealed: On the one hand there are points of null group velocity, located at $\mathbf{k} = (0, \pm\pi)$ and at $\mathbf{k} = (\pm\pi, 0)$, in correspondence with the saddle points observed in Fig 3.1. On the other hand there are five *singular* points at $\mathbf{k} = (0, 0)$ as well as at the four corners. These points are singular because the group velocity is undefined at them (they look like sources or sinks). We note that these points coincide with the diabolical points in Fig 3.1.

We find it worth mentioning that in two–dimensional QWs with coin operators other that the Grover, diabolical points are also found, as we have checked by using the DFT coin [59] that displays several conical intersections. In this case of the DFT coin none of the four leaves of the dispersion relation is constant. We mention too that a behavior very similar to that of the 2D Grover walk is found in the Alternate QW [53], except for the fact that in this last case there are no constant surfaces in the dispersion relation (and hence no localization phenomena).

3.4.2 Eigenvectors

The eigenvectors of the 2D Grover walk matrix (3.49) are given by [16]. Use of these eigenvalues in (3.23) allows finally to compute the state of the system at any time.

Whenever $\mathbf{k}$ is not close to a diabolical point these eigenvectors vary smoothly around $\mathbf{k}$. Here we just want to study the behavior of the eigenvectors close to the diabolical point at $\mathbf{k} = \mathbf{k}_{\mathrm{D}} \equiv (0, 0)$ –at the corners the conclusions are similar. We find it convenient to use polar coordinates $(k_1, k_2) = (k\cos\theta, k\sin\theta)$.

Performing the limit for $k \to 0$ we find

$$\phi^{(1)}_{\mathbf{k}} = \frac{1}{2\sqrt{2}} \begin{pmatrix} 1+\sqrt{2}\cos\theta \\ 1-\sqrt{2}\cos\theta \\ -1-\sqrt{2}\sin\theta \\ -1+\sqrt{2}\sin\theta \end{pmatrix},$$

$$\phi^{(2)}_{\mathbf{k}} = \frac{1}{2\sqrt{2}} \begin{pmatrix} 1-\sqrt{2}\cos\theta \\ 1+\sqrt{2}\cos\theta \\ -1+\sqrt{2}\sin\theta \\ -1-\sqrt{2}\sin\theta \end{pmatrix},$$

$$\phi^{(3)}_{\mathbf{k}} = \frac{1}{\sqrt{2}} \begin{pmatrix} \sin\theta \\ -\sin\theta \\ \cos\theta \\ -\cos\theta \end{pmatrix}, \quad \phi^{(4)}_{\mathbf{k}} = \frac{1}{2} \begin{pmatrix} 1 \\ 1 \\ 1 \\ 1 \end{pmatrix}. \tag{3.55}$$

Hence, close to the diabolical point $\mathbf{k}_{\mathrm{D}}$, there are three eigenvectors, corresponding to $s = 1, 2, 3$, displaying a strong azimuthal dependence, while $\phi^{(4)}_{\mathbf{k}}$ is constant around $\mathbf{k}_{\mathrm{D}}$ (its variations are smooth and hence tend to zero as $\mathbf{k} \to \mathbf{k}_{\mathrm{D}}$). Thus, even if only $\phi^{(1)}_{\mathbf{k}}$ and $\phi^{(2)}_{\mathbf{k}}$ participate in the conical intersection and define the diabolical point, $\phi^{(3)}_{\mathbf{k}}$ is also affected by this feature because it is associated with eigenvalue $\lambda^{(3)}_{\mathbf{k}} = -1$, which is degenerate with $\lambda^{(s=1,2)}_{\mathbf{k}_{\mathrm{D}}}$. The fact that the diabolical point is singular is easy to understand: depending on the direction we approach to it the eigenvectors of the problem are different.

Just at the diabolical point $\lambda^{(s=1,2,3)}_{\mathbf{k}} = -1$ and hence there is a 3D eigensubspace formed by all vectors orthogonal to the fourth eigenvector, namely $\phi^{(4)}_{\mathbf{k}_{\mathrm{D}}} = \frac{1}{2}\,\mathrm{col}\,(1,1,1,1)$, which is equal to $\phi^{(4)}_{\mathbf{k}}$: see (3.55). A sensible choice for these eigenvectors follows from noting that $\phi^{(1)}_{\mathbf{k}} + \phi^{(2)}_{\mathbf{k}}$ in (3.55) is independent of the azimuth and is orthogonal to $\phi^{(4)}_{\mathbf{k}}$. Hence one of the basis elements for this 3D degenerate subspace can chosen as

$$\phi_{\mathrm{D}} = \frac{\phi^{(1)}_{\mathbf{k}} + \phi^{(2)}_{\mathbf{k}}}{\sqrt{2}} = \frac{1}{2}\,\mathrm{col}\,(1,1,-1,-1)\,, \tag{3.56}$$

which has the outstanding property of being the single vector that projects, close to the diabolical point $\mathbf{k}_{\mathrm{D}}$, only onto $\phi^{(s=1,2)}_{\mathbf{k}}$, i.e. onto the eigenspaces of the diabolo. As for the other two eigenvectors we just impose their orthogonality with ϕ_{D} and $\phi^{(4)}_{\mathbf{k}_{\mathrm{D}}}$ and we choose them arbitrarily as

$$\phi'_{\mathrm{D}} = \frac{1}{\sqrt{2}}\,\mathrm{col}\,(1,-1,0,0)\,, \quad \phi''_{\mathrm{D}} = \frac{1}{\sqrt{2}}\,\mathrm{col}\,(0,0,-1,1)\,. \tag{3.57}$$

Note that we are using a "primed" notation instead of keeping the notation with the label s, except for $s = 4$, because none of these eigenvectors keeps being an eigenvector for $\mathbf{k} \neq \mathbf{k}_{\mathrm{D}}$ (only for special directions θ) and hence there is no sense in attaching any of these eigenvectors to a particular sheet of the dispersion relation. To conclude we list the projections of these eigenvectors onto the eigenvectors (3.55) in the neighborhood of $\mathbf{k}_{\mathrm{D}}$:

$$\begin{aligned}
&\langle \phi_{\mathrm{D}} \mid \phi^{(1)}_{\mathbf{k}} \rangle = \langle \phi_{\mathrm{D}} \mid \phi^{(2)}_{\mathbf{k}} \rangle = \tfrac{1}{\sqrt{2}}, && \langle \phi_{\mathrm{D}} \mid \phi^{(3)}_{\mathbf{k}} \rangle = 0, \\
&\langle \phi'_{\mathrm{D}} \mid \phi^{(1)}_{\mathbf{k}} \rangle = -\langle \phi'_{\mathrm{D}} \mid \phi^{(2)}_{\mathbf{k}} \rangle = \tfrac{\cos\theta}{\sqrt{2}}, && \langle \phi'_{\mathrm{D}} \mid \phi^{(3)}_{\mathbf{k}} \rangle = -\sin\theta, \\
&\langle \phi''_{\mathrm{D}} \mid \phi^{(1)}_{\mathbf{k}} \rangle = -\langle \phi''_{\mathrm{D}} \mid \phi^{(2)}_{\mathbf{k}} \rangle = \tfrac{\sin\theta}{\sqrt{2}}, && \langle \phi''_{\mathrm{D}} \mid \phi^{(3)}_{\mathbf{k}} \rangle = \cos\theta,
\end{aligned} \tag{3.58}$$

and $\langle \phi_{\mathrm{D}} \left| \phi^{(4)}_{\mathbf{k}} \right\rangle = \langle \phi'_{\mathrm{D}} \left| \phi^{(4)}_{\mathbf{k}} \right\rangle = \langle \phi''_{\mathrm{D}} \left| \phi^{(4)}_{\mathbf{k}} \right\rangle = 0$. All this has strong consequences on the QW dynamics near $\mathbf{k}_{\mathrm{D}}$ as we will show below.

3.4.3 Continuous wave equations

In order to illustrate how the evolution of the QW can be controlled via an appropriate choice of the initial conditions, we will show some results obtained numerically from the evolution of the 2D quantum walk with the Grover operator. Unless otherwise specified, the initial profile in position space is a Gaussian centered at the origin with cylindrical symmetry (independent of s):

$$\mid \psi_{\mathbf{x},0} \rangle = e^{i\mathbf{k}_0 \cdot \mathbf{x}} F_{\mathbf{x},0} \, |\phi\rangle \,, \tag{3.59}$$

where $|\phi\rangle$ represents the initial state of the coin, and

$$F_{\mathbf{x},0} = \mathcal{N} e^{-\frac{x_1^2 + x_2^2}{2\sigma^2}}, \tag{3.60}$$

with $\mathbf{x} = (x_1, x_2)$, which implies that in the continuous limit we also have a Gaussian, in momentum space, centered at $\mathbf{k}_0 = (k_1, k_2)$. Here, $\mathcal{N}$ is a constant that guarantees the normalization of the state. In the numerics, we have taken a sufficiently large value $\sigma = 50$ for the Gaussian, so as to make it possible the connection with the continuous limit, although we will also discuss the situation for smaller values of σ in order to show the robustness of the results.

Let us first consider a simple case having $k_1 = k_2 = \pi/2$, with an initial coin state $\frac{1}{\sqrt{2}}(\mid \phi^{(1)}_{\mathbf{k}_0}\rangle + \mid \phi^{(2)}_{\mathbf{k}_0}\rangle)$, where $\mid \phi^{(1)}_{\mathbf{k}_0}\rangle = \frac{1}{\sqrt{2}} \operatorname{col}(1, 0, -1, 0)$ and $\mid \phi^{(2)}_{\mathbf{k}_0}\rangle = \frac{1}{\sqrt{2}} \operatorname{col}(0, 1, 0, -1)$ that projects on the $s = 1$ and $s = 2$ branches with equal weights. The group velocity is given by $\mathbf{v}_{\mathrm{g}}^{(s)}(\mathbf{k}_0) = \pm(\frac{1}{2}, \frac{1}{2})$, respectively for

$s = 1, 2$, implying that the original Gaussian will split into two pieces that will move along the diagonal of the lattice in opposite directions, as shown in Fig. 3.3. It must be noticed that, since the second derivatives vanish at this point ($\varpi_{ij} = 0$), the Gaussian distribution moves with no appreciable distortion. On the right bottom panel of this figure, we show the result for $\sigma = 5$ and we observe that, in this case, the results obtained for large σ are very robust even for such a low value of σ.

However, if we choose an initial value $\mathbf{k}_0$ close to the origin, then the second derivatives take a large value, with the consequence that now the two pieces experience a considerable distortion along the line perpendicular to the line of motion, as can be seen from Fig. 3.4, where $k_1 = k_2 = 0.01\pi$, implying a curvature $\varpi_{ij} \simeq 7.96$ in the perpendicular direction.

In this case, at variance with the case considered in Fig.3.3, we have to face a peculiar situation, as the distribution is now peaked around a value close to the diabolical point $\mathbf{k}_D = (0, 0)$. As far as the initial distribution does not contain this point with a significant probability (i.e., for a large value of σ), the behavior will be as described above. However, if σ decreases below a certain limit, the evolution is dominated by the singular behavior of the diabolic point (to be studied in detail in the next subsection). This transition is clearly observed in Fig.3.5, where the resulting evolution is depicted as σ is increased from $\sigma = 5$ to $\sigma = 30$, the latter subpanel already showing a close resemblance with the result in Fig. 3.4. Distributions initially centered around non-singular points, however, are much more robust against a smaller σ, as previously shown in Fig. 3.3.

A completely different situation arises when $\mathbf{k}_0$ corresponds to one of the saddle points (such as the one located at $\mathbf{k}_{sp} = (0, \pi)$). As the group velocity vanishes at that point, i.e., $\mathbf{v}_g^{(1,2)}(\mathbf{k}_0) = (0, 0)$, the center of the probability distribution is expected to remain at rest but will spread in time analogously to diffracting optical waves, as Eq. (3.37) reduces to the paraxial wave equation of optical diffraction [84]. In our case, by considering $s = 1$ as the initial coin state, one finds $\varpi_{11} = -1/2, \varpi_{12} = \varpi_{21} = 0, \varpi_{22} = 1/2$. Therefore, Eq. (3.37) becomes

$$\mathrm{i}\frac{\partial A^{(1)}(\mathbf{X}, t)}{\partial t} = -\frac{1}{4}\frac{\partial^2 A^{(1)}}{\partial X_1^2} + \frac{1}{4}\frac{\partial^2 A^{(1)}}{\partial X_2^2}. \tag{3.61}$$

This wave equation is similar to that of paraxial optical diffraction [84], differing from it in that the sign of spatial derivatives are different for the two spatial directions. Hence this hyperbolic equation describes a situation in which there is diffraction in one direction and anti-diffraction in the other direction, as it

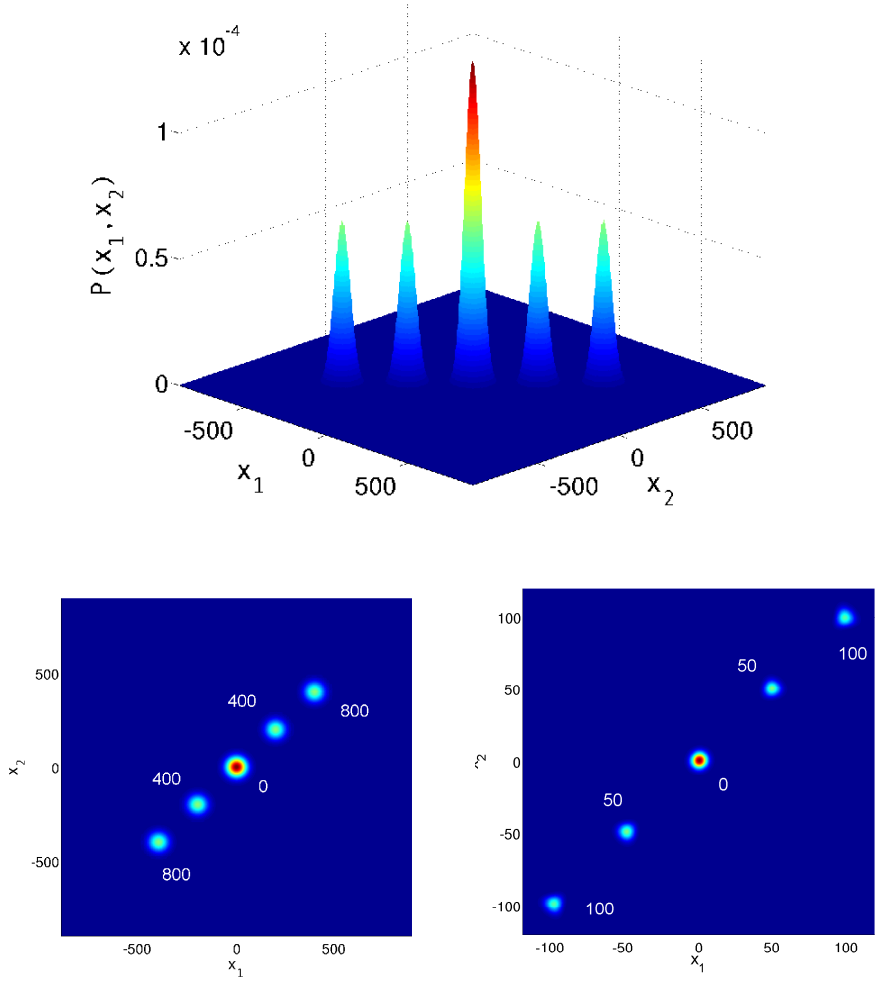

Figure 3.3: Probability distribution, as a function of the dimensionless (x_1, x_2) position and for the three times t=0, 400, 800. The initial condition (3.59) is given by the coin state $|\phi\rangle = \frac{1}{\sqrt{2}}(|\ \phi^{(1)}_{\mathbf{k}_0}\rangle + |\ \phi^{(2)}_{\mathbf{k}_0}\rangle)$ with $k_1 = k_2 = \pi/2$. (Top panel): 3D plot; the central peak corresponds to $t = 0$, and produces two symmetric peaks that move away from the origin: Each pair of symmetric peaks corresponds to a different value of the time t. (Bottom panel): Top view of the previous figure, both for $\sigma = 50$ (left) and $\sigma = 5$ (right). The numbers indicate, in each case, the value of time for different snapshots.

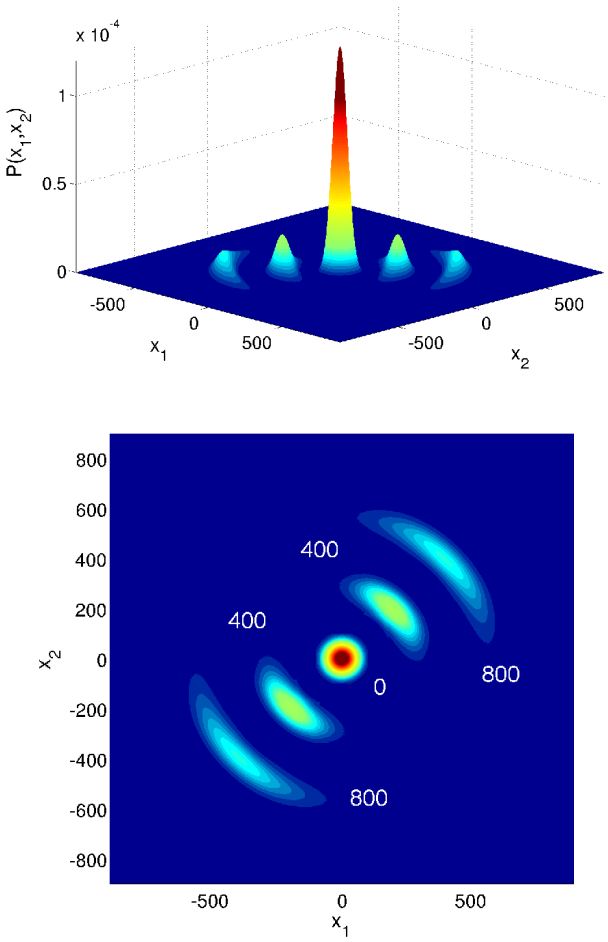

Figure 3.4: Probability distribution, as a function of the dimensionless (x_1, x_2) position and for the three times t=0, 400, 800. The initial condition (3.59) is given by the coin state $|\phi\rangle = \frac{1}{\sqrt{2}}(|\ \phi^{(1)}_{\mathbf{k}_0}\rangle + |\ \phi^{(2)}_{\mathbf{k}_0}\rangle)$ with $k_1 = k_2 = 0.01\pi$. (Top panel): 3D plot; as in Fig. 3, the central peak corresponds to $t = 0$, and produces two symmetric distributions that move away from the origin: Each pair of symmetric distributions corresponds to a different value of the time t. (Bottom panel): Top view of the previous figure, showing the value of the corresponding times.

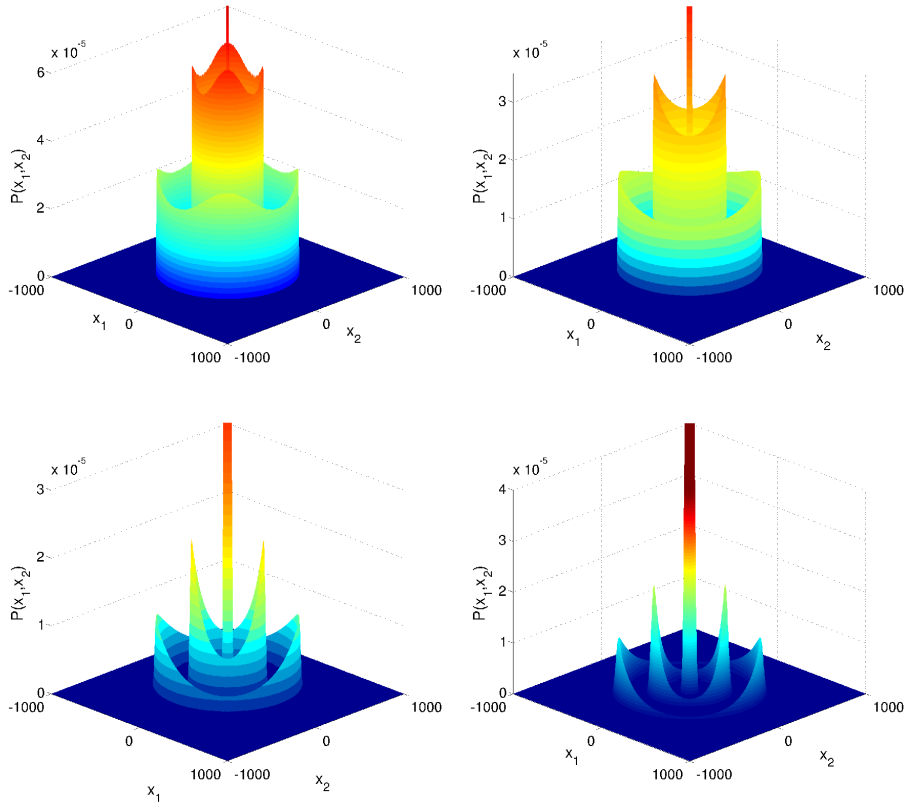

Figure 3.5: Same as Fig. 3.4, corresponding to four different values of σ. From left to right and from top to bottom: $\sigma = 5$, $\sigma = 10$, $\sigma = 20$ and $\sigma = 30$, respectively. The initial condition (3.59) is given by the coin state $|\phi\rangle = \frac{1}{\sqrt{2}}(|\ \phi^{(1)}_{\mathbf{k}_0}\rangle + |\ \phi^{(2)}_{\mathbf{k}_0}\rangle)$ and $k_1 = k_2 = 0.01\pi$. The distribution is shown for three times t=0, 400, 800. The central peak corresponds to $t = 0$, and expands from the origin in a manner that depends on the value of σ. For $\sigma = 5$ and $\sigma = 10$, the probability distribution has an almost cylindrical shape for each value of time. As σ is increased, the probability distribution becomes similar to the one found (for each value of t) in Fig. 3.4.

happens in certain optical systems [85]. This causes that the cylindrical symmetry proper of diffraction is replaced by a rectangular symmetry. Basing on the analogy with diffraction, it is possible to tailor the initial distribution in order to reach a desired asymptotic distribution as we already demonstrated in the one-dimensional QW [9]. Hence if we want to reach a final homogeneous (top hat) distribution, we must use an initial condition of the form [9, 84]

$$F_{\mathbf{x},0} = \mathcal{N} e^{i\mathbf{k}_0\cdot\mathbf{x}} e^{-\frac{x_1^2+x_2^2}{2\sigma^2}} sinc\left(x_1/\sigma_0\right)\ sinc\left(x_2/\sigma_0\right), \tag{3.62}$$

with $sinc\left(x\right) = \sin\left(\pi x\right)/\pi x$ and σ_0 a constant that accounts for the width of the distribution. In Fig. 3.6 we observe the evolution of the Grover walk with the above initial condition and the initial coin $\left|\phi^{(1)}_{\mathbf{k_0},0}\right\rangle = \frac{1}{2\sqrt{2}} col\left(1+i, 1+i, 1-i, 1-i\right)$, equal for all populated sites. The figure shows a final distribution that is quite homogeneous along most of its support, except in its outer borders, where it shows a smooth but rapid fall out (the ratio σ/σ_0 has been chosen to optimize the result [9]). This is the expected result, but Fig. 3.6 also shows a central peak that has been cut for a better display, the height of this central peak being quite large (around $1.5\cdot 10^{-5}$) as compared to the plateau (around $4\cdot 10^{-7}$). The existence of that central peak is a consequence of the common initial coin $|\phi_{\mathbf{k_0},0}\rangle$. This coin state guarantees that the initial distribution projects just onto the relevant branch of the dispersion relation at its central spatial frequency but, as the width of the distribution is finite, for the larger values of $|\mathbf{k}-\mathbf{k}_0|$ it will provide a non–negligible projection onto the static branches of the dispersion relation and the localized part of these projections are what we see as a central peak in Fig. 3.6.

3.4.4 Dynamics at the diabolical points

In this case $N=2$, $\mathrm{d}^N\Omega = \mathrm{d}\theta$, with θ the azimuth, and

$$\left|\mathbf{E}^{(s)}_{\mathbf{x}}\left(k\right)\right\rangle = \int_0^{2\pi} \mathrm{d}\theta \exp\left(\mathrm{i}\mathbf{k}\cdot\mathbf{x}\right) \langle\phi^{(s)}_{\mathbf{k}_\mathrm{D}+\mathbf{k}} \mid \Xi\rangle \mid \phi^{(s)}_{\mathbf{k}_\mathrm{D}+\mathbf{k}}\rangle. \tag{3.63}$$

We remind that here $|\Xi\rangle$ is assumed to project just onto $\left|\phi^{(s=1,2)}_{\mathbf{k}_\mathrm{D}+\mathbf{k}}\right\rangle$. This means that $|\Xi\rangle$ coincides with $|\phi_\mathrm{D}\rangle$, see (3.56). According to the projections (3.58) and

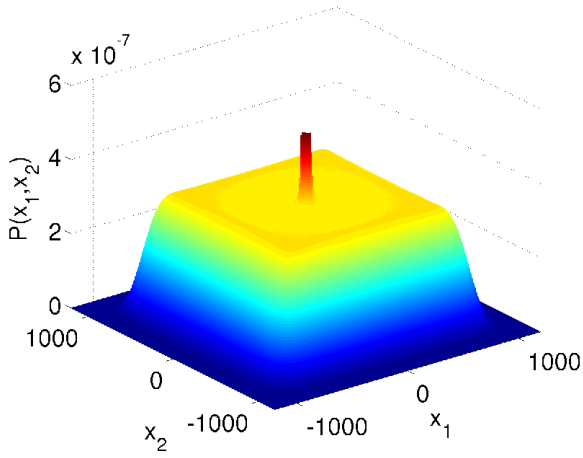

Figure 3.6: Probability distribution as a function of the dimensionless (x_1, x_2) position at time t=9000, for initial conditions at the saddle point $\mathbf{k}_0 = (0, \pi)$. The coin initial state is $|\ \phi^{(1)}_{\mathbf{k}_0}\rangle = \frac{1}{2\sqrt{2}}\,\mathrm{col}\,(1+i, 1+i, 1-i, 1-i)$, and the starting space distribution as given by Eq. (3.62). We have taken a value $\sigma_0 = 15$ for this simulation. The central peak has been cut for a better display of the rest of the features.

to the vectors (3.55) we can write, in matrix form,

$$\mathbf{E}_{\mathbf{x}}^{(s)}(k)=\frac{1}{4}\int_0^{2\pi}\mathrm{d}\theta\exp\left(\mathrm{i}\mathbf{k}\cdot\mathbf{x}\right)\begin{pmatrix}1\pm\sqrt{2}\cos\theta\\1\mp\sqrt{2}\cos\theta\\-1\mp\sqrt{2}\sin\theta\\-1\pm\sqrt{2}\sin\theta\end{pmatrix},\tag{3.64}$$

where the upper (lower) sign in $\pm$ or $\mp$ corresponds to $s=1(2)$, respectively, and we remind that $\mathbf{k}=(k\cos\theta,k\sin\theta)$. Upon writing $\mathbf{k}\cdot\mathbf{x}=kx\cos(\theta-\varphi)$, where $\mathbf{x}=x(\cos\varphi,\sin\varphi)$ and performing the integral we arrive to

$$\mathbf{E}_{\mathbf{x}}^{(s)}(k)=\frac{\pi}{2}\begin{pmatrix}J_0(kx)\pm\mathrm{i}\sqrt{2}J_1(kx)\cos\varphi\\J_0(kx)\mp\mathrm{i}\sqrt{2}J_1(kx)\cos\varphi\\-J_0(kx)\mp\mathrm{i}\sqrt{2}J_1(kx)\sin\varphi\\-J_0(kx)\pm\mathrm{i}\sqrt{2}J_1(kx)\sin\varphi\end{pmatrix},\tag{3.65}$$

where J_n are the Bessel functions of the first kind of order n. Using this result in (3.47) we get, in matrix form,

$$\mathbf{F}_{\mathbf{x},t}^{(s)}=(2\pi)^{-2}\int\mathrm{d}k\exp\left(\mp\mathrm{i}kct\right)k\tilde{F}_k\mathbf{E}_{\mathbf{x}}^{(s)}(k).\tag{3.66}$$

Let us compute the probability of finding the walker at some point, regardless the coin state, as given by (3.6), (3.22), (3.43) and (3.66). After simple algebra we obtain

$$P_{\mathbf{x},t}=\sum_{s,s'}\left[\mathbf{F}_{\mathbf{x},t}^{(s)}\right]^{\dagger}\cdot\mathbf{F}_{\mathbf{x},t}^{(s')}=\left[p_{\mathbf{x},t}^{(0)}\right]^2+\left[p_{\mathbf{x},t}^{(1)}\right]^2,\tag{3.67}$$

where

$$p_{\mathbf{x},t}^{(0)}=(2\pi)^{-1}\int_0^{\infty}\mathrm{d}k\cos(kct)J_0(kx)k\tilde{F}_k,\tag{3.68}$$

$$p_{\mathbf{x},t}^{(1)}=(2\pi)^{-1}\int_0^{\infty}\mathrm{d}k\sin(kct)J_1(kx)k\tilde{F}_k,\tag{3.69}$$

are amplitude probabilities. We see that the spatial dependence of the probability amplitude on the azimuth φ in (3.66,3.65) disappears when looking at the full probability $P_{\mathbf{x},t}$. This means that a coin-sensitive measurement of the probability should display angular features.

As a summary of what we know up to here about the neighborhood of the diabolical point, we can say that when the initial coin $|\Xi\rangle$ coincides with $|\phi_{\mathrm{D}}\rangle$, see (3.56), we predict (i) no localization and, (ii) when the initial wave packet $F_{\mathbf{x},0}$

is radially symmetric (it only depends on $x = |\mathbf{x}|$), an evolution of the probability $P_{\mathbf{x},t}$ that keeps the radial symmetry along time, according to (3.67,3.68,3.69).

Equations (3.68) and (3.69) describe the evolution of the probability of an initial wave packet centered at a diabolical point and with radial symmetry. The actual probability $P_{\mathbf{x},t}$ can be computed from them numerically, but little can be said in general. In order to gain some insight we consider next the relevant long time limit, which turns out to be analytically tractable. First of all it is convenient to scale the radial wavenumber k to the (loosely defined) width of the initial state in real space, $F_{\mathbf{x},0}$, which we denote by σ. Accordingly we define $\kappa = \sigma k$ so that (3.68) and (3.69) become

$$p^{(0)}_{\mathbf{x},t} = \left(2\pi\sigma^2\right)^{-1} \int_0^\infty \mathrm{d}\kappa \cos\left(\frac{ct}{\sigma}\kappa\right) J_0\left(\frac{x}{\sigma}\kappa\right) \kappa \tilde{f}_\kappa, \tag{3.70}$$

$$p^{(1)}_{\mathbf{x},t} = \left(2\pi\sigma^2\right)^{-1} \int_0^\infty \mathrm{d}\kappa \sin\left(\frac{ct}{\sigma}\kappa\right) J_1\left(\frac{x}{\sigma}\kappa\right) \kappa \tilde{f}_\kappa, \tag{3.71}$$

where $\tilde{f}_\kappa = \tilde{F}_{k=\kappa/\sigma}$ is non null only for $\kappa \lesssim 1$. Hence when $ct \gg \sigma$, $\cos\left(\frac{ct}{\sigma}\kappa\right)$ and $\sin\left(\frac{ct}{\sigma}\kappa\right)$ are strongly oscillating functions of κ, around zero, what would make $p^{(0,1)}_{\mathbf{x},t}$ to vanish. However in the integrals defining such amplitude probabilities other oscillating functions, $J_0\left(\frac{x}{\sigma}\kappa\right)$ and $J_1\left(\frac{x}{\sigma}\kappa\right)$, appear. Thus it can be expected that when the oscillations of the latter and the ones of the former are partially in phase, a non null value of the integrals is got. According to the asymptotic behavior of $J_n(z)$ at large z, $J_n(z) \approx \sqrt{2/\pi z}\cos\left(z - n\pi/2 - \pi/4\right)$ for $z \gg \left|n^2 - 1/4\right|$ [86], this partial phase matching occurs when $x \approx ct$, which is expected from physical considerations. Hence we are led to consider the limit $x = ct + \sigma\xi$, with $ct \gg \sigma$, where ξ is the scaled radial offset with respect to ct, in which case (3.70) and (3.71), after expressing the products of trigonometric functions as sums, become

$$\begin{aligned} p^{(0)}_{\mathbf{x},t} &= p^{(1)}_{\mathbf{x},t} \\ &\approx \left(2\pi\sigma^2\right)^{-1} \sqrt{\frac{\sigma}{2\pi ct}} \int_0^\infty \mathrm{d}\kappa \sin\left(\kappa\xi + \pi/4\right) \sqrt{\kappa}\tilde{f}_\kappa = \\ &\left(2\pi\right)^{-1} / \sqrt{2\pi ct} \int_0^\infty \mathrm{d}k \sin\left(k\sigma\xi + \pi/4\right) \sqrt{k}\tilde{F}_k, \end{aligned} \tag{3.72}$$

to the leading order, where the approximation follows from disregarding highly oscillating terms. As an application of this result we consider next the Gaussian case $\tilde{F}_k = 2\sigma\sqrt{\pi}\exp\left(-\frac{1}{2}\sigma^2 k^2\right)$, where σ is the standard deviation of the initial

probability in real space, Eq. (3.60). We readily obtain

$$p^{(0)}_{\mathbf{x},t} = p^{(1)}_{\mathbf{x},t} = \frac{1}{8\sqrt{\sigma ct}} e^{-\xi^2/4} \times \left\{ \xi\sqrt{|\xi|}\left[I_{-1/4}\left(\xi^2/4\right) - I_{3/4}\left(\xi^2/4\right)\right] + \frac{\xi^2 I_{5/4}\left(\xi^2/4\right) - \left(\xi^2-2\right) I_{1/4}\left(\xi^2/4\right)}{\sqrt{|\xi|}} \right\}, \tag{3.73}$$

where $\xi = \frac{x-ct}{\sigma}$ and I_n is the modified Bessel function of the first kind of order n. The total probability $P_{\mathbf{x},t} \equiv P(\xi)$ follows from using (3.73) in (3.67), from which we observe that the initial width σ acts only as a scale factor for the height and shape of the probability at long times ($ct \gg \sigma$). A plot of the probability can be seen in Fig. 3.8, where two unequal spikes, whose maxima are located at $\xi = -1.74623$ and at $\xi = 0.550855$, separated by a zero at $\xi = -0.765951$, are apparent. We remind that $x = ct + \sigma\xi$ is a radial coordinate, hence these maxima correspond to two concentric rings separated by a dark ring. The situation is fully analogous to the so-called "Poggendorff rings" appearing in the paraxial propagation of a beam incident along an optic axis of a biaxial crystal, a situation in which a conical intersection (a diabolical point) is present. Remarkably the result we have obtained for $P_{\mathbf{x},t}$ fully coincides with that described in [71] whose Fig. 7 is to be compared to our Fig. 3.8.

As an example that illustrates the above features, we have studied the evolution of a state of the form Eq. (3.60) for the diabolic point $\mathbf{k}_{\mathrm{D}} = (0,0)$, and a coin state as defined in Eq. (3.56). As seen from Fig. 3.7, the probability distribution keeps its cylindrical symmetry while it expands in position. It can also be seen from this figure that the general features remain valid for a wider distribution (in k space) corresponding to $\sigma = 5$, even if the distribution in spatial coordinates is narrower for a given time step. The Poggendorff rings can be appreciated in Fig. 3.8, which shows a radial cut of the previous figure. We also plot for comparison our analytical result, as obtained form Eqs. (3.67) and (3.73) , which shows a good agreement with the (exact) numerical result, as can be seen from this figure.

All these features crucially depend on the choice of the coin initial conditions, as clearly observed when these conditions are chosen differently. As an example, we show in Fig. 3.9 the evolution after 200 time steps, of the probability distribution when we start from a state, also centered around the diabolic point, but the vector coin is now $\left|\phi^{(2)}_{\mathbf{k}_{\mathrm{D}}}\right\rangle$ with $\theta = \pi/2$. Most of the probability is directed along the positive x_2 axis, which corresponds to the choice of θ. In fact, by changing the value of this parameter one can, at will, obtain a chosen direction for propagation.

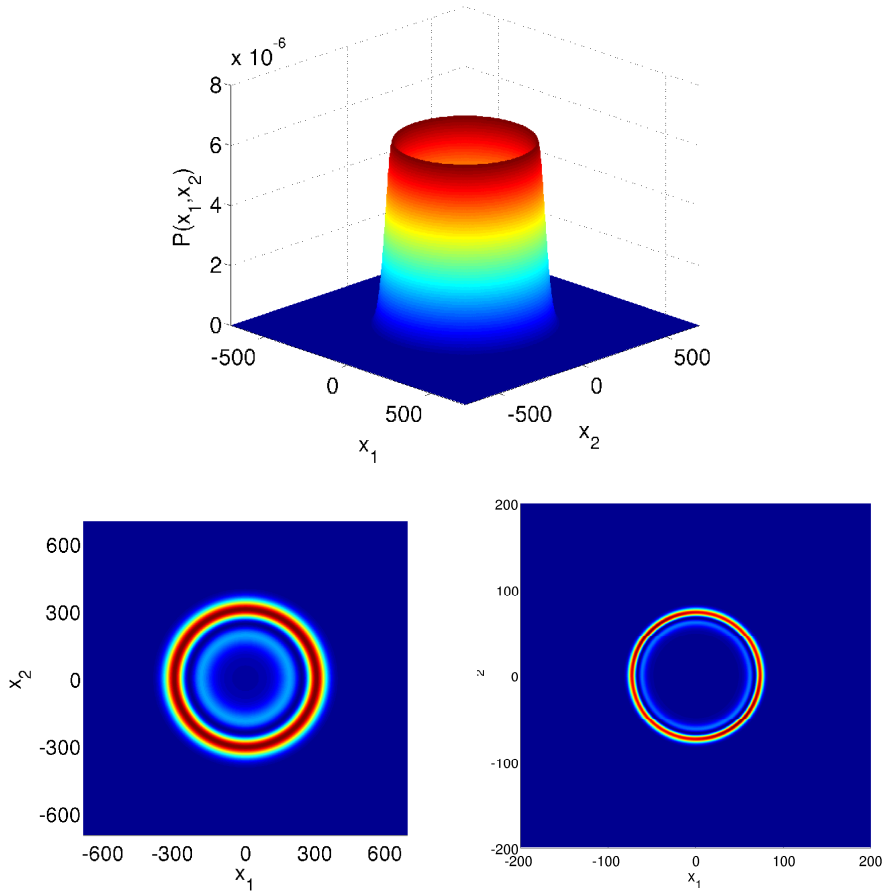

Figure 3.7: (Top panel): Probability distribution as a function of the dimensionless (x_1, x_2) position, at time $t = 400$. The initial condition is given by Eq. (3.56) around the diabolic point $\mathbf{k}_{\mathrm{D}} = (0, 0)$, with $\sigma = 50$. (Bottom panel): Top view of the previous figure with $\sigma = 50$ (left) and $\sigma = 5$ (right), but now at time $t = 100$.

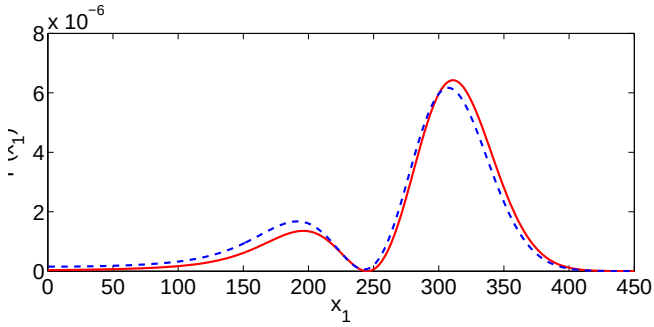

Figure 3.8: Radial cut, with $x_2 = 0$, for the top panel of Fig. 3.7 (blue, dotted curve), showing the Poggendorff rings (see the text for explanation). Also shown for comparison is our analytical result, as obtained form Eqs. (3.67) and (3.73) (solid, red curve).

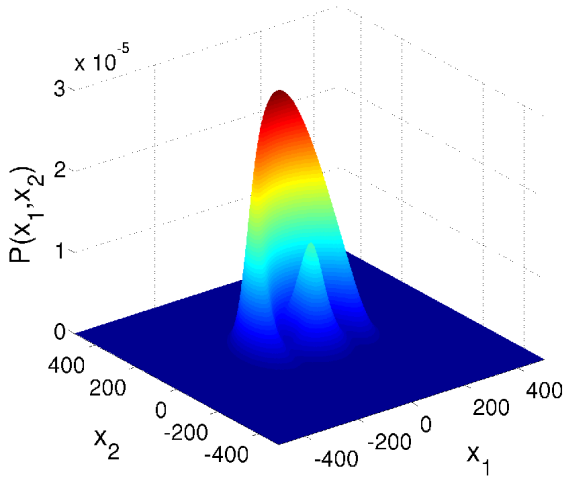

Figure 3.9: Probability distribution as a function of the dimensionless (x_1, x_2) position, at time $t = 200$. The initial condition is given by $\left|\phi^{(2)}_{\mathbf{k}_D}\right\rangle$ around the diabolic point with $\theta = \pi/2$.

3.5 Application to the 3D Grover QW

In this section we briefly analyze the three–dimensional Grover QW in order to illustrate similarities and differences with the two–dimensional case. In 3D, the Grover-coin operator reads

$$C = \frac{1}{3}\begin{pmatrix} -2 & 1 & 1 & 1 & 1 & 1 \\ 1 & -2 & 1 & 1 & 1 & 1 \\ 1 & 1 & -2 & 1 & 1 & 1 \\ 1 & 1 & 1 & -2 & 1 & 1 \\ 1 & 1 & 1 & 1 & -2 & 1 \\ 1 & 1 & 1 & 1 & 1 & -2 \end{pmatrix}, \tag{3.74}$$

and the diagonalization of the corresponding matrix $C_{\mathbf{k}}$ (3.17), with $\mathbf{k} = (k_1, k_2, k_3)$, yields six eigenvalues $\lambda_{\mathbf{k}}^{(s)} = \exp\left(-\mathrm{i}\omega_{\mathbf{k}}^{(s)}\right)$ with

$$\omega_{\mathbf{k}}^{(1,2)} = \pm\Omega_{\mathbf{k}}^{(+)},\ \omega_{\mathbf{k}}^{(3,4)} = \pm\Omega_{\mathbf{k}}^{(-)},\ \omega_{\mathbf{k}}^{(5)} = 0,\ \omega_{\mathbf{k}}^{(6)} = \pi, \tag{3.75}$$

where

$$\cos\Omega_{\mathbf{k}}^{(\pm)} = -\frac{1}{3}\left[\sum_{i=1,2,3}\cos k_i \pm \sqrt{\sum_{i=1,2,3}^{j>i}(\cos^2 k_i - \cos k_i \cos k_j)}\right]. \tag{3.76}$$

Remember that adding a multiple integer of 2π to any of the ω's does not change anything because time is discrete and runs in steps of 1. This implies that $\omega = -\pi$ and $\omega = \pi$ represent the same frequency.

The graphical representation is more complicated in the 3D case: Plots of the dispersion relations (3.75) for particular values of k_3 and for particular values of ω are given in Figs. 3.10 and 3.11, respectively.

A large variety of propagation properties can be expected depending on the particular region in k-space that the initial distribution occupies. Notice the existence of two constant dispersion relations, $\omega_{\mathbf{k}}^{(5,6)}$, which will give rise to localization phenomena, as already discussed in the 2D case.

There exist several degeneracies in the above dispersion relations, appearing in the crossings of several dispersion curves. For $\omega = \pi$, there is a 5-fold degeneracy at $\mathbf{k} = \mathbf{0}$, where $\omega_{\mathbf{k}}^{(j)} = \pi$ for $j = 1, 2, 3, 4, 6$. There is also a 3-fold degeneracy occurring when $\mathbf{k}$ takes the form $\mathbf{k} = \mathbf{k}_{||} \equiv k\mathbf{e}_i$, where $\mathbf{e}_i$ is one of the vectors of the canonical basis in $\mathbb{R}^3$(i.e., $\mathbf{k}_{||}$ has two null components and an arbitrary third component), where $\omega_{\mathbf{k}}^{(j)} = \pi$ for $j = 1, 2, 6$. For $\omega = 0$ these degeneracies migrate

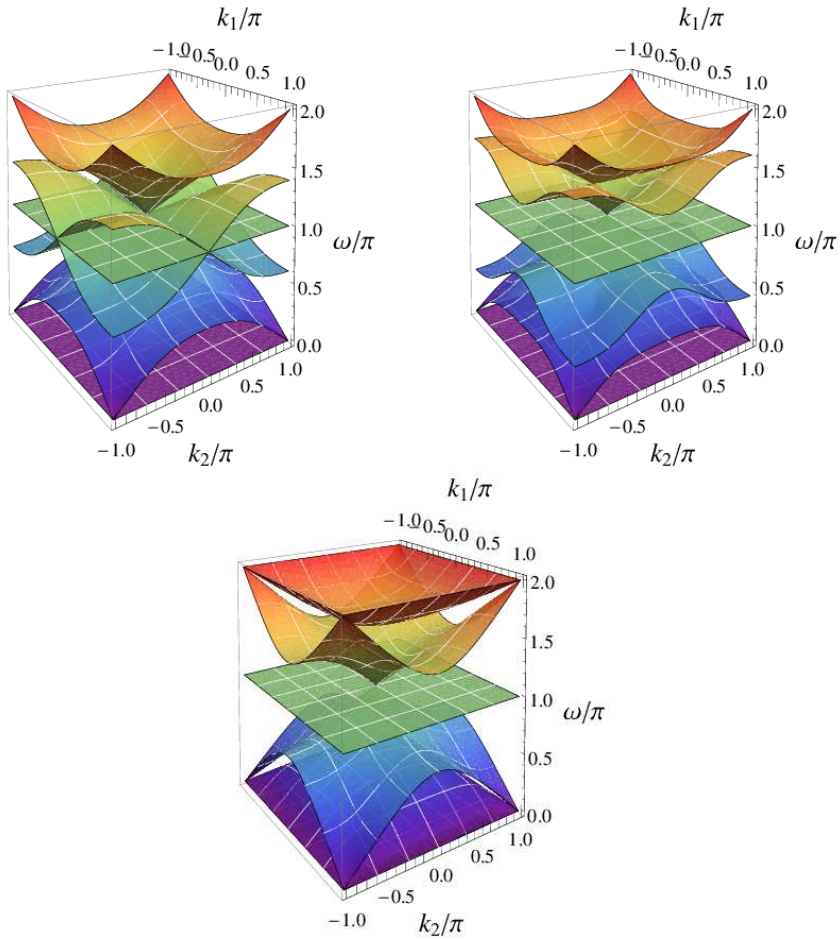

Figure 3.10: Representations of the Grover 3D six dispersion relation surfaces for $k_3 = 0$ (left), $\pi/2$ (center), and π (right).

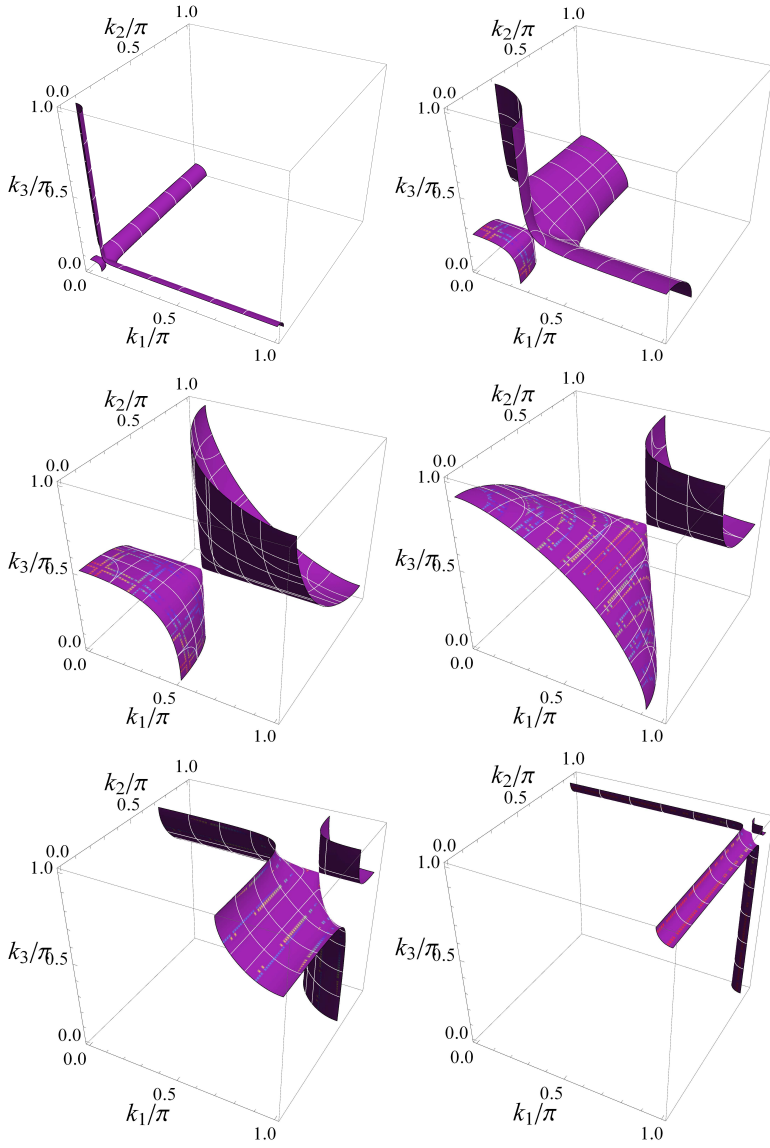

Figure 3.11: Representations of the Grover 3D isofrequency surfaces, as obtained from $\Omega_{\mathbf{k}}^{(+)}$ in the first octant of the Brillouin zone for $\omega = 0.95\pi$ (a), 0.8π (b), 0.6π (c), 0.4π (d), 0.2π (e), and 0.05π (f). For $\omega = \pi$ the two dispersion relation coincides with the cube axes and the cube origin, whilst for $\omega = 0$ they have migrated to the opposite side of the cube.

to the corners and borders, respectively, of the first Brillouin zone, see Fig. 3.11. The frequencies $\Omega_{\mathbf{k}}^{(\pm)}$, close to the degeneracies for $\omega = \pi$, read

$$\cos\Omega_{\mathbf{k}}^{(\pm)}\Big|_{\mathbf{k}=0} \simeq -1 + \frac{1}{6}|\mathbf{k}|^2 \mp \frac{1}{6}\sqrt{|\mathbf{k}|^4 - 3\left(k_x^2k_y^2 + k_x^2k_z^2 + k_y^2k_z^2\right)} + O\left(k^4\right). \tag{3.77}$$

In the case that $\mathbf{k}$ takes the form $\mathbf{k} = \mathbf{k}_{||} \equiv k\mathbf{e}_i$, we obtain

$$\cos\Omega_{\mathbf{k}}^{(+)} = -1 \tag{3.78}$$

$$\cos\Omega_{\mathbf{k}}^{(-)} = -\frac{1}{3}(1 + 2\cos k) \tag{3.79}$$

which shows the above-mentioned degeneracy.

We see that the point degeneracy occurring at $\mathbf{k} = 0$, $\cos\Omega_{\mathbf{k}}^{(+)} = -1$, is not a true diabolical point because, for fixed frequency, the dispersion relation has not spherical symmetry (hence the dispersion relation surface is not a hyperdiabolo). This implies that the theory developed in Sec. III.B cannot be applied to this case. (We notice, however, that it can be applied when coins different to the Grover one are used as it occurs, for example, in the Alternate 3D QW, where true 3D diabolical points exist [53].)

Its not difficult to see that the group velocities

$$\mathbf{v}_{\mathrm{g}}^{(1,2,3,4)}(\mathbf{k}) = \pm\nabla_{\mathbf{k}}\Omega_{\mathbf{k}}^{(\pm)}, \tag{3.80}$$

have now the expression

$$\left(\mathbf{v}_{\mathrm{g}}^{(1,2)}(\mathbf{k})\right)_i = \mp\frac{(2\cos\Omega_{\mathbf{k}}^{(+)} + \sum_{j\neq i}\cos k_j)\sin k_i}{2\left(3\cos\Omega_{\mathbf{k}}^{(+)} + \sum_j \cos k_j\right)\sin\Omega_{\mathbf{k}}^{(+)}}, \tag{3.81}$$

$$\left(\mathbf{v}_{\mathrm{g}}^{(3,4)}(\mathbf{k})\right)_i = \mp\frac{(2\cos\Omega_{\mathbf{k}}^{(-)} + \sum_{j\neq i}\cos k_j)\sin k_i}{2\left(3\cos\Omega_{\mathbf{k}}^{(-)} + \sum_j \cos k_j\right)\sin\Omega_{\mathbf{k}}^{(-)}}, \tag{3.82}$$

and $\mathbf{v}_{\mathrm{g}}^{(5,6)}(\mathbf{k}) = 0$.

We see that the extrema of the dispersion relations for branches 1,2,3 and 4 giving points of null velocity (those for which a Schrödinger type equation is a priori well suited for extended initial conditions) occur, in particular, when all $\sin k_i = 0$. At some of these points we find the just discussed degeneracies, hence

at them a Schrödinger type equation is not appropriate. However, some of the points of null velocity do not correspond to degeneracies, in particular those $\mathbf{k}$ with two null components and the third one equal to $\pm\pi$. Consider, for example, the point $\mathbf{k}_0 = (0, 0, \pm\pi)$ at which $\Omega_{\mathbf{k}}^{(+)}$ presents degeneracies but not $\Omega_{\mathbf{k}}^{(-)}$, which takes the value $\Omega_{\mathbf{k}}^{(-)} = \arccos 1/3$. In order to particularize the wave equation (3.1) to this case we must calculate the nine coefficients

$$\varpi_{ij}^{(3,4)} = \pm\, \partial^2 \Omega_{\mathbf{k}}^{(-)} / \partial k_i \partial k_j \Big|_{\mathbf{k}=\mathbf{k}_0}, \tag{3.83}$$

which turn out to be $\varpi_{11}^{(3,4)} = \varpi_{22}^{(3,4)} = -\varpi_{33}^{(3,4)}/4 = \mp 1/4\sqrt{2}$ the rest being zero. Hence the continuous description in this case is given by

$$\mathrm{i}\frac{\partial A^{(3,4)}}{\partial t} = \pm\frac{1}{8\sqrt{2}}\left(\frac{\partial^2}{\partial X_1^2} + \frac{\partial^2}{\partial X_2^2} - 4\frac{\partial^2}{\partial X_3^2}\right) A^{(3,4)}, \tag{3.84}$$

which exhibits an anisotropic diffraction (diffraction in the (X_1, X_2) plane and anti-diffraction, with a different coefficient, in the X_3 direction). For $\mathbf{k}_0 = (\pi, 0, 0)$ and $\mathbf{k}_0 = (0, \pi, 0)$ the result is the same after making the changes $X_1 \to X_3$ and $X_2 \to X_3$, respectively. Eq. (3.84) can be solved via a Fourier transform method. For a starting Gaussian profile as given below, the solution will factorize in three one dimensional functions of the form

$$\frac{e^{-\frac{ix^2}{2t\varpi + 2i\sigma^2}}}{\sqrt{\sigma^2 - it\varpi}} \tag{3.85}$$

(except for an overall constant), where ϖ is any of the coefficients ϖ_{ij} that appear in Eq. (3.84), and x represents one of the coordinates X_i with $i = 1, 2, 3$. This implies a characteristic time scale $t \sim \sigma^2/|\varpi|$ for the Gaussian to broaden.

We now show two examples that illustrate the above results. As in the 2D cases, we start with an initial condition (3.41) defined by a Gaussian shape

$$F_{\mathbf{x},0} = \mathcal{N} e^{i\mathbf{k}_0\cdot\mathbf{x}} e^{-\frac{x_1^2 + x_2^2 + x_3^2}{2\sigma^2}}, \tag{3.86}$$

with $\mathcal{N}$ an appropriate constant defining the normalization, and $|\Xi\rangle$ a constant (position-independent) vector in the coin space, which is chosen to be one of the eigenvectors of the matrix $C_{\mathbf{k}}$ (3.17) at the point $\mathbf{k} = \mathbf{k}_0$. We have not explored those cases where $\mathbf{k}_0$ lies at, or very close to, any of the degeneracies discussed above. The problem at these points seems to be much more involved than in the 2D case. For example, the extension of the eigenvectors obtained in [16] to this case encounters a singular behavior at the axis (which are degeneracy lines). One

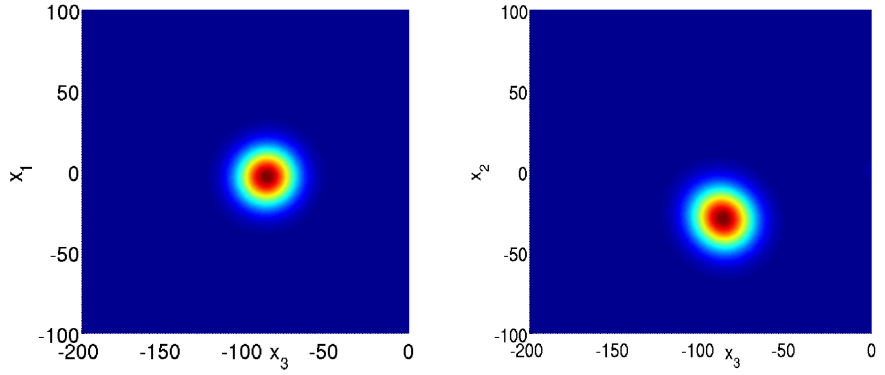

Figure 3.12: Top view of the probability distribution in position space on the $x_2 = 0$ plane (left) and on the $x_1 = 0$ plane (right) for a time step $t = 125$. The initial distribution is given by Eqs. (3.41) and (3.86), with $\mathbf{k}_0 = (0.1, 0.2, 0.3)\pi$ and $|\Xi\rangle$ the eigenvector of the coin operator corresponding to $s = 3$.

needs to carefully take care of the appropriate limit as one approaches these lines, and perform a systematic study in order to find the relevant linear combinations providing a sensible time evolution. Such a study is beyond the scope of this thesis.

We first start with a value $\mathbf{k}_0 = (0.1, 0.2, 0.3)\pi$ that lies far from any degeneracy or points with zero group velocity. For $s = 3$, the group velocity is $\mathbf{v}_{\mathrm{g}}^{(3)}(\mathbf{k}_0) = (-0.028, -0.232, -0.704)$. In Fig. 3.12 we show two different views corresponding to the evolved probability distribution. Within the timescale displayed on this Figure, the initial Gaussian has not appreciably broaden, and we can instead observe the motion of the center of the wave packet according to what is expected from the group velocity. A somehow opposite behavior is observed if we choose a point giving a zero velocity, such as $\mathbf{k}_0 = (0, 0, \pi)$. As described above, we expect no motion of the center and a broadening which depends on the axis we choose. This broadening can be approximately described by Eq. (3.84) and, for the values of σ we are assuming here, one needs to follow the time evolution during a considerably larger time scale. As a consequence, higher order effects neglected in deriving Eq. (3.84) may accumulate. In Fig. 3.13 we show two different radial cuts of the 3D probability distribution. As observed from this Figure, the accumulated discrepancy between the exact numerical evolution and

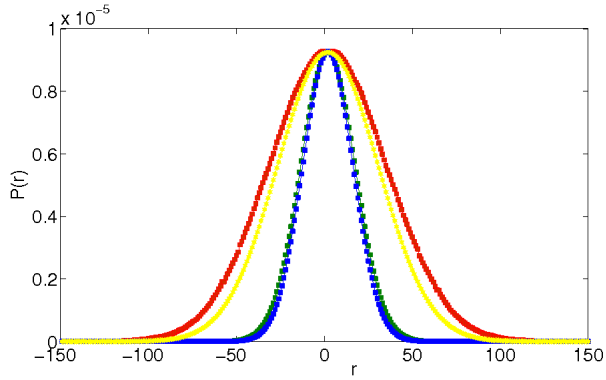

Figure 3.13: Two different radial cuts of the evolved probability distribution, represented by $P(r)$, where r is the coordinate along the cut, at $t = 1000$ when the initial distribution is a spherically symmetric Gaussian function with $\sigma = 20$, with $\mathbf{k}_0 = (0, 0, \pi)$ and $|\Xi\rangle$ the eigenvector of the coin operator corresponding to $s = 3$. The figure also shows for comparison the analytical result as obtained from Eq. (3.84). The curve with red symbols corresponds to a cut along the x_3 axis, to be compared with the analytical approximation (yellow curve). The curve with blue symbols is the plot for a cut along the x_3 axis, to be compared with the analytical approximation (green).

the approximated analytical Eq. (3.84) may depend on the spatial direction. However, given all these considerations, we see that our derived analytical result gives a reasonable description for the main features of the time evolution, even in 3D.

4 Quantum Walks and Non-Markovian behavior

4.1 Introduction

There are many phenomena in nature for which the variables that describe them vary irregularly or randomly with time. Such processes are called stochastic processes. The study of stochastic processes is very important in the field of physics since there are many phenomena that depend on time in complex ways, such as the Brownian motion of a particle. These processes can be described by all the different states that a system can occupy, and its evolution through the transitions from one state to another. Markovian processes are a type of widely studied stochastic processes. Such processes are characterized by the fact that the transitions at a given time depend only on the value of the random variables at that time, and not on the previous history. The classical random walk is an example of a Markovian process that has found applications in many fields.

In quantum mechanics, the concept of Markovianity can be applied to the evolution of some open quantum system interacting with an environment. Important physical processes leading to decoherence can be analyzed by means of simple Markovian models. This is often the case in quantum optics where, under some reasonable assumptions, the time evolution of an open system can be described by a (non-unitary) master equation, written as a Lindblad equation [87].

In this chapter, we briefly introduce the concept of Markovianity and non-Markovianity both for discrete and continuous time classical systems. The concept of Markovianity and non-Markovianity in quantum systems is also discussed. The quantification of non-Markovianity remains an open question, and hence many different measures have been proposed. Next, the asymptotic QW behavior with and without decoherence is studied. To this end, we make use of the method proposed in Ref. [88] which was designed to characterize the non-Markovian behavior in quantum systems.

4.2 Classical Markovian processes

4.2.1 Discrete Time Markov Chains

A stochastic process is a collection of random values used to represent the evolution of some random variable, or system, over time. Let $X_n, n = 0, 1, 2, 3...$ be a variable corresponding to a discrete time stochastic process with a state space S. Let $P(A|B)$ be the conditional probability which measures the probability of an event A, given that another event B has occurred. This process is called a Markov chain if, for all times $n \geqslant 0$ and all states $i_0, i_1...i_n \in S$,

$$P(X_{n+1} = i_{n+1}|X_n = i_n, X_{n-1} = i_{n-1}, ..., X_0 = i_0) = P(X_{n+1} = i_{n+1}|X_n = i_n) \tag{4.1}$$

In this case, the probabilities associated with future states depend solely on the current state, they do not depend on any previous state of the system. In this sense, the process is called memoryless. The conditional probabilities $p_{ij} = P(X_{n+1} = j|X_n = i)$ are named the single-step transition probabilities and give the conditional probability of transitions from state $x_n = i$ to state $x_{n+1} = j$ within one time-step. The single step transition probabilities $p_{ij}(n)$ can be written as a transition probability matrix,

$$P(n) = \begin{pmatrix} p_{11}(n) & p_{12}(n) & ... & p_{1n}(n) \\ ... & & & \\ ... & & & \\ p_{n1}(n) & p_{n2}(n) & ... & p_{nn}(n) \end{pmatrix}$$

$P(n)$ satisfies the following properties:

$$0 \leqslant p_{ij}(n) \leq 1 \tag{4.2}$$

$$\sum_{j=1}^{n} p_{ij} = 1 \tag{4.3}$$

Any matrix satisfying Eqs. (4.2-4.3) is called a Markov or Stochastic matrix. A Markov chain is said to be time-homogeneous if, for all states i and j, it satisfies that,

$$P(X_{n+1} = j|X_n = i) = P(X_{n+m+1} = j|X_{n+m} = i) = p_{ij} \tag{4.4}$$

This implies that the transition probability matrix $P(n)$ is independent of n.

The Sojourn Time

It is possible that the system remains in state i at the next step if the diagonal elements of the transition matrix P are different from zero. Let T_i be the sojourn time or holding time of the state, i.e. the time spent in state i, before moving to state j. The probability that the systems remains in state i after one time-step is p_{ii}. The transition probability to a different state j is then given by,

$$\sum_{i \neq j} p_{ij} = 1 - p_{ii}$$

The sojourn time at state i is itself a random variable, with the following probability distribution

$$P(T_i = n) = (1 - p_{ii}) p_{ii}^{(n-1)}$$

This probability has a geometric distribution with parameter $1 - p_{ii}$. The geometric distribution is the only discrete distribution that has the memoryless property. This result is only valid when the Markov chain is time-homogeneous.

Higher order transition probabilities. The Chapman-Kolmogorov equations

The m-step transition probability $p_{ij}^{(m)}$, is the probability of moving from state i to state j after m steps. For a homogeneous discrete time Markov chain, given $0 < l < m$, $p_{ij}^{(m)}$ satisfies

$$\begin{aligned} p_{ij}^{(m)} = P(X_m = j | X_0 = i) = \sum_k P(X_m = j, X_l = k | X_0 = i) = \\ \sum_k P(X_m = j | X_l = k, X_0 = i) P(X_l = k | X_0 = i) = \\ \sum_k P(X_m = j | X_l = k) P(X_l = k | X_0 = i) = \sum_k p_{kj}^{(m-l)} p_{ik}^{(l)} \end{aligned} \tag{4.5}$$

Eq. (4.5) is called Chapman-Kolmogorov Equation.

It is possible to write any m-step homogeneous transition probability matrix as the product of l-step and $(m - l)$-step transition probability matrices. Let $\pi^{(0)}$ be the row vector of the initial probability distribution of the Markov chain. Then the probability after the first time step is given by the product of $\pi^{(0)} P$,

$$\pi^{(1)} = \pi^{(0)} P$$

In general, after n steps,

$$\pi^{(n)} = \pi^{(n-1)}P = \pi^{(0)}P^{(n)}$$

Notice that calculating transition probabilities is computationally equivalent to computing powers of the transition matrix.

4.2.2 Continuous Markov process

A stochastic process $\{X(t) : t \geq 0\}$ is called a continuous-time Markov chain if for all $t \geq 0$, $s \geq 0$, $i, j, k \in S$, and $0 \leq u \leq s$ we have

$$P(X(s+t) = j|X(s) = i, X(u) = k) = P(X(s+t) = j|X(s) = i) = p_{ij}(s,t) \tag{4.6}$$

p_{ij} gives the probability that the system which was in state i, changes to state j, after a time interval t. If the continuous Markov chain is homogeneous, the transition probabilities only depend on the time difference

$$p_{ij}(\tau) = P(X(s+\tau) = j|X(s) = i)$$

To be able to describe the evolution of the system, we need the rates per unit time $q_{ij}(t)$ at which transitions occur. The continuous Markov chain is characterized by a matrix of transition rates $Q(t)$, related to the transition probabilities by

$$q_{ij}(t) = \lim_{\Delta t \to 0} \frac{p_{ij}(\Delta t)}{\Delta t}$$

In matrix notation

$$Q(t) = \lim_{\Delta t \to 0} \frac{P(\Delta t) - I}{\Delta t} \tag{4.7}$$

For an homogeneous continuous-time Markov chain the transition rates q_{ij} are independent of time.

The Sojourn time

Let T_i be the random variable corresponding to the time that the system stays in the state i before a transition to another state occurs. By time homogeneity, we assume that the process starts out in state i. For $s \geq 0$ the event $\{T_i > s\}$ is equivalent to the event $\{X(u) = i \ \ for \ \ 0 \leq u \leq s\}$. Similarly, for s, $t \geq 0$ the

event $\{T_i > s+t\}$ is equivalent to the event $\{X(u) = i \ \ for \ \ 0 \leq u \leq s+t\}$. Therefore,

$$\begin{aligned} & P(T_i > s+t | T_i > s) \\ &= P(X(u) = i \ \ for \ \ 0 \leq u \leq s+t | X(u) = i \ \ for \ \ 0 \leq u \leq s) \\ &= P(X(u) = i \ \ for \ \ s < u \leq s+t | X(u) = i \ \ for \ \ 0 \leq u \leq s) \\ &= P(X(u) = i \ \ for \ \ s < u \leq s+t | X(s) = i) \\ &= P(X(u) = i \ \ for \ \ 0 < u \leq t | X(0) = i) \\ &= P(T_i > t), \end{aligned} \tag{4.8}$$

where the second equality follows from the simple fact that $P(AB|A) = P(B|A)$, where we let $A = \{X(u) = i \ \ for \ \ 0 \leq u \leq s\}$ and $B = \{X(u) = i \ \ for \ \ s < u \leq s+t\}$. The third equality follows from the Markov property and the fourth equality follows from time homogeneity. Multiplying the Eq.(4.8) by $P(T_i > s)$ we obtain:

$$P(T_i > s+t | T_i > s) P(T_i > s) = P(T_i > t | T_i > s) P(T_i > s) \tag{4.9}$$

In other words

$$P(T_i > s+t) = P(T_i > t | T_i > s) P(T_i > s) \tag{4.10}$$

if $F(t) = P(T_i > t)$

$$F(s+t) = F(t)F(s) \tag{4.11}$$

The exponential function $F(t) = e^{-\mu t}$ is the only function that satisfies Eq. (4.11) and is the only continuous distribution that has the memoryless property. Thus the sojourn time must be exponentially distributed. After the sojourn time, the system makes a transition into state j according to the transition probability p_{ij}, regardless of the past. Each time this happens through a new T_i, independent of the past, determines a new time the system will spend in state i.

Higher order transition probabilities. The Chapman-Kolmogorov equations

For a non-homogeneous continuous-time Markov chain, the Chapman-Kolmogorov Equation Eq. (4.5) is easy to obtain using the Markov property. When the continuous-time Markov chain is homogeneous, the Chapman-Kolmogorov equation can be written in matrix form as

$$P(u+t) = P(u)P(t) \tag{4.12}$$

Recalling the derivation of the probability transition matrix and the definition of Q, Eq.(4.7) we define,

$$\begin{aligned}\frac{dP}{dt} = \lim_{\Delta t \to 0} \frac{P(t+\Delta t) - P(t)}{\Delta t} = \\ \lim_{\Delta t \to 0} \frac{P(t)P(\Delta t) - P(t)}{\Delta t} = \\ \lim_{\Delta t \to 0} P(t)\frac{P(\Delta t) - I}{\Delta t} = \\ P(t)Q\end{aligned} \tag{4.13}$$

Eq. (4.13) is known as the forward Kolmogorov differential equation. If we change the side on which we factorize $P(t)$, we obtain the backward Kolmogorov differential equation $\frac{dP}{dt} = QP(t)$.

The solution to the equation (4.13) under the condition $P(0) = I$ is uniquely given by:

$$P(t) = e^{Qt} = \sum_k \frac{(Qt)^k}{k!} \tag{4.14}$$

Therefore, if we know Q we can work out the transition probability matrix for any future time. As in the discrete case, we can write the row vector of the probability distribution after evolution as a function of the transition probability matrix and the row vector of the initial probability distribution:

$$\pi(t) = \pi(0)P(t). \tag{4.15}$$

We can regard Eq. (4.15) as the evolution of a classical dynamical map i.e., the evolution of the probability vector $\pi(0)$ can be described by a time dependent stochastic matrix $P(t)$. If we take into account Eq. (4.12) and the fact that $P(t)$ is by itself a stochastic matrix, then the classical map is divisible, later we will gain in-depth knowledge about this concept.

4.3 Classical Semi-Markovian and non-Markovian processes

Semi-Markovian processes can be understood as a generalization of a Markov chain. The transitions are governed by a transition probability matrix, and the next state to be occupied depends only on the current state and not on the full history of the process. In this sense, the process is still memoryless. However

semi-Markovian processes differ from the Markovian processes in that the transition probability depends on the amount of time the process has already spent in that state. In a semi-Markovian process the time spent in each state may follow any arbitrary distribution. If the sojourn time T_i, does not have an exponential distribution as in the case of continuous Markov chain, nor a geometric distribution as in the case of discrete Markov chain but rather a general distribution, then the process is called semi-Markovian process. In contrast, in a non-Markovian process, the transition probability does depend on the initial probability vector and thus the process can not be considered memoryless.

4.4 Open Quantum systems and Quantum Markovian processes

The common approach to the description of open quantum systems consists in separating the total system in two parts, the quantum system of interest and the *environment*, which are coupled to each other, and together form a closed quantum system that is assumed to follow an unitary evolution [87]. Consider a composite system formed by the system of interest S and the environment E. The Hilbert space of the total system is given by the tensor product of the Hilbert space of the system $\mathcal{H}_{\mathcal{S}}$ and the Hilbert space of the environment $\mathcal{H}_{\mathcal{E}}$, $\mathcal{H} = \mathcal{H}_{\mathcal{S}} \otimes \mathcal{H}_{\mathcal{E}}$. The total Hamiltonian is the sum of the Hamiltonian of each systems plus a term H_I responsible for the interaction between the system and the environment,

$$H(t) = H_S \otimes I_E + I_S \otimes H_E + H_I(t)$$

The matrix ρ represents the physical state of the total system, it is a positive definite trace class operator on $\mathcal{H}$ with unit trace, i.e, $\rho \geq 0$ which means that ρ is self-adjoint with non-negative eigenvalues, and $tr\rho = 1$. The states of the subsystem S and E are given by the partial trace over $\mathcal{H}_{\mathcal{S}}$ and $\mathcal{H}_{\mathcal{E}}$,

$$\rho_S = tr_E\rho; \qquad\qquad \rho_E = tr_S\rho;$$

For the subsystem S, it is possible to write the evolution of the density matrix using the von Neumann equation:

$$\frac{d}{dt}\rho_S(t) = -itr_E[H(t), \rho(t)] \tag{4.16}$$

However, studying the dynamics of the reduced system with the exact equation (4.16) is not always easy. Some approximations are usually done to render the problem tractable.

If initially the system and the environment are uncorrelated, $\rho_{SE}(0) = \rho_S(0) \times \rho_E(0)$, the evolution of the subsystem S can be expressed as

$$\rho_S(t) = V(t,0)[(\rho_S(0))] \equiv tr_E\{U(t,0)[\rho_{SE}(0)]U^\dagger(t,0)\} \tag{4.17}$$

For the homogeneous-time case, equation (4.17) defines a map from the space $B(\mathcal{H}_\mathcal{S})$ of density matrix states of the reduced system into itself.

$$V(t,0) : B(\mathcal{H}_\mathcal{S}) \to B(\mathcal{H}_\mathcal{S}) \tag{4.18}$$

This map, describing the state change of the open system over time, is called a dynamical map. It is easy to check that it preserves trace and Hermiticity

$$[V(t,0)[A]]^\dagger = V(t,0)[A^\dagger] \tag{4.19}$$

and

$$tr_S\{V(t,0)[A]\} = tr_S\{A\} \tag{4.20}$$

Additionally, $V(t,0)$ maps positive operators to positive operators, so that $V(t,0)\rho$ is a valid density operator for any input density operator ρ

$$A \geq 0 \to V(t,0)[A] \geq 0 \tag{4.21}$$

This property remains true if the operation is applied to any part of the total system and then is said to be completely positive. Consider any possible extension of $\mathcal{H}_\mathcal{S}$ to the tensor product $\mathcal{H}_\mathcal{S} \otimes \mathcal{H}_\mathcal{A}$; then $V(t,0)$ is completely positive on $\mathcal{H}_\mathcal{S}$ if $V(t,0) \otimes I_A$ is positive for all such extensions.

In general, a quantum process of an open system is given by a completely positive and trace-preserving (CPT) quantum dynamical map. There is a specially interesting subclass of maps, called Markovian process, where, additionally, the following semigroup composition law is satisfied

$$V(t_1,0)V(t_2,0) = V(t_1+t_2,0) \tag{4.22}$$

If a dynamical map follows this law with both $V(t_1)$ and $V(t_2)$ being completely positive, the dynamical map is called divisible. In this case the map $V(t)$ can be written as

$$V(t) = e^{\mathcal{L}t}$$

where $\mathcal{L}$ is the generator of the semigroup. The reduced density matrix is easily obtained as a first-order differential equation,

$$\frac{d}{dt}\rho_S(t) = \mathcal{L}\rho_S(t). \tag{4.23}$$

Eq. (4.23) represents a Markovian master equation. The most general time-independent infinitesimal generator $\mathcal{L}$ of a quantum dynamical semigroup [89, 90] for the case of finite dimensional Hilbert space, is a super-operator which has the following form,

$$\mathcal{L}\rho_S = -i[H, \rho_S] + \sum_{k=1}^{N^2-1} \gamma_k (A_k \rho_S A_k^\dagger - \frac{1}{2} A_k^\dagger A_k \rho_S - \frac{1}{2} \rho_S A_k^\dagger A_k) \tag{4.24}$$

where N is the dimension of the Hilbert space $\mathcal{H}_S$. The commutator with the Hamiltonian of the system H represents the unitary part of the evolution. The operators A_k are the Lindblad operators describing the decay modes of the system, and $\gamma_k \geq 0$ are the corresponding decay rates. This equation characterizes a quantum dynamical semigroup which describes a Markovian process.

This kind of description is appropriate for physical systems in which the time scales for the decay of environmental correlations are smaller than the characteristic time scale of the system evolution: and one can neglect memory effects in the environment. This approximation allows to treat the evolution of the subsystem as a Markovian process and write the dynamics of the reduced system in terms of a quantum dynamical semigroup.

4.5 Quantum non-Markovian processes

In order to apply a quantum Markovian master equation to describe the evolution of the system, we have to perform some approximation to ensure that the process is memoryless. However, in many open quantum systems there are evidences of strong memory effects, in particular in the case when there is strong coupling between the system and the environment. Due to those problems, the study by means of the dynamical semigroup becomes tricky. Different techniques have been thus developed to derive master equations beyond the Markovian approximation. Following the projection operator technique developed by Nakajima-Zwanzig in Ref. [91, 92], a natural non-Markovian generalization of Eq. (4.23) would result in an integrodifferential master equation,

$$\frac{d}{dt}\rho_S(t) = \int d\tau K(\tau)\rho_S(t-\tau), \tag{4.25}$$

which takes into account memory effects through the memory kernel $K(\tau)$. The rate of change of the state $\rho(t)$ at time t then depends on its whole history.

However, even if analytical solutions can be achieved, the generalized master equations becomes soon too complicated. An alternative approach is desirable.

It is possible to obtain a first order differential equation for the reduced density matrix of the system through an alternative approach, called the time-convolutionless projection operator technique (TCL) [93]. The goal of the TCL is to achieve an equation of motion which is local in time, in contrast to the Nakajima-Zwanzing equation, which is non-local in time. In this case, the reduced density matrix of the system $\rho_s(t)$ is given by the master equation

$$\frac{d}{dt}\rho_S(t) = \mathcal{L}\rho_S = -i[H,\rho_S] + \sum_{k=1}^{N^2-1} \gamma_k(t)[A_k(t)\rho_S(t)A_k^\dagger(t) - \frac{1}{2}A_k^\dagger(t)A_k(t)\rho_S(t) - \frac{1}{2}\rho_S(t)A_k^\dagger(t)A_k(t)] \tag{4.26}$$

Where $H(t)$ is the Hamiltonian of the system, $A_k(t)$ are the Lindblad operators describing the decay modes of the system, and $\gamma_k(t)$ are the corresponding decay rates. For arbitrary time-dependent operators $H(t)$ and $A_k(t)$, and for $\gamma_k(t) \geq 0$ equation (4.26) yields a completely positive dynamical transformations, in which the evolution over any time interval is completely positive, and can be considered as a time-dependent quantum Markovian process. However, in the non-Markovian case, the rates $\gamma_k(t)$ have oscillations and take negative values. The memory effects are taken into account through the sign of the $\gamma_k(t)$ and reflect the flow of information between the system and the environment.

It is always possible to write the composition law

$$V(t_2,t_1)V(t_1,0) = V(t_2,0) \tag{4.27}$$

and the map

$$V(t_2,t_1) = \mathcal{T}e^{\int_{t_1}^{t_2}\mathcal{L}(t')dt'} \qquad (t_2 \geq t_1 \geq 0) \tag{4.28}$$

where $\mathcal{T}$ is the time-ordering operator. When this time local master equation describes a Markovian process, the dynamical map $V(t_2,t_1)$ is trace-preserving and completely positive. However, in the non-Markovian case, the dynamical map $V(t_2,t_1)$, may not be completely positive due to the negative rate, $\gamma_k(t)$. Therefore a quantum dynamical semigroup is not generated.

It is worth stressing that the master equation (4.26) produces physical states, it preserves the positivity of the density matrix. It is necessary that $V(t_2,0)$ be completely positive to be a dynamical map, however, $V(t_2,t_1)$ may not be completely positive.

Due to the negative decay rates, one can see that Eq (4.28) violates the complete positivity, and then divisibility. Several approaches to quantify non-Markovianity are based on these features, divisibility and complete positivity of the dynamical maps, although there is no single measure of non-Markovianity.

Non-Markovian behavior is attracting a lot of attention due to the need to control applications on quantum technologies. Whit this goal in mind, several methods to define the limit between Markovian and non-Markovian quantum dynamics and several proposed measures to assess the degree of memory have been developed. In this thesis we will follow a method recently introduced in Ref. [88]. The measure, that takes into account the divisibility of the map matching a direct equivalence between divisibility and positive rates in the time-local master equations, is based on the trace distance, which quantifies the distinguishability of quantum states, and can be interpreted in terms of the information flow between the open system and its environment. The measure takes nonzero values whenever there is a flow of information from the environment back to the open system. It has already been used in different contexts [94].

4.6 Operator sum representation

Useful for our discussion is the operator sum representation of the dynamical maps. We are focusing, as described above, on the dynamical evolution of a subsystem S. We assume that the system and the environment start in a product state $\rho_S \otimes \rho_E$, and there are no correlations between them. A partial trace over the environment can be performed to obtain the reduced state of the system:

$$\varepsilon(\rho) = tr_E[U(\rho_S \otimes \rho_E)U^\dagger] \tag{4.29}$$

We can rewrite the Eq. (4.29) in terms of operators acting on the Hilbert space of the system $\mathcal{H}_\mathcal{S}$. Let $\mid \mu\rangle_E$ be an orthonormal basis for $\mathcal{H}_\mathcal{E}$, and consider that the initial state of the environment is given by a pure state $\mid 0\rangle_E$, then

$$\varepsilon(\rho) = \sum_\mu {}_E\langle\mu \mid U(\rho_S \otimes \mid 0\rangle_{EE}\langle 0 \mid)U^\dagger \mid \mu\rangle_E = \sum_\mu M_\mu \rho_S M_\mu^\dagger \tag{4.30}$$

where $M_\mu \equiv {}_E\langle\mu \mid U \mid 0\rangle_E$ is an operator on the state space of the system S. Equation (4.30) defines a liner map ε that takes linear operators to linear operators. Equation (4.30) is known as the Kraus representation or the operator sum representation, and the set of operators $\{M_\mu\}$ are known as the Kraus operators or operation elements for the quantum operation ε. Since we can perform the

partial trace in any basis, the operator sum representations, of a given superoperator, ε is not unique. Notice that, if there is only one term in the operator sum representation, we then have an unitary evolution of ρ_S. Superoperators provide us a formalism for studying decoherence, i.e. the evolution of pure states into mixed states.

4.7 Discrete time Quantum Markovian and non-Markovian processes

As in the case of the continuous time quantum evolution, when the evolution of the system can not be expressed by an unitary evolution due to the fact that our system is composed by two subsystems which interact with each other, we are talking about open systems and we need a more sophisticated description. In the case of discrete time evolution of the system, the dynamics of open systems is also given by the mathematical tool of semigroup of completely positive (CP) trace-preserving dynamical maps.

The map $\varepsilon : \rho \to \rho'$ that transforms a density matrix ρ into a density matrix ρ', has to satisfy the following properties to be trace-preserving and completely positive

1. ε is linear $\varepsilon(\lambda\rho_1 + (1-\lambda)\rho_2) = \lambda\varepsilon(\rho_1) + (1-\lambda)\varepsilon(\rho_2)$
2. ε preserves hermiticity $\rho'^{\dagger} = \sum_\mu M_\mu \rho \dagger M_\mu^\dagger = \rho$
3. ε is trace-preserving $tr(\rho') = \sum_\mu tr(\rho M_\mu^\dagger M_\mu) = tr(\rho) = 1$
4. ε is completely positive

Given the initial condition $\rho(0)$ for the system, we can then write the successive evolutions of the system as $\rho(t) = \varepsilon^t(\rho(0))$ where ε^t indicates t applications of the map. Hence, the evolution obeys a forward composition law and is called a discrete time quantum dynamical semigroup. Therefore, trace-preserving completely positive maps describe general dynamics. When M_μ does not depend on the past states the dynamical map ε represent a discrete time Markovian process.

One can generalize the process for a time dependent CP map $\varepsilon(t)$, and then the map is Markovian if $\varepsilon(t)$ is divisible. We can write this condition as

$$\varepsilon(t) = \varepsilon_t \varepsilon(t-1) \tag{4.31}$$

with some sequence of CP maps $\varepsilon_1\varepsilon_2 ..., \varepsilon_t$. To be clear, we require that

$$\varepsilon(1) = \varepsilon_1, \qquad \varepsilon(2) = \varepsilon_2\varepsilon_1, \qquad \varepsilon(3) = \varepsilon_3\varepsilon_2\varepsilon_1 \tag{4.32}$$

If $\varepsilon(t)$ is not divisible, i.e., such a sequence $\varepsilon_1\varepsilon_2..., \varepsilon_t$ does not exist, then the process is non-Markovian.

4.8 Quantum Walks and non-Markovian behavior

The asymptotic behavior of the QW has been recently investigated focusing on the chirality or spin reduced density matrix, obtained when the position degree of freedom is traced out [95–98]. This matrix has a long-time limit that depends on the initial conditions. One finds thus the following situation: the dynamical evolution of the QW is a unitary process, however the asymptotic behavior of the reduced density matrix has some properties which are shared by some diffusive Markovian processes. This allows to amalgamate concepts such as thermodynamic equilibrium with the idea of a system that follows a unitary evolution. Refs. [96, 98] have developed a thermodynamic theory to describe the QW equilibrium between the position and chirality degrees of freedom; it is possible to introduce the concept of temperature for an isolated quantum system that evolves in a composite Hilbert space (i.e. the tensor product of several subspaces). Additionally, Ref. [96] has shown that the transient behavior towards thermodynamic equilibrium is described by a master equation with a time-dependent population rate.

In this section we study the asymptotic QW behavior with and without decoherence, and exploit the measure proposed in Ref. [88] to evaluate its non-Markovianity. We show that, without decoherence, the reduced density matrix dynamics has a clear time dependence and a well-defined limit, that can be calculated in terms of the initial conditions. This corresponds, when comparing the evolution of two different initial states, to a reduced asymptotic trace distance. The introduction of decoherence translates, as the long-time limit is concerned, into a trivial result, since all states evolve towards the maximally decohered state (proportional to the identity matrix).

The evolution during the first time steps of the QW features an interesting phenomenon, i.e. the presence of oscillations in the trace distance between pairs of states, which is interpreted as a signature of a non-Markovian process. Such oscillations occur both with and without decoherence, even though they become more and more attenuated as the level of noise increases. In agreement with

our observations for the asymptotic limit, the trace distance tends to zero when decoherence affects the system.

4.9 Asymptotic reduced density matrix for the QW

The density matrix of the quantum system is

$$\rho(t) = |\Psi(t)\rangle\langle\Psi(t)|. \tag{4.33}$$

To study the Hadamard QW time dependence on the initial conditions, we take the initial state of the walker as sharply localized at the origin with pure state of chirality, thus

$$|\Psi(0)\rangle = |0\rangle \otimes |\Phi_0\rangle\,. \tag{4.34}$$

Here

$$|\Phi_0\rangle = \begin{pmatrix} \cos\frac{\gamma}{2} \\ e^{i\varphi}\sin\frac{\gamma}{2} \end{pmatrix}, \tag{4.35}$$

with $\gamma \in [0,\pi]$ and $\varphi \in [0,2\pi]$ defining a point on the three-dimensional Bloch sphere. In this case the initial density matrix is

$$\rho(0) \quad = \quad |0\rangle\langle 0| \otimes |\Phi_0\rangle\langle\Phi_0|\,, \tag{4.36}$$

where

$$|\Phi_0\rangle\langle\Phi_0| = \begin{pmatrix} \cos^2\frac{\gamma}{2} & \frac{e^{-i\varphi}}{2}\sin\gamma \\ \frac{e^{i\varphi}}{2}\sin\gamma & \sin^2\frac{\gamma}{2} \end{pmatrix}. \tag{4.37}$$

In order to use the affine map approach [99, 100], Eq. (4.37) can be transformed to express the two-by-two matrix as a four-dimensional column vector, obtaining

$$\begin{aligned} |\Phi_0\rangle\langle\Phi_0| &= r_0 I + r_1\sigma_1 + r_2\sigma_2 + r_3\sigma_3 \\ &= \begin{pmatrix} r_0 \\ r_1 \\ r_2 \\ r_3 \end{pmatrix} = \frac{1}{2}\begin{pmatrix} 1 \\ \cos\varphi\sin\gamma \\ -\sin\varphi\sin\gamma \\ \cos\gamma \end{pmatrix}, \end{aligned} \tag{4.38}$$

with σ_i $(i = 1,2,3)$ the Pauli matrices, and

$$r_i = \frac{1}{2}\mathrm{tr}((|\Phi_0\rangle\langle\Phi_0|)\sigma_i). \tag{4.39}$$

The reduced density operator is defined as

$$\rho_c(t) = \mathrm{tr_s}(\rho(t)) = \sum_{x=-\infty}^{\infty} \langle x|\rho(t)|x\rangle, \tag{4.40}$$

where the partial trace is taken over the positions. Following the method introduced in Ref. [99] and generalized in Ref. [100], Eq. (4.40) can be transformed into

$$\rho_c(t) = \int_{-\pi}^{\pi} \frac{dk}{2\pi} L_k^t(|\Phi_0\rangle \langle\Phi_0|), \tag{4.41}$$

with L_k the superoperator defined as

$$L_k = \begin{pmatrix} 1 & 0 & 0 & 0 \\ 0 & 0 & \sin 2k & \cos 2k \\ 0 & 0 & -\cos 2k & \sin 2k \\ 0 & 1 & 0 & 0 \end{pmatrix}. \tag{4.42}$$

In order to obtain the eigenvalues of L_k, it is necessary to find the eigenvalues of the following associated matrix

$$M_k = \begin{pmatrix} 0 & \sin 2k & \cos 2k \\ 0 & -\cos 2k & \sin 2k \\ 1 & 0 & 0 \end{pmatrix}. \tag{4.43}$$

The eigenvalues of Eq. (4.43) are

$$\lambda_1 = 1, \quad \lambda_2 = e^{i(\alpha+\pi)}, \quad \lambda_3 = e^{-i(\alpha+\pi)}, \tag{4.44}$$

where

$$\cos\alpha = \frac{1}{2}(1 + \cos 2k) = (\cos k)^2. \tag{4.45}$$

The corresponding eigenvectors are

$$\begin{aligned} \vec{v_1} &= \begin{pmatrix} v_{11} \\ v_{21} \\ v_{31} \end{pmatrix} \\ &= \frac{\sqrt{2}\cos k}{\sqrt{3+\cos 2k}} \begin{pmatrix} 1 \\ (1-\cos 2k)/\sin 2k \\ 1 \end{pmatrix}, \end{aligned} \tag{4.46}$$

$$\begin{aligned}\vec{v_2} &= \begin{pmatrix} v_{12} \\ v_{22} \\ v_{32} \end{pmatrix} \\ &= \frac{1}{N_2}\begin{pmatrix} e^{i(\alpha+\pi)} \\ -(e^{i(\alpha+\pi)} - 2\cos 2k)/(2\sin 2k) \\ 1 \end{pmatrix}, \end{aligned} \tag{4.47}$$

$$\begin{aligned}\vec{v_3} &= \begin{pmatrix} v_{13} \\ v_{23} \\ v_{33} \end{pmatrix} \\ &= \frac{1}{N_3}\begin{pmatrix} e^{-i(\alpha+\pi)} \\ -(e^{-i(\alpha+\pi)} - 2\cos 2k)/(2\sin 2k) \\ 1 \end{pmatrix}, \end{aligned} \tag{4.48}$$

with N_2 and N_3 normalization factors. It is now straightforward to obtain $(L_k)^t$ using the diagonal expression for L_k, that is

$$(L_k)^t = B\begin{pmatrix} 1 & 0 & 0 & 0 \\ 0 & 1 & 0 & 0 \\ 0 & 0 & e^{it(\alpha+\pi)} & 0 \\ 0 & 0 & 0 & e^{-it(\alpha+\pi)} \end{pmatrix} B^\dagger. \tag{4.49}$$

Here, B is the eigenvector matrix

$$B = \begin{pmatrix} 1 & 0 & 0 & 0 \\ 0 & v_{11} & v_{12} & v_{13} \\ 0 & v_{21} & v_{22} & v_{23} \\ 0 & v_{31} & v_{32} & v_{33} \end{pmatrix}, \tag{4.50}$$

and $B^\dagger$ its conjugate transpose. Substituting Eq. (4.50) into Eq. (4.49) and exploiting the stationary phase theorem to neglect the oscillatory terms $e^{\pm it(\alpha+\pi)}$ when time goes to infinity, one finds the following asymptotic equation

$$(L_k)^t \longrightarrow \begin{pmatrix} 1 & 0 & 0 & 0 \\ 0 & |v_{11}|^2 & v_{11}v_{21}^* & v_{11}v_{31}^* \\ 0 & v_{21}v_{11}^* & |v_{21}|^2 & v_{21}v_{31}^* \\ 0 & v_{31}v_{11}^* & v_{31}v_{21}^* & |v_{31}|^2 \end{pmatrix}. \tag{4.51}$$

The reduced density matrix in the asymptotic regime, $\widetilde{\rho_c}$, can be calculated using Eq. (4.41) as

$$\widetilde{\rho_c} \equiv \lim_{t\to\infty} \rho_c(t) \quad = \lim_{t\to\infty} \int_{-\pi}^{\pi} \frac{dk}{2\pi} L_k^t \left|\Phi_0\right\rangle \left\langle\Phi_0\right| . \tag{4.52}$$

In order to work out this expression, it is necessary to solve the following integrals

$$\int_{-\pi}^{\pi} \frac{\left|v_{11}\right|^2}{2\pi} dk = 1 - \frac{1}{\sqrt{2}}, \tag{4.53}$$

$$\int_{-\pi}^{\pi} \frac{\left|v_{21}\right|^2}{2\pi} dk = \sqrt{2} - 1, \tag{4.54}$$

$$\int_{-\pi}^{\pi} \frac{\left|v_{31}\right|^2}{2\pi} dk = 1 - \frac{1}{\sqrt{2}}, \tag{4.55}$$

$$\int_{-\pi}^{\pi} \frac{v_{11} v_{31}^*}{2\pi} dk = 1 - \frac{1}{\sqrt{2}}, \tag{4.56}$$

$$\int_{-\pi}^{\pi} \frac{v_{11} v_{21}^*}{2\pi} dk = \int_{-\pi}^{\pi} \frac{v_{21} v_{31}^*}{2\pi} dk = 0. \tag{4.57}$$

Therefore, we obtain analytically the QW reduced density matrix in the asymptotic regime,

$$\begin{aligned} \widetilde{\rho_c} &= \begin{pmatrix} r_0 \\ \left(1 - \frac{1}{\sqrt{2}}\right)(r_1 + r_3) \\ \left(\sqrt{2} - 1\right) r_2 \\ \left(1 - \frac{1}{\sqrt{2}}\right)(r_1 + r_3) \end{pmatrix} \\ &= \frac{1}{2} \begin{pmatrix} 1 \\ \left(1 - \frac{1}{\sqrt{2}}\right)(\cos\varphi \sin\gamma + \cos\gamma) \\ \left(\sqrt{2} - 1\right) \sin\varphi \sin\gamma \\ \left(1 - \frac{1}{\sqrt{2}}\right)(\cos\varphi \sin\gamma + \cos\gamma) \end{pmatrix}. \end{aligned} \tag{4.58}$$

Going back to the 2×2 matrix formalism, the reduced density matrix in the asymptotic regime can be finally written as

$$\widetilde{\rho_c} = \begin{pmatrix} \Pi_L & Q_0 \\ Q_0^* & \Pi_R \end{pmatrix}, \tag{4.59}$$

where

$$\begin{aligned}
\Pi_L &= \frac{1}{2}\left[1+\left(1-\frac{1}{\sqrt{2}}\right)(\cos\varphi\sin\gamma+\cos\gamma)\right], \\
\Pi_R &= \frac{1}{2}\left[1-\left(1-\frac{1}{\sqrt{2}}\right)(\cos\varphi\sin\gamma+\cos\gamma)\right], \\
Q_0 &= \frac{1}{2}\left(1-\frac{1}{\sqrt{2}}\right)\left[(\cos\varphi\sin\gamma+\cos\gamma)\ -i\sqrt{2}\sin\varphi\sin\gamma\right].
\end{aligned} \tag{4.60}$$

4.10 QW map equation

The aim of this section is to study the populations of the reduced density matrix for the standard (decoherence-free) QW. Using Eq. (4.33), and Eq. (4.40), this matrix is expressed as

$$\rho_c(t) = \begin{pmatrix} P_L(t) & Q(t) \\ Q^*(t) & P_R(t) \end{pmatrix}, \tag{4.61}$$

where

$$P_L(t) = \sum_{k=-\infty}^{\infty} |a_k(t)|^2, \tag{4.62}$$

$$P_R(t) = \sum_{k=-\infty}^{\infty} |b_k(t)|^2, \tag{4.63}$$

$$Q(t) \equiv \sum_{k=-\infty}^{\infty} a_k(t) b_k^*(t). \tag{4.64}$$

The global chirality distribution (GCD) is defined as the distribution

$$\begin{bmatrix} P_L(t) \\ P_R(t) \end{bmatrix}, \tag{4.65}$$

with $P_R(t) + P_L(t) = 1$.

It is shown in Ref. [95] that the GCD satisfies the following map

$$\begin{aligned}
\begin{bmatrix} P_L(t+1) \\ P_R(t+1) \end{bmatrix} &= \begin{pmatrix} \cos^2\theta & \sin^2\theta \\ \sin^2\theta & \cos^2\theta \end{pmatrix} \begin{bmatrix} P_L(t) \\ P_R(t) \end{bmatrix} \\
&\quad + \mathrm{Re}\,[Q(t)] \sin 2\theta \begin{bmatrix} 1 \\ -1 \end{bmatrix}.
\end{aligned} \tag{4.66}$$

We observe that, if the "interference term"

$$\mathrm{Re}\,[Q(t)]\sin 2\theta \begin{bmatrix} 1 \\ -1 \end{bmatrix} \tag{4.67}$$

in Eq. (4.66) is neglected, the time evolution of the GCD could be described by a classical Markovian process. The two-dimensional matrix

$$\begin{pmatrix} \cos^2\theta & \sin^2\theta \\ \sin^2\theta & \cos^2\theta \end{pmatrix} \tag{4.68}$$

can be interpreted as the corresponding transition probability matrix for a Markov chain, since it satisfies the necessary requirements: all its elements are positive and the sum over the elements of any column or row is equal to one. However $Q(t)$ (together with $P_L(t)$ and $P_R(t)$) is a time-dependent function. This implies that the map defined by Eq. (4.66) does not correspond to a classical Markovian process. It is important to stress that, here, we are just analyzing the GCD (i.e. the left and right populations of the chiral degree of freedom) in terms of classical Markovian behavior. A study of quantum Markovianity requires, on the other hand, to consider the evolution of the complete matrix $\rho_c(t)$ and will be performed in section 4.12.

In spite of the time dependence manifested by Eq. (4.66), the GCD does possess a long-time limiting value, as obtained in previous section. Eq. (4.66) can be used to derive a consistency condition relating Π_L, Π_R, and Q_0, by taking the limit $t \to \infty$. One then finds

$$\begin{bmatrix} \Pi_L \\ \Pi_R \end{bmatrix} = \frac{1}{2}\begin{bmatrix} 1 + 2\mathrm{Re}(Q_0)/\tan\theta \\ 1 - 2\mathrm{Re}(Q_0)/\tan\theta \end{bmatrix}. \tag{4.69}$$

When $\theta = \pi/4$, Eq. (4.69) agrees with the expressions given by Eq. (4.60). This interesting result shows that the long-time probability to find the system with left or right chirality only depends on the asymptotic interference term. Although the dynamical evolution of the QW is unitary, the evolution of its GCD has an asymptotic limit, a feature which is characteristic of a diffusive behavior. The situation is even more surprising if we compare our case with the case of the QW on finite graphs [101], where it is shown that there is no convergence to a stationary distribution. In order to quantify how much the asymptotic limit keeps track of the initial state, we use the trace distance

$$D(\rho_1 - \rho_2) = \frac{1}{2} tr|\rho_1 - \rho_2|,$$

which gives us a measure for the distinguishability of two quantum states. Here, $|\rho| = \sqrt{\rho^\dagger \rho}$. We calculate this quantity for two reduced density matrices (in the chiral space) that correspond to two different initial states of Eq. (4.37). Following the notation defined in Eq. (4.61), we write

$$\rho_1(t) - \rho_2(t) = \begin{pmatrix} P_{1L}(t) - P_{2L}(t) & Q_1(t) - Q_2(t) \\ Q_1^*(t) - Q_2^*(t) & P_{1R}(t) - P_{2R}(t) \end{pmatrix}. \tag{4.70}$$

We now evaluate the trace distance between the asymptotic reduced density matrices for the QW without decoherence while, in next section, we extend the investigation to the scenario that takes into account decoherence introduced by broken links. Considering two different initial conditions, the difference between their asymptotic reduced density matrices is

$$\tilde{\rho}_{12} = \begin{pmatrix} \Pi_{1L} - \Pi_{2L} & Q_{10} - Q_{20} \\ Q_{10}^* - Q_{20}^* & \Pi_{1R} - \Pi_{2R} \end{pmatrix}. \tag{4.71}$$

Therefore, the distance between the asymptotic reduced density matrices is defined as

$$D(\tilde{\rho}_{12}) = \frac{1}{2} tr\, |\tilde{\rho}_{12}|\,. \tag{4.72}$$

After some algebra, taking into account Eq. (4.69) with $\theta = \pi/4$, the asymptotic trace distance can be expressed, in terms of the initial conditions, as

$$D(\tilde{\rho}_{12}) = \sqrt{2\left[\mathfrak{Re}\left(Q_{10} - Q_{20}\right)\right]^2 + \left[\mathfrak{Im}\left(Q_{10} - Q_{20}\right)\right]^2}. \tag{4.73}$$

Here, $\mathfrak{Re}(Q_0)$ ($\mathfrak{Im}(Q_0)$) is the real (imaginary) part of Q_0, and Q_0 is given by Eq. (4.60). In order to study the dependence on the initial conditions, we consider the evolution of pairs of independent states under the QW map. We fix the initial conditions for the first state and study Eq. (4.73) by considering different points on the Bloch sphere as the initial conditions for the second state.

Figures 4.1 and 4.2 show our results in two non-equivalent scenarios. As can be seen from these figures, the asymptotic trace distance has a non trivial behavior as a function of the second state, once the first one is fixed. The left panel gives an idea on how much the trace distance is reduced (the minimum reduction being of the order of 1/2 in the case represented in Fig. 4.1, whereas lower values are reached for the parameters that correspond to Fig. 4.2). The contour levels can be mapped to the points of the Bloch sphere associated with the second state (right panel), thus providing a closer relationship to physical states. As we see by comparing the two figures, changing the first state does not translate into a simple rotation of the Bloch sphere representation, the reason being that the coin operator does not commute with arbitrary rotations.

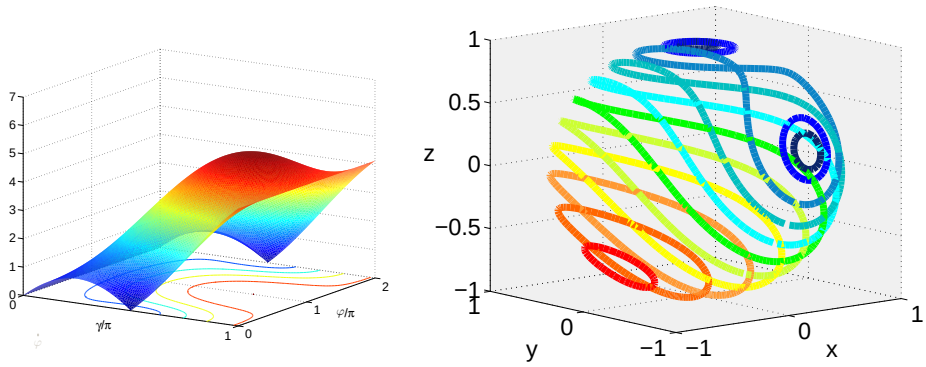

Figure 4.1: Left panel: Asymptotic trace distance as a function of the angles γ and φ, representing the initial conditions of ρ_2. The initial conditions of ρ_1 are given by $\gamma = 0$. Right panel: The contour levels corresponding to the left panel are mapped to the Bloch sphere, using the same color convention.

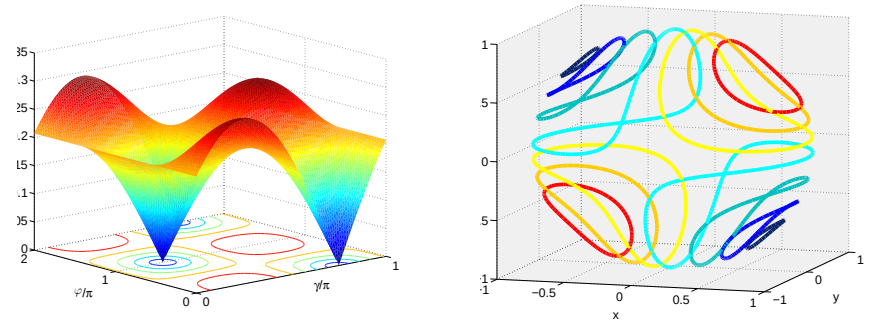

Figure 4.2: Same as Fig. 4.1, but now the initial conditions for ρ_1 are given by $\gamma = \pi/4$ and $\varphi = \pi$.

4.11 Asymptotic density matrix with decoherence

We now study the dynamics of the reduced density matrix for the QW under the effect of decoherence. We exploit the model, known as *broken links*, that was proposed for the first time in Ref. [102] and analyzed in the frame of previous section in Ref. [100]. It induces decoherence in both degrees of freedom, coin and position. Similar results to those presented here can also be found for other decoherence models.

At each time step t, the state of the links in the line is defined. Each link has a probability p of breaking in a given time step. Clearly, for $p = 0$, the ideal decoherence-free QW is recovered. During the movement stage, if the walker is in a site with both the links on right and left broken (this happens with probability p^2), the walker does not move. With probability $(1-p)^2$ both links are not broken and, in this case, the evolution normally occurs. With probability $p(1-p)$ only one link is broken and the walker is *forced* to move to the other direction. Notice, however, that the limit $p \longrightarrow 1$ implies that the walker is forced to stay at the initial position, since the links with neighboring sites are broken with probability one (or close to one), and only the coin operator acts. This limit is no longer connected with the QW and, for this reason, we restrict ourselves to small values of p.

Reference [100] obtains the superoperator L_k that determines the dynamical evolution of the QW with broken links

$$L_k = \begin{pmatrix} 1 & 0 & 0 & 0 \\ 0 & 0 & e & f+p^2 \\ 0 & 0 & p^2-f & e \\ 0 & 1-2p & -2g & -2h \end{pmatrix}, \tag{4.74}$$

where

$$\begin{aligned} e &= (1-p)^2 \sin 2k, \\ f &= (1-p)^2 \cos 2k, \\ g &= p\,(1-p) \sin k, \\ h &= p\,(1-p) \cos k. \end{aligned} \tag{4.75}$$

The dynamics of the reduced density matrix is again described by Eq. (4.52) but

now L_k is given by Eq. (4.74). Redefining M_k as

$$M_k = \begin{pmatrix} 0 & e & f+p^2 \\ 0 & p^2-f & e \\ 1-2p & -2g & -2h \end{pmatrix}, \tag{4.76}$$

its eigenvalues $\{\lambda_i : i = 1, 2, 3\}$ satisfy $|\lambda_i| < 1$ for $0 < p < 1$. If A is the matrix constructed from the eigenvectors of M_k, and Λ the diagonal matrix with the corresponding eigenvalues as elements, it is straightforward to prove that

$$\lim_{t\to\infty} M_k^t = \lim_{t\to\infty} (A\Lambda^t A^\dagger) = 0. \tag{4.77}$$

In this case Eq. (4.52) gives us

$$\widetilde{\rho}_c = \int_{-\pi}^{\pi} \frac{dk}{2\pi} \begin{pmatrix} 1 & 0 & 0 & 0 \\ 0 & 0 & 0 & 0 \\ 0 & 0 & 0 & 0 \\ 0 & 0 & 0 & 0 \end{pmatrix} \begin{pmatrix} r_0 \\ r_1 \\ r_2 \\ r_3 \end{pmatrix}. \tag{4.78}$$

In other words, going back to the formalism of 2×2 matrices, the reduced density matrix in the asymptotic regime is simply

$$\widetilde{\rho}_c = \frac{1}{2} \begin{pmatrix} 1 & 0 \\ 0 & 1 \end{pmatrix}, \tag{4.79}$$

regardless of the initial state. Thus, in the presence of noise, the trace distance between any two different initial states approaches zero, i.e.

$$\lim_{t\to\infty} D(\rho_1(t) - \rho_2(t)) = 0. \tag{4.80}$$

4.12 Short-time behavior

So far we have investigated the properties of the reduced density matrix in the long-time regime. We have obtained a well-defined limit for both the decoherence-free scenario and the case with decoherence. We now discuss the situation where one considers not the asymptotic limit but a finite number of steps in the QW. Our study, as before, is focused on the time evolution of $D(\rho_1 - \rho_2)$.

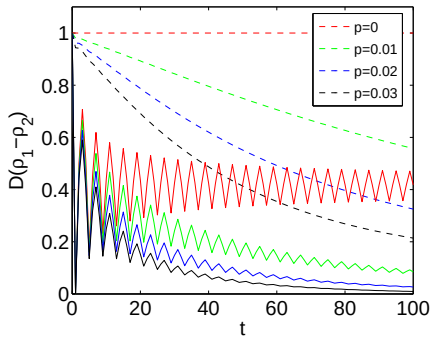

Figure 4.3: Trace distance, as a function of the number of time steps, between the whole density matrices (dashed lines) and between the corresponding reduced density matrices (solid lines). The initial state $\rho_1(0)$ is defined by Eq. (4.37) with $\gamma = 0$, while $\rho_2(0)$ with $\gamma = \pi$. Different values of the decoherence parameter p have been considered.

The measure of quantum non-Markovianity given by Ref. [88] is based on the rate of change [1] of the trace distance

$$\sigma(t, \rho_{1,2}(0)) = \frac{d}{dt} D(\rho_1(t) - \rho_2(t)). \tag{4.81}$$

Figure 4.3 shows the time evolution of the trace distance, both for the whole density matrices and for the corresponding reduced density matrices. We have taken, as initial conditions, the pair of states giving the maximum value of the measure (see below). If one starts from a different pair of states, the curves look qualitatively similar, although the overall scale is smaller.

We have considered various values of the decoherence parameter p, the case $p = 0$ corresponding to the absence of decoherence. Without decoherence, the QW evolves unitarily, so the trace distance between two total states is preserved. If $p > 0$, the evolution for the total state is clearly Markovian, as indicated by a monotonous decrease in the trace distance (this happens of course for any possible pair of initial states). The reduced density matrices, however, show a completely different behavior. Analyzing first the case $p = 0$, we observe the presence of oscillations. In other words, the trace distance increases during some

[1] For the QW considered here, t takes only discrete values $t \in \mathbb{N}$, therefore time derivatives and integrals in time have to be understood as finite differences and sums.

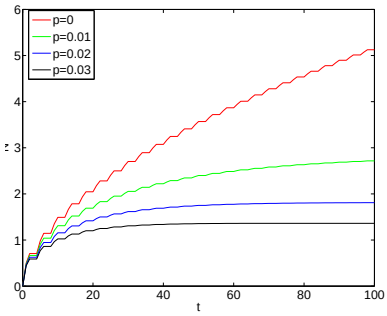

Figure 4.4: Contribution to the non-Markovianity measure, as a function of the number of time steps, evaluated for the pair of initial states $\rho_1(0)$ and $\rho_2(0)$ that maximizes the integral in Eq. (4.82). Different values of the decoherence parameter p have been considered.

time intervals, giving a positive value of σ in Eq. (4.81). As discussed in Ref. [88], this feature is a clear signature of a quantum non-Markovian process. We notice that the amplitude of these oscillations decreases with t. For values $p > 0$, we also observe the presence of such oscillations. In fact, the curves look similar during the first time steps. However, as t increases, the oscillations are more strongly damped than in the decoherence-free case. This effect is even more pronounced for larger values of p. In addition to these features, we also notice that the trace distance goes asymptotically to zero, consistently with our results in section 4.9.

To obtain a quantitative idea about the degree of the non-Markovianity observed in the previous plots, the authors in Ref. [88] suggest, as a figure of merit, the accumulated area of the trace distance variation for those time intervals where the trace distance is increasing, which amounts to calculating

$$N_{max} = \max_{\rho_1,\rho_2} \int_{\sigma>0} \sigma(\tau, \rho_{1,2}(0)) d\tau. \tag{4.82}$$

The maximization is performed over all the possible pairs of initial states $\rho_1(0)$ and $\rho_2(0)$. We have checked numerically that the pair of states maximizing Eq. (4.82) is the same both with and without decoherence, and corresponds to the North and South poles of the Bloch sphere. We have verified, by performing several numerical simulations, that this does not depend either on the total number of time steps considered or on the value of p. We have therefore plotted in Fig.

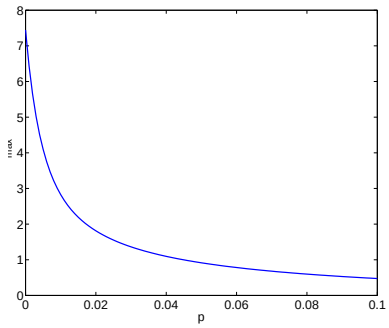

Figure 4.5: Contribution to the non-Markovianity measure, as a function of the decoherence parameter, calculated for the pair of initial states $\rho_1(0)$ and $\rho_2(0)$ that maximizes the integral in Eq. (4.82), and for the time interval $[0, 200]$.

4.4 the value

$$N(t) = \int_{\sigma>0;\tau\in[0,t]} \sigma(\tau, \rho_{1,2}(0))d\tau, \tag{4.83}$$

evaluated for this pair of initial states. $N(t)$ can be seen as the contribution to the non-Markovianity measure in the time window $[0, t]$. Even if in the time window allowed by our computational power it is not possible to evaluate (if any) the asymptotic value of $N(t)$ for $t \to \infty$ (i.e. the non-Markovianity measure N_{max}) in the decoherence-free case, the results reported in Fig. 4.4 give already a very precise picture of how the decoherence affects the degree of non-Markovianity of the coin evolution. The non-Markovianity is stronger as the magnitude of decoherence decreases, with the largest value of its measure corresponding to the decoherence-free case. This feature is clearly shown in Fig. 4.5, where we have plotted the contribution to the non-Markovianity measure N_{max} calculated for the time interval $[0, 200]$ as a function of p, for the North-South pair of states.

Part II

Wigner function

5 Introduction to quantum mechanics in phase space

In classical mechanics the state of a particle is completely determined if its position and momentum are known, i.e, all the information about the state of a particle can be represented as a point in phase space. The state of a particle with n degrees of freedom can be described by a point in $2n$ dimensional phase space and the configuration of the total system is decribed by the generalized coordinates $\vec{q} = (q_1, q_2, ..., q_n)$ and $\vec{p} = (p_1, p_2, ..., p_n)$ where q is the position coordinate and p the conjugate momentum coordinate. The evolution of a particle is described by the Hamiltonian function $H(\vec{q}, \vec{p}, t)$. A function $\rho(\vec{q}, \vec{p})$ giving the density probabilty to find the particle in one point of the phase space can be defined and then, $\rho(\vec{q}, \vec{p})d^n q d^n p$ denotes the probability that the system be in a volume element $d^n q d^n p$ on the phase space. In this scheme the Liouville equation governs the evolution of $\rho(p, q; t)$ in time t.

In quantum mechanics the description of a system is represented by a state vector in the complex Hilbert space or by a density matrix, and the evolution of the state is generated by a self-adjoint Hamiltonian operator acting in the Hilbert space according to the Schrödinger equation. The description of quantum mechanics in phase space can not be easily transferred due to the impossibility to extend the concept of a density probability function since the non-commutative character of position and momentum variables and the uncertainty principle. The precision which allows us to know a state must satisfy the uncertainty principle $\Delta p \Delta q \geq \hbar/2$. However, it is possible to construct a **quasi-probability distribution**, which in conceptual and operational terms is equivalent to the classical probability functions. One of the most used quasi-probability distributions in phase space is the Wigner function.

The formalism of Wigner functions and the formulation of quantum mechanics in phase space have been used since the early days of quantum physics. Originally motivated by the attempt to describe quantum effects in thermal ensembles by Wigner in 1932 [103], various quasi-probability distribution functions have been

developed and applied to many different fields in quantum physics, as alternative formalisms which provide useful computational tools and facilitate physical insight into the quantum nature of states [104, 105]. In particular, in the field of quantum optics, the phase-space descriptions of quantum states have found extensive application. Specially interesting from the experimental point of view is the ability to reconstruct the Wigner function (and thus the quantum state) from measurements of the electromagnetic field quadratures, thus making it a very powerful tool for state tomography [106–108]. Remarkably, the fact that the Wigner function is not positive definite has itself a practical use, since the negative volume in phase space has been proposed as a measure of non-classicality of the state [109].

In analogy to the classical situation, in which a state can be completely described in terms of its phase-space density, a quantum state can also be entirely characterized by its Wigner function, and the expectation values of all observables can be computed as a sum over the whole phase-space weighted by this function. In contrast to the classical case, in the quantum scenario probability distributions cannot be defined simultaneously over position and momentum. Thus the Wigner function is not a true probability distribution, as it becomes apparent by the fact that it can adopt negative values. Instead, it can be interpreted as a quasi-probability distribution whose marginals reproduce the true probability distributions over single observables. Operators and dynamics can also be accommodated in the phase-space picture [110], so that quantum mechanics can be entirely formulated in this framework.

The second part of this thesis consists in the definition of the Wigner function for a quantum system with a **discrete, infinite dimensional Hilbert space** such as a spinless particle moving on an one dimensional lattice. We discuss the peculiarities of this scenario and of the associated phase space construction, propose a meaningful definition of the Wigner function in this case, and characterize the set of pure states for which it is non-negative. Later, we extend the definition of a Wigner function to include an extra degree of freedom such as a spin 1/2 particle that moves on an infinite one-dimensional lattice. Using these definitions, we study the dynamics of the particle subject to a potential in both cases: for a particle with spin and for a spinless particle. In order to establish a clear comparison with our research, we start by reviewing the definition of the Wigner function in continuous space.

5.1 Continuous Wigner Function

In Wigner's formulation, the quantum description of a system S is based on the density matrix ρ, which contains all the physical information of the system. For a quantum one-dimensional system in continuous space, the Wigner function can be written [103] as [1].

$$W_{\mathrm{c}}(x,p) = \frac{1}{\pi}\int_{-\infty}^{\infty} dy \langle x+y|\rho|x-y\rangle \; e^{-i2py}, \tag{5.1}$$

where ρ is the density matrix of the system, and $|x\rangle$ represents the eigenbasis of the position operator, $\hat{X}$

It is also possible to define the Wigner function axiomatically [106]. The fundamental properties that it must satisfy are usually formulated as follows.

1. Reality: due to the hermiticity of the density matrix, the Wigner function is required to be real.
2. Projection: the integral of the Wigner function along any direction, (α, β), in phase space, yields the probability distribution for the outcomes of measuring the observable $\alpha\hat{X} + \beta\hat{P}$, being $\hat{P}$ the momentum operator. In particular, then, the marginal distributions for position and momentum can be obtained, respectively.[2]
3. Inner product: the inner product of two states, given by their density operators, ρ_1 and ρ_2, can be computed from their Wigner functions as $\mathrm{tr}\,(\rho_1\rho_2) = 2\pi \int dxdpW_1(x,p)W_2(x,p)$ where W_1 and W_2 are the Wigner functions of ρ_1 and ρ_2, respectively

From these properties, other features of the Wigner function can be derived, such as the following ones.

- The expectation value of any observable can be reconstructed from the knowledge of the Wigner function,

$$\mathrm{tr}\left(\rho\hat{O}\right) = 2\pi \int dxdpW_O(x,p)W(x,p),$$

where $W_O(x,p) \equiv \frac{1}{\pi}\int_{-\infty}^{\infty} dy\langle x+y|\hat{O}|x-y\rangle \; e^{-i2py}$ is the Wigner representation of the operator $\hat{O}$.

[1] We use natural units, such that $\hbar = 1$.

[2] In the rest of the thesis, unspecified integral (or sum) limits will be understood as extending over the whole range of the integrated (summed) variable. as $\int dpW(x,p) = P(x)$ and $\int dxW(x,p) = P(p)$.

- Following from property 2, the Wigner function is normalized when integrated over the whole phase space, $\int dxdpW(x,p) = 1$.

The Wigner function can also be constructed from the *phase-point operators*, defined for all points in the phase space as

$$A(x,p) \equiv \frac{1}{\pi}\mathcal{D}(x,p)\Pi\mathcal{D}(x,p)^{\dagger}, \tag{5.2}$$

where $\mathcal{D}(x,p) = e^{-i(x\hat{P}-p\hat{X})}$ are displacement operators and $\Pi \mid x\rangle = \mid -x\rangle$ is the parity reflection. The phase-point operators form a complete set, spanning all Hermitian operators. In particular, the Wigner function corresponds to the coefficients of the density matrix in this basis,

$$W(x,p) = \mathrm{tr}\left(\rho A(x,p)\right), \tag{5.3}$$

so that the full state can be reconstructed by

$$\rho = \int dxdpW(x,p)A(x,p). \tag{5.4}$$

Properties equivalent to (1)-(3) can be formulated for phase-point operators, leading to an equivalent definition of the phase space. According to these properties the operators $A(x,p)$ should be Hermitian and satisfy an orthogonality condition, and integrating $A(x,p)$ along a line in phase space must yield a projector.

The Wigner-Weyl formalism establishes a bijective correspondence between a classical phase space function, $F(x,p)$, and a quantum observable $\hat{F}(\hat{X},\hat{P})$. In order to quantize the classical phase space function $F(x,p)$, the Wigner-Weyl formalism establishes that the first step is to write $F(x,p)$ in terms of its Fourier expansion

$$F(x,p) = \int\int d\sigma d\tau f(\sigma,\tau)e^{i(\sigma x+\tau p)} \tag{5.5}$$

Now, to construct the corresponding operator for $F(x,p)$, the variables x and p have to be replaced by the respective quantum operators

$$\hat{F}(X,P) = \int\int d\sigma d\tau f(\sigma,\tau)e^{i(\sigma X+\tau P)}. \tag{5.6}$$

As an example, we show the Wigner-Weyl quantization of the product xp. Using the inverse of Eq. (5.5) in Eq.(5.6) we obtain

$$\hat{F}(\hat{X},\hat{P}) = \int\int\int\int dxdpd\sigma d\tau F(x,p)e^{i(\sigma(\hat{X}-x)+\tau(\hat{P}-p))} \tag{5.7}$$

Making use of the Weyl map expressed in terms of the integral kernel matrix elements

$$\langle x \mid \hat{F}(\hat{X},\hat{P}) \mid y\rangle = \frac{1}{2\pi}\int dp e^{ip(x-y)} F(\frac{x+y}{2},p) \tag{5.8}$$

We have

$$\begin{aligned}\langle x \mid \hat{F}(\hat{X},\hat{P}) \mid y\rangle = \frac{1}{2\pi}\int dp e^{ip(x-y)}\frac{x+y}{2}p = \frac{-i}{2\pi}\frac{x+y}{2}\frac{\partial}{\partial x}\int dp e^{ip(x-y)} = \\ \frac{-i}{2\pi}\frac{x+y}{2}\frac{\partial}{\partial x}2\pi\delta(x-y) = \frac{x+y}{2}\frac{\partial}{\partial x}\langle x \mid y\rangle = \frac{x+y}{2}\langle x \mid \hat{P} \mid y\rangle \\ = \langle x \mid \frac{\hat{P}\hat{X}+\hat{X}\hat{P}}{2} \mid y\rangle \end{aligned} \tag{5.9}$$

The Wigner function and the Weyl transformation are inverse of each other. In this sense, the Wigner function associates to each quantum operator, a corresponding phase space function.

Besides the Wigner function, other probability distributions have been defined. The differences in their construction are based on the definition of the phase space operators. For the definition of the Wigner function, a symmetric ordering of the operators $\hat{P}$ and $\hat{X}$ for the displacement operator is used, $\mathcal{D}(x,p) = e^{-i(x\hat{P}-p\hat{X})}$. It is also possible to use an anti-normal or normal ordering of the operator. For a normal ordering, $D(x,p) = e^{ix\hat{P}}e^{ip\hat{X}}$ the Glauber-Sudarshan or P distribution can be generated and for an anti-normal ordering $D(x,p) = e^{ip\hat{X}}e^{ix\hat{P}}$ the Husimi or Q distribution can be generated.

The P distribution was proposed by Glauber and Sudarshan [111, 112] for a representation of the electromagnetic field. It was formulated as a description of a statistical mixture of coherent states, and for these states it is analogous to a classical probability distribution since it is positive. For other states, however, it can take negative values and therefore it can also be considered as a indication of non-classicality [113, 114]. The P distribution can be interpreted as a weighted mixture of coherent states.

The Husimi or Q distribution proposed by Husimi [115] is built from the diagonal matrix elements of the density operator in the coherent state set. Notice, however, that coherent states form an overcomplete basis for the Hilbert space, therefore they do not constitute an orthonormal basis. Due to the fact that the coherent states form an overcomplete basis, the Q distribution can characterize any state. The Q function is strictly non-negative and it does not reproduce the correct marginal distributions.

6 Wigner function for a particle in an infinite lattice

6.1 Discrete finite case

The original definition, and the applications mentioned above make use of a Wigner function defined in continuous space. It is nevertheless possible to introduce also a sensible Wigner function for systems on a discrete space. A valid generalization of the Wigner function to the case of a discrete Hilbert space involves generalizing the concept of phase space and the definition of phase point operators. Several approaches have been proposed in the literature for the case of a finite dimensional, periodic Hilbert space. Here we briefly describe the two main alternatives, emphasizing their relation to the continuous case, and we establish the basis for our definitions (see [105, 116] for more comprehensive reviews).

Wootters [117] generalized the definition of the Wigner function to discrete periodic Hilbert spaces of prime dimension, N. In Wootter's original construction the phase space was a two dimensional $N \times N$ array, indexed by integers. Complete sets of parallel lines in this phase space, or *striations*, which are defined using arithmetics modulo N, were associated to projective measurements. For more general cases, such as power of prime dimensions or composite systems with both discrete and continuous degrees of freedom, the phase space could be constructed as a Cartesian product of the fundamental pieces.

A related, more general construction, valid for systems whose dimension is an integer power of a prime number, was put forward in [118]. In the general construction the discrete phase space has also size $N \times N$, and was labelled by a finite field. To give a physical interpretation to the discrete phase space, each line is assigned to a pure quantum state. The set of all lines parallel to a given one corresponds to an orthogonal basis, and the distinct sets are mutually unbiased basis [119]. This assignment of states to lines determines the particular definition of the Wigner function for the system, which is therefore not unique. Although closely connected to quantum information concepts and useful to describe sys-

tems of n qubits [120, 121], the lack of a unique physical interpretation and the restriction to dimensions which are powers of primes makes this approach less appropriate for the kind of system we want to describe.

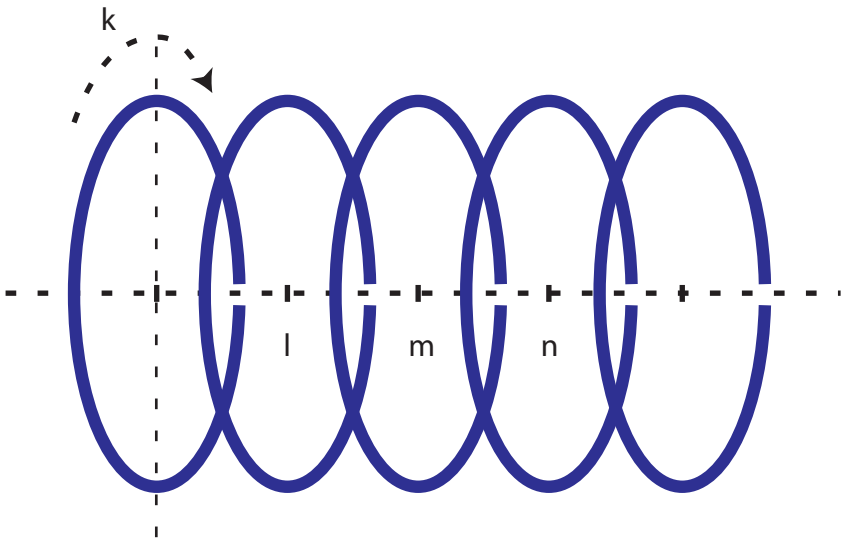

Figure 6.1: Graphical representation of the phase space for an infinite one-dimensional lattice. The *momentum-like* coordinate is continuous and periodic, $k \in [-\pi, \pi[$, and the *position-like* coordinate is discrete, labelled by integer values, m.

Leonhardt [122] introduced another definition, more closely connected to the continuous construction, in which the labels of the phase space axis could be connected to discrete position and momentum base of the physical system. For the case of an odd dimensional system, the discretized version of the continuous definitions is enough to obtain a valid definition of the Wigner function. However, in the case of even dimensional Hilbert spaces, the naive discretization does not suffice to guarantee a Wigner function with the desired properties. Instead, half-odd labels had to be introduced between the integer points of the phase space axis, so that the size of the grid has to be increased to $2N \times 2N$ (see also [123] for a discussion).

A similar approach was pursued in [124], where the construction followed from the definition of discrete phase-point operators and was then applied to the analysis of quantum algorithms [125]. In [126], this approach was also combined with

Wootters' prescription to compose degrees of freedom and employed for the study of quantum teleportation. Our approach builds up on this construction, easily connected to the physical interpretation of the continuous phase space.

Another scenario studied in the literature that relates closely to our construction is that of a pair of quantum variables, the angular momentum and angle [127–129]. The structure of the associated phase space is completely analogous to the one in our problem (see figure 6.1). As discussed in [127], the choice of a Wigner function in that case is not unique, but different Wigner representations are possible for the same system. The prescription presented in the following section can be seen as an alternative to that in [127], which offers the advantage of a more compact expression that can be computed explicitly for some interesting cases and a more direct connection to the Wigner functions for the finite-dimensional case discussed above.

As we will see in the following section, the phase space associated with our problem possesses the topological structure $S^1 \times Z$, where S^1 represents the unit circle. In the continuous case, the phase space becomes $R \times R$. The problem of studying a phase space with this kind of topology has been a recurrent topic since the beginning of quantum mechanics, due to the presence of the angular variable running on S^1, the difficulty being motivated by the fact that the angle is a multivalued or discontinuous variable (see [130, 131], and references therein, for a review). Thus, if one faces the quantization of such a phase space as a starting point, one has to cope with these problems. Another interesting feature that arises as a consequence of the quantization procedure is the possibility of a fractional orbital angular momentum, a theoretical possibility that may find an experimental correspondence in scenarios such as Bloch waves in ideal crystals or the Aharanov–Bohm and fractional quantum Hall effects. In this thesis, we are mostly concerned with the properties of the Wigner function on the infinite lattice, as an alternative to the standard quantum approach; see the above references for a detailed study of the quantization of the corresponding phase space.

6.2 Definition of the Wigner function in the infinite discrete lattice

We consider here a single particle moving on a discrete one-dimensional lattice, with inter-site spacing a. We can define a discrete position basis, given by orthonormal states $|n\rangle$, with $n \in \mathbb{Z}$. Its Fourier transform defines then a quasi-

momentum basis, $|q\rangle = \sqrt{\frac{a}{2\pi}} \sum_n e^{iqna}|n\rangle$, which can be restricted to the first Brillouin zone, $q \in [-\frac{\pi}{a}, \frac{\pi}{a}[$.

Unlike the discrete cases considered above, the Hilbert space of this system is not periodic and has infinite dimension. The continuum limit is recovered as $a \to 0$, and $\frac{1}{\sqrt{a}}|n\rangle \to |x = na\rangle$. We may require that the Wigner function for this system, besides fulfilling the defining properties, also reproduces in that limit the usual one for a particle in the continuum, (5.1).

In [122, 124] the problems in the direct discretization of Eq.(5.2) were connected to the fact that, in the case of even dimensions, such a definition does not generate enough number of independent operators. We may thus wonder whether the fact of having an infinite dimensional system is enough to solve this problem. However, the direct discretization of (5.2), in spite of producing an infinite number of operators, does not suffice either in this case to obtain a Wigner function that fulfills the desired properties in the case of interest as we see now.

Here we follow closely the construction of [124], starting with a definition of the discrete phase space and the associated phase-point operators that then produce the Wigner function. A direct discretization of the phase-point operators leads to

$$A_{\text{direct}}(m,k) = \frac{1}{2\pi} U^{2m} \hat{\Pi} V(-\frac{2k}{a}) e^{i2km}, \tag{6.1}$$

where U is the discrete translation operator, shifting the lattice by one site, $U^m|n\rangle = |n+m\rangle$, and $V(q)$ is the continuous momentum translation, defined by its action on the momentum basis as $V(q')|q\rangle = |q+q'\rangle$. Notice the hybrid character of the phase space in this case, with discrete and unbounded values of m and continuous, periodic $k \in [-\pi, \pi[$. It is easy to see that A_{direct} has periodicity π in the momentum coordinate, $A_{\text{direct}}(n, k \pm \pi) = A_{\text{direct}}(n,k)$. The Wigner function following from these phase-point operators does not fulfill the defining properties. In particular, summing over positions does not produce the correct marginal. Instead,

$$\sum_n W_{\text{direct}}(n,k) \propto \left\langle \tfrac{k}{a}|\rho|\tfrac{k}{a}\right\rangle + \left\langle \tfrac{k+\pi}{a}|\rho|\tfrac{k+\pi}{a}\right\rangle. \tag{6.2}$$

As a consequence, the resolution in k is not enough to retrieve all the information on the state from the Wigner function (see [122, 123] for a discussion of this effect).

The problem does not appear if we integrate over the momentum coordinate, and is thus an effect arising purely from the discrete character of the position basis. It is not surprising, then, that the strategy in [124], consisting in doubling the number of points in the phase space, serves us to define also here an appropriate set of phase-point operators. In our case, the doubling should only affect

the position coordinate, and is equivalent to adopting the definition

$$A(m,k) = \frac{1}{2\pi} U^m \hat{\Pi} V(-\tfrac{2k}{a}) e^{imk}. \tag{6.3}$$

In the position basis, the phase-point operators can then be written as $A(m,k) = \frac{1}{2\pi}\sum_n |m-n\rangle\langle n| e^{-i(2n-m)k}$, and the Wigner function for our system reads

$$W(m,k) \equiv \mathrm{tr}\left[\rho A(m,k)\right] = \frac{1}{2\pi}\sum_n \langle n|\rho|m-n\rangle e^{-i(2n-m)k}. \tag{6.4}$$

This corresponds to a phase space with the structure depicted in figure 6.1, where the m coordinate takes integer values, whereas k is continuous and periodic, taking values in $[-\pi, \pi[$. Notice that $(m,\ k)$ cannot be directly interpreted as discrete positions, and quasimomentum. Instead, they have to be understood as labels of the phase space points. To make the distinction clear, we reserve symbols m and k for the phase space and n, q for the position and quasimomentum states of the lattice. We observe that the Wigner function in (6.4) restricted to even values of m is equivalent to the straightforward discretization from (6.1).

Although the periodicity of $A(m,k)$ is now 2π, it is important to notice that not all the operators are independent. Indeed, $A(m, k \pm \pi) = (-1)^m A(m,k)$, from which it follows

$$W(m, k \pm \pi) = (-1)^m W(m,k). \tag{6.5}$$

It is easy to check that the definition (6.4) fulfills the main properties we require from a valid Wigner function. In particular it is real, as follows from the Hermiticity of (6.3). The inner product property (3) is also easy to check, given operators $\hat{A}$ and $\hat{B}$,

$$2\pi \sum_{m=-\infty}^{\infty} \int_{+\pi}^{-\pi} dk W A(m,k) W B(m,k) = \mathrm{tr}\left(\hat{A}\hat{B}\right), \tag{6.6}$$

In a very similar way, we obtain the explicit expression of the density operator in terms of the Wigner function,

$$\rho = 2\pi \sum_m \int_{-\pi}^{+\pi} dk W(m,k) A(m,k). \tag{6.7}$$

Due to the relation (6.5), the orthogonality relation between phase-point operators adopts the following form,

$$\mathrm{tr}\langle A(m_1,k_1)A(m_2,k_2)\rangle = \frac{1}{4\pi}\delta_{m_1 m_2}\langle \delta(k_1-k_2) + (-1)^{m_1}\Theta(k_2)\delta(k_1-k_2+\pi)\rangle. \\ +(-1)m1\Theta(-k_2)\delta(k_1-k_2-\pi), \tag{6.8}$$

where $\Theta(k)$ is the Heaviside step function. To obtain this relation we made use of $\sum_n e^{ink} = 2\pi \sum_r \delta(k+2\pi r)$, where the sum runs over all $r \in \mathbb{Z}$. Eq. (6.8) reflects the fact that operators associated to phase space points whose k coordinate is shifted by π are not independent, but differ only in a phase.

We may also compute the marginal distributions of (6.4), and obtain

$$\sum_{m=-\infty}^{+\infty} W(m,k) = \tfrac{1}{a}\langle \tfrac{k}{a}|\rho|\tfrac{k}{a}\rangle, \tag{6.9}$$

and

$$\int_{-\pi}^{+\pi} dk W(m,k) = \sum_n \delta_{m,2n}\langle n|\rho|n\rangle. \tag{6.10}$$

The last equations make evident the distinction between the coordinates of the momentum space points, $m \in \mathbb{Z}$, $k \in [-\pi, \pi[$, and the position and quasimomentum bases, $|\, n\rangle$, $|\, q\rangle$. The k coordinate is adimensional and does not directly represent a momentum value, but is connected to $q = k/a$. The *spatial* label m in phase-space is only connected to a discrete position, s, for even values , $m = 2s$, while the odd values of m are analogous to the odd half-integer phase space grid points in [122, 124].

Keeping these considerations in mind, we can take the continuum limit that transforms our discrete lattice into real space. This limit is attained by letting $a \to 0$, with $na \to x \in \mathbb{R}$. With this prescription, we can easily see that the continuum limit of Eq. (6.4) yields (up to a proportionality factor) the proper continuum Wigner function,

$$W(m,k) \underset{a\to 0}{\to} \frac{1}{2} W_{\mathrm{c}}(y = \frac{ma}{2}, q = \frac{k}{a}) = \\ \frac{1}{2\pi}\int_{-\infty}^{+\infty} dz \langle \frac{ma}{2} + z \mid \rho \mid \frac{ma}{2} - z\rangle e^{-i2z\frac{k}{a}}, \tag{6.11}$$

as can be checked from the definition (5.1) after a simple change of variable. Together with the discussion above, this result shows how the proper continuum limit is attained in the phase space coordinates. Indeed, as the spacing is decreased, $m\frac{a}{2} \to x$ and $\frac{k}{a} \to q$. The Wigner function is a quasi-probability distribution, and the physically meaningful quantities are given by integrals over the phase space. The measure of the integration must be modified according to this change of variables, so that we obtain the correspondence, for the integral over any region of the phase space,

$$\sum \int dk W(m,k) \underset{a\to 0}{\longrightarrow} \int dy \int dq W(y,q). \tag{6.12}$$

6.3 Non-classicality of states: negativity of the Wigner function

The fact that the Wigner function is not positive definite over the phase space is interpreted as a quantum feature, since it follows from the incompatibility of quantum observables. This property has been applied to separate quantum states from classical ones. In the continuous case, it is known that the only pure states with non-negative Wigner function are Gaussian states [132]. The classification is not so clear for mixed states, where nevertheless some bounds are known for states with positive Wigner function [133]. From a quantitative point of view, the volume of the negative part of the Wigner function can be used as a measure of non-classicality [109]. More recently, it has been shown that the smallest distance to a state with positive Wigner function can also be used to measure the non-classicality of a state, without needing full tomography [134].

In the context of discrete systems the negativity of the Wigner function has also been explored, but the different prescriptions discussed in the previous section lead to different conclusions. For the direct discretization, a discrete version of Hudson's theorem was proven by Gross [135, 136] for the case of a Hilbert space with odd dimension. In that case the only pure states with non-negative Wigner functions are stabilizer states. For the class of discrete Wigner functions defined as in [118] a characterization was given in [137], where the set of non-negative states was identified with the convex hull of stabilizer states when the Hilbert space dimension was small. Another scenario studied in the literature, which closely relates to our construction, is that of a pair of quantum variables, angular momentum and angle, and their associated phase space [127, 128] which has the same mixed discrete continuous structure of (6.1). For that case, it has been shown that the only states with non-negative Wigner functions are those of well defined angular momentum.

For the situation studied in this thesis, a similar reasoning to that in [127] leads to the conclusion that a pure state has a non negative Wigner function if and only if it is a state of well defined position in the lattice, i.e. the components of the state vector in the position basis are given by a delta function (see the section 6.4.1 for details).

With our definition, however, phases (6.5) imply that any state with a non-vanishing Wigner function on some phase space point with odd-valued position-like coordinate, $W(m = 2s + 1, k) \neq 0$, will necessarily have a contribution of opposite sign at points $(m, k \pm \pi)$. These signs are fundamental in order to ensure that the Wigner function reproduces the momentum and position probability distributions, but are not related to the *quantumness* of the different states. Therefore a naive calculation of the volume of the negative part of the function, i.e. applying the discrete version of the definition in [109], will not be a valid measure of non-classicality, as it would result in a non-vanishing value even for states expected to be *classical*, such as the discrete version of Gaussian states.

A similar phenomenon has been observed in different contexts. In the field of signal analysis, where Wigner functions have also been widely employed, the discrete time Wigner distribution shows similar features, which are related to aliasing [138], and various alternative definitions have been proposed to construct alias-free distributions, and to allow a reconstruction of the continuum time signal from a discrete sample. In the context of finite dimensional quantum systems, a proposal for a *ghost free* Wigner function was put forward in [139]. In all such cases, the negative values of the Wigner function respond to the very structure of the discretized phase space and not to the features of the state or the signal. We would thus like to define a new quantity which serves to estimate non-classicality of states in our system, and allows for a connection to the well-defined continuum limit. In particular, we expect that this non-classicality measure vanishes for all Gaussian states, so as to reproduce the well-known continuum limit, and that it does not include the spurious negative parts from the extended phase space. Notice that these criteria can be considered necessary, but not sufficient for a sensible definition of such measure.

The definition (6.4) leads to a discrete Wigner function which contains two *images*, one in each half of the momentum domain. According to (6.5), they have the same magnitude, but on odd position-like coordinates m, their sign is reverted, as can be seen in (6.3) for the case of a pure Gaussian state. Although in the continuum limit (6.4) reduces to the original expression for the Wigner function, and the second, *ghost* image disappears, we would like to have a quantity that characterizes the *non-classicality* of discretized states. In particular, we require that the criterion is consistent with that for the analogous continuous states, in the cases when such exist.

The so-called ghost image exhibits alternating signs between even and odd space-like coordinates (see, for instance 6.4a), while the regular image is smooth.

In the continuum limit, a single value x corresponds to a pair of even and odd discrete values of the space-like coordinate in the phase space, and the oscillating image vanishes. We would thus like to use as a measure of the non-classicality the negativity restricted to the regular image. However its position in the phase space plane is not fixed, but changes with momentum shifts. A momentum displacement, q_0, translates into a displacement $q_0 a$ in the k coordinate. As the lattice spacing vanishes the regular image lies on the central region of the phase space, while the ghost image is pushed towards the edge, which in the continuum is mapped to infinity.

Instead of trying to locate the regular image, so as to restrict the sum to the corresponding phase-space region, we may apply a filter that eliminates the spurious sign oscillations from odd values of m, and effectively produces two copies of the regular image. We thus define the following quantity,

$$\eta(\rho) \equiv \sum_{m=-\infty}^{+\infty} \int_{-\pi}^{+\pi} dk \left[|W^{(s)}(m,k)| - W^{(s)}(m,k) \right], \tag{6.13}$$

where $W^{(s)}$ is the result of filtering out the sign oscillations for odd m. If the filtering is perfect, in the continuum limit $\eta(\rho)$ will yield twice the negativity of the Wigner function as defined in [109].

Different filtering operations can be tried to this aim. In particular, we propose to use a sign-averaged Wigner function, defined by

$$W^{(s)}(m,k) \equiv \begin{cases} W(m,k) & m \text{ even} \\ \chi(m,k)|W(m,k)| & m \text{ odd}, \end{cases} \tag{6.14}$$

with $\chi(m,k) = \text{sign}[2\ \text{sign}(W(m-1,k)) + \text{sign}(W(m,k)) + 2\ \text{sign}(W(m+1,k))]$, i.e. the even components are unchanged, and the sign of the odd ones is corrected according to a majority criterion that takes into account the sign of the two closest neighboring even points [1]. This produces approximately two copies of the regular image (see 6.4b), so that $\eta(\rho)$ is equivalent to twice the negativity restricted to the half space where this image is supported.

6.4 Particular cases

To illustrate the definitions introduced in the previous sections, we explicitly compute here the Wigner functions and negativities for several pure states.

[1] The factor 2 takes care of the situation when one of the adjacent even points has vanishing $W(m,k)$.

6.4.1 Localized state

We may consider the simplest case, in which the position of the particle is well defined, $|\Psi_\delta\rangle = |n_0\rangle$, so that, in position basis, $\langle n|\Psi_\delta\rangle = \delta_{n\,n_0}$. The Wigner function can then be computed exactly,

$$W_\delta(m,k) = \frac{1}{2\pi}\delta_{m\,2n_0}. \tag{6.15}$$

This function, represented in figure 6.2, is non-negative everywhere, so that $\eta(\delta) = 0$.

As a mentioned before, the only state with positive Wigner function is a delta function. The following proof this affirmation. Analogous to the result in [127] for a conjugate pair of angle and angular momentum variables, with the present definition the Wigner function of a pure state is non negative if and only if it is an eigenstate of the discrete position operator, i.e. $\langle n|\Psi\rangle = \delta_{n\,n_0}$. The first part of the theorem is trivial, since the Wigner function of a localized state (6.15) is non negative.

To show the converse, let us assume a pure state with non-negative Wigner function, $W(m,k) \geq 0$, $\forall m \in \mathbb{Z}$, $k \in [-\pi, \pi[$. From 6.5 it follows that the Wigner function can only be non-vanishing on points of the phase space with even space-like coordinate, $m = 2n$,

$$W(2n+1,k) = 0 \quad \forall n \in \mathbb{Z}. \tag{6.16}$$

The rest of the demonstration follows closely that in [127], and we sketch it here only for completeness, with the proper modifications to match the definition in (6.4).

The proof relies on the following two lemmas, proven in [127], for complex periodic functions and their (discrete) Fourier transform.

1. Let $g(q)$ be a continuous, complex, $2\pi-$periodic function. If its Fourier transform is non-negative, then the integration kernel $g(q-q')$ is non-negative.

2. Given a function $f : \mathbb{Z} \to \mathbb{C}$, if its inverse Fourier transform has constant modulus, then $\sum_{n\in\mathbb{Z}} f(n)f^*(n+m) = 0$, $\forall m \neq 0$.

It is easy to see that, for a pure state, the Wigner function can be written as

$$W(m,k) = \frac{1}{2\pi}\int_{-\pi/a}^{\pi/a} dq e^{iqma}\tilde{\psi}(\tfrac{k}{a}+q)\tilde{\psi}^*(\tfrac{k}{a}-q) \tag{6.17}$$

where $\tilde{\psi}(k) = \langle k|\psi\rangle$ are the components of the state in the quasi-momentum basis. It is thus the Fourier transform of the function $g(q) = \frac{1}{a\sqrt{2\pi}}\tilde{\psi}((k+q)/a)\tilde{\psi}^*((k-q)/a)$. From lemma 1, $\int_{-\pi}^{\pi} dq' \chi^*(q) g(q-q')\chi(q') \geq 0$ for any χ. In particular, requiring the inequality for all functions $\chi(q) = a_1\delta_{2\pi}(q-c_1) + a_2\delta_{2\pi}(q-c_2)$, where $\delta_{2\pi}(q) \equiv \sum_{r\in\mathbb{Z}} \delta(q-2r\pi)$, $a_{1,2} \in \mathbb{C}$, $c_{1,2} \in \mathbb{R}$, implies

$$|\tilde{\psi}(q)|^2 \geq |\tilde{\psi}(q+\Delta)||\tilde{\psi}(q-\Delta)|, \quad \forall \Delta \in \mathbb{R}, \quad q \in [-\tfrac{\pi}{a}, \tfrac{\pi}{a}[. \tag{6.18}$$

This requires that $|\tilde{\psi}(q)|$ is constant, so that also $|g(q)|$ must be constant. Applying now lemma (2)

$$\sum_j W(m,k)W(m+j,k) = 0 \quad \forall j \neq 0. \tag{6.19}$$

So that, for a given value of k, there can at most be a single space-like component, $m_0(k)$, for which the Wigner function does not vanish. Combining this with (6.16), we obtain that such component must be even, $m_0(k) = 2n_0(k)$, so that, using normalization, $W(m,k) = \frac{1}{2\pi}\delta_{m,2n_0(k)}$.

It only remains to be shown that this component is the same for all values of k. This can be seen, as in [127], by making use of the expression for the Wigner function for a product in terms of individual Wigner functions,

$$W_{\varrho_2\varrho_1}(m,k) = \frac{1}{2\pi}\sum_{m_1,m_2}\int_{-\pi}^{\pi} dk_1 \int_{-\pi}^{\pi} dk_2 W_{\varrho_1}(m+m_1, k+k_1) \\ W_{\varrho_2}(m+m_2, k+k_2) e^{i(m_2k_1 - m_1k_2)}. \tag{6.20}$$

In particular, taking $\rho_1 = \rho_2 \equiv \rho$, the pure state we are considering, for which $W(m,k) = \frac{1}{2\pi}\delta_{m,2n_0(k)}$, and looking at the (real) component for $m = 2n_0(0) \equiv 2n_0$, $k = 0$,

$$4\pi^2 = \int_{-\pi}^{\pi} dk_1 \int_{-\pi}^{\pi} dk_2 \cos\left(2k_2[n_0(k_1) - n_0] - 2k_1[n_0(k_2) - n_0]\right). \tag{6.21}$$

To fulfill this equality, the argument of the cosine has to be an integer multiple of 2π for all values of $k_{1,2}$, which is only possible if $n_0(k) = n_0$ $\forall k$, and thus

$$W(m,k) = \frac{1}{2\pi}\delta_{m,2n_0}. \tag{6.22}$$

Using 6.7 it is easy to show that the pure state corresponding to this Wigner function is $|\Psi_\delta\rangle = |n_0\rangle$.

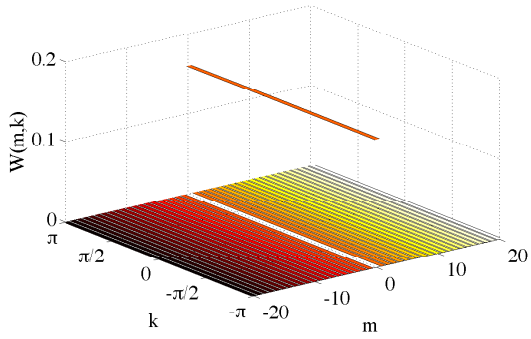

Figure 6.2: Wigner function for a state localized at the origin $n_0 = 0$, assuming $a = 1$. Notice that a plane projection of the phase space is represented, although it is periodic in k, and the edges $k = \pm\pi$ have to be identified.

6.4.2 Gaussian state

In the case of continuous degrees of freedom, Gaussian states play a fundamental role. In particular, pure Gaussian states are the only pure states with non negative Wigner function [132]. It makes then sense to consider the discretization of a state $\Psi(x) = \frac{1}{(\sigma\sqrt{\pi})^{\frac{1}{2}}} e^{-\frac{(x-x_0)^2}{2\sigma^2}} e^{iq_0 x}$, namely $|\Psi_G\rangle = \frac{1}{N}\sum_n e^{-\frac{(n-n_0)^2}{2\sigma^2}} e^{iq_0 na}|n\rangle$, for $n_0 \in \mathbb{Z}$ being $\sigma \equiv \sigma/a$ the width measured in units of the lattice spacing. The correct normalization in the discrete case, $N^2 = \sum_n e^{-\frac{(n-n_0)^2}{\sigma^2}} \equiv \theta_3(0, e^{-\frac{1}{\sigma^2}})$, is expressed in terms of the Jacobi theta function, defined as $\theta_3(z,q) \equiv \sum_n q^{n^2} e^{2izn}$ for complex arguments q, z, with $|q| < 1$ [140].

The Wigner function for this state can also be computed exactly,

$$W_G(m,k) = \frac{1}{2\pi} e^{i(k-q_0 a)m} e^{-\frac{(m-n_0)^2+n_0^2}{2\sigma^2}} \frac{\theta_3(k - q_0 a + i\frac{m}{2\sigma^2}, e^{-\frac{1}{\sigma^2}})}{\theta_3(0, e^{-\frac{1}{\sigma^2}})}, \tag{6.23}$$

and shown in figure 6.3 for the particular case $\sigma = 2$, $n_0 = 0$, $q_0 = 0$. The figure shows clearly the regular image, centered around $k = 0$, and the *ghost* image, exhibiting the sign oscillations on odd sites. If we consider instead a displaced Gaussian, with $q_0 \neq 0$, the whole figure is correspondingly shifted in momentum space, as shown in figure 6.4a. To illustrate the meaning of the sign-averaged function defined in (6.14), we also plot it in figure 6.4b for this state. Obviously, $\eta(\Psi_G) = 0$ for any pure Gaussian state.

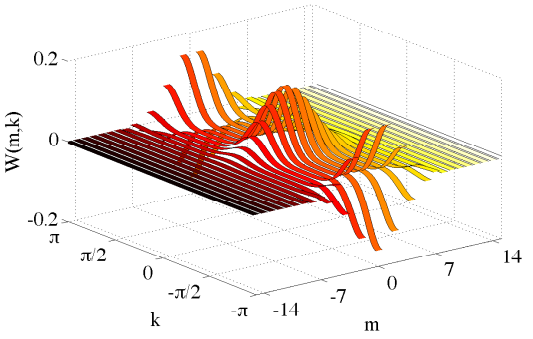

Figure 6.3: Wigner function for a discretized Gaussian state with $\sigma = 2$, $q_0 = 0$ and $n_0 = 0$, taking $a = 1$.

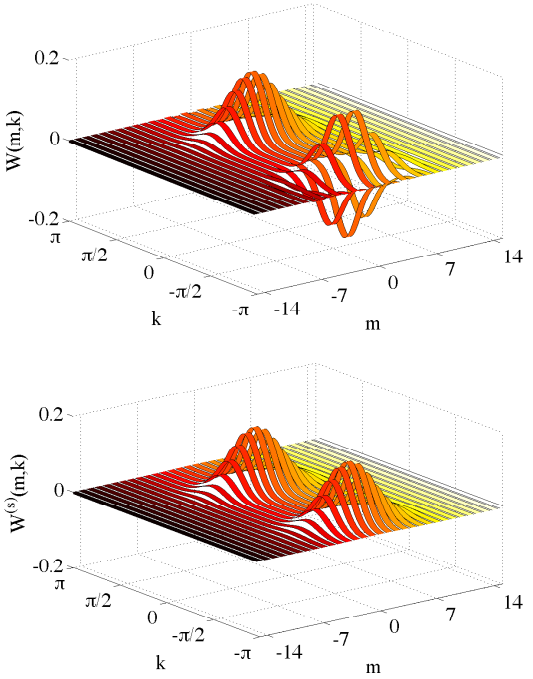

Figure 6.4: Wigner function (top) for a discretized Gaussian state identical to that in (6.3) with a displacement in momentum $q_0 a = \pi/3$. On the bottom, the sign-averaged Wigner function (6.14).

The cases discussed above are limited to pure states. Indeed, in the continuum case, also mixed Gaussian states have a non-negative Wigner function. We have also studied numerically the discretized version of a general single-mode Gaussian state in coordinate representation [141],

$$\langle n \mid \rho_G \mid n' \rangle = \frac{1}{N_{\rho_G}} e^{\frac{-a}{2}n^2 - \frac{a^*}{2}n'^2 + cnn'}, \tag{6.24}$$

where $N_{\rho_G} = \Theta_3(0, e^{-Re(a)+c})$. For this state the Wigner function reads

$$W_{\rho_G}(m,k) = \frac{1}{2\pi\Theta_3(0,e^{-Re(a)+c}} e^{ikm} e^{\frac{-a^{*2}}{2}} \Theta_3(k+i(a^*+c)\frac{m}{2}, e^{-Re(a)-c}). \tag{6.25}$$

We computed the value of η for varying parameters a, c and found no state with η different from zero, within the numerical precision of our calculation. Although the study is not exhaustive, and there could still exist some mixed Gaussian state for which the non-negativity property is not satisfied in the discrete case, it serves as an additional consistency check for the proposed measure.

6.4.3 Superposition of deltas

The Gaussian case has vanishing negativity, as expected from its correspondence in the continuum limit. It actually includes the case of a localized state, too, which can be interpreted as a Gaussian in the limit of a vanishing width, σ. Superpositions of such states will instead have more *quantum* features.

We may in particular consider an arbitrary superposition of two localized states, such as $|\Psi_{2\delta}\rangle = \frac{1}{\sqrt{1+|\alpha|^2}} \sum_n (\delta_{nn_1} + \alpha\delta_{nn_2}) |n\rangle$, for any $n_1 \neq n_2 \in \mathbb{Z}$ and $\alpha \in \mathbb{C}$. The corresponding Wigner function can be easily calculated,

$$W_{2\delta}(m,k) = \frac{1}{2\pi(1+|\alpha|^2)} \left\{ \delta_{m,2n_1} + |\alpha|^2 \delta_{m,2n_2} + 2|\alpha| \delta_{m,n_1+n_2} \cos[\Delta n\ k + \phi] \right\}, \tag{6.26}$$

where ϕ is the phase of the complex coefficient α, and $\Delta n = n_2 - n_1$. In this case, the Wigner function vanishes everywhere except for three particular values of the space-like phase space coordinate, namely $m = 2n_1, 2n_2, n_1 + n_2$. Figure 6.5 shows the particular case of $n_1 = -n_2 = 4$, $\alpha = 1$.

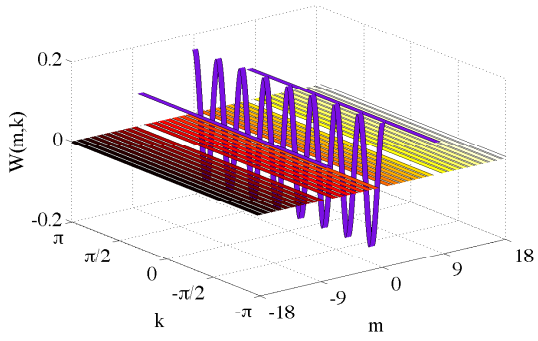

Figure 6.5: Wigner function for the superposition of two deltas located at $n_1 = -n_2 = 4$, assuming lattice spacing $a = 1$. The function vanishes everywhere except on three isolated strips, colored purple in the figure.

It is easy to see that $W^{(s)}_{2\delta}(m,k) = W_{2\delta}(m,k)$, since none of the terms changes sign under (6.14). Indeed, the first two terms are non-vanishing only on even values of m, while the last term can be supported on odd m if n_1 and n_2 have different parity, but in that case, $W_{2\delta}(m \pm 1, k) = 0$. Therefore, we can analytically compute the quantity 6.13 as

$$\eta(\Psi_{2\delta}) = \sum_m \int_{-\pi}^{\pi} [|W(m,k)| - W(m,k)]dk$$
$$= \frac{|\alpha|}{\pi(1+|\alpha|^2)} \int_{-\pi}^{\pi} dk\, [|\cos(\Delta n k + \phi)| - \cos(\Delta n k + \phi)]$$
$$= \frac{4|\alpha|}{\pi(1+|\alpha|^2)}, \tag{6.27}$$

independent of the separation between the localized states, Δn, and reaching its maximum value, $\eta_{\max(\Psi_{2\delta})} = 2/\pi$, for $|\alpha| = 1$.

6.4.4 Superposition of Gaussian states

Another family of states for which the Wigner function defined above can be computed analytically is that of superpositions of pure Gaussian states. We may consider an arbitrary superposition of two discretized pure Gaussian states,

$$|\Psi_{2G}\rangle = \frac{1}{\mathcal{N}} \sum_n \left\{ e^{-\frac{(n-n_1)^2}{2\sigma_1^2}} e^{iq_1 na} + \alpha e^{-\frac{(n-n_2)^2}{2\sigma_2^2}} e^{iq_2 na} \right\} |n\rangle, \tag{6.28}$$

for arbitrary $n_{1,2} \in \mathbb{Z}$, $q_{1,2} \in [-\pi/a, \pi/a[$ and $\alpha \in \mathbb{C}$. For such state, the Wigner function can be expressed as a sum

$$W_{2G} = W_1 + |\alpha|^2 W_2 + \alpha W_{12} + \alpha^* W_{21}, \tag{6.29}$$

where W_1 and W_2 are (up to the normalization factor) equivalent to the Wigner function of a single Gaussian (6.23), while W_{12} and W_{21} contain the crossed terms,

$$\begin{aligned} W_{12}(m,k) = \frac{1}{\pi\mathcal{N}^2} e^{i(k-q_2 a)m} e^{-\frac{n_1^2}{2\sigma_1^2}} e^{-\frac{(m-n_2)^2}{2\sigma_2^2}} \\ \times \theta_3\left(k - a\tfrac{q_1+q_2}{2} + i\left(\tfrac{m-n_2}{2\sigma_2^2} + \tfrac{n_1}{2\sigma_1^2}\right), e^{-\frac{\sigma_1^2+\sigma_2^2}{2\sigma_1^2\sigma_2^2}}\right), \end{aligned} \tag{6.30}$$

and $W_{21} = W_{12}(1 \leftrightarrow 2)$.

In the symmetric case, $\alpha = 1$, $n_1 = -n_2 \equiv n_0$, $\sigma_1 = \sigma_2 \equiv \sigma$, $q_1 = q_2 = 0$, the above expression adopts the compact form

$$W_{2G}(m,k) = \frac{e^{ikm}}{\pi\mathcal{N}^2} e^{-\frac{m^2}{2\sigma^2}} \left\{ e^{-\frac{n_0^2}{\sigma^2}} \cosh\frac{m n_0}{\sigma^2} + \cos(2kn_0) \right\} \times \theta_3\left(k + i\frac{m}{2\sigma^2}, e^{-\frac{1}{\sigma^2}}\right),$$

with $\mathcal{N}^2 = 2(1 + e^{-n_0^2/\sigma^2})\theta_3(0, e^{-1/\sigma^2})$. Using the properties of the θ_3 function, we can further simplify the expression, so that, for even $m = 2s$,

$$W_{2G}(2s,k) = \frac{e^{-\frac{s^2}{\sigma^2}}}{\pi\mathcal{N}^2} \theta_3(k, e^{-\frac{1}{\sigma^2}}) \left\{ e^{-\frac{n_0^2}{\sigma^2}} \cosh\frac{2sn_0}{\sigma^2} + \cos(2kn_0) \right\}, \tag{6.31}$$

and for odd $m = 2s+1$,

$$\begin{aligned} W_{2G}(2s+1,k) = \frac{e^{ik}}{\pi\mathcal{N}^2} e^{-\frac{(s+1/2)^2}{\sigma^2}} e^{-\frac{1}{4\sigma^2}} \theta_3(k + \frac{i}{2\sigma^2}, e^{-\frac{1}{\sigma^2}}) \\ \times \left\{ e^{-\frac{n_0^2}{\sigma^2}} \cosh\frac{(2s+1)n_0}{\sigma^2} + \cos(2kn_0) \right\}. \end{aligned} \tag{6.32}$$

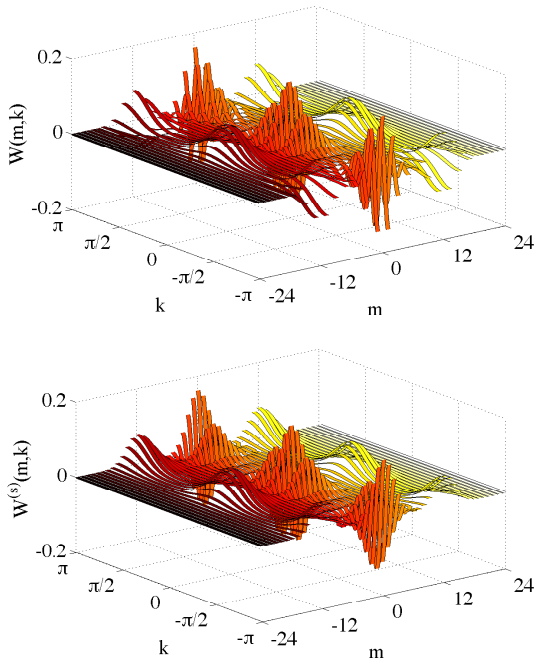

Figure 6.6: Wigner function (top) for the symmetric superposition of two Gaussian states with center in $\pm n_0$, for $n_0 = 6$, and width $\sigma = 1.5$, assuming lattice spacing $a = 1$. The bottom panel shows the sign-averaged $W^{(s)}$, for comparison.

In the limit $\sigma \to 0$, (6.31) results in the expression for the superposition of two localized states discussed in the previous section, while (6.32) vanishes.

Figure 6.6a shows the full Wigner function for the particular case $n_0 = 6$, $\sigma = 1.5$. The central part, around $k = 0$, corresponds to the regular image, showing the usual Gaussian peaks and a central interference region. This survives in the continuum limit, giving rise to a genuine negativity. The ghost image in this case lives on the half phase-space with larger momenta, and exhibits the characteristic sign oscillation when moving along the space-like axis. The sign average defined in (6.14) transforms this image in a copy of the genuine one, as shown in figure 6.6b, so that $\eta(\Psi_{2G})$ will be twice the negativity of the regular image.

Although there is no closed analytical expression for the non-classicality $\eta(\Psi_{2G})$,

even in the simplest case discussed above, we can compute it numerically, as shown in figure 6.7a for the symmetric superposition of two Gaussian states of the same width, centered at $\pm n_0$ and with momentum displacements, $q_1 = 0$ and $q_2 \equiv q_0$. As shown in the plot, η vanishes only for $n_0 = 0$ and $q_0 = 0, \pi$, when the situation reduces to a single Gaussian. For small distances, $2n_0$, the value of η depends on n_0 and q_0, while for larger separations it becomes less sensitive to q_0, and soon enough it reaches its maximal value, and stays constant. As shown in figure 6.7b, this asymptotic value is sensitive to the Gaussian width only when the latter is comparable to the lattice spacing. When σ is large enough, instead, the asymptotic negativity is constant. In the limit $\sigma \to 0$, on the other hand, the negativity for a superposition of two deltas is recovered.

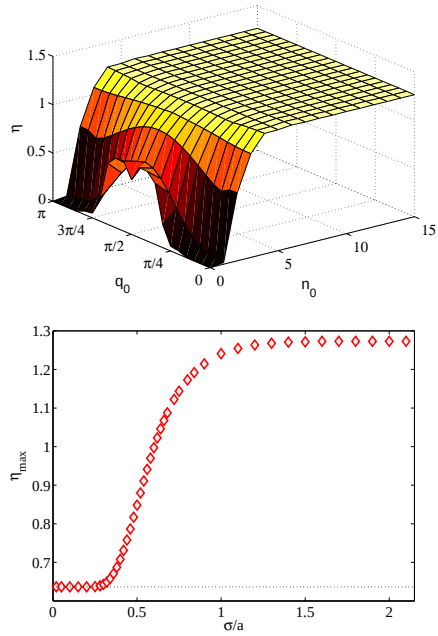

Figure 6.7: Negativity of a superposition of two discretized Gaussian states of the same width. The left plot shows the case $\sigma = 1.2$, as a function of their half-distance, n_0, and the relative momentum displacement, q_0, taking $a = 1$. On the right, we show the asymptotic value reached for varying width, σ.

6.5 Definition of the Wigner function in the infinite discrete lattice for a particle with spin

We are interested in the phase space description of a spin 1/2 particle that is allowed to move on an infinite 1D lattice. A paradigmatic example is the quantum walk, where a particle moves along the sites of a 1D lattice.

We now would like to incorporate the additional degree of freedom arising from the spin of the particle. As discussed previously, there are different approaches in the literature to describe finite dimensional Hilbert spaces, such as the spin of a particle. One can combine both degrees of freedom (spin and spatial) by a tensor multiplication of the corresponding point operators, as done in [142] for angular momentum and spin states. Our choice consists in defining a Wigner function matrix as already introduced in [143] (a similar treatment is made in [144]). We consider the Hilbert space $\mathcal{H} = \mathcal{H}_l \otimes \mathcal{H}_s$, where $\mathcal{H}_l$ stands for the motion on the lattice, and $\mathcal{H}_s$ describes the spin states. The composed Hilbert space is spanned by the basis $\mid n, \alpha\rangle \equiv \mid n\rangle \otimes \mid \alpha\rangle$; with $n \in \mathbb{Z}$ and $\alpha \in 0, 1$ designate the eigenvectors of the σ_z Pauli matrix (these states might also correspond to the computational basis of a qubit, or to the levels of a two level system). Following similar steps to [143], we introduce the following definition for the Wigner matrix

$$W_{\alpha\beta}(m,k) \equiv \frac{1}{2\pi} \sum_n \langle n, \alpha | \rho | m-n, \beta \rangle e^{-i(2n-m)k}. \tag{6.33}$$

We then have a set of four functions $W_{\alpha\beta}(m,k)$, $\alpha, \beta = 0, 1$ forming a 2×2 matrix. Each function, as before, is defined on the phase space of points (m,k), with $m \in \mathbb{Z}$, and k takes values in $[-\pi, \pi[$. A similar definition can be made for any operator $\mathcal{O}$ acting on $\mathcal{H}$:

$$W^{\mathcal{O}}_{\alpha\beta}(m,k) \equiv \frac{1}{2\pi} \sum_n \langle n, \alpha | \mathcal{O} | m-n, \beta \rangle e^{-i(2n-m)k}. \tag{6.34}$$

Unlike the spatial variables, where the relationship with phase space points is non trivial, there is a direct correspondence between spin indices in the state of the system and indices in the matrix Wigner function. This implies that operations on the spin space, such as rotations, change of basis or interactions with a spin-dependent force, as studied below, become more transparent using the matrix Wigner function than other kind of representations for the spin. Moreover, the definition Eq. (6.33) keeps a closer analogy, for pure states, to the relativistic Wigner function used in Quantum Field Theory. For such states one has $\rho =$

$|\Psi\rangle\langle\Psi|$ and we can write

$$W_{\alpha\beta}(m,k) \equiv \frac{1}{2\pi}\sum_n \Psi_\alpha(n)\Psi^*_\beta(m-n)e^{-i(2n-m)k} \tag{6.35}$$

with $\Psi_\alpha(n) \equiv \langle n,\alpha|\Psi\rangle$. In the continuum limit, the functions $\Psi_\alpha(n)$ can be interpreted as the components of a Pauli spinor or a Dirac spinor. In this case, Eq. (6.35) can be related to the relativistic Wigner function already mentioned.

Some of the properties discussed in section 6.2, can be easily generalized for the matrix Wigner function.

- We have
$$W_{\beta\alpha}(m,k) = W^*_{\alpha\beta}(m,k), \tag{6.36}$$
which implies that the matrix Wigner function in Hermitian.

- The normalization condition becomes
$$\sum_\alpha\sum_m \int_{-\pi}^{+\pi} dk W_{\alpha\alpha}(m,k) = 1. \tag{6.37}$$

- Also,
$$W_{\alpha\beta}(m,k\pm\pi) = (-1)^m W_{\alpha\beta}(m,k). \tag{6.38}$$

- Given two operators C, D and their corresponding Wigner matrices $W^C_{\alpha\beta}(m,k)$, $W^D_{\alpha\beta}(m,k)$ one has
$$2\pi\sum_{\alpha,\beta}\sum_{m=-\infty}^{\infty}\int_{-\pi}^{+\pi} dk W^C_{\alpha\beta}(m,k)W^D_{\beta\alpha}(m,k) = \mathrm{tr}\,(CD)\,. \tag{6.39}$$

- A complete knowledge of the Wigner function can be used to reconstruct the density operator ρ:
$$\langle\alpha|\rho|\beta\rangle = 2\pi\sum_m\int_{-\pi}^{+\pi} dk W_{\alpha\beta}(m,k)A(m,k). \tag{6.40}$$

- The marginal distributions of (6.33) are related to matrix elements of the density operator
$$\sum_{m=-\infty}^{+\infty} W_{\alpha\beta}(m,k) = \tfrac{1}{a}\langle\tfrac{k}{a},\alpha|\rho|\tfrac{k}{a},\beta\rangle, \tag{6.41}$$

and

$$\int_{-\pi}^{+\pi} dk W_{\alpha\beta}(m,k) = \sum_n \delta_{m,2n} \langle n,\alpha|\rho|n,\beta\rangle. \tag{6.42}$$

As already discussed in section 6.2, these equations reflect the distinction between the coordinates of the phase space points, $m \in \mathbb{Z}$, $k \in [-\pi, \pi[$, and the position and quasimomentum bases, n, q. The k coordinate is adimensional and does not directly represent a momentum value, but is connected to $q = k/a$. The *spatial* label m in phase-space is only connected to a discrete position, s, for even values, $m = 2s$, while the odd values of m are analogous to the odd half-integer phase space grid points in [122, 124].

6.6 Particular cases

In order to obtain some insight about the characteristics of the matrix Wigner function Eq. (6.33), we will give the explicit form it takes for some particular cases.

6.6.1 Product state

We start by considering a product state of spatial and spin degrees of freedom

$$\rho = \rho_L \otimes \rho_S, \tag{6.43}$$

where ρ_L represents a general state on the lattice, and ρ_S is an arbitrary spin state. In this case, we readily obtain

$$W_{\alpha\beta}(m,k) = W_L(m,k)\langle\alpha|\rho_S|\beta\rangle, \tag{6.44}$$

with

$$W_L(m,k) \equiv \frac{1}{2\pi} \sum_n \langle n|\rho_L|m-n\rangle e^{-i(2n-m)k}. \tag{6.45}$$

6.6.2 Superposition of two deltas

Let us consider the Wigner function for the state formed by a superposition of two localized states at lattice sites $|n_1\rangle$ and $|n_2\rangle$ with $n_1 \neq n_2 \in \mathbb{Z}$

$$|\,\Psi_{2\delta}\rangle = \frac{1}{\sqrt{1+|\,\alpha\,|^2}}(|n_1\rangle\,|\,0\rangle + \alpha\,|n_2\rangle\,|\,1\rangle), \tag{6.46}$$

where α is an arbitrary complex number that represents the relative weight of the state $|n_2\rangle$. For $\alpha = 1$ we obtain a Schrödinger-cat state. The corresponding Wigner function can be easily calculated. Written in matrix form in the above spin basis,

$$W(m,k) = \frac{1}{2\pi(1+\mid \alpha \mid^2)} \begin{pmatrix} \delta_{m,2n_1} & \alpha^* e^{-ik(n_1-n_2)}\delta_{m,n_1+n_2} \\ \alpha e^{ik(n_1-n_2)}\delta_{m,n_1+n_2} & \mid \alpha \mid^2 \delta_{m,2n_2} \end{pmatrix} \tag{6.47}$$

In this case, the Wigner matrix is zero everywhere except for three particular values of the space-like phase coordinate, $m = 2n_1, 2n_2, n_1 + n_2$. It is interesting to compare the structure provided by Eq. (6.47) with the corresponding superposition of two localized states without spin, given by

$$\mid \Psi_{2\delta}^{no\ spin}\rangle = \frac{1}{\sqrt{1+\mid \alpha \mid^2}}(|n_1\rangle + \alpha\,|n_2\rangle). \tag{6.48}$$

In that case, the Wigner matrix is a scalar function

$$\begin{aligned} W_{2\delta}^{no\ spin}(m,k) \quad = \quad & \frac{1}{2\pi(1+|\alpha|^2)} \left\{\delta_{m,2n_1} + |\alpha|^2\delta_{m,2n_2}\right. \\ & \left. +2|\alpha|\delta_{m,n_1+n_2}\cos[\Delta n\ k+\phi]\right\}, \end{aligned} \tag{6.49}$$

where ϕ is the phase of the complex coefficient α, and $\Delta n = n_2 - n_1$. One observes the different terms in (6.49) appear distributed on different matrix positions in Eq. (6.47). In particular, the out of diagonal term in (6.47) corresponds to the interference, oscillating term in (6.49). This term plays an interesting role related to the non positivity of the Wigner function. We will return to this point later.

6.6.3 Superposition of two Gaussian states

The superposition of two discretized pure Gaussian states with orthogonal spin components is another interesting state for which the Wigner matrix defined in this thesis can be computed analytically. Such a state is defined as

$$|\Psi_{2G}\rangle = \frac{1}{\sqrt{2}\mathcal{N}} \sum_n \left\{ e^{-\frac{(n-a)^2}{2\sigma^2}} \mid 0\rangle + e^{-\frac{(n-b)^2}{2\sigma^2}} \mid 1\rangle \right\} |n\rangle, \tag{6.50}$$

for arbitrary $a, b \in \mathbb{Z}$, $\sigma \in \mathbb{R}^+$. For such state, the Wigner function can be expressed as a matrix in the same $\{|0\rangle, |1\rangle\}$ basis

$$W(m,k) = \frac{1}{2}\begin{pmatrix} W_a(m,k) & W_{ab}(m,k) \\ W^*_{ab}(m,k) & W_b(m,k) \end{pmatrix} \tag{6.51}$$

where

$$W_l(m,k) = \frac{1}{2\pi\mathcal{N}^2} e^{-\frac{l^2+(m-l)^2}{2\sigma^2}} e^{ikm}\theta_3(k+\frac{im}{2\sigma^2}, e^{-\frac{1}{\sigma^2}}), \;\; l=a,b \tag{6.52}$$

$$W_{ab}(m,k) = \frac{1}{2\pi\mathcal{N}^2} e^{-\frac{a^2+(m-b)^2}{2\sigma^2}} e^{ikm}\theta_3(k+\frac{i(m-b+a)}{2\sigma^2}, e^{-\frac{1}{\sigma^2}}) \tag{6.53}$$

with $\mathcal{N} = \sqrt{\theta_3(0, e^{-\frac{1}{\sigma^2}})}$ the normalization constant. The Jacobi theta function $\theta_3(z,q)$ is defined as $\theta_3(z,q) \equiv \sum_n q^{n^2} e^{2izn}$ for complex arguments q, z, with $|q| < 1$ [140]. As in the previous example, we find an important difference with the Wigner function for the case without spin, since the components in the scalar function appear here distributed as the components of the matrix Wigner function. In the limit $a = -b \gg \sigma$ with $\sigma \to 0$ we recover the result for the two deltas (6.47) corresponding to the case $n_1 = -n_2 = a$ and $\alpha = 1$.

Figure 6.8 shows the four components of the Wigner matrix for a two-Gaussian state, as given by Eqs. (6.51-6.53). One can immediately observe on each component the presence of a secondary image that reflects the property Eq. (6.5) discussed for the definition for a spinless particle.

6.7 Negativity

We previously discussed that in the context of continuous variables, it is well known that the Wigner function may present some zones in phase space where it is negative. This is interpreted as an indication of quantumness, in the sense that the state would not have a classical analogous.

The positive character of the Wigner function has also been studied for discrete systems. In the finite dimensional case, and for odd dimension, Gross showed [135] that the only pure states with positive Wigner function are stabilizer states. The presence of negative values in the Wigner function has been in this case connected to a quantum resource, related to a possible quantum speedup [121,

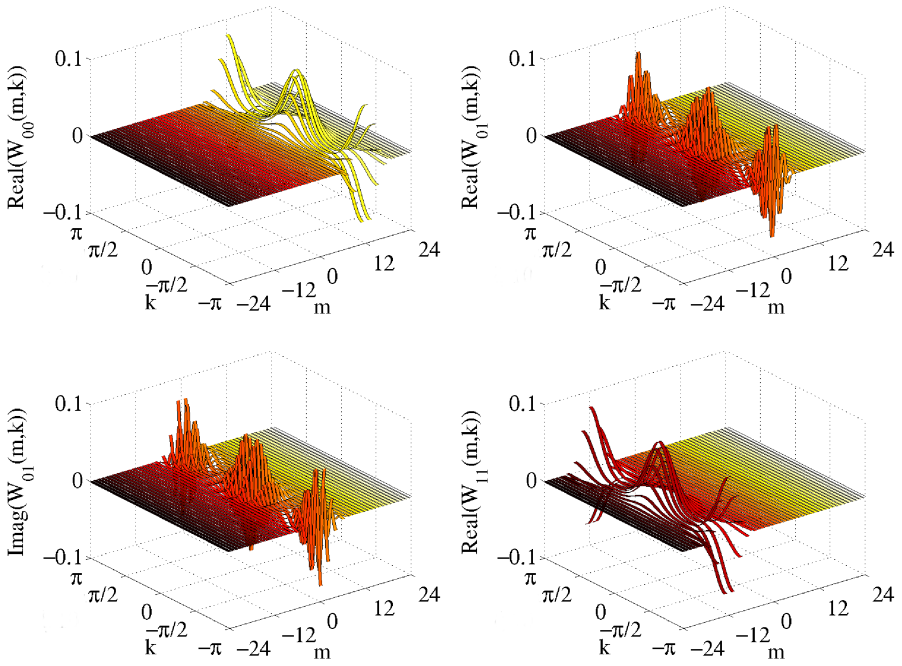

Figure 6.8: Matrix components of the Wigner function for two Gaussians, as given by Eqs. (6.51-6.53). Panel a) represents $W_a(m,k)$, panel b) is the real part of $W_{ab}(m,k)$, while the imaginary part is plotted on panel c). Finally, panel d) shows the $W_b(m,k)$ component. In these plots, $a = -b = 6$ and $\sigma = 1.5$.

137] or the non-simulability of certain quantum computations involving states with non-positive Wigner function [145, 146].

In the case of spin $\frac{1}{2}$, the Wigner function defined by Wootters [117] has been used to establish a separability criterion for a system of two particles [147]. A connection between entanglement and negative Wigner functions was established also in [134] for two particles in a continuous space, when the state is a hyperradial s-wave.

We have studied in the previous section 6.3 that even without the additional degree of freedom, the discreteness of the Hilbert space causes the appearance of spurious negative terms in the Wigner function, which do not correspond directly to non-classical features of the state, but are due to the structure of the discrete phase space itself. Nevertheless, we have [148] introduce a modified negativity measure which excludes such negative contributions and contains information about the quantumness of the states, consistent with the continuum limit.

The discussion above indicates that the meaning of a negativity measure will strongly depend on the definition used for the Wigner function and on the characteristics of the system. It is nevertheless worth investigating what the natural extension of the negativity will be when we consider a particle in a discrete lattice and include the spin degree of freedom.

Obviously, if we start with our definition (6.33) and trace the spin, we are left with a scalar Wigner function representing the state of the spatial degree of freedom, which in general will be mixed. To this function we can immediately apply the definition of negativity discussed in 6.3. Our purpose, however, is to define a negativity $\eta(\rho)$ that preserves some spin information.

An alternative is to define a negativity for the Wigner function with spin, as introduced in [149],

$$\eta(\rho) = \sum_n \int_{-\pi}^{\pi} [|| \, W(m,k) \, ||_1 - Tr(W(m,k))] dk = \sum_n \int_{-\pi}^{\pi} || \, W(m,k) \, || \, dk - 1, \tag{6.54}$$

where $|| \, A \, ||_1 \equiv Tr\sqrt{A^\dagger A}$ is the trace norm of matrix A, and the second equality follows from normalization. We can easily check that this quantity fulfills the following desirable properties

1. It reduces to Eq. (6.13) for product states in the continuum limit, with $W_c(x,p)$ obtained from $W_L(m,k)$ (see 6.44);

2. It is invariant under rotations in spin space.

The first property is also satisfied by the negativity computed after tracing out the spin.

The second property, on the other hand, can be illustrated with the following example. We consider an electron, subject to an external magnetic field. To simplify, the electron is confined to a site on the lattice, so that its state is factorisable. The effect of the magnetic field manifests on the precession of the spin, which continuously changes the spin state of the electron. This property ensures that the value of the negativity is not influenced by the precession. In other words, simply changing the spin direction will not alter the negativity properties of the Wigner matrix. Notice that, for some alternative definitions of the Wigner function for a particle with spin [117], the function can contain negative values in the phase space for some states, while being completely positive for other states.

We can further explore the significance of the definition (6.54) by considering different examples. We may then investigate, as in [147], whether this quantity holds information about the entanglement in the state.

We start by analysing the cat state, $\mid \psi\rangle = \frac{1}{\sqrt{1+|\beta|^2}}(\mid a\rangle \mid \sigma_1\rangle + \beta \mid b\rangle \mid \sigma_2\rangle)$ where $a, b \in \mathcal{Z}$ label two different sites on the lattice, $\beta \in \mathbb{C}$ is a constant, and $\{|\sigma_1\rangle, |\sigma_2\rangle\}$ are two arbitrary, orthogonal spin states. The negativity of this state takes the form: $\eta = \frac{2|\beta|}{1+|\beta|^2}$. It is easy to check that in this case the entanglement and the negativity have the same behavior.

However, this is not a generic behavior, as illustrated by the Werner state [150], $\rho = \frac{1-z}{4} I + z \mid \psi\rangle\langle\psi \mid$, where $\mid \psi\rangle = \frac{1}{\sqrt{2}}(\mid a\rangle \mid 0\rangle + \mid b\rangle \mid 1\rangle$ and $a, b \in \mathcal{Z}$ label two different sites on the lattice. This state is entangled whenever $z \geq \frac{1}{3}$. The Wigner matrix for this state takes the form

$$W(m,k) = \begin{pmatrix} \frac{1+z}{4} W_{aa}(m,k) + \frac{1-z}{4} W_{bb}(m,k) & \frac{z}{2} W_{ab}(m,k) \\ \frac{z}{2} W_{ab}(m,k) & \frac{1-z}{4} W_{aa}(m,k) + \frac{1+z}{4} W_{bb}(m,k) \end{pmatrix}, \tag{6.55}$$

with the definition $W_{ln}(m,k) = \frac{1}{2\pi} \delta_{m,l+n} e^{-ik(l-n)}$ and $l, n \in \{a, b\}$. The corresponding negativity is simply $\eta(\rho) = z$. This result implies that for these states, entanglement and negativity are not correlated.

Another scenario where this quantity might carry a clear physical meaning can be found in the context of decoherent dynamics. Indeed, we will show in section 7.3 how for some simple models, the negativity (6.54) keeps track of the disappearance of coherence due to dissipation.

Although it is obvious from this discussion that in the presence of spin the negativity does not have the clear unique physical meaning it has in the purely

spatial case (either continuous or discrete), the quantity η introduced here may be useful to characterize some features of the quantum state or the dynamics, specially when the study is restricted to particular families of states. The topic is nevertheless far from being closed, and could be the subject of further debate.

7 Dynamics in the discrete Wigner function

The Wigner function formalism can be used, not only to allow for a description of a given state, but also to analyze the dynamics, and to visualize it in phase space. Our purpose is to study the motion of a particle on a lattice in terms of the corresponding Wigner function. We start from the simplest case, which corresponds to the spinless particle, and then move to a more general situation,where a particle with spin may be subject to a spin-dependent potential. The time evolution will be first considered with continuous time, a situation that can be applied to most problems in physics, and can be described by the Von Neumann equation. This equation of motion can be generalized for the Wigner matrix and we solve this equation in some simple cases. Finally, we study the effect of decoherence for the system we are studying. We show how one can make use of the Wigner matrix to investigate the dynamics that appear in some discrete time problems, and consider the particular example of the quantum walk. As before, we show the effect that decoherence may have on such problems.

7.1 Dynamics for a particle without spin in continuous time

Let us consider a spinless particle moving on a lattice under the influence of a potential V that depends on the lattice site. We concentrate on the following Hamiltonian

$$H = J(T_+ + T_-) + V, \tag{7.1}$$

that appears as a consequence of the tight-binding approximation in crystals, where the parameter J is a characteristic of the system which is related to the hoping probability of an electron to the nearest neighbor, and the displacement operators $T_\pm$ are defined by $T_\pm \mid n\rangle = \mid n \pm 1\rangle$. Notice that the Hamiltonian (7.1)

can also be considered as a discretized version of

$$H_{cont} = -\frac{\nabla^2}{2M} + V(x) \tag{7.2}$$

(with M the mass of the particle) if one defines $J = -\frac{1}{2Ma^2}$.

The wave function can be written as $\psi(n,t)$, with t the time, so that the Schrödinger equation

$$i\frac{\partial}{\partial t}\psi(n,t) = J\left[\psi(n+1,t) + \psi(n-1,t) - 2\psi(n,t)\right] + V_n\psi(n,t), \tag{7.3}$$

with $V_n \equiv \langle n \mid V \mid n\rangle$. The last term inside the brackets in Eq. (6.4) can be easily reabsorbed into the definition of the coefficients V_n (it can be also understood as a term proportional to the identity in the Hamiltonian, thus contributing only as a position-independent phase as time evolves). Therefore we omit that term.

It is straightforward to derive an evolution equation satisfied by the Wigner function for the above problem. We begin with the von Neumann equation for the density operator

$$\frac{\partial}{\partial t}\rho(t) = -i[H, \rho(t)], \tag{7.4}$$

Making use of (6.4) one arrives to

$$\begin{aligned}\frac{\partial}{\partial t}W(m,k,t) = 2J\sin k\left[W(m+1,k,t) - W(m-1,k,t)\right] - \\ \frac{i}{2\pi}\sum_l e^{-i(2l-m)k}(V_l - V_{m-l})\langle l \mid \rho(t) \mid m-l\rangle,\end{aligned} \tag{7.5}$$

where we have explicitly showed the time dependence of ρ and $W(m,k)$ for the sake of clarity.

Let us consider that $V(x)$ is a continuous and infinitely derivable function. In this case, one can obtain a closed form of the above expression for the Wigner function, as showed in the Appendix. As a result, one arrives to the following expression

$$\begin{aligned}\frac{\partial}{\partial t}W(m,k,t) = 2J\sin k\left[W(m+1,k,t) - W(m-1,k,t)\right] + \\ \sum_{s=0}^{\infty}\frac{(-1)^s a^{2s+1}}{2^{2s}(2s+1)!}\left.\frac{d^{2s+1}V(x)}{dx^{2s+1}}\right|_{x=ma/2}\frac{\partial^{2s+1}W(m,k,t)}{\partial k^{2s+1}}.\end{aligned} \tag{7.6}$$

It must be noticed that Eq. (7.6) also holds for the Wigner matrix (6.33) if we introduce the spin of the particle, by simply replacing $W(m,k,t) \longrightarrow W_{\alpha\beta}(m,k,t)$, since none of the spatial operations in this equation can affect the spin indices.

Before we go on, we will consider the continuous limit ($a \to 0$) of Eq. (7.6). In this limit, our Wigner function has to be replaced by the corresponding function $W_{\rm c}(x,q,t)$ following the prescription followed in the previous chapter.

$$W(m,k,t) \underset{a\to 0}{\longrightarrow} \frac{1}{2} W_{\rm c}(x = \frac{ma}{2}, q = \frac{k}{a}, t). \tag{7.7}$$

By replacing $J = -\frac{1}{2Ma^2}$ and substituting (7.7) in (7.6), and taking the limit ($a \to 0$), one obtains the equation

$$\frac{\partial}{\partial t} W_c(x,q,t) + \frac{q}{M} \frac{\partial}{\partial x} W_c(x,q,t) = \sum_{s=0}^{\infty} \frac{(-1)^s}{2^{2s}(2s+1)!} \left. \frac{d^{2s+1}V(x)}{dx^{2s+1}} \right|_{x=ma/2} \frac{\partial^{2s+1} W_c(x,q,t)}{\partial q^{2s+1}}. \tag{7.8}$$

Eq. (7.8) is the equation of motion for the Wigner function under the effect of an external potential $V(x)$ in continuous space, where q represents the momentum of the particle (ranging from $-\infty$ to ∞) (see, for example [104]).

As an interesting particular case, we will study the particular case of a linear potential, i.e. $V(x) = \lambda x$, with λ a real constant. Eq. (7.6) adopts a simple form

$$\frac{\partial}{\partial t} W(m,k,t) = 2J \sin k \left[W(m+1,k,t) - W(m-1,k,t) \right] + \lambda a \frac{\partial}{\partial k} W(m,k,t). \tag{7.9}$$

To solve this equation, we perform a Fourier transformation on the variable m by introducing the function

$$\tilde{W}(q,k,t) \equiv \frac{1}{\sqrt{2\pi}} \sum_m e^{iqm} W(m,k,t), \tag{7.10}$$

the new variable q taking values on the interval $[-\pi, \pi[$. With the help of this function, we can rewrite Eq. (7.10) as

$$\frac{\partial}{\partial t} \tilde{W}(q,k,t) = -4iJ \sin k \sin q \tilde{W}(q,k,t) + \lambda a \frac{\partial}{\partial k} \tilde{W}(q,k,t). \tag{7.11}$$

The change of function

$$\tilde{W}(q,k,t) \equiv e^{-\frac{4iJ \cos k \sin q}{\lambda a}} f(q,k,t) \tag{7.12}$$

leads to the following equation for the function $f(q,k,t)$:

$$\frac{\partial}{\partial t}f(q,k,t) = \lambda a \frac{\partial}{\partial k}f(q,k,t), \tag{7.13}$$

which implies that the function $f(q,k,t)$ must be of the form $f(q,k,t) = g(q,k+\lambda at)$, with $g(q,k)$ an unknown function that can be determined by the initial $(t=0)$ condition in Eq. (7.12), giving

$$g(q,k) = e^{\frac{4iJ\cos k \sin q}{\lambda a}}\tilde{W}(q,k,0). \tag{7.14}$$

We finally obtain, after some algebra

$$\tilde{W}(q,k,t) = \exp[-8i\frac{J}{\lambda a}\sin(k+\frac{\lambda at}{2})\sin(\frac{\lambda at}{2})\sin q]\tilde{W}(q,k+\lambda at,0). \tag{7.15}$$

To derive an expression for the Wigner function, we need the inverse relation of Eq. (7.10), given by

$$W(m,k,t) = \frac{1}{\sqrt{2\pi}}\int_{-\pi}^{\pi} dq e^{-iqm}\tilde{W}(q,k,t), \tag{7.16}$$

and make use of the formula [151]

$$J_n(z) = \frac{1}{2\pi}\int_{-\pi}^{\pi} dq e^{-inq}e^{iz\sin q}, \tag{7.17}$$

where $n \in \mathbb{Z}$, $z \in \mathbb{C}$, and $J_n(z)$ are the Bessel functions of the first kind. After substituting Eq. (7.15) into (7.16) we arrive to the final expression

$$W(m,k,t) = \sum_l J_{m-l}\left[-8\frac{J}{\lambda a}\sin(k+\frac{\lambda at}{2})\sin\frac{\lambda at}{2}\right]W(l,k+\lambda at,0). \tag{7.18}$$

Notice that, in the latter equation, the argument $k+\lambda at$ is to be understood modulo 2π. Using this fact, one can readily obtain that the above solution exhibits a time periodicity

$$W(m,k,t+\frac{2\pi}{\lambda a}) = W(m,k,t), \tag{7.19}$$

which corresponds to the well known phenomenon of Bloch oscillations, that can be observed for electrons confined in a periodic potential (the lattice) subject to a constant force, as for example a constant electric field. The corresponding frequency $\omega_B = \mid \lambda \mid a$ is precisely what is expected for our linear potential $V(x) = \lambda x$.

Directly related to the above treatment, it appears quite natural to attempt a parallelism with a situation that describes the dynamics of a particle under the effect of a constant gravitational field, $V(x) = m_g g x$, where m_g is the gravitational mass and g the acceleration of gravity. Notice that, for the following discussion to make sense, one should design a physical system that is described by this potential, and that Eq. (7.3) can be considered as a discretized approximation to (7.2), with $J = -\frac{1}{2Ma^2}$. We will return to this discussion later.

We find it convenient to use the symbol m_i instead of M to represent the *inertial mass,* and to recover the Planck constant. We observe that the argument of the Bessel functions in Eq. (7.18) depends upon the combination

$$-\frac{J}{\lambda a} = \frac{\hbar^2}{2m_i m_g g a^3} \equiv \frac{1}{(k_g a)^3}, \tag{7.20}$$

where $k_g \equiv (\frac{2m_i m_g g}{\hbar^2})^{1/3}$ is a characteristic wave vector that modulates the spatial dependence of energy eigenstates in a gravitational field in continuous space [152]. As the authors of this work discuss, this is one of the possible effects of quantum particles under the effect of gravity, where various combinations of (powers of) m_g and m_i may appear depending on the problem under consideration, thus paving the way to measuring these two quantities independently.

The dynamics on the lattice we just considered offers a similar perspective. The time evolution in Eq. (7.18) is governed by the product $k_g a$, which involves the lattice spacing as a new parameter, thus allowing an extra degree of freedom in the design of experiments, if they are performed on a lattice instead of in continuous space. However, one has to be careful about this point: Only if the design of the experiment is such that J and $V(x)$ correspond to the above hypothesis, the previous discussion can make sense.

To illustrate the behavior of the Wigner function, we plotted in figure 7.1 several snapshots obtained by evolving an initial Gaussian state of the form (6.23). The time evolution is governed by Eq. (7.18). One observes several features on this plot. First, the position of the maximum shows oscillations for the variable m, as corresponding to the Bloch oscillations discussed above, while variable k evolves linearly (and periodically) with time. During the evolution, the Wigner function also experiences a distortion that is similar to the one observed in continuous space [152]. One also observes the presence of a secondary image which manifests as vertical strips.

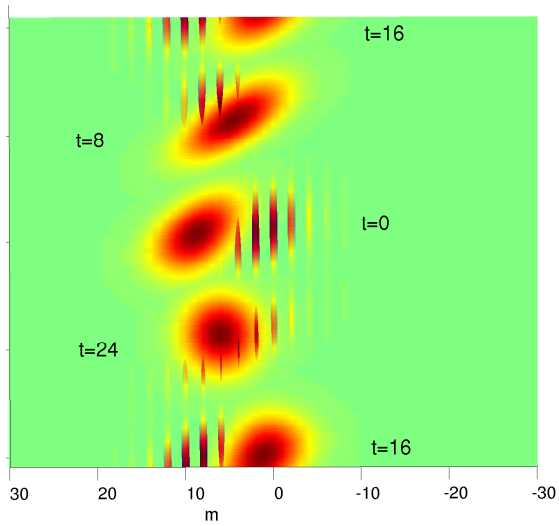

Figure 7.1: Snapshots corresponding to the time evolution of the Wigner function, as given by Eq. (7.18) with an initial Gaussian state of the form (6.23) with $a = 3$ and $\sigma = 2$. The parameters of the Hamiltonian are $J = 1$ and $\lambda a = 1$. The labels indicate different values of time.

7.2 Dynamics for a particle with spin in continuous time

Our purpose is to analyze the dynamics for a particle with spin, and compare it with the spinless case studies in the previous section. To do so, we need to introduce some spin-dependent potential, otherwise the different components in the Wigner matrix will evolve exactly in the same way, and the results of the previous section apply. In order to make this comparison as close as possible, we will consider the time evolution under the effect of a Hamiltonian of the form

$$H = J(T_+ + T_-) + \sigma_z V, \tag{7.21}$$

where V is, as before, a site-dependent scalar potential. It is possible to obtain an evolution equation, similar to (7.6), when the particle is subject to the above Hamiltonian in the lattice. This derivation is made in the Appendix, the main difference with the spinless case being that the diagonal and off-diagonal components of the Wigner matrix evolve differently. In what follows, we concentrate on the particular example of a discretized linear potential $V_n = \lambda a n$, with λ a real constant. Then, Eq. (9.6) particularizes to

$$\frac{\partial}{\partial t} W_{\alpha\alpha}(m,k,t) = 2J \sin k \left[W_{\alpha\alpha}(m+1,k,t) - W_{\alpha\alpha}(m-1,k,t) \right] + (-1)^{\alpha} \lambda a \frac{\partial}{\partial k} W_{\alpha\alpha}(m,k,t), \tag{7.22}$$

and

$$\frac{\partial}{\partial t} W_{\alpha\beta}(m,k,t) = 2J \sin k \left[W_{\alpha\beta}(m+1,k,t) - W_{\alpha\beta}(m-1,k,t) \right] - i(-1)^{\alpha} \lambda a m W_{\alpha\beta}(m,k,t), \tag{7.23}$$

(valid for $\alpha \neq \beta$).

The first equation can be easily solved by comparison to (7.9). We only have to perform the replacement $\lambda \longrightarrow (-1)^{\alpha}\lambda$. Therefore, we can write the solution using the same procedure as in the case with no spin, to obtain

$$W_{\alpha\alpha}(m,k,t) = \sum_l J_{m-l} \left[-8 \frac{J}{\lambda a} \sin(k + (-1)^{\alpha} \frac{\lambda a t}{2}) \sin \frac{\lambda a t}{2} \right] W_{\alpha\alpha}(l, k + (-1)^{\alpha} \lambda a t, 0). \tag{7.24}$$

The same comments made in the previous section hold here: $W_{\alpha\alpha}(m,k,t)$ is periodic in time, with frequency given by $\omega_B =\mid \lambda \mid a$. Eq. (7.23) can be solved by introducing a Fourier transform, as made with (7.9). We arrive, after some algebra, at

$$W_{\alpha\beta}(m,k,t) = e^{(-1)^\alpha im\frac{\lambda a t}{2}} \sum_l e^{(-1)^\alpha il\frac{\lambda a t}{2}} J_{m-l}\left[-8\frac{J}{\lambda a}\sin k \sin\frac{\lambda a t}{2}\right] W_{\alpha\beta}(l,k,0). \tag{7.25}$$

(valid when $\alpha \neq \beta$).

To illustrate the evolution of the Wigner matrix elements under the effect of the Hamiltonian (7.21) with a linear potential, we followed this evolution for an initial separable state of the form (6.44), with ρ_S defined by the pure state $\frac{1}{\sqrt{2}}(|0\rangle + |1\rangle)$ and $W_L(m,k)$ corresponding to a Gaussian state, given by (c.f. Eq. (6.52))

$$W_L(m,k) = \frac{1}{2\pi\mathcal{N}^2} e^{-\frac{a^2+(m-a)^2}{2\sigma^2}} e^{ikm}\theta_3(k+\frac{im}{2\sigma^2}, e^{-\frac{1}{\sigma^2}}) \tag{7.26}$$

and $\mathcal{N} = \sqrt{\theta_3(0, e^{-\frac{1}{\sigma^2}})}$ the normalization constant. The results are presented in figure 7.2, which shows different snapshots of the diagonal components $W_{00}(m,k,t)$ and $W_{11}(m,k,t)$ of the Wigner matrix. We observe that both components present similar features to the case without spin, plotted in figure 7.1. However, they evolve differently on the m axis: Initially, the $W_{00}(m,k,t)$ component moves to the left, while the $W_{11}(m,k,t)$ component moves to the right, as a consequence of the different time dependence $(-1)^\alpha \lambda a t$ in (7.24), a phenomenon which is reminiscent of the splitting into two beams on the Stern-Gerlach experiment, where the basic piece of the interaction is analogous to (7.21).

Decoherence

Another dynamical scenario of great relevance for the study of quantum systems is the presence of decoherence, which can be caused by interaction with the environment. In the following we show how the Wigner function formalism we are discussing accommodates also such situation. In particular, we explore some typical cases, in which the spin structure of the Wigner matrix allows a simple visualization of the decoherence effects.

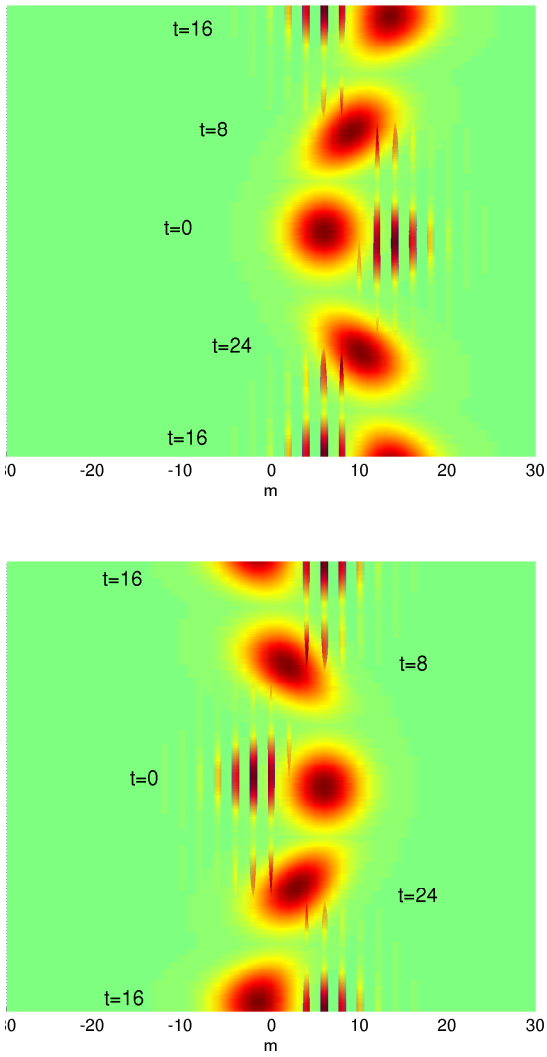

Figure 7.2: The two panels show the diagonal components of the Wigner matrix at four different times (labeled by the corresponding t), for a particle subject to the interaction Hamiltonian (7.21) in a lattice. Left panel corresponds to $W_{00}(m,k,t)$, whereas right panel shows $W_{11}(m,k,t)$. The initial state is a separable state (see the main text for explanation) with $a=3$, $\sigma=2$. The parameters of the interaction Hamiltonian are $J=\lambda a=1$.

We consider the case where the interaction with the environment can be described by a Lindblad-type equation [153]

$$\frac{\partial}{\partial t}\rho = -i[H,\rho] + \sum_k \gamma_k (A_k \rho A_k^\dagger - \frac{1}{2} A_k^\dagger A_k \rho - \frac{1}{2}\rho A_k^\dagger A_k), \tag{7.27}$$

where A_k are the Lindblad operators, and γ_k represent the corresponding coupling constants.

If these operators act only on the spin space, the Lindbland (noise) term Eq. (7.27) immediate translates in an analogous equation for the Wigner matrix. In other words, under this hypothesis we can write for the Wigner matrix

$$\frac{\partial}{\partial t} W(m,k,t) = \frac{\partial}{\partial t} W(m,k,t)|_H + \sum_k \gamma_k (A_k W(m,k,t) A_k^\dagger - \frac{1}{2} A_k^\dagger A_k W(m,k,t) - \frac{1}{2} W(m,k,t) A_k^\dagger A_k). \tag{7.28}$$

In the latter equation, $\frac{\partial}{\partial t} W(m,k,t)|_H$ denotes the contribution of the Hamiltonian to the dynamics (without decoherence), and we used a matrix notation, so that spin indices are omitted.

As a simple example, let us consider the case when we only have a Lindblad operator $A_1 = \sigma_z$ with $\gamma_1 \equiv \gamma$. We then have

$$\frac{\partial}{\partial t} W(m,k,t) = \frac{\partial}{\partial t} W(m,k,t)|_H + \begin{pmatrix} 0 & -2\gamma W_{01}(m,k,t) \\ -2\gamma W_{10}(m,k,t) & 0 \end{pmatrix}, \tag{7.29}$$

which solution can be readily obtained, and expressed as

$$W(m,k,t) = \begin{pmatrix} W_{00}(m,k,t)|_H & e^{-2\gamma t} W_{01}(m,k,t)|_H \\ e^{-2\gamma t} W_{10}(m,k,t)|_H & W_{11}(m,k,t)|_H \end{pmatrix}. \tag{7.30}$$

In other words, in this example decoherence leaves the diagonal terms unaltered, while the off-diagonal terms are exponentially damped with time.

Our second example is provided by the Lindblad operator $A_1 = \sigma_x$ with $\gamma_1 \equiv \gamma$. In this case, Eq. (7.28) becomes

$$\frac{\partial}{\partial t} W(m,k,t) = \frac{\partial}{\partial t} W(m,k,t)|_H + \gamma \begin{pmatrix} W_{11}(m,k,t) - W_{00}(m,k,t) & W_{10}(m,k,t) - W_{01}(m,k,t) \\ W_{01}(m,k,t) - W_{10}(m,k,t) & W_{00}(m,k,t) - W_{11}(m,k,t) \end{pmatrix}. \tag{7.31}$$

This set of equations can be solved by elementary operations. We concentrate on the diagonal terms, for which the final solution reads

$$W_{00}(m,k,t) = \frac{1}{2}(1+e^{-2\gamma t})W_{00}(m,k,t)|_H + \frac{1}{2}(1-e^{-2\gamma t})W_{11}(m,k,t)|_H, \quad (7.32)$$

$$W_{11}(m,k,t) = \frac{1}{2}(1-e^{-2\gamma t})W_{00}(m,k,t)|_H + \frac{1}{2}(1+e^{-2\gamma t})W_{11}(m,k,t)|_H. \quad (7.33)$$

Similar equations can be obtained involving $W_{01}(m,k,t)$ and $W_{10}(m,k,t)$. As a result, in the limit $t \longrightarrow \infty$ both $W_{00}(m,k,t)$ and $W_{11}(m,k,t)$ become an equally weighted mixture (the same happens with the off-diagonal terms).

7.3 Dynamics for a particle with spin in discrete time

Quantum walk

The examples studied in the previous section arise as a consequence of the continuous interaction of a particle with an external potential acting on the lattice. However, we can envisage some situations in which we act on the particle with subsequent short pulses, or via some actions that appear suddenly, but regularly in time. A paradigmatic example of this kind is provided by the quantum walk. The QW dynamics can be described entirely in terms of the Wigner matrix [149], via a recursion formula that relates $W(m,k,t+1)$ to other components of this function at time t. Using Eq. (2.2) one obtains, after some algebra:

$$\begin{aligned} W(m,k,t+1) = {} & M_R W(m-2,k,t)M_R^\dagger + e^{-2ik}M_R W(m,k,t)M_L^\dagger \\ & + e^{2ik}M_L W(m,k,t)M_R^\dagger + M_L W(m+2,k,t)M_L^\dagger, \end{aligned} \quad (7.34)$$

where $M_L = (|L\rangle\langle L|)C(\theta)$ and $M_L = (|R\rangle\langle R|)C(\theta)$. A complete analysis of the time evolution in phase space with the help of the Wigner function can be found in [149]. Notice that a different definition of the Wigner function was used in [125] for the reduced density matrix of the walker (after tracing the coin) to the study of the evolution and the effects of decoherence for the quantum walk.

The time evolution of the component W_{00} can be seen on Fig. 7.3. One can observe an intricate structure, arising from interference effects. Notice, for example, the similarity with the threads mentioned in [154]. It is interesting to mention that, although the Wigner function expands in space, as the walker distribution broadens, it keeps the same structure. The rest of components of the Wigner function show a similar appearance.

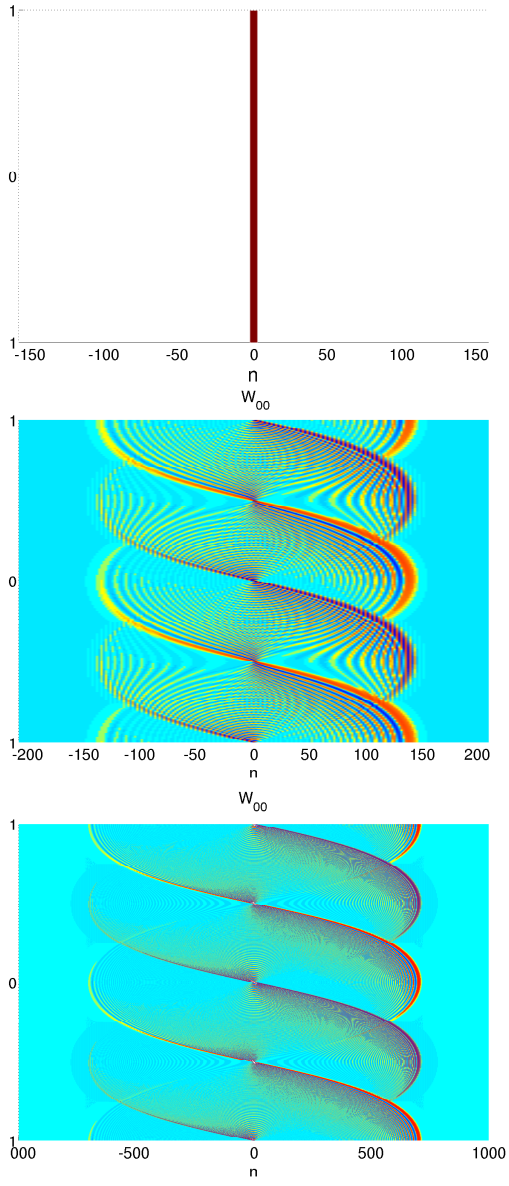

Figure 7.3: Contour plots showing the time evolution of the W_{00} component of the Wigner function starting the QW from the localized state $\mid \phi_{ini}\rangle = \frac{1}{\sqrt{2}}(\mid R\rangle + i \mid L\rangle)\otimes \mid 0\rangle$. From left to right, the sub figures correspond to $t = 0$, $t = 100$ and $t = 500$, respectively.

Decoherence in discrete time

The Wigner function formalism can easily accommodate the description of the general transformation of the quantum state via a completely positive (CP) map. In particular, we consider here trace preserving maps. These could, for instance, represent a decoherent QW process, with Kraus operators modeling the interaction of the system with the environment. The discrete evolution is represented by

$$\rho(t+1) = \sum_i E_i \rho(t) E_i^\dagger, \tag{7.35}$$

where E_i are Kraus operators with the property $\sum_i E_i^\dagger E_i = I$. As an example, we analyze two simple models of decoherence which are applied as projective measurements in the different degrees of freedom of the system. The first model is defined as projectors in spin space, while the second model is defined by projecting in the lattice sites. We use the notation Π_i to designate the different projectors, which satisfy $\Pi_i^\dagger = \Pi_i$ and $\Pi_i \Pi_j = \delta_{ij} \Pi_i$. With probability p, the system is projected onto the spin (or space) basis, so that Eq. (7.35) will be rewritten as

$$\rho(t+1) = (1-p)\rho(t) + p \sum_i \Pi_i \rho(t) \Pi_i. \tag{7.36}$$

By iteration of the above equation and making use of the properties of projectors, one can derive the following formula relating the final and initial density operators of the system,

$$\rho(t) = (1-p)^t \rho(0) + [1-(1-p)^t] \sum_i \Pi_i \rho(t) \Pi_i. \tag{7.37}$$

We start from a state consisting of superposition of two deltas with orthogonal spin components, Eq. (6.46) with $\alpha = 1$. For the first projective model we apply the spin projectors $\Pi_i = |i\rangle \langle i|$, $i = 0, 1$, while for the site projection they are given by $\Pi_n = |n\rangle \langle n|, n \in \mathbb{Z}$. The iterated density operator $\rho(t)$ that is obtained from Eq. (7.37) is the same in both cases, the reason being the spin and position entanglement structure in Eq. (6.46). The result is

$$\rho(t) = \frac{1}{2} \begin{pmatrix} \mid n_1\rangle\langle n_1 \mid & (1-p)^t \mid n_1\rangle\langle n_2 \mid \\ (1-p)^t \mid n_2\rangle\langle n_1 \mid & \mid n_2\rangle\langle n_2 \mid \end{pmatrix}. \tag{7.38}$$

The corresponding Wigner matrix becomes

$$W(m,k,t) = \frac{1}{4\pi}\begin{pmatrix} \delta_{m,2n_1} & (1-p)^t\delta_{m,n_1+n_2}e^{-ik(n1-n2)} \\ (1-p)^t\delta_{m,n_1+n_2}e^{ik(n1-n2)} & \delta_{m,2n_2} \end{pmatrix}. \tag{7.39}$$

Thus, as a consequence of the projective measurements, the non-diagonal components in the Wigner matrix (7.39) tend to zero with time. This was expected from the intuitive idea that these components appear from interference between the two spin states in Eq. (6.46) (or, correspondingly, between the two occupied positions): Once decoherence acts, this kind of interference is reduced and the responsible terms are consequently diminished. Interestingly, these interference terms are non positive and tend to disappear as decoherence is acting.

It is thus reasonable to study how the negativity, η, changes under these effects of decoherence. To do so, we consider this very simple situation, in which the initial state subject to decoherence is the double delta and restrict ourselves to the discrete time dynamics with decoherence arising from projections on spin or lattice sites. Similar qualitative conclusions can be drawn if we allow for a continuous time dynamics, or if we consider a double Gaussian state (6.50) and introduces projective measurements on the lattice states, although calculations are more involved. A simple application of (6.54) to Eq. (7.39) leads to the result

$$\eta(t) = (1-p)^t \tag{7.40}$$

for the negativity as a function of time. This simple result can be interpreted as the damping of the out-of-diagonal terms in Eq. (7.39). As time goes on, these interference terms tend to fade away, and one is left with an incoherent state with a positive Wigner function. This transition from a coherent superposition to an incoherent one is, of course, a well known phenomenon in the theory of open quantum systems which shows as a change in the nature of the Wigner function that is monitored by our definition of the corresponding negativity.

8 Conclusions

In the first part of this thesis, different aspects of the QW have been studied. In chapter 3 we have formally solved the standard multidimensional QW, taking into account extended initial conditions of arbitrary shape and width. In the limit of large width, the continuous limit is particularly well suited and clearly reveals the wave essence of the walk. The use of the dispersion relations is the central argument behind this view as their analysis allows a great deal of insight into the propagation properties of the walk, and even tailoring of the initial state in order to reach a desired asymptotic distribution, as we have demonstrated. We must insist here that our goal was not to obtain approximate solutions to the QW, thus quantifying their degree of accuracy, but rather to get qualitative insight into the long term solutions. The equations we have derived will be quite accurate for wide initial conditions, but the interesting point is that they provide a good qualitative description for relatively narrow initial distributions, specially far from degeneracies.

We have also shown that the two-dimensional Grover QW exhibits diabolical points in the dispersion relation, and have analyzed in detail the dynamics around this point, closely connecting the Grover walk with the phenomenon of conical refraction [71, 72]. In the three–dimensional Grover walk we have found other types of degeneracies whose influence on the dynamics we have not illustrated. The detailed study of the construction of the eigenvectors providing a clear qualitative interpretation turns out to be much more complicated in the 3D than in the 2D case, and we leave this extensive study for a future work.

It is worth stressing that the asymptotic distributions found in the continuous limit, valid for extended initial distributions, can be qualitatively reached for not very broad distributions, say $\sigma \sim 5$, and this should be easy to implement in systems such as the optical interferometers of Ref. [43, 155]. An exception to this general rule are those distributions which are peaked close to the diabolic point, since in this case a broad distribution will be dominated by the singular nature of that point.

We would like to point out, on the one hand, that the multidimensional QW can be viewed as a simulator of a large variety of linear differential equations

depending on the particular region of the dispersion relation that governs the evolution of the initial wave–packet. On the other hand, we stress that continuous approximations to the QW must follow the dispersion relation if they are to be taken as good approximations.

In chapter 4 we have analyzed both the short-time behavior and the asymptotic limit of the chiral density matrix for the discrete time QW on a one-dimensional lattice. We have found that this reduced system shows clear features which can be associated to a non-Markovian evolution. First, we have considered the case where the QW proceeds without decoherence. The chiral density matrix possesses a well-defined asymptotic limit in time. This allows us to calculate the limiting value of the trace distance for pairs of different initial states, which gives us the distinguishability of the states and then the presence of memory effects in the system.

We have studied the effect of decoherence, modeled as the random presence of broken links on the lattice. The case with decoherence possesses a trivial asymptotic limit, since all states converge to (one half of) the identity, so that the trace distance between pairs of them always tends to zero and then, no memory of the initial state remains.

The short-time behavior of the reduced system features quite interesting results. One observes the presence of oscillations in the trace distance for reduced matrices that correspond to two different initial states, a phenomenon that clearly indicates a non-Markovian time evolution. These oscillations appear even when the system does not suffer from decoherence, and they are damped as the number of time steps increases, thus allowing for a convergence of the trace distance, in accordance with our previous observations. As the level of noise becomes larger, the amplitude of the oscillations is also reduced, for a given number of time steps. In addition, the trace distance approaches asymptotically zero, as already predicted from our long-time analysis. The contribution to the non-Markovianity measure reported in Eq. (4.82), as a function of the number of time steps, then tends to a value that decreases as the level of decoherence increases.

We have found and characterized a non-Markovian behavior for a relatively simple and yet non-trivial system as the coin in a QW on a line. The results that we have presented for the particular model of decoherence chosen here can also be found for other models, as the one investigated in Ref. [97]. They can provide a step forward in our understanding of phenomena like the transition from unitary to diffusive processes and of the thermalization of quantum systems, and thus deserve further attention.

In the second part of this thesis, in chapter 6, we have extended the formalism of the Wigner function to the case of a quantum system with a discrete, infinite dimensional Hilbert space. For instance, this would be the case for a spinless particle moving on a one dimensional lattice. The prescription presented here appears to be the natural one for this problem, as it satisfies the defining mathematical properties of the phase-space representation and recovers the correct continuum limit for vanishing lattice spacing.

The quantification of non-classicality, as signaled by the negative part of the Wigner function in the case of continuous degrees of freedom, has to be redefined in this case to exclude negative contributions due to the structure of the discrete phase space itself. We have proposed a negativity measure for this case, and have illustrated it with the explicit results for localized and Gaussian states, and for superpositions of each. Our results support the meaningfulness of this measure to characterize the states of a particle on a one-dimensional lattice.

A natural extension of this work is to combine the phase space introduced here with additional degrees of freedom, such as internal ones for the particle, or to extend it to the case of several particles or dimensions. Wootter's prescription [117] to construct composite phase spaces by combining the phase-space point operators of different degrees of freedom via their tensor product can be applied in this case.

We have elaborated the previously introduced Wigner formalism for a particle in an infinite 1D lattice, in order to account for the presence of an additional, finite-dimensional, degree of freedom. We introduce a definition for the Wigner matrix that incorporates the spin of the particle. We have illustrated the construction of the Wigner matrix by analyzing first some simple static examples, like the "Schrödinger cat" double delta or two-Gaussian states. For these states, the position and spin variables are entangled, and this entanglement manifests in a particular structure of the Wigner matrix. Finally, we have explored a possible extension of the concept of negativity, as defined for the scalar WF, to the spin 1/2 case.

While it is not evident what the physical meaning of such negativity might be in general, the quantity we propose fulfills a number of physically sound conditions, and carries well-defined physical information in restricted scenarios. In particular, we have illustrated how for given families of states it can be connected to entanglement, although Werner states show this is not the general case. For simple decoherence scenarios, this negativity can track the loss of coherence, as was shown in chapter 7. We think that it is worth studying further the relation-

ship of the Wigner description to the quantum properties of general states in a lattice.

As for other cases, in which the phase-space formalism can also account for the dynamics of the system, it would be possible to formulate the evolution of such system fully in terms of its Wigner function, and to study the time evolution of the proposed negativity measure η. Although the examples presented in this thesis are focused on pure states, the same concepts apply also to mixed states. In chapter 7, we described the dynamics on the phase space associated to this problem.

We have studied the time evolution of the Wigner function for some simple cases. We have explicitly shown the equation governing the evolution of the Wigner function for a general space-dependent potential. This equation, however, can only be exactly solved for some special cases, as we have done for the case of a linear potential, where one recovers the well known phenomenon of Bloch oscillations. A similar statement is valid for a Hamiltonian that can be factored as a scalar part and a spin operator. We have obtained the equation of motion for a general scalar term, and solved it in the linear case, what allows us to compare with the dynamics in the spinless case. The presence of a "spin dependent force" introduces new features on the dynamics that manifest in phase space. To complete the above description, we have incorporated the role of decoherence which, for some simple examples, can be implemented for the Wigner matrix in a closed form.

Although we have concentrated, for simplicity, on the case where such additional degree of freedom corresponds to a spin 1/2, one can envisage more general situations where higher spins, or different properties, such as the polarization of a photon, are considered. As we have shown, the matrix formalism is specially well suited to describe the interaction of the particle with a spin-dependent Hamiltonian on a fixed basis, and keeps a close resemblance to the relativistic WF formalism [156, 157], a fact that might be useful in the investigation of the non relativistic limit of a given problem.

In some physical situations, the interaction appears as short pulses acting on the particle, a paradigmatic example being the Quantum Walk. It is possible to analyze the role of decoherence also in these cases, and we have analyzed a simple example for the double delta state, when decoherence appears as projections either on the spatial or in the original spin basis. We have shown that both type of mechanisms produce the same effect, which translates into a damping of the off-diagonal matrix components.

9 Appendix A. Dynamics of the Wigner function for a particle subject to a potential

We will derive the differential equation that is obeyed by the Wigner matrix in two cases: I) A particle interacting with a position-dependent potential $V(x)$ and II) A spin 1/2 particle under the effect of a spin-position Hamiltonian of the form (7.21).

I) Particle interacting with a position-dependent potential V(x)

We start with the Hamiltonian defined in (7.1). The interaction in this case only affects the phase space variables (m, k), therefore spin indices can be omitted for the moment, but can be recovered in the final expression by replacing $W(m,k,t) \longrightarrow W_{\alpha\beta}(m,k,t)$. Of course, for a spinless particle no replacement is necessary.

The evolution equation is obtained from the von Neumann equation for the density operator (7.4). Using the properties of the $T_{\pm}$ operators one obtains (7.5).

$$\frac{\partial}{\partial t}W(m,k,t) = 2J\sin k\left[W(m+1,k,t) - W(m-1,k,t)\right] + D, \tag{9.1}$$

where

$$D \equiv -\frac{i}{2\pi}\sum_{l} e^{-i(2l-m)k}(V_l - V_{m-l})\left\langle l|\rho(t)|m-l\right\rangle . \tag{9.2}$$

We assume that $V(x)$ is continuous and infinitely derivable at any point. Remembering that $V_l = V(la)$, we Taylor expand both V_l and V_{m-l} around the

point $\frac{m}{2}a$, so that

$$D = -\frac{i}{2\pi}\sum_l e^{-i(2l-m)k}\sum_{p=0}^{\infty}\frac{a^p}{p!}\left.\frac{d^pV(x)}{dx^p}\right|_{x=ma/2} \frac{(2l-m)^p}{2^p}[1-(-1)^p]\,\langle l|\rho(t)|m-l\rangle\,. \tag{9.3}$$

With the help of the Wigner function definition, Eq. (6.33), one arrives to

$$D = -i\sum_{p=0}^{\infty}\frac{a^p}{p!}\left.\frac{d^pV(x)}{dx^p}\right|_{x=ma/2}\frac{1}{(-2i)^p}[1-(-1)^p]\frac{\partial^pW(m,k,t)}{\partial k^p}. \tag{9.4}$$

Notice that even values of p do not contribute in the above sum, so we restrict ourselves to odd values $p = 2s+1$ with $s \in \mathbb{N}$. After simplifying, we finally obtain

$$\frac{\partial}{\partial t}W(m,k,t) = 2J\sin k\,[W(m+1,k,t)-W(m-1,k,t)] + \sum_{s=0}^{\infty}\frac{(-1)^s a^{2s+1}}{2^{2s}(2s+1)!}\left.\frac{d^{2s+1}V(x)}{dx^{2s+1}}\right|_{x=ma/2}\frac{\partial^{2s+1}W(m,k,t)}{\partial k^{2s+1}}. \tag{9.5}$$

II) Spin 1/2 particle under the effect of a spin-position Hamiltonian

We now develop an equation of motion for a spin 1/2 particle which is subject to a spin position dependent interaction given by Eq. (7.21). Following similar steps to the previous case, and making use of $\sigma_z\,|\alpha\rangle = (-1)^\alpha\,|\alpha\rangle$, $\alpha = 0, 1$, one gets

$$\frac{\partial}{\partial t}W_{\alpha\beta}(m,k,t) = 2J\sin k\,[W_{\alpha\beta}(m+1,k,t)-W_{\alpha\beta}(m-1,k,t)] + D_{\alpha\beta}, \tag{9.6}$$

with

$$D_{\alpha\beta} \equiv -\frac{i}{2\pi}\sum_l e^{-i(2l-m)k}\left[(-1)^\alpha V_l - (-1)^\beta V_{m-l}\right]\langle n,\alpha|\rho|m-n,\beta\rangle. \tag{9.7}$$

After expanding V_l and V_{m-l} around the point $\frac{m}{2}a$ as before, we arrive to

$$D_{\alpha\beta} = -\frac{i}{2\pi}\sum_l e^{-i(2l-m)k}\sum_{p=0}^{\infty}\frac{a^p}{p!}\left.\frac{d^pV(x)}{dx^p}\right|_{x=ma/2} \frac{(2l-m)^p}{2^p}(-1)^\alpha[1-(-1)^p(-1)^{\alpha+\beta}]\,\langle l|\rho(t)|m-l\rangle\,. \tag{9.8}$$

In terms of the Wigner matrix,

$$D_{\alpha\beta} = -i \sum_{p=0}^{\infty} \frac{a^p}{p!} \left. \frac{d^p V(x)}{dx^p} \right|_{x=ma/2}$$
$$\frac{1}{(-2i)^p} (-1)^{\alpha} [1 - (-1)^p (-1)^{\alpha+\beta}] \frac{\partial^p W_{\alpha\beta}(m,k,t)}{\partial k^p}. \tag{9.9}$$

In order to determine the values of p that contribute to the above sum, one has to consider two different cases.

If $\alpha = \beta$, only odd values $p = 2s + 1$ with $s \in \mathbb{N}$ have to be considered, and one is lead to

$$D_{\alpha\alpha} = (-1)^{\alpha} \sum_{s=0}^{\infty} \frac{(-1)^s a^{2s+1}}{(2s+1)!} \frac{1}{2^{2s}} \left. \frac{d^{2s+1} V(x)}{dx^{2s+1}} \right|_{x=ma/2} \frac{\partial^{2s+1} W_{\alpha\alpha}(m,k,t)}{\partial k^{2s+1}}, \tag{9.10}$$

whereas for the off-diagonal elements $\alpha \neq \beta$ we have now only the contribution from even values of $p = 2s$, and we can easily obtain

$$D_{\alpha\beta} = -2i(-1)^{\alpha} \sum_{s=0}^{\infty} \frac{(-1)^s a^{2s}}{(2s)!} \frac{1}{2^{2s}} \left. \frac{d^{2s} V(x)}{dx^{2s}} \right|_{x=ma/2} \frac{\partial^{2s} W_{\alpha\beta}(m,k,t)}{\partial k^{2s}}. \tag{9.11}$$

Bibliography

[1] Heinz-Peter Breuer, Elsi-Mari Laine, and Jyrki Piilo. Measure for the Degree of Non-Markovian Behavior of Quantum Processes in Open Systems. *Phys. Rev. Lett.*, 103:210401, Nov 2009. vi

[2] Quantum Walks On Graphs: Proc ACM Symposium on Theory of Computation (STOC'01) (Association for Computing Machinery, New York, July 2001). page 50, 2001. 5, 25, 43

[3] Andris Ambainis, Eric Bach, Ashwin Nayak, Ashvin Vishwanath, and John Watrous. One-dimensional quantum walks. In *STOC*, pages 37–49, 2001. 5, 13, 15, 25, 32, 34, 43, 49

[4] Andrew M. Childs, Edward Farhi, and Sam Gutmann. An Example of the Difference Between Quantum and Classical Random Walks. *Quantum Information Processing*, 1:35–43, 2002. 10.1023/A:1019609420309. 5, 13, 25, 32, 43

[5] Edward Farhi and Sam Gutmann. Quantum computation and decision trees. *Phys. Rev. A*, 58(2):915–928, Aug 1998. 5, 25, 43

[6] Andrew M. Childs. Universal Computation by Quantum Walk. *Phys. Rev. Lett.*, 102(18):180501, May 2009. 6, 25, 43

[7] Neil B. Lovett, Sally Cooper, Matthew Everitt, Matthew Trevers, and Viv Kendon. Universal quantum computation using the discrete-time quantum walk. *Phys. Rev. A*, 81(4):042330, Apr 2010. 6, 25, 43

[8] Ashwin Nayak and Ashvin Vishwanath. Quantum Walk on the Line. 2007. 13, 19, 32, 38

[9] Germán J de Valcárcel, Eugenio Roldán, and Alejandro Romanelli. Tailoring discrete quantum walk dynamics via extended initial conditions. *New Journal of Physics*, 12(12):123022, 2010. 18, 37, 45, 46, 69

[10] Carl M. Bender and Steven A. Orszag. Advanced Mathematical Methods for Scientists and Engineer s . *International Series in Pure and Applied Mathematics. McGr aw-Hill, Inc., New York,*, 1978. 19, 38

[11] Norman Bleistein and Richard A. Handelsman. Asymptotic Expansions of Integrals . *nstitute of Mathematical Statistics, Hayward, Californ ia*, 1988. 19, 38

[12] N. Konno. Symmetry of distribution for the one-dimensional hadamard walk. *Interdisciplinary Information Sciences*, 10:11–22, 2004. 20, 39

[13] N. Konno. Limit theorem for continuous-time quantum walk on the line. *Phys. Rev. E*, 72(026113), 2005. 20, 39

[14] N. Konno. A new type of limit theorems for the one-dimensional quantum random walk. *ournal of the Mathematical Society of Japan*, 57:1179–1195, 2005. 20, 39

[15] N. Konno. A path integral approach for disordered quantum walks in one dimension. *Fluctuation and Noise Letters*, 5:529–537, 2005. 20, 39

[16] Kyohei Watabe, Naoki Kobayashi, Makoto Katori, and Norio Konno. Limit distributions of two-dimensional quantum walks. *Phys. Rev. A*, 77:062331, Jun 2008. 20, 39, 45, 62, 80

[17] Neil Shenvi, Julia Kempe, and K. Birgitta Whaley. Quantum random-walk search algorithm. *Phys. Rev. A*, 67(5):052307, May 2003. 20, 39, 45

[18] Andrew M. Childs, Richard Cleve, Enrico Deotto, Edward Farhi, Sam Gutmann, and Daniel A. Spielman. Exponential Algorithmic Speedup by a Quantum Walk. In *Proceedings of the Thirty-fifth Annual ACM Symposium on Theory of Computing*, STOC '03, pages 59–68, New York, NY, USA, 2003. ACM. 20, 39

[19] B. C. Travaglione and G. J. Milburn. Implementing the quantum random walk. *Phys. Rev. A*, 65(3):032310, Feb 2002. 21, 22, 40, 41

[20] C. Monroe, D. M. Meekhof, B. E. King, and D. J. Wineland. A "Schrödinger Cat" Superposition State of an Atom. *Science*, 272(5265):1131–1136, 1996. 21, 40

[21] Barry C. Sanders, Stephen D. Bartlett, Ben Tregenna, and Peter L. Knight. Quantum quincunx in cavity quantum electrodynamics. *Phys. Rev. A*, 67:042305, Apr 2003. 21, 40

[22] W. Dür, R. Raussendorf, V. M. Kendon, and H.-J. Briegel. Quantum walks in optical lattices. *Phys. Rev. A*, 66(5):052319, Nov 2002. 21, 40

[23] K. Eckert, J. Mompart, G. Birkl, and M. Lewenstein. One- and two-dimensional quantum walks in arrays of optical traps. *Phys. Rev. A*, 72:012327, Jul 2005. 21, 40

[24] Eugenio Roldán and J. C. Soriano. Optical implementability of the two-dimensional quantum walk. *Journal of Modern Optics*, 52(18):2649–2657, 2005. 21, 40

[25] Jiangfeng Du, Hui Li, Xiaodong Xu, Mingjun Shi, Jihui Wu, Xianyi Zhou, and Rongdian Han. Experimental implementation of the quantum random-walk algorithm. *Phys. Rev. A*, 67(4):042316, Apr 2003. 22, 41

[26] Olaf Mandel, Markus Greiner, Artur Widera, Tim Rom, Theodor W. Hänsch, and Immanuel Bloch. Coherent Transport of Neutral Atoms in Spin-Dependent Optical Lattice Potentials. *Phys. Rev. Lett.*, 91:010407, Jul 2003. 22, 41

[27] C. A. Ryan, M. Laforest, J. C. Boileau, and R. Laflamme. Experimental implementation of a discrete-time quantum random walk on an NMR quantum-information processor. *Phys. Rev. A*, 72(6):062317, Dec 2005. 22, 41

[28] H. Schmitz, R. Matjeschk, Ch. Schneider, J. Glueckert, M. Enderlein, T. Huber, and T. Schaetz. Quantum Walk of a Trapped Ion in Phase Space. *Phys. Rev. Lett.*, 103:090504, Aug 2009. 22, 41

[29] Peng Xue, Barry C. Sanders, and Dietrich Leibfried. Quantum Walk on a Line for a Trapped Ion. *Phys. Rev. Lett.*, 103:183602, Oct 2009. 22, 41

[30] F. Zähringer, G. Kirchmair, R. Gerritsma, E. Solano, R. Blatt, and C. F. Roos. Realization of a Quantum Walk with One and Two Trapped Ions. *Phys. Rev. Lett.*, 104:100503, Mar 2010. 22, 41

[31] R Matjeschk, Ch Schneider, M Enderlein, T Huber, H Schmitz, J Glueckert, and T Schaetz. Experimental simulation and limitations of quantum walks with trapped ions. *New Journal of Physics*, 14(3):035012, 2012. 22, 41

[32] Michal Karski, Leonid Förster, Jai-Min Choi, Andreas Steffen, Wolfgang Alt, Dieter Meschede, and Artur Widera. Quantum Walk in Position Space with Single Optically Trapped Atoms. *Science*, 325(5937):174–177, 2009. 22, 41

[33] Hagai B. Perets, Yoav Lahini, Francesca Pozzi, Marc Sorel, Roberto Morandotti, and Yaron Silberberg. Realization of Quantum Walks with Negligible Decoherence in Waveguide Lattices. *Phys. Rev. Lett.*, 100:170506, May 2008. 22, 41

[34] Alberto Peruzzo, Mirko Lobino, Jonathan C. F. Matthews, Nobuyuki Matsuda, Alberto Politi, Konstantinos Poulios, Xiao-Qi Zhou, Yoav Lahini, Nur Ismail, Kerstin Wörhoff, Yaron Bromberg, Yaron Silberberg, Mark G. Thompson, and Jeremy L. OBrien. Quantum Walks of Correlated Photons. *Science*, 329(5998):1500–1503, 2010. 23, 42

[35] J O Owens, M A Broome, D N Biggerstaff, M E Goggin, A Fedrizzi, T Linjordet, M Ams, G D Marshall, J Twamley, M J Withford, and A G White. Two-photon quantum walks in an elliptical direct-write waveguide array. *New Journal of Physics*, 13(7):075003, 2011. 23, 42

[36] Linda Sansoni, Fabio Sciarrino, Giuseppe Vallone, Paolo Mataloni, Andrea Crespi, Roberta Ramponi, and Roberto Osellame. Two-Particle Bosonic-Fermionic Quantum Walk via Integrated Photonics. *Phys. Rev. Lett.*, 108:010502, Jan 2012. 23, 42

[37] J. Svozilík, R. de J. León-Montiel, and J. P. Torres. Implementation of a spatial two-dimensional quantum random walk with tunable decoherence. *Phys. Rev. A*, 86:052327, Nov 2012. 23, 42

[38] Weeler and Zurec. Quantum theory and measurament. *Princenton university press, Princton, NJ*, 1984. 23, 42

[39] Yoon-Ho Kim, Rong Yu, Sergei P. Kulik, Yanhua Shih, and Marlan O. Scully. Delayed "Choice" Quantum Eraser. *Phys. Rev. Lett.*, 84:1–5, Jan 2000. 23, 42

[40] Alberto Peruzzo, Peter Shadbolt, Nicolas Brunner, Sandu Popescu, and Jeremy L. O'Brien. A Quantum Delayed-Choice Experiment. *Science*, 338(6107):634–637, 2012. 23, 42

[41] Florian Kaiser, Thomas Coudreau, Pérola Milman, Daniel B. Ostrowsky, and Sébastien Tanzilli. Entanglement-Enabled Delayed-Choice Experiment. *Science*, 338(6107):637–640, 2012. 23, 42

[42] Jeong Youn-Chang, Di Franco Carlo, Lim Hyang-Tag, Kim M.S., and Kim Yoon-Ho. Experimental realization of a delayed-choice quantum walk. *Nat Commun*, 4, sep 2013. 23, 42

[43] Andreas Schreiber, Aurél Gábris, Peter P. Rohde, Kaisa Laiho, Martin Štefaňák, Václav Potoček, Craig Hamilton, Igor Jex, and Christine Silberhorn. A 2D Quantum Walk Simulation of Two-Particle Dynamics. *Science*, 336(6077):55–58, 2012. 23, 42, 161

[44] Takuya Kitagawa, Mark S. Rudner, Erez Berg, and Eugene Demler. Exploring topological phases with quantum walks. *Phys. Rev. A*, 82:033429, Sep 2010. 24, 42

[45] Yutaka Shikano, Kota Chisaki, Etsuo Segawa, and Norio Konno. Emergence of randomness and arrow of time in quantum walks. *Phys. Rev. A*, 81:062129, Jun 2010. 24, 42

[46] Antoni Wójcik, Tomasz Łuczak, Paweł Kurzy, Andrzej Grudka, Tomasz Gdala, and Małgorzata Bednarska-Bzd. Trapping a particle of a quantum walk on the line. *Phys. Rev. A*, 85:012329, Jan 2012. 24, 42

[47] Hideaki Obuse and Norio Kawakami. Topological phases and delocalization of quantum walks in random environments. *Phys. Rev. B*, 84:195139, Nov 2011. 24, 42

[48] J. K. Asbóth. Symmetries, topological phases, and bound states in the one-dimensional quantum walk. *Phys. Rev. B*, 86:195414, Nov 2012. 24, 42

[49] Graciana Puentes, Ilja Gerhardt, Fabian Katzschmann, Christine Silberhorn, Jörg Wrachtrup, and Maciej Lewenstein. Observation of Topological Structures in Photonic Quantum Walks. *Phys. Rev. Lett.*, 112:120502, Mar 2014. 24, 42

[50] Frederick W. Strauch. Connecting the discrete- and continuous-time quantum walks. *Phys. Rev. A*, 74(3):030301, Sep 2006. 34

[51] S E Venegas-Andraca. Quantum Inf. Proc. *Quantum Inf. Proc.*, 110:1015–106, 2012. 39

[52] Peter L. Knight, Eugenio Roldán, and J. E. Sipe. Quantum walk on the line as an interference phenomenon. *Phys. Rev. A*, 68(2):020301, Aug 2003. 40

[53] Eugenio Roldán, Carlo Di Franco, Fernando Silva, and Germán J. de Valcárcel. N-dimensional alternate coined quantum walks from a dispersion-relation perspective. *Phys. Rev. A*, 87:022336, Feb 2013. 45, 46, 55, 62, 79

[54] A. Kempf and R. Portugal. Group velocity of discrete-time quantum walks. *Phys. Rev. A*, 79:052317, May 2009. 45

[55] M. Štefaňák, I. Bezděková, and I. Jex. Continuous deformations of the Grover walk preserving localization. *The European Physical Journal D*, 66(5):1–7, 2012. 45

[56] Takuya Machida. A quantum walk with a delocalized initial state: contribution from a coin-flip operator. *International Journal of Quantum Information*, 11(05):1350053, 2013. 45

[57] Peter P Rohde, Andreas Schreiber, Martin Štefaňák, Igor Jex, and Christine Silberhorn. Multi-walker discrete time quantum walks on arbitrary graphs, their properties and their photonic implementation. *New Journal of Physics*, 13(1):013001, 2011. 45

[58] C. Di Franco, M. Mc Gettrick, T. Machida, and Th. Busch. Alternate two-dimensional quantum walk with a single-qubit coin. *Phys. Rev. A*, 84:042337, Oct 2011. 45

[59] T D Mackay, S D Bartlett, L T Stephenson, and B C Sanders. Quantum walks in higher dimensions. *Journal of Physics A: Mathematical and General*, 35(12):2745, 2002. 45, 62

[60] Ben Tregenna, Will Flanagan, Rik Maile, and Viv Kendon. Controlling discrete quantum walks: coins and initial states. *New Journal of Physics*, 5(1):83, 2003. 45

[61] Norio Inui, Yoshinao Konishi, and Norio Konno. Localization of two-dimensional quantum walks. *Phys. Rev. A*, 69:052323, May 2004. 45, 61

[62] Ivens Carneiro, Meng Loo, Xibai Xu, Mathieu Girerd, Viv Kendon, and Peter L Knight. Entanglement in coined quantum walks on regular graphs. *New Journal of Physics*, 7(1):156, 2005. 45

[63] William Adamczak, Kevin Andew, Bergen Leon, Dillon Ethier, Peter Hernberg, Jennifer Lin, and Christiano Tamon. Non-uniform mixing of quantum walk on cycles. *International Journal of Quantum Information*, 05(06):781–793, 2007. 45

[64] F. L. Marquezino, R. Portugal, G. Abal, and R. Donangelo. Mixing times in quantum walks on the hypercube. *Phys. Rev. A*, 77:042312, Apr 2008. 45

[65] Salvador Elías Venegas-Andraca. Quantum Walks for Computer Scientists. *Synthesis Lectures on Quantum Computing*, 1(1):1–119, 2008. 45

[66] A. C. Oliveira, R. Portugal, and R. Donangelo. Decoherence in two-dimensional quantum walks. *Phys. Rev. A*, 74:012312, Jul 2006. 45

[67] Y. Omar, N. Paunković, L. Sheridan, and S. Bose. Quantum walk on a line with two entangled particles. *Phys. Rev. A*, 74:042304, Oct 2006. 45

[68] M Štefaňák, B Kollár, T Kiss, and I Jex. Full revivals in 2D quantum walks. *Physica Scripta*, 2010(T140):014035, 2010. 45

[69] M. Štefaňák, T. Kiss, and I. Jex. Recurrence properties of unbiased coined quantum walks on infinite d-dimensional lattices. *Phys. Rev. A*, 78:032306, Sep 2008. 45

[70] M V Berry and M Wilkinson. Diabolical points in the spectra of triangles. *Prox. R. Soc. Lond.*, 392(15), 1984. 46, 59

[71] M V Berry. Conical diffraction asymptotics: fine structure of Poggendorff rings and axial spike. *J. Opt. A: Pure Appl. Opt.*, 6(289), 2004. 46, 59, 73, 161

[72] M V Berry and M R Jeffrey. Conical diffraction: Hamilton's diabolical point at the heart of crystal optics. *Prog. Opt.*, 50(13), 2007. 46, 59, 161

[73] Y. Hatsugai, T. Fukui, and H. Aoki. Topological aspects of graphene. *The European Physical Journal Special Topics*, 148(1):133–141, 2007. 46, 59

[74] Aaron Bostwick, Taisuke Ohta, Jessica L McChesney, Konstantin V Emtsev, Thomas Seyller, Karsten Horn, and Eli Rotenberg. Symmetry breaking in few layer graphene films. *New Journal of Physics*, 9(10):385, 2007. 46, 59

[75] Taisuke Ohta, Aaron Bostwick, J. L. McChesney, Thomas Seyller, Karsten Horn, and Eli Rotenberg. Interlayer Interaction and Electronic Screening in Multilayer Graphene Investigated with Angle-Resolved Photoemission Spectroscopy. *Phys. Rev. Lett.*, 98:206802, May 2007. 46

[76] I. Pletikosić, M. Kralj, P. Pervan, R. Brako, J. Coraux, A. T. N'Diaye, C. Busse, and T. Michely. Dirac Cones and Minigaps for Graphene on Ir(111). *Phys. Rev. Lett.*, 102:056808, Feb 2009. 46

[77] A. H. Castro Neto, F. Guinea, N. M. R. Peres, K. S. Novoselov, and A. K. Geim. The electronic properties of graphene. *Rev. Mod. Phys.*, 81:109–162, Jan 2009. 46

[78] C. Alden Mead and Donald G. Truhlar. Erratum: On the determination of Born–Oppenheimer nuclear motion wave functions including complications due to conical intersections and identical nuclei [J. Chem. Phys. 70, 2284 (1979)]. *The Journal of Chemical Physics*, 78(10):6344–6344, 1983. 46, 59

[79] Lorenz S. Cederbaum, Ronald S. Friedman, Victor M. Ryaboy, and Nimrod Moiseyev. Conical Intersections and Bound Molecular States Embedded in the Continuum. *Phys. Rev. Lett.*, 90:013001, Jan 2003. 46, 59

[80] Machi Zhang, Hsiang-hsuan Hung, Chuanwei Zhang, and Congjun Wu. Quantum anomalous Hall states in the p-orbital honeycomb optical lattices. *Phys. Rev. A*, 83:023615, Feb 2011. 46, 59

[81] Daniel Torrent and José Sánchez-Dehesa. Acoustic Analogue of Graphene: Observation of Dirac Cones in Acoustic Surface Waves. *Phys. Rev. Lett.*, 108:174301, Apr 2012. 46, 59

[82] Takuya Kitagawa. Topological phenomena in quantum walks: elementary introduction to the physics of topological phases. *Quantum Information Processing*, 11(5):1107–1148, 2012. 46

[83] O M Friesch, I Marzoli, and W P Schleich. Quantum carpets woven by Wigner functions. *New Journal of Physics*, 2(1):4, 2000. 49

[84] J W Goodman. Introduction to Fourier Optics. *Englewood, CO: Roberts and Company*, 2005. 65, 69

[85] Stanis Kolpakov, Adolfo Esteban-Martín, Fernando Silva, Javier García, Kestutis Staliunas, and Germán J. de Valcárcel. Experimental Demonstration of Hyperbolic Patterns. *Phys. Rev. Lett.*, 101:254101, Dec 2008. 69

[86] I. S. Gradshteyn and I. M. Ryzhik. Table of Integrals, Series and Products. *Academic Press,*, 1994. 72

[87] H. P. Breuer and F. Petruccione. The Theory of Open Quantum Systems. *Oxford University Press, Oxford*, 2002. 85, 91

[88] Heinz-Peter Breuer, Elsi-Mari Laine, and Jyrki Piilo. Measure for the Degree of Non-Markovian Behavior of Quantum Processes in Open Systems. *Phys. Rev. Lett.*, 103:210401, Nov 2009. 85, 95, 97, 108, 109

[89] G Lindblad. On the generators of quantum dynamical semigroups. *Commun. Math. Phys.*, 48(119), 1976. 93

[90] V. Gorini, A. Kossakowski, and E.C.G Sudarshan. Completely positive semigroups of N-level systems. *J. Math. Phys*, 17(21), 1976. 93

[91] Robert Zwanzig. Ensemble Method in the Theory of Irreversibility. *Journal of Chemical Physics*, 33(5):1338–1341, 1960. 93

[92] Sadao Nakajima. On Quantum Theory of Transport Phenomena. *Progress of Theoretical Physics*, 20(6):948–959, 1958. 93

[93] S. Chaturvedi and F. Shibata. Time-convolutionless projection operator formalism for elimination of fast variables. Application to Brownian motion. *Z. Phys.*, B85:297–308, 1979. 94

[94] Tony J. G. Apollaro, Carlo Di Franco, Francesco Plastina, and Mauro Paternostro. Memory-keeping effects and forgetfulness in the dynamics of a qubit coupled to a spin chain. *Phys. Rev. A*, 83:032103, Mar 2011. 95

[95] Alejandro Romanelli. Distribution of chirality in the quantum walk: Markov process and entanglement. *Phys. Rev. A*, 81:062349, Jun 2010. 97, 102

[96] Alejandro Romanelli. Thermodynamic behavior of the quantum walk. *Phys. Rev. A*, 85:012319, Jan 2012. 97

[97] A. Pérez and A. Romanelli. Spatially Dependent Decoherence and Anomalous Diffusion of Quantum Walks. *Journal of Computational and Theoretical Nanoscience*, 10(7), 2013. 97, 162

[98] Alejandro Romanelli and Gustavo Segundo. The entanglement temperature of the generalized quantum walk. *Physica A: Statistical Mechanics and its Applications*, 393(0):646–654, 2014. 97

[99] Todd A. Brun, H. A. Carteret, and Andris Ambainis. Quantum random walks with decoherent coins. *Phys. Rev. A*, 67:032304, Mar 2003. 98, 99

[100] Mostafa Annabestani, Seyed Javad Akhtarshenas, and Mohamad Reza Abolhassani. Decoherence in a one-dimensional quantum walk. *Phys. Rev. A*, 81:032321, Mar 2010. 98, 99, 106

[101] Y. Aharonov, L. Davidovich, and N. Zagury. Quantum random walks. *Phys. Rev. A*, 48:1687–1690, Aug 1993. 103

[102] A. Romanelli, R. Siri, G. Abal, A. Auyuanet, and R. Donangelo. Decoherence in the quantum walk on the line. *Physica A: Statistical Mechanics and its Applications*, 347(0):137–152, 2005. 106

[103] E. Wigner. On the Quantum Correction For Thermodynamic Equilibrium. *Phys. Rev.*, 40(5):749–759, Jun 1932. 113, 115

[104] M. Hillery, R. F. O'Connell, M. O. Scully, and E. P. Wigner. Distribution functions in physics: Fundamentals. *Physics Reports*, 106(3):121–167, 1984. 114, 149

[105] Christopher Ferrie. Quasi-probability representations of quantum theory with applications to quantum information science. *Reports on Progress in Physics*, 74(11):116001, 2011. 114, 119

[106] J. Bertrand and P. Bertrand. A tomographic approach to Wigner's function. *Foundations of Physics*, 17:397–405, 1987. 114, 115

[107] K. Vogel and H. Risken. Determination of quasiprobability distributions in terms of probability distributions for the rotated quadrature phase. *Phys. Rev. A*, 40:2847–2849, Sep 1989. 114

[108] Wolfgang P. Schleich. *Quantum Optics in Phase Space*. Wiley-VCH, Berlin, 1 edition, February 2001. 114

[109] Anatole Kenfack and Karol Zyczkowski. Negativity of the Wigner function as an indicator of non-classicality. *Journal of Optics B: Quantum and Semiclassical Optics*, 6(10):396, 2004. 114, 125, 126, 127

[110] Jose Moyal. Quantum Mechanics as a Statistical Theory. *Proc. Camb. Phil. Soc.*, 45:99–124, 1949. 114

[111] E. C. G. Sudarshan. Equivalence of Semiclassical and Quantum Mechanical Descriptions of Statistical Light Beams. *Phys. Rev. Lett.*, 10:277–279, 1963. 117

[112] E. C. G. Sudarshan. Equivalence of Semiclassical and Quantum Mechanical Descriptions of Statistical Light Beams. *Phys. Rev. Lett.*, 10:277–279, Apr 1963. 117

[113] Th. Richter and W. Vogel. Nonclassicality of Quantum States: A Hierarchy of Observable Conditions. *Phys. Rev. Lett.*, 89:283601, Dec 2002. 117

[114] Werner Vogel. Nonclassical States: An Observable Criterion. *Phys. Rev. Lett.*, 84:1849–1852, Feb 2000. 117

[115] Kôdi Husimi. Some Formal Properties of the Density Matrix. *Proc. Phys. Math. Soc. Jpn*, 22:264–314, 1940. 117

[116] A. Vourdas. Quantum systems with finite Hilbert space. *Reports on Progress in Physics*, 67(3):267, 2004. 119

[117] William K. Wootters. A Wigner-function formulation of finite-state quantum mechanics. *Annals of Physics*, 176(1):1–21, 1987. 119, 143, 144, 163

[118] Kathleen S. Gibbons, Matthew J. Hoffman, and William K. Wootters. Discrete phase space based on finite fields. *Phys. Rev. A*, 70(6):062101, Dec 2004. 119, 125

[119] W. K. Wootters. Quantum mechanics without probability amplitudes. *Foundations of Physics*, 16(4):391–405, 1986. 119

[120] Juan Pablo Paz, Augusto José Roncaglia, and Marcos Saraceno. Qubits in phase space: Wigner-function approach to quantum-error correction and the mean-king problem. *Phys. Rev. A*, 72(1):012309, Jul 2005. 120

[121] Cecilia Cormick, Ernesto F. Galvão, Daniel Gottesman, Juan Pablo Paz, and Arthur O. Pittenger. Classicality in discrete Wigner functions. *Phys. Rev. A*, 73:012301, Jan 2006. 120, 141

[122] Ulf Leonhardt. Discrete Wigner function and quantum-state tomography. *Phys. Rev. A*, 53(5):2998–3013, May 1996. 120, 122, 124, 139

[123] J Zak. Doubling feature of the Wigner function: finite phase space. *Journal of Physics A: Mathematical and Theoretical*, 44(34):345305, 2011. 120, 122

[124] César Miquel, Juan Pablo Paz, and Marcos Saraceno. Quantum computers in phase space. *Phys. Rev. A*, 65:062309, Jun 2002. 120, 122, 124, 139

[125] Cecilia C. López and Juan Pablo Paz. Phase-space approach to the study of decoherence in quantum walks. *Phys. Rev. A*, 68:052305, Nov 2003. 120, 157

[126] Juan Pablo Paz. Discrete Wigner functions and the phase-space representation of quantum teleportation. *Phys. Rev. A*, 65:062311, Jun 2002. 120

[127] I. Rigas, L. L. Sánchez-Soto, A. B. Klimov, J. Řeháček, and Z. Hradil. Nonnegative Wigner functions for orbital angular momentum states. *Phys. Rev. A*, 81:012101, Jan 2010. 121, 125, 128, 129

[128] I. Rigas, L.L. Sánchez-Soto, A.B. Klimov, J. Řeháček, and Z. Hradil. Orbital angular momentum in phase space. *Annals of Physics*, 326(2):426–439, 2011. 121, 125

[129] João P. Bizarro. Weyl-Wigner formalism for rotation-angle and angular-momentum variables in quantum mechanics. *Phys. Rev. A*, 49:3255–3276, May 1994. 121

[130] H.A. Kastrup. Quantization of the optical phase space $\mathcal{S}^2 = \{\varphi \bmod 2\pi, I > 0\}$ in terms of the group $SO^{\uparrow}(1,2)$. *Fortschritte der Physik*, 51(10-11):975–1134, 2003. 121

[131] H. A. Kastrup. Quantization of the canonically conjugate pair angle and orbital angular momentum. *Phys. Rev. A*, 73:052104, May 2006. 121

[132] R.L. Hudson. When is the wigner quasi-probability density non-negative? *Reports on Mathematical Physics*, 6(2):249–252, 1974. 125, 130

[133] A. Mandilara, E. Karpov, and N. J. Cerf. Extending Hudson's theorem to mixed quantum states. *Phys. Rev. A*, 79:062302, Jun 2009. 125

[134] A. Mari, K. Kieling, B. Melholt Nielsen, E. S. Polzik, and J. Eisert. Directly Estimating Nonclassicality. *Phys. Rev. Lett.*, 106:010403, Jan 2011. 125, 143

[135] David Gross. Hudson's theorem for finite-dimensional quantum systems. *J. Math. Phys.*, 47:122107, 2006. 125, 141

[136] D. Gross. Non-negative Wigner functions in prime dimensions. *Applied Physics B: Lasers and Optics*, 86:367–370, 2007. 125

[137] Ernesto F. Galvão. Discrete Wigner functions and quantum computational speedup. *Phys. Rev. A*, 71:042302, Apr 2005. 125, 141

[138] F. Peyrin and R. Prost. A unified definition for the discrete-time, discrete-frequency, and discrete-time/Frequency Wigner distributions. *Acoustics, Speech and Signal Processing, IEEE Transactions on*, 34(4):858–867, aug 1986. 126

[139] Arturo Argüelles and Thomas Dittrich. Wigner function for discrete phase space: Exorcising ghost images. *Physica A: Statistical Mechanics and its Applications*, 356(1):72–77, 2005. 126

[140] Milton Abramowitz and Irene A. Stegun. *Handbook of Mathematical Functions with Formulas, Graphs, and Mathematical Tables*. Dover, New York, 1972. 130, 141

[141] A. Mann and M. Revzen. Gaussian Density Matrices: Quantum Analogs of Classical States. *Fortschr. Phys*, 41:431–446, 1993. 132

[142] Alfredo Luis. Scalar Wigner function for vectorial fields and spatial-angular Stokes parameters. *Optics Communications*, 246(4–6):437–443, 2005. 137

[143] S. Wallentowitz, R. L. de Matos Filho, and W. Vogel. Determination of entangled quantum states of a trapped atom. *Phys. Rev. A*, 56:1205–1211, Aug 1997. 137

[144] R. Martínez-Herrero, P. M. Mejías, and J. M. Movilla. Spatial characterization of general partially polarized beams. *Opt. Lett.*, 22(4):206–208, Feb 1997. 137

[145] A. Mari and J. Eisert. Positive Wigner Functions Render Classical Simulation of Quantum Computation Efficient. *Phys. Rev. Lett.*, 109:230503, Dec 2012. 143

[146] Victor Veitch, Christopher Ferrie, David Gross, and Joseph Emerson. Negative quasi-probability as a resource for quantum computation. *New Journal of Physics*, 14(11):113011, 2012. 143

[147] R. Franco and V. Penna. Discrete Wigner distribution for two qubits: a characterization of entanglement properties. *J. Phys. A: Math. Gen.*, 39:5907–5919, 2006. 143, 144

[148] M. Hinarejos, A. Pérez, and M.C. Bañuls. Wigner function for a particle in an infinite lattice. *New Journal of Physics*, 14(10):103009, 2012. 143

[149] M. Hinarejos, M.C. Bañuls, and A. Pérez. A study of Wigner functions for discrete-time quantum walks. *Journal of Computational and Theoretical Nanoscience*, 10(7):1626–1633, 2013. 143, 157

[150] Reinhard F. Werner. Quantum states with Einstein-Podolsky-Rosen correlations admitting a hidden-variable model. *Phys. Rev. A*, 40:4277–4281, Oct 1989. 144

[151] I. S. Gradshteyn and I. M. Ryzhik. Table of integrals, series, and products. *Elsevier/Academic Press, Amsterdam*, 2007. 150

[152] E Kajari, N.L. Harshman, E.M. Rasel, S. Stenholm, G Süssmann, and W.P. Schleich. Inertial and gravitational mass in quantum mechanics. *Applied Physics B*, 43-60, 2010. 151

[153] Heinz-Peter Breuer and Francesco Petruccione. The Theory of Open Quantum Systems. *Oxford University Press*, 2007. 156

[154] C. C. Lopez and J. P. Paz. Phase-space approach to the study of decoherence in quantum walks. *Phys. Rev. A*, 68,:052305, 2003. 157

[155] A. Schreiber, K. N. Cassemiro, V. Potoček, A. Gábris, P. J. Mosley, E. Andersson, I. Jex, and Ch. Silberhorn. Photons Walking the Line: A Quantum Walk with Adjustable Coin Operations. *Phys. Rev. Lett.*, 104(5):050502, Feb 2010. 161

[156] P. Carruthers and F. Zachariasen. Relativistic quantum transport theory approach to multiparticle production. *Phys. Rev. D*, 13:950–960, Feb 1976. 164

[157] Rémi Hakim. *Introduction to relativistic statistical mechanics: classical and quantum*. World scientific, Singapore, 2011. 164

List of publications

- M. Hinarejos, A. Pérez, and M.C. Bañuls. Wigner function for a particle in an infinite lattice. *New Journal of Physics*, 14(10):103009, 2012.
- M. Hinarejos, M.C. Bañuls, and A. Pérez. A study of Wigner functions for discrete-time quantum walks. *Journal of Computational and Theoretical Nanoscience*, 10(7):1626–1633, 2013.
- Margarida Hinarejos; Germán J. de Valcárcel, Eugenio Roldán, Alejandro Romanelli, A.Pérez. Understanding and controlling N-dimensional quantum walks via dispersion relations. Application to the 2D and 3D Grover walk: Diabolical points and more *New Journal of Physics* 15 073041, 2013
- Margarida Hinarejos, Carlo Di Franco, Alejandro Romanelli, and Armando Pérez . Chirality asymptotic behavior and non-Markovianity in quantum walks on a line. *Phys. Rev. A* 89, 052330, 2014
- M Hinarejos, M C Bañuls, A Pérez. Wigner formalism for a particle on an infinite lattice: dynamics and spin. arXiv:1405.2944, 2014